1-1-2011

Opposing effects of recirculated gases during cranking on cold start of diesel engines

Rafik N. Rofail
Wayne State University,

OPPOSING EFFECTS OF RECIRCULATED GASES DURING CRANKING ON COLD START OF DIESEL ENGINES

by

RAFIK N. ROFAIL

DISSERTATION

Submitted to the Graduate School

of Wayne State University,

Detroit, Michigan

in partial fulfillment of the requirements

for the degree of

DOCTOR OF PHILOSOPHY

2011

MAJOR: MECHANICAL ENGINEERING

Approved by

_____

Advisor Date

_____

_____

_____

_____

DEDICATION

To my wife Celine, my son Mark, my daughter Maria and my whole family (Especially my grandma, my mother, my father and my in-laws) in my hometown in Cairo, Egypt.

ACKNOWLEDGMENTS

I would like to genuinely express my gratefulness to Professor Naeim A. Henein, who served as my advisor throughout the period of my graduate study, for the chance and support he has provided for me to work on the challenging topics, for all the expert guidance, superb insight and valuable advice, his patience and encouragement throughout these years. I would like to thank my committee members, Prof. Dinu Taraza, Prof. Walter Bryzik, Prof. Trilochan Singh, Prof. Harpreet Singh and Dr. Peter Schihl for their help and support throughout my dissertation work and valuable opinions.

I am also greatly grateful for the technical support from Sam Hashemi at Ford Motor Company.

A special thankfulness to Ms Lidia Nedeltcheva, in Mechanical Engineering Department Lab, for her generous, valuable, and in time help in trouble shooting throughout my work. The help from machine shop, Mr. Eugene Snowden, Mr. Dave Griffin and Mr. Marvin Santure and help from electric shop, Mr. Randy Zabla are heartily appreciated.

I also appreciate the sincere efforts of the colleagues and friends of the Center for Automotives Research (CAR), Dr. Jansons Marcis, Steve Gruenewald, Rohit Tanksale, Anshul Sharma and other members for their help and support.

A special THANK to my parents and especially my father in law who came especially from Egypt to attend my Ph.D. final defense.

Finally, I would like to express my deepest and everlasting gratitude to my wife Celine for her support, encouragement and understanding during the years of my graduate work.

TABLE OF CONTENTS

Dedication…… **ii**

Acknowledgement…… **iii**

List of Tables …… **xi**

List of Figures …… **xii**

Nomenclature …… **xx**

Introduction …… **1**

Goal …… **2**

CHAPTER 1: LITERATURE REVIEW …….. 3

1.1 Factors Affecting Cold Start ……..…..... 3

1.1.1 Ambient temperature.……..…….. 3

1.1.2 Engine speed ……..…..…… 4

1.1.3 Altitude ……..…..…… 5

1.1.4 Fuel injection timing ……..……..…… 6

1.1.5 Injection rate ……..... 7

1.1.6 Chamber design ……. 9

1.1.7 Common rail pressure …….. 9

1.1.8 Cetane number ……..... 10

1.2 Cold Start Aids …… 11

1.3 Effect of Adding Folmaldehyde on Ignition Delay …….. 12

CHAPTER 2: EXPERIMENTAL SETUP AND INSTRUMENTATION 13

2.1 Introduction ……..…… 13

2.2 CGR System and Engine Features ……. 15

2.2.1 CGR system …….. 15

2.2.2 Valve train ……... 17

2.2.3 Fuel injection ……. 17

2.2.4 Combustion bowl ……. 17

2.2.5 Port deactivation ……. 18

2.3 Instrumentation and Measurements ……. 18

2.3.1 In cylinder pressure ……... 19

2.3.2 Intake manifold pressure ……... 20

2.3.3 Pressure before and after turbocharger ……. 22

2.3.4 Exhaust temperature ……. 24

2.3.5 Air intake temperature …….. 25

2.3.6 Needle lift ……. 26

2.3.7 Fuel pressure …….. 27

2.3.8 Turbocharger speed ……... 28

2.3.9 Engine RPM ……. 29

2.3.10 Unburnt hydrocarbon emissions …….. 30

2.3.11 NOx emissions …….. 31

2.3.12 Fuel consumption ……. 32

2.3.13 Air mass flow ……. 33

2.3.14 Blow-By flow …….. 34

2.4 Engine Control …… 35

2.4.1 Variables that can only be monitored …….. 35

2.4.2 Engine variables that can be controlled …….. 36
2.5 Detailed Steps with Illustrations for a Single Run ……. 37
CHAPTER 3: EXPERIMENTAL RESULTS AND DISCUSSIONS …… 47
3.1 Introduction …….. 47
3.2 Baseline Test …….. 47
3.3 Effect of Low Rates of CGR on Cranking Period and Unburned HC Emissions ……..... 50
3.4 Effect of High Rates of CRG on Cranking Period and Unburned HC Emissions at a Reduced Fuel Injection ……... 53
3.4.1 Effect of applying the highest rates of CGR ……. 53
3.4.2 Effect of applying controlled rates of CGR at 3 ℃ ambient temperature ……. 56
3.4.3 Effect of applying controlled rates of CGR at -3 ℃ ambient temperature ……. 59
3.4.4 Effect of varying fuel injection rate at a constant CGR rate 61
CHAPTER 4: SIMULATION RESULTS AND DISCUSSIONS …….. 63
4.1 Introduction …….. 63
4.2 Heterogeneous Charge ……. 64
4.2.1 Effect of adding three different concentrations of HCHO to the intake charge on ignition delay at 25 mg/stroke fuel injected using CFD simulation …….. 65

4.2.2 Effect of adding different HCs with different concentrations to the intake charge on ignition delay at 25 mg/stroke fuel injected using CFD simulation ……. 66
4.3 Homogeneous Charge …….. 68
4.3.1 Effect of adding 0 to 900 ppm HCHO to the intake charge on ignition delay using Chemkin at different equivalence ratios …….. 70
4.3.2 Effect of adding 0 to 900 ppm of different species of HCs to the intake charge on ignition delay at different equivalence ratios 74
4.4 Investigation of Ignition Delay …….. 80
4.4.1 Effect of temperature on ignition delay ……. 80
4.4.2 Species that affect the start of combustion ……. 81
4.4.3 A new parameter to indicate if firing will occur in a cycle based on the ratio between HCHO and H2O2 mole fractions ……. 86
4.4.4 Effect of adding hydrocarbon species on ignition delay and applying the HCHO/H2O2 parameter to indicate if firing will occur ……. 88
4.4.4.1 Effect of adding Propene (C3H6) on ID ... 89
4.4.4.2 Effect of adding Propane (C3H8) on ID ... 91
4.4.5 Summary and conclusions ……... 94

4.4.5.1 Check the applicability of firing and misfiring zones of HCHO/H2O2 graph on the cases of different concentrations of formaldehyde addition …….. 95

4.5 Reaction Path Analysis for OH Formation and Ignition Delay with Formaldehyde addition …….. 98

4.5.1 Investigation of ignition delay retard ……..…….. 103

4.5.2 Investigation using reaction path analysis ……..… 105

4.5.2.1 At 0.01750 Seconds ……. 106

4.5.2.2 At 0.01875 Seconds ……. 116

4.5.2.3 At 0.02000 Seconds ……. 121

4.5.3 Summary …….. 127

4.6 Reaction Path Analysis for OH Formation and Ignition Delay with Propene addition ……. 128

4.6.1 Investigation of ignition delay retard …….. 129

4.6.2 Investigation using Reaction Path Analysis …… 131

4.6.2.1 At 0.01750 seconds ……. 133

4.6.2.2 At 0.01875 seconds ……. 143

4.6.3 Summary …….. 144

CHAPTER 5: CONCLUSIONS AND RECOMMENDATIONS ……... 145

5.1 Conclusions …….. 145

5.2 Recommendations …….. 147

APPENDIX A – Valves Timing ……. 148

APPENDIX B – Nozzle Geometry …….. 149

APPENDIX C – Reaction Path Analysis for OH Formation and Ignition Delay with Ethane addition …….. 150

APPENDIX D – Reaction Path Analysis for OH Formation and Ignition Delay with Methane addition ……. 168

References …… 182

Abstract ……..…… 191

PUBLICATIONS ……... 194

Autobiographical Statement …… 195

LIST OF TABLES

Table 4.1	DIATA engine specifications ……..…….	63
Table 4.2	Effect of adding 150 ppm HC species concentration on ignition delay ……..……...	67
Table 4.3	Effect of adding 150, 1000 and 1500 ppm HC species concentration on ignition delay ..……	68

LIST OF FIGURES

Figure 2.1	Layout of experimental setup and instrumentation	14
Figure 2.2	GR valve and its opening controller ..….....	16
Figure 2.3	Exhaust butterfly valve and its electronic controller ..……	16
Figure 2.4	In cylinder pressure transducers and their charge amplifiers	20
Figure 2.5	Cylinder pressure ..……..……	20
Figure 2.6	Intake manifold transducer and its charge amplifier	21
Figure 2.7	Intake manifold pressure ..……....	21
Figure 2.8	Before turbocharger pressure transducer and its charge amplifier ..……..	22
Figure 2.9	After turbocharger pressure transducer and its charge amplifier ..……..	22
Figure 2.10	Pressure before turbocharger ..……..	23
Figure 2.11	Pressure after turbocharger ..……....	23
Figure 2.12	Thermocouple for exhaust temperature and its charge amplifier ..……..	24
Figure 2.13	Exhaust temperatures ..……..	24
Figure 2.14	Thermocouple for intake temperature and its charge amplifier …….....	25
Figure 2.15	Intake temperatures ……...……	25
Figure 2.16	Needle lift sensor and its charge amplifier ……..……	26

Figure 2.17 Pressure after turbocharger ……..…… 26

Figure 2.18 Fuel pressure sensor and its charge amplifier ..…….. 27

Figure 2.19 Pressure in fuel lines ……..…. 27

Figure 2.20 Turbocharger speed sensor and its charge amplifier ….. 28

Figure 2.21 Turbocharger speed ……..…….. 28

Figure 2.22 Engine speed ……..…….. 29

Figure 2.23 Fast responses FID ……..…… 30

Figure 2.24 Unburned hydrocarbons concentration ……..…….. 30

Figure 2.25 Fast responses NOx ……..……..…… 31

Figure 2.26 NOx concentration ……..……. 32

Figure 2.27 Fuel consumption, mass flow meter ……..…… 32

Figure 2.28 Fuel consumption ……..……... 33

Figure 2.29 Air mass flowmeter ……..…. 33

Figure 2.30 Air Mass flow …… 34

Figure 2.31 Blow-by flow meter and its filter ……..……... 34

Figure 2.32 Blow-by volumetric capacities ……..…….. 35

Figure 3.1.a Gas pressure and instantaneous engine speed with 25 mg/stroke. SOI: 12° BTDC, T_{amb}:15℃, 0%CGR ……. 48

Figure 3.1.b HCs emissions with 25 mg/stroke. SOI: 12° BTDC, T_{amb}: 15℃, 0%CGR ……. 48

Figure 3.2.a First 5 cycles of gas pressure and instantaneous engine speed with 25 mg/stroke. SOI: 12° BTDC, T_{amb}:15℃, 0%CGR 49

Figure 3.2.b First 5 cycles of HCs emissions with 25 mg/stroke. SOI: 12° BTDC, T_{amb}: 15℃, 0%CGR ……. 49

Figure 3.3.a Gas pressure and instantaneous engine speed with 25 mg/stroke. SOI: 12° BTDC, T_{amb}:15℃, 100%CGR…….. 51

Figure 3.3.b HCs emissions with 25 mg/stroke. SOI: 12° BTDC, T_{amb}:15℃, 100%CGR …….. 51

Figure 3.4.a Effect of different CGR (0, 20, 40, 60, 80 and 100%) on cranking period with 25 mg/stroke. SOI: 12° BTDC, T_{amb}: 15℃ ……. 52

Figure 3.4.b Effect of different CGR (0, 20, 40, 60, 80 and 100%) on HC at the exhaust manifold with 25 mg/stroke. SOI: 12° BTDC, T_{amb}: 15℃ 52

Figure 3.5.a Gas pressure and instantaneous engine speed with 25 mg/stroke. SOI: 12° BTDC, T_{amb}: 16℃, 100%CGR and 100% BF close ……. 54

Figure 3.5.b HCs emissions with 25 mg/stroke. SOI: 12° BTDC, T_{amb}: 16℃, 100%CGR and 100% BF close ……..... 54

Figure 3.6.a Gas pressure and instantaneous engine speed with 20 mg/stroke. SOI: 12° BTDC, T_{amb}:16℃, 100%CGR and 100% BF close ……..... 55

Figure 3.6.b HCs emissions with 20 mg/stroke. SOI: 12° BTDC, T_{amb}: 16℃, 100%CGR and 100% BF close ……..... 55

Figure 3.7.a Gas pressure and instantaneous engine speed with 25 mg/stroke. SOI: 12° BTDC, T_{amb}:3℃, 40%GR valve and 50% BF valve …….. 57

Figure 3.7.b HCs emissions with 25 mg/stroke. SOI: 12° BTDC, T_{amb}: 3℃, 40%GR valve and 50% BF valve ……..... 57

Figure 3.8.a Gas pressure and instantaneous engine speed with 25 mg/stroke. SOI: 12° BTDC, T_{amb}:3℃, 60%GR valve and 50% BF valve …….. 58

Figure 3.8.b HCs emissions with 25 mg/stroke. SOI: 12° BT DC, T_{amb}:3℃, 60%GR valve and 50% BF valve ……..... 58

Figure 3.9.a Gas pressure and instantaneous engine speed with 25 mg/stroke. SOI: 12° BTDC, T_{amb}: -3℃, 80%GR valve and 50% BF valve ……. 60

Figure 3.9.b HCs emissions with 25 mg/stroke. SOI: 12° BT DC, T_{amb}:-3℃, 80%GR valve and 50% BF valve ……. 60

Figure 3.10.a Effect of different fuel quantity (20, 21, 22, 23 & 24 mg/stroke/ 12℃BTDC) on cranking period with 60% CGR and 50% BF valve close during cold start. T_{amb}:16℃ 62

Figure 3.10.b Effect of different fuel quantity (20, 21, 22, 23 & 24 mg/stroke/ 12℃BTDC) on HC with 60% CGR and 50% BF valve close during cold start. T_{amb}: 16 ℃ ……. 62

Figure 4.1 Effect of adding HCHO on ignition delay at 25 mg/stroke injection ……..……. 66

Figure 4.2.a Gas pressure vs CAD at different equivalence ratios (0.8, 1.0 and 1.2) without adding HCHO ……..……. 70

Figure 4.2.b Gas pressure vs CAD at different equivalence ratios (0.8, 1.0 and 1.2) with adding 100ppm HCHO ……..... 71

Figure 4.2.c Gas pressure vs CAD at different equivalence ratios (0.8, 1.0 and 1.2) with adding 250ppm HCHO ……..……. 71

Figure 4.2.d Gas pressure vs CAD at different equivalence ratios (0.8, 1.0 and 1.2) with adding 300ppm HCHO ..……..... 72

Figure 4.3 Gas pressure vs CAD at different equivalence ratios (0.8, 1.0 and 1.2) with adding 350ppm HCHO ……..... 72

Figure 4.4 Effect of adding HCHO on ignition delay at equivalence ratios of 0.8, 1.0 and 1.2 ……..……..... 73

Figure 4.5 Effect of adding C3H6 on ignition delay at equivalence ratios of 0.8, 1.0 and 1.2 ……..... 75

Figure 4.6 Effect of adding C2H6 on ignition delay at equivalence ratios of 0.8, 1.0 and 1.2 ……..... 76

Figure 4.7 Effect of adding C2H5 on ignition delay at equivalence ratios of 0.8, 1.0 and 1.2 ……... 76

Figure 4.8 Effect of adding C2H, C2H2, C2H3, C3H2, C3H3, CH2, CH3 and C3H7 on ignition delay at equivalence ratios of 0.8, 1.0 and 1.2 ……. 78

Figure 4.9 Effect of adding C2H4, C3H8, C4H10, C4H6 and CH4 on ignition delay at equivalence ratios of 0.8, 1.0 and 1.2 ……..... 79

Figure 4.10 Effect of different cylinder gas temperatures at SOI on ignition delay …….. 81

Figure 4.11.a In-Cylinder pressure and the corresponding H2O2, HCHO, OH vs time at SOI temperature of 344 ℃ …….. 82

Figure 4.11.b In-Cylinder pressure and the corresponding H2O2, HCHO, OH vs time at starting temperature of 343 ℃ … 82

Figure 4.12 Absolute rate of the reaction of H2O2 at starting temperature of 344 ℃ …….. 83

Figure 4.13.a Temperature vs time at different SOI temperatures …… 85

Figure 4.13.b Pressure vs time at different SOI temperatures …….. 86

Figure 4.14 In-Cylinder pressure and the corresponding HCHO/H2O2 vs time at SOI temperature of 344 ℃ ….. 8 7

Figure 4.15 In-Cylinder pressure and the corresponding HCHO/H2O2 vs time at SOI temperature of 343 ℃ ….. 8 7

Figure 4.16 Comparison between the HCHO/H2O2 at different SOI temperatures varying from 343 ℃ to 344 ℃ ……... 88

Figure 4.17.a HCHO/H2O2 vs time without C3H6 addition ……... 89

Figure 4.17.b HCHO/H2O2 vs time with the addition of 600 ppm C3H6 ……... 90

Figure 4.18 Ratio of HCHO to H2O2 vs time at different C3H6 addition ……... 90

Figure 4.19 Effect of Propane addition on Ignition Delay at Equivalence Ratio 1.0 …….. 91

Figure 4.20.a Ratio of HCHO to H2O2 vs time at 0 ppm C3H8 addition ……... 92

Figure 4.20.b Ratio of HCHO to H2O2 vs time at 600 ppm C3H8 addition ……... 93

Figure 4.20.c Ratio of HCHO to H2O2 vs time at 1000 ppm C3H8 addition ……... 93

Figure 4.21 Firing and Misfiring zones based on [HCHO / H2O2] parameter ……... 94

Figure 4.22 Ratio of HCHO to H2O2 vs time at 0 ppm HCHO addition ……... 95

Figure 4.23 Ratio of HCHO to H2O2 vs time at 300 ppm HCHO addition ……... 96

Figure 4.24 Ratio of HCHO to H2O2 vs time at 500 ppm HCHO addition ……... 97

Figure 4.25 DIATA engine specifications ……. 99

Figure 4.26 Reactions involving NC7H16 …….. 100

Figure 4.27 Effect of HCHO addition on ignition delay at equivalence ratio 1.0 ……... 102

Figure 4.28 In-cylinder Pressure and OH mole fractions at different HCHO concentrations versus CAD ……... 103

Figure 4.29 In-cylinder pressure and OH mole fractions at different HCHO concentrations versus time ……..... 104

Figure 4.30.a Rate of formation of OH at 0.01750 seconds with zero and 200ppm HCHO …….. 107

Figure 4.30.b Comparison using superposition between the rate of formation of OH at 0.01750 seconds with zero and 200ppm HCHO …….. 109

Figure 4.31 Effect of HCHO addition on the pressure and temperature …… 110

Figure 4.32 Comparison of Net rate of OH production at zero and 200ppm HCHO and by 3 major reactions at 0.01750 seconds …….. 116

Figure 4.33.a Rate of formation of OH at 0.018750 seconds with zero and 200ppm HCHO …….. 117

Figure 4.33.b Comparison using superposition between the rate of formation of OH at 0.018750 seconds with zero and 200ppm HCHO ……..... 118

Figure 4.34 Comparison of Net rate of OH production at zero and 200ppm HCHO and by 3 major reactions at 0.018750 seconds ……..…. 121

Figure 4.35.a Rate of formation of OH at 0.020 seconds with zero and 200ppm HCHO ……..……... 122

Figure 4.35.b Comparison using superposition between the rate of formation of OH at 0.020 seconds with zero and 200 ppm HCHO ……..……..…... 123

Figure 4.36 Comparison using superposition between the rate of formation of OH at 0.02175 seconds with zero and 200ppm HCHO and some other reactions contributing towards OH formation ……..... 126

Figure 4.37 Effect of C3H6 addition on ignition delay at equivalence ratio 1.0 ……..…… 128

Figure 4.38 In-cylinder pressure and OH mole fractions at different HCHO concentrations versus CAD ……..……..... 129

Figure 4.39 In-cylinder pessure and OH mole fractions at different HCHO concentrations versus time ……..…..... 130

Figure 4.40 Reaction path diagram for C3H6OH ……..…..... 135

Figure 4.41.a Rate of formation of OH at 0.01750 seconds with zero and 200ppm C3H6 ……..……. 139

Figure 4.41.b Comparison using superposition between the rate of formation of OH at 0.01750 seconds with zero and 200ppm C3H6 ……..……. 140

Figure 4.42 Rate of formation of OH at 0.018750 seconds with zero and 200ppm C3H6 ……. 144

NOMENCLATURE

BF: Butterfly

BTDC: Before Top Dead Center

CAD: Crank Angle Degree

CGR: Cranking Gases Recirculation

DIATA: Direct-Injection, Aluminum, Through-bolt Assembly

EGR: Exhaust Gas Recirculation

FID: Flame Ionization Detector

HC: Hydrocarbon

HCHO: Formaldehyde

HCR: Hydrocarbon Recirculation

HCs: Hydrocarbons

PPM: Part Per Million

PRF80: A mixture of Primary Reference Fuels comprising 80% iso-octane and 20% n-heptane by volume

Rm Temp: Room Temperature

RPA: Reaction Path Analysis

RPM: Revolution Per Minute

ULSD: Ultra Low Sulfur Diesel

INTRODUCTION

Cold startability of diesel engines can be defined as the ability of an engine to quickly start and run with minimum assistance from the starting motors and to continue to run without hesitation. The incomplete combustion and misfire of diesel engines during starting result in unwanted white smoke (Unburned hydrocarbons), long cranking period and increase in fuel consumption.

Wide attention has been paid on the diesel engine emissions as their population increases, corresponding emission control regulations have been enacted to control the emissions and the standards become more and more stringent. HC emissions under the cold start conditions are a significant part of overall emissions. The drop in ambient temperature combined with the low ignition quality of the fuel result in long cranking periods, the emission of large amounts of HCs which appear as white smoke, instable combustion and complete failure to start.

This study explains the opposing effect of recirculated cranking gases on unburned hydrocarbons, cranking periods and fuel consumption. By using low rates of CGR (Cranking Gases Recirculation), a prompt cold start with minimal hydrocarbon emissions and less fuel consumption will result. The advantages of the new technique are demonstrated on the cold starting of a multi-cylinder diesel engine at different ambient temperatures. This new concept has been explained and validated using 0D and 3D simulation.

GOAL

Reducing the cranking periods required before the engine fires and the unburned hydrocarbons emissions which appear as white smoke are among the most critical issues in the design of diesel engines .

The technique proposed is contingent on the fact that a stoichiometric fuel-vapor-air mixture is formed in the cylinder in order to promote prompt combustion. This can be achieved by recirculating some of the HC species emitted during cranking to enhance the autoignition process and improve cold startability at different ambient temperatures.

In the proposed technique, the cranking gases are recirculated to the intake manifold. The rate of recirculated gases is controlled using 2 valves. The first is a butterfly valve, referred to as gas recirculation (GR) valve, installed between the exhaust and intake manifold. The second is a butterfly (BF) valve, installed in the exhaust system after the turbocharger to increase the back pressure, hence the rate of recirculated gases. Since there is no combustion during cranking, these gases contain evaporated hydrocarbons and partial oxidation products, mostly formaldehyde HCHO.

In order to apply the technique of CGR, it is necessary to understand the effect of cranking gases species on ignition delay using the simulation.

CHAPTER 1

LITERATURE REVIEW

Diesel engines are becoming important prime movers that power different types of machinery and transportation equipment. However, long cranking periods, the emission of large amounts of unburned hydrocarbons (HCs) which appear as white smoke, unstable combustion and even complete engine failure to start [1-4] are considered as major problems that need to be solved.

1.1 Factors Affecting Cold Start

Previous research work in diesel engine showed that several factors affect the combustion and emissions in the diesel engines. Several factors , such as ambient temperature and pressure [1, 5-10, 11], the combustion chamber design [11, 12, 13], the fuel properties [14, 15, 16], the injection process [1, 6, 7, 17], cranking speed [6, 7, 11, 17], residuals composition, equivalence ratio, surface temperature and the inlet charge temperature [14, 18-20, 21-40], affect the combustion process and engine-out emissions.

1.1.1 Ambient Temperature

Probably, the effect of ambient temperature is the most critical or important factor affecting the starting of the Diesel engine, which can lead to large cranking period, excessive white smoke in the exhaust, oil starvation and poor idle stability. It is obvious that the lower the ambient temperature, the less the chance the engine has to start. Zahdeh, Henein and Bryzik [41] verified this

behavior in a single-cylinder direct injection (DI) engine, which had a compression ratio of 17 and a total piston displacement of 673 cm^3. The testing was done at an ambient temperature of 263 K and the engine was observed to operate on an 8-stroke-cycle (where combustion failed every second cycle) and on a 12-stroke-cycle (where combustion failed in two consecutive cycles after a firing cycle).

Later, Gonzalez [42] verified that borderline conditions of misfire and skipped cycles occur at ambient temperatures below 263 K, while at temperatures below 241 K specific starting kits were needed for a positive start.

Regardless of the compression ratio and cranking speeds. the startability improves with the increased ambient temperature. If the compressed air temperature at the time of fuel injection is high enough for the fuel to evaporate and form a combustible fuel air mixture, an excellent chance of a successful start exists. This depends on many parameters such as cranking speed and injection timing. Phatak and Nakamura [43] supported their conclusion by the fact that a cold engine with warm air continued to fire after the first few cranking cycles. This is quite likely because of a continuous increase in the charge temperature since it is unlikely that, in such short time, engine parts such as piston, head and cylinder were warmed up sufficiently to influence combustion.

1.1.2 Engine Speed

Under cold starting, the engine goes through several speeds; cranking is followed by acceleration after firing and deceleration to idle speed. The cranking

speed and period depends upon the ambient temperature, the quality of the fuel and the design parameters of the combustion chamber and the injection system.

Austen and Lyn [17] found that the effect of cranking speed on compression pressure and temperature is very important especially at low speeds, below 200 rpm. An increase from 100 to 200 rpm causes an increase of about 70℃ in the compression temperature which confirms the importance of maintaining high cranking speeds under cold starting conditions as it is one of the most effective means of obtaining high compression temperatures. According to Phatak and Nakamura [11] at higher cranking speeds, the loss of time for auto-ignition reactions far outweighs any marginal gains in peak temperatures because of reduced blowby.

Matsui and Sugihara [44] found that for extremely small and constant amount of fuel injected, HC emissions increased remarkably as the engine speed went up.

1.1.3 Altitude

At higher altitudes, the ambient pressure and temperatures are lower than at sea level. Accordingly, the compression pressure and temperature are lower and auto-ignition and combustion reactions are slower. This might lead to longer cranking periods and more white smoke.

Kato et al. [45 stated that for each fuel, there is an altitude limit beyond which the white smoke starts to appear and increase dramatically. The lower the cetane number, the lower the altitude at which white smoke becomes a problem.

1.1.4 Fuel Injection Timing

Injection timing directly effects the ignition delay and HC emissions. Under steady state warmed up operation the optimum injection timing is designed in such a way that it gives minimum ignition delay. As the injection timing is changed from the position giving the minimum ignition delay, HC emissions increase.

Austen and Lyn [17] found that an optimum timing for normal operation is generally too early for optimum cold start which lies between 10° and 20° BTDC by static timing. At extremely low speeds such as cranking speed, because of the increase in heat loss and blow-by, cylinder air temperature is lower than that at high speed. Therefore, the required time for ignition delay becomes longer at starting, but the required crank angle degrees for ignition delay becomes much less.

Greeves et al. [46] investigated the effect of injection timing and ignition delay on HC emissions on four different engines. They found that the injection timing corresponding to minimum ignition delay gave minimum HC emissions. They also found that as the injection timing is retarded from this point, the HC emissions increased at the same rate as the ignition delay.

Yu et al. [47], on the other hand, found that HC emissions decrease with advancing the timing from 3.5 ATDC to 4 BTDC. Their experiments covered a very narrow range and it was not clear whether these timings were before or after the minimum optimum injection timing corresponding to the minimum ignition

delay. They attributed the effect of timing on HC emissions to the changes in the ignition delay since timing had a little direct effect on the mixing rate. For retarded timing, the start of combustion is delayed into the expansion stroke and as a result of rapid drop in the gas temperature and pressure, quenching of the oxidation reactions might occur resulting in higher HC emissions.

Keppeler [48] reported that the pilot injection quantity should reduce the ignition delay by providing radicals in the combustion chamber. It is desired that this fuel does not burn before the start of main injection, to avoid an excessive increase of the particulate emission. His tests recommended a dwell of 10 deg and of 30 deg for the various tests performed.

Osuka et al. [49] reduced starting time and white smoke emission by using pilot injection. They indicated that the cool flame produced during pilot injection promoted ignition of the later main injection. Han et al [7] found that the mismatch between the injection parameters and the instantaneous engine speed could lead to a misfire. The mismatch included the injection timing and the shift from main injection to pilot-main injection.

1.1.5 Injection Rate

The injection rate is a measure of how much fuel is injected per cycle. The amount of fuel injected per cycle affects the overall equivalence ratio of the charge and this affects the course of combustion and emissions. During cold starting, the amount of fuel injected during the cranking period is directly related to the concentration of HC emitted upon firing.

Heywood [14] and Bosch [50] refer to the importance of governor characteristics; increased fuel quantity is required in starting ignition as compared to an idling combustion. Unfortunately, this quantity is also the source of unburned hydrocarbons. Since the total amount of fuel injected is not completely burnt, the residual fuel shows up as the major part emissions.

Karim et al. [51] studied the effect of injection rate on HC emissions under very cold ambient temperatures (down to -40C). He indicated that in order to keep the idling speed constant, the fueling rate needed to be increased rapidly as the air intake temperature was lowered to very low temperatures, during which the ignition delay was being increased at high rate. The corresponding smoke density increased significantly as the temperature was lowered. At such low temperatures, the injected fuel was high and a greater fraction of injected fuel was not fully utilized and thus would appear in the form of white smoke aerosol.

Yu et al. [47] studied the effect of fuel flow rate on HC emissions. Their results sho0wed that under idling and low load conditions, hydrocarbon emissions decreased as the fuel flow rate increases. They indicated that reduction in HC emission is attributed to the decrease in ignition delay resulting less local over mixing.

Campbell et al. [52] found that increasing the fuel injection rate at the same injection timing reduces the smoke opacity originated from HC emissions. Nakakita et al. [53] indicated that with increased injection pressure, the ignition delay is shortened and consequently HC emissions decreased.

Tatsuya and Kawase [54] showed that as the injector nozzle spring constant increase, white smoke emissions were improved. They related the effect of higher nozzle injection rate with fuel droplet size and distribution. Higher spring constant gave an accelerated fuel atomization with smaller fuel droplets that took less time to evaporate thus improving HC emissions.

1.1.6 Chamber Design

Tsunemoto, et al [13], studied the influence of combustion chamber shape and depth on the adhering fuel to the chamber walls in a direct injection diesel engine. They concluded that, in shallow combustion chambers, the distance from injection nozzle to the combustion chamber wall with bowl and cavities is far, and fuel evaporates before impinging on the wall reducing the amount of remaining fuel. The work of Phatak and Nakamura [43] indicated that the combustion chamber design and the resulting fuel-air mixing process have a significant influence on the cold startability of a DI diesel engine.

1.1.7 Common Rail Pressure

The high emission level during start-up process of common rail diesel engine is still a problem for ultra-low emission control. The electronic map-loaded engine start-up process goes through the initialization of injection and rail pressure build-up process and then the fuel injection rate is not stable. The time taken to build up the common rail pressure can be further subjected to engine speed variety.

Woermann, Theuerkauf and Heinrich [55] summarized the real reaction on the rapid change of the demand rail pressure. The ECU control algorithm adjusts the system pressure to the demand by stimulating the regulation valve. After two seconds, the actual pressure remains stable inside a narrow band. In terms of calibration complexity, it is easy to optimize parameters of the control algorithm implemented in the ECU.

Roy, Tsunemoto [56] investigated injection pressure and split injection and concluded that with the high-pressure at idle, there is an optimum injection pressure where the ignition delay is the shortest, which causes less fuel to adhere to the combustion chamber walls. Moreover, the fuel air mixture is improved and more homogeneous. The shorter ignition delay and the more fine the particles in the homogeneous mixture are produced, the less aldehydes and total hydrocarbons content in the exhaust.

Osuka et al. [49] mentioned that the injection parameters of the initial phase of engine start-up have large effects on the start-up time and smoke emissions. Common rail is being aggressively pursued for development because of its high injection pressure, flexible multiple injection and the minimal changes needed to the engine body.

1.1.8 Cetane Number

Studies have confirmed that cetane number affects the starting and white smoke in modern heavy duty diesel engines. The effect of cetane number is most significant at the minimum starting temperature because below this temperature,

the engine will be inoperable. Clerc [16] reported that a decrease in fuel cetane number from 45 to 40 would increase minimum starting temperature of light-duty and heavy-duty engines by less than 3℃.

1.2 Cold Start Aids

Henein [57] and Bielaczyc [58] brought forward a cold starting strategy for DI diesel engines by cutting off fuel injection during the first few revolutions of cold starting process. The results of experiments suggested that emissions were significantly improved when compared with the standard cold start procedure, where a large amount of fuel is injected upon motoring the engine.

Lindl, Schmitz [59] investigated the effect of different starting aids such as glow plug, electrical intake air heater and intake manifold, by observing the acceleration to a governed engine speed, the HC-emission or the exhaust gas opacity. The results of the various studies indicates the necessity of aids for a reliable cold start (even for modern diesel engines) for the desired starting convenience, smoothness during the ramp-up and warm-up phase, the reduction in noise and the need to meet future emission standard regulations. This resulted in the minimization of specific fuel consumption.

Intake manifold burner, electric intake air heaters or glow plugs with fast preheat time of less than 4 seconds can provide post-heat temperature level of 1400 K

Girotra et al [60] used split injection to improve the cold starting of a direct injection, 4-cylinder diesel engine. The improvement in cold starting was found to

depend on the amount of fuel delivered in each injection event as well as the dwell between the two events.

Gruenwald [61] conducted preliminary experiments on the engine used in this investigation to explore the effect of HCR (Hydrocarbon Recirculation) on cold starting of the engine.

1.3 Effect of Adding Formaldehyde on Ignition Delay

The kinetic effect of formaldehyde (HCHO) on autoignition has been studied by Sjöberg and Dec [31] in HCCI combustion. The authors found that HCHO has an advancing effect on autoignition for iso-octane, but a retarding effect for PRF80 mixture.

Jansons [40] reported formaldehyde has a retarding effect on autoignition under lean conditions in an optically accessible diesel engine.

In conclusion, the literature review shows that no investigations have been done on the opposing effect of recirculated gases during the cranking period on cold starting of multi-cylinder D.I. diesel engines at different low ambient temperatures.

This investigation is aimed at gaining a better understanding of the effect of CGR on the autoignition process and reducing the cranking period.

CHAPTER 2

EXPERIMENTAL SETUP AND INSTRUMENTATIONS

2.1 Introduction

Introducing a combination of HCs and HCHO into the intake manifold has been investigated experimentally by recirculating part of the exhaust gases to the intake manifold and checking the effect of different recirculated percentage on the cranking period and the exhaust hydrocarbons.

Figure 2.1 shows the layout of the setup and instrumentation. The engine is 1.2L Ford DIATA 4-cylinder, 16-valve, 70 mm bore, 78 mm stroke, direct injection, turbocharged, intercooled, water cooled and 19.5 compression ratio diesel engine equipped with a common rail injection system. The engine is installed in a cold room and is motored by its electric starter and battery system. Each of the cylinders is instrumented with a flush mounted piezo pressure transducer and a charge amplifier. The engine was soaked for at least 8 hours at the desired ambient temperature before starting the test by turning on the electric starter which cranks the engine at 200 rpm. The data recording began as soon as the crankshaft started to rotate at every 0.05 CAD, and continued till after the electric starter disengaged and the engine ran at idle speed. After each test the engine was run till it was warmed up before it was shut down. Each test had been repeated at least three times to ensure the reproducibility of the results. The CGR percentage was controlled by the openings positions of the CGR valve and the exhaust butterfly valve. Two types of recirculation are examined. The first is

a low pressure recirculation of engine-out gases into the intake manifold where their rate is controlled by a gas recirculation (GR) valve installed between the exhaust and intake manifold. The second is a high pressure recirculation obtained by restricting the flow of the engine-out gases using a butterfly (BF) valve installed in the exhaust system after the turbocharger in order to increase the back pressure and the rate of recirculated gases. Since there is no combustion during cranking, these gases contain evaporated hydrocarbons and partial oxidation products, mostly formaldehyde HCHO. The unburned hydrocarbons were measured in ppm at the intake and the exhaust manifolds using two channels of the fast FID analyzer instrument. The results reported in this thesis are for the effect of low and higher rates of recirculated gases at different ambient temperatures.

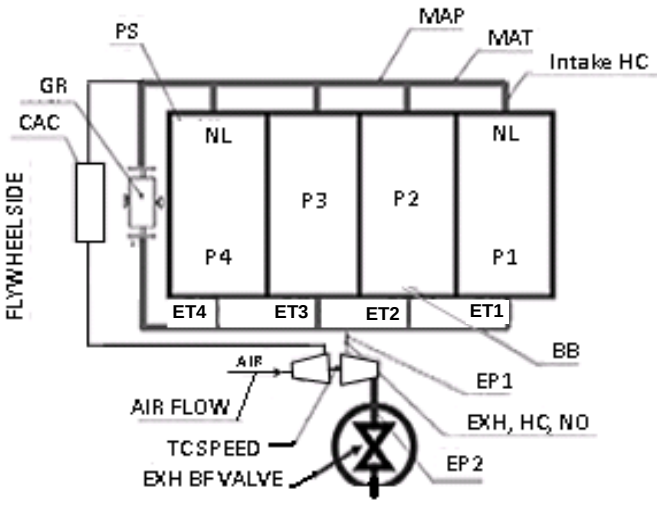

Instrumentation	
BB	Blow-by meter
EP1	Exhaust pressure before TC
EP2	Exhaust pressure after TC
ET1	Exhaust temperature, cylinder 1
ET2	Exhaust temperature, cylinder 2
ET3	Exhaust temperature, cylinder 3
ET4	Exhaust temperature, cylinder 4
GR	Gases recirculation valve
MAP	Intake manifold pressure
MAT	Intake manifold temperature
NL	Needle lift sensor
P1	Gas pressure, cylinder 1
P2	Gas pressure, cylinder 2
P3	Gas pressure, cylinder 3
P4	Gas pressure, cylinder 4
PS	Position Sensor

Figure 2.1 - Layout of experimental setup and instrumentation.

2.2 CGR system and engine features

80 miles per gallon was the goal to be achieved in 2000 by the hybrid concept car “Ford PRODIGY’. Part of this electric hybrid vehicle project was the state-of-the-art Ford DIATA engine where DIATA stands for Direct Injection Aluminum Through-bolt Assembly. The DIATA engine specifications are given in appendix I. The goal of this project was to downsize the engine as much as possible, while improving vehicle fuel economy with minimal emissions and undesirable NVH (Noise Vibration and Harshness) behavior. Ford product design guidelines and FEV publications were the main source of the engine features materials while the cold start diesel engine lab at Wayne State University is the source of CGR system materials.

2.2.1 CGR system

The CGR (Cranking Gases Recirculation) system is composed of 2-butterfly valves. The first is the GR (Gases Recirculation) valve which connects the exhaust manifold to the intake manifold to control the amount of gases recirculated. The GR valve is controlled by using 2 gears for accurate measurements as shown in figure 2.2. This valve should be cleaned regularly to avoid any carbon deposit on the valve which can affect the valve area and the opening percentage. The second is the exhaust butter-fly valve which is mounted in the exhaust system after the turbocharger to restrict the flow of gases in order to increase the rate of gases recirculated. The exhaust butter-fly valve is electronically controlled as shown in figure 2.3.

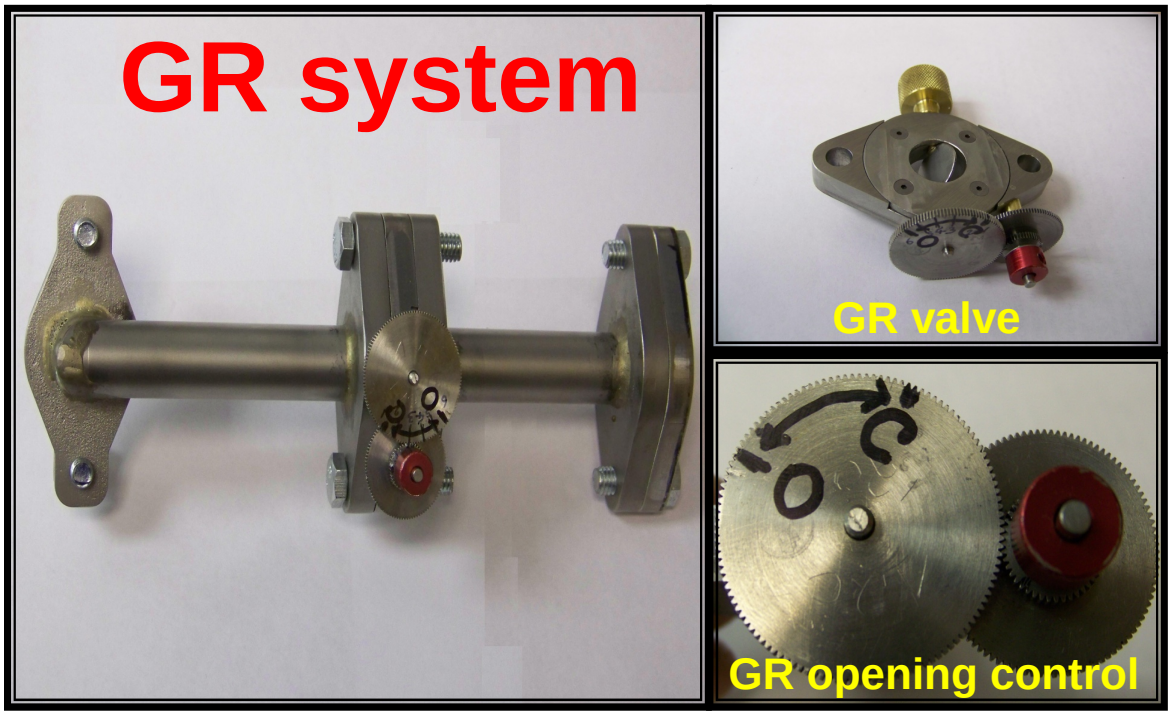

Figure 2.2 – GR valve and its opening controller.

Figure 2.3 – Exhaust butterfly valve and its electronic controller.

2.2.2 Valve Train

The valve train concept includes dual overhead camshafts (DOHC), roller finger followers and hydraulic lash adjusters. A bore hole in each camshaft distributes oil to the camshaft bearings, as well as to the high-pressure fuel pump coupling. The hydraulic lash adjusters receive their oil via two drilled oil galleries. The camshaft at the exhaust side is driven directly from the crankshaft by a primary chain and as second chain synchronizes the two camshafts.

2.2.3 Fuel Injection

Injectors are arranged close to the cylinder center line, where a clamping mechanism is used, which allows for disassembly of the injectors without opening the valve cover. All high and low pressure fuel lines are located outside the oil room. The rail is mounted on top of the intake manifold plenum chamber to enable the use of short injection lines. The nozzle geometry details are given in appendix II.

2.2.4 Combustion Bowl

The combustion bowl design is very similar to the designs used for engines in 2.0 liter class, but downsized to account for the smaller engine displacement. The mixture formation is improved due to the higher in-bowl swirl of the smaller combustion bowl. However, as a part of the downsizing process, the surface-to-volume ratio was increased by approximately 25%, which increases the relative heat losses of the combustion chamber walls.

2.2.5 Port Deactivation

A suitable method to improve maximum torque at low engine speeds is the usage of port deactivation at full load. The deactivation flap arrangement with the bigger port of the two always open and the smaller port is the controllable port with a flap valve. All of the intake ports with flap valve are coupled together and can be controlled through a single lever. Opening the smaller port counters the flow from other port reducing the swirl ratio inside the cylinder. Using the flap valve, the swirl ratio can be changed from 1.5 to 4, which is when the short port is completely closed and larger port is open.

2.3 Instrumentation and measurements

A Ford DIATA engine is used for the investigation. The cylinder head is designed by FEV and the block is developed at Ford Motor Company.

The following engine parameters can be measured:

- In Cylinder pressure
- Intake manifold pressure
- Pressure before and after turbocharger
- Exhaust temperature
- Air intake temperature
- Needle lift
- Fuel pressure
- Turbocharger speed

- Engine RPM
- Unburnt Hydrocarbon Emissions
- NOx emissions
- Fuel consumption
- Air mass flow
- Blow-By flow

2.3.1 In- Cylinder pressure

A quartz crystal pressure transducer (Kistler 6061B) water-cooled pressure sensor is used for in-cylinder pressure measurements. A dual-mode charge amplifier (Kistler 5010B) is used with this transducer as shown in figure 2.4. These transducers are mounted in the glow plug holes in the cylinder head. They have inbuilt cooling jackets to keep the transducer temperature low. The transducers and the respective charge amplifiers are factory calibrated.

The pressure at the end of the intake stroke is used as the reference pressure which is equal to the value of the intake manifold pressure transducer.

Figure 2.5 shows a sample of the cylinder pressure versus the cycle number.

Figure 2.4 – In cylinder pressure transducers and their charge amplifiers.

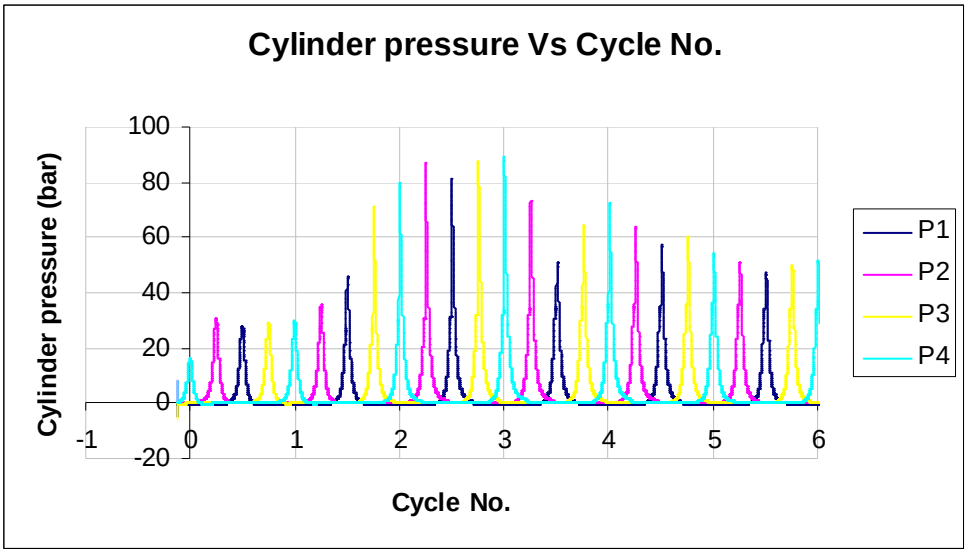

Figure 2.5 – Cylinder pressure.

2.3.2 Intake manifold pressure:

An Omega sensor (PX-176/177) is used for the intake manifold pressure measurements as shown in figure 2.6.

Figure 2.6 – Intake manifold transducer and its charge amplifier.

Using the following calibration equation: $\left(\frac{Signal}{100}-1\right)\left(\frac{1}{0.2}\right)(0.068948)$ bar to calculate the air intake pressure as shown in figure 2.7

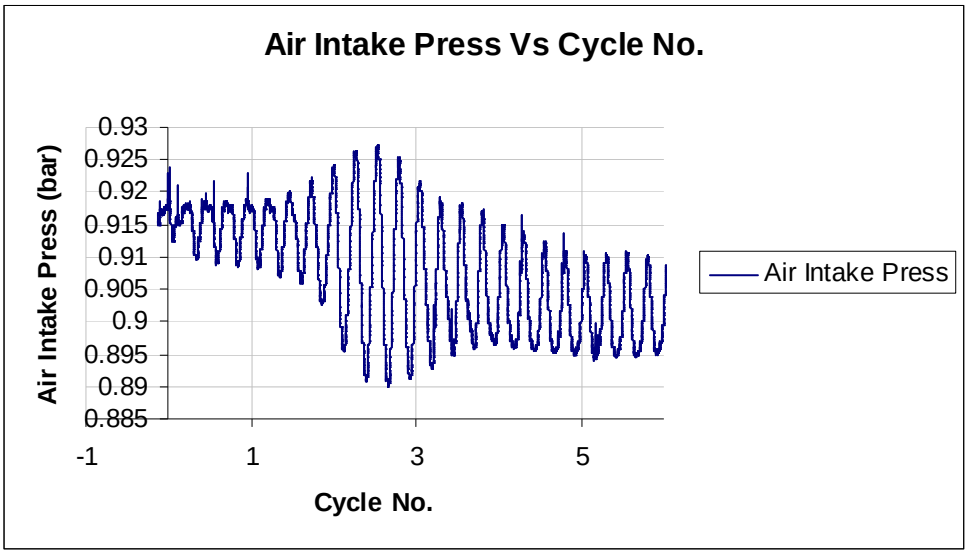

Figure 2.7 – Intake manifold pressure.

2.3.3 Pressure before and after turbocharger (Exhaust Pressure):

Omega (PX-176/177) sensors are used for exhaust pressure measurements before and after turbocharger as shown in figure 2.8 and 2.9.

Figure 2.8 – Before turbocharger pressure transducer and its charge amplifier.

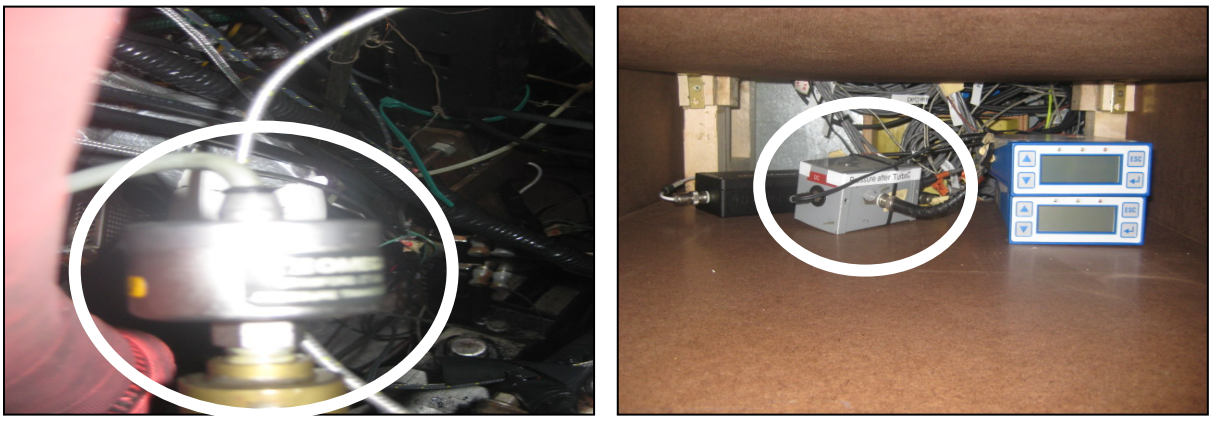

Figure 2.9 – After turbocharger pressure transducer and its charge amplifier.

The pressures before and after the turbocharger are calculated using the following calibration equation as shown in figure 2.10 and 2.11.

$$\left(\frac{Signal}{100}-1\right)\left(\frac{1}{0.1}\right)(0.068948) \text{ bar}$$

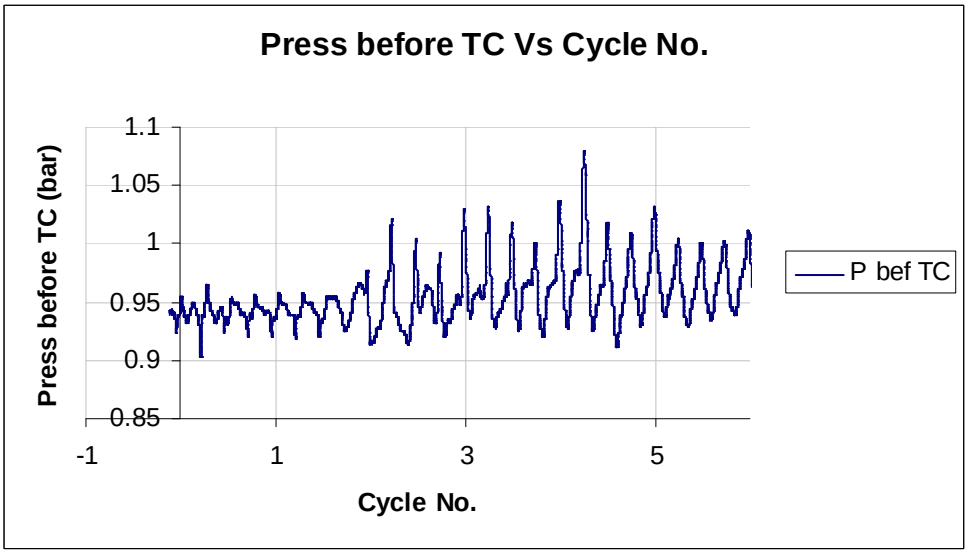

Figure 2.10 – Pressure before turbocharger.

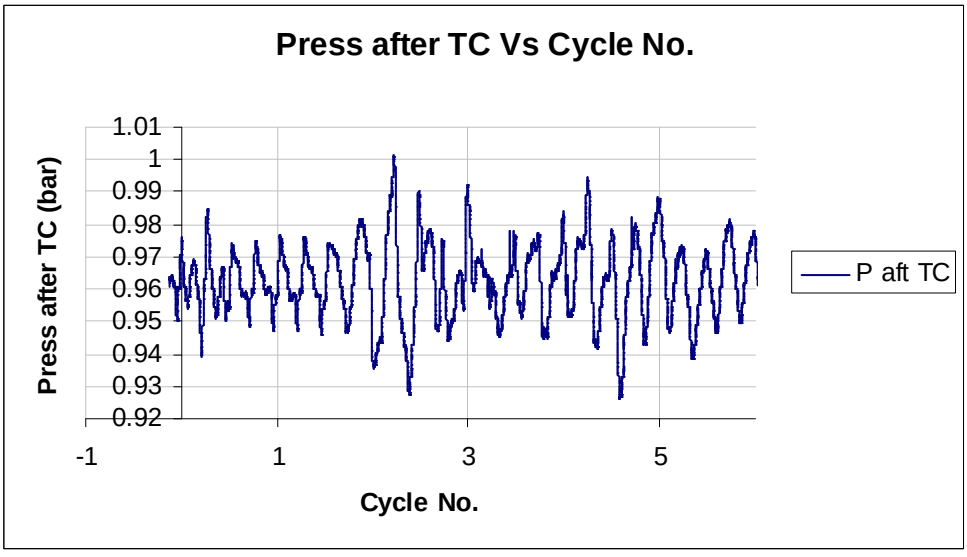

Figure 2.11 – Pressure after turbocharger.

2.3.4 Exhaust Temperature:

Omega K-type 0.005-inch thermocouples are used with a 5B37 module for exhaust temperature measurements for each cylinder as shown in figure 2.12.

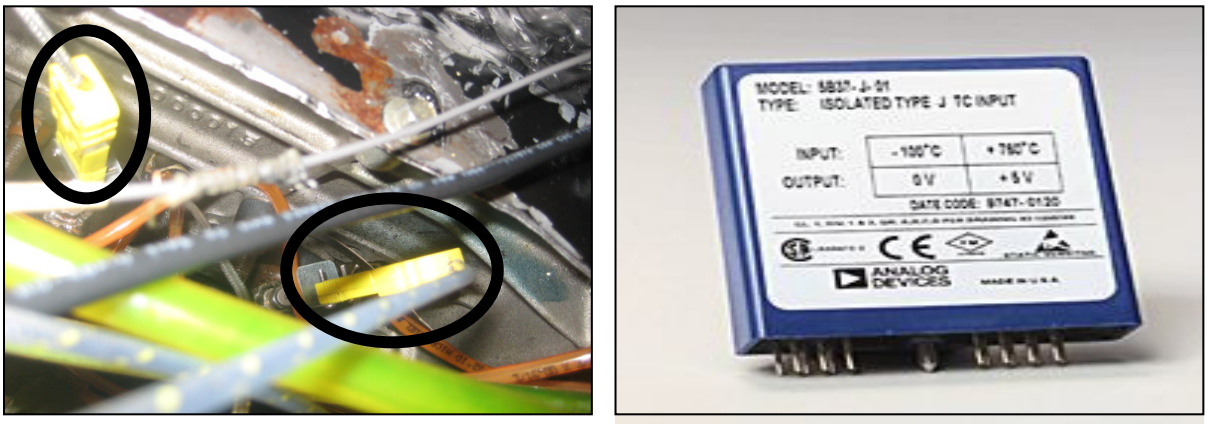

Figure 2.12 – Thermocouple for exhaust temperature and its charge amplifier.

Figure 2.13 shows the exhaust temperature using the following calibration equation: $\left(\frac{Signal}{100} * 290\right) - 100 \quad ℃$

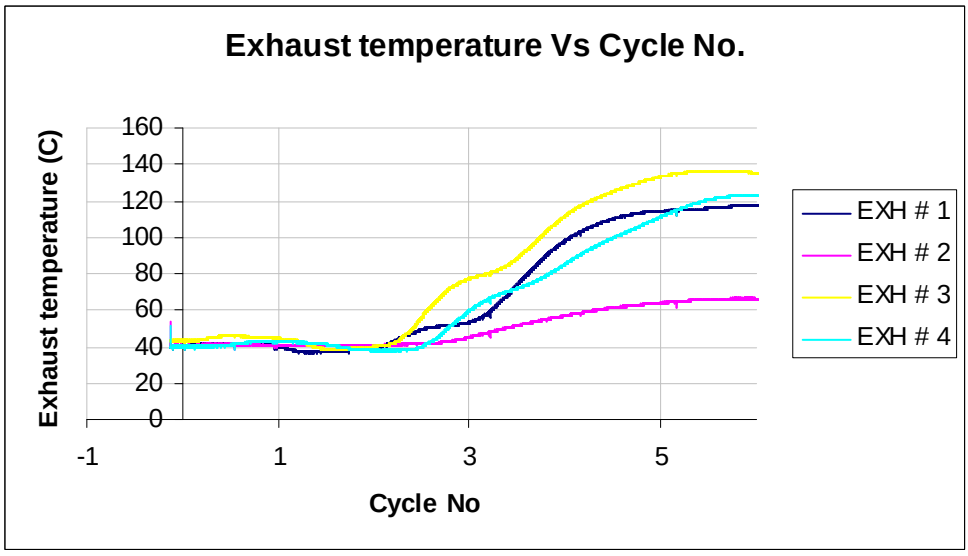

Figure 2.13 – Exhaust temperature.

2.3.5 Air Intake Temperature:

An Omega K-type 0.005-inch thermocouples is used with a 5B37 module for air intake temperature measurements as shown in figure 2.14.

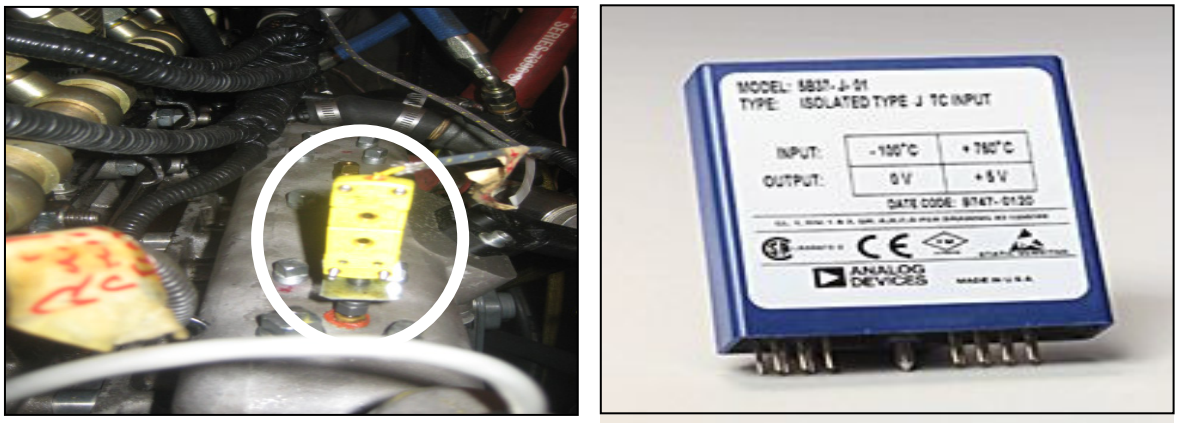

Figure 2.14 – Thermocouple for intake temperature and its charge amplifier.

Figure 2.15 shows the intake temperature using the following calibration equation: $\left(\frac{Signal}{100} * 290\right) - 100$ ℃

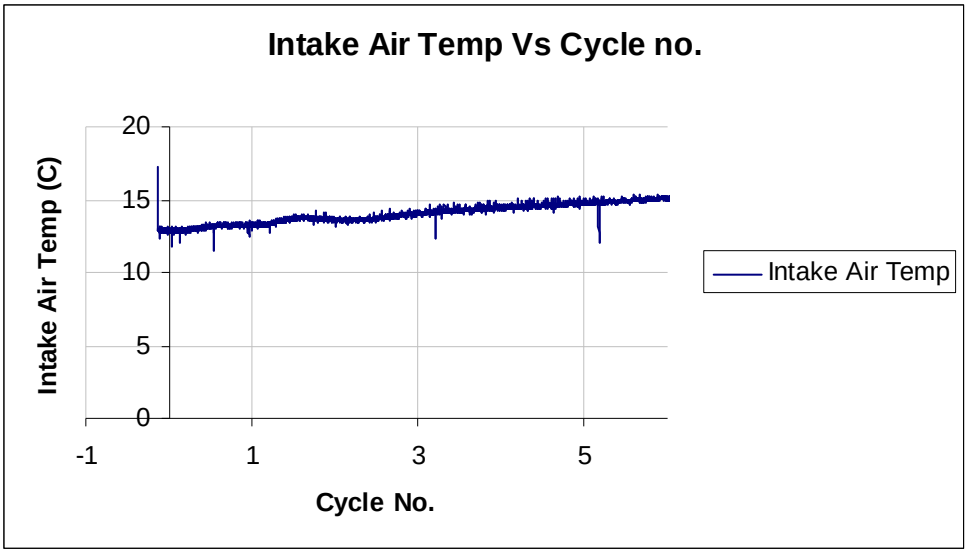

Figure 2.15 – Intake temperature.

2.3.6 Needle lift:

Micro Epsilon Needle lift sensors (ES-04) are used with their respective amplifiers to check the needle lift movement as shown in figure 2.16.

Figure 2.16 – Needle lift sensor and its charge amplifier.

Figure 2.17 shows the traces of the needles lifts.

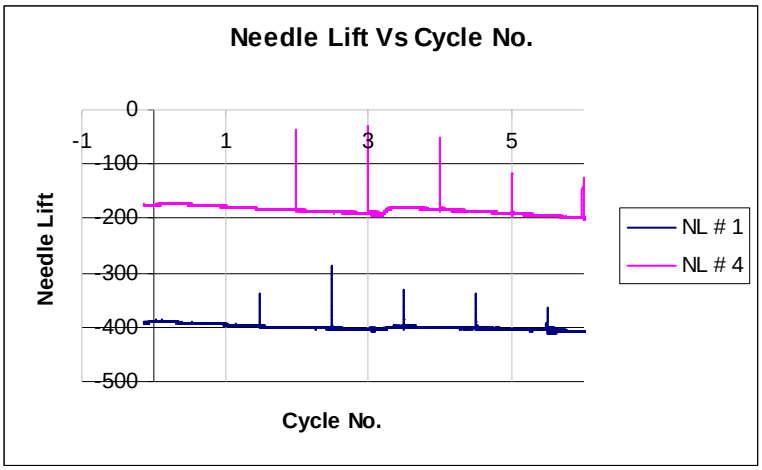

Figure 2.17 – Pressure after turbocharger.

2.3.7 Fuel Pressure:

Kistler-integrated sensors are used with their respective amplifiers (0-3000bar) for the fuel pressure measurements for each cylinder fuel line and the common rail as shown in figure 2.18.

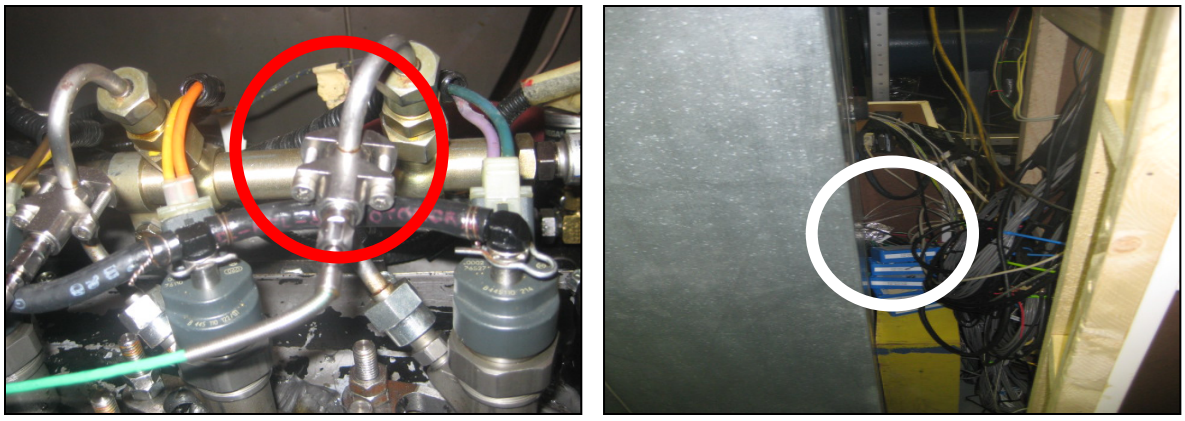

Figure 2.18 – Fuel pressure sensor and its charge amplifier.

The following calibration equation is used to calculate the pressure in the fuel lines as shown in figure 2.19: $(Signal * 100 * 3)$ bar

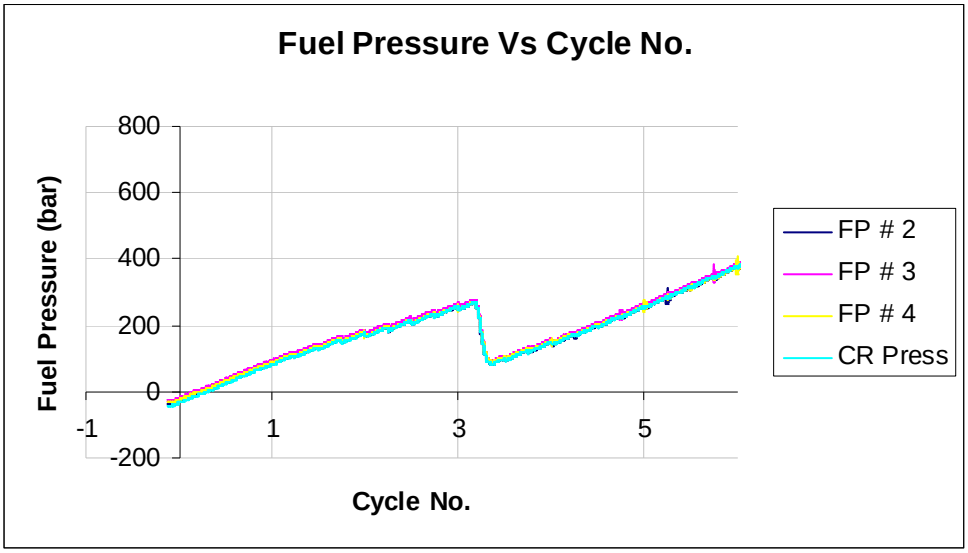

Figure 2.19 – Pressure in fuel lines.

2.3.8 Turbocharger speed:

A Micro Epsilon speed sensor (ES-04) is used with its respective amplifier for the turbocharger speed measurements as shown in figure 2.20.

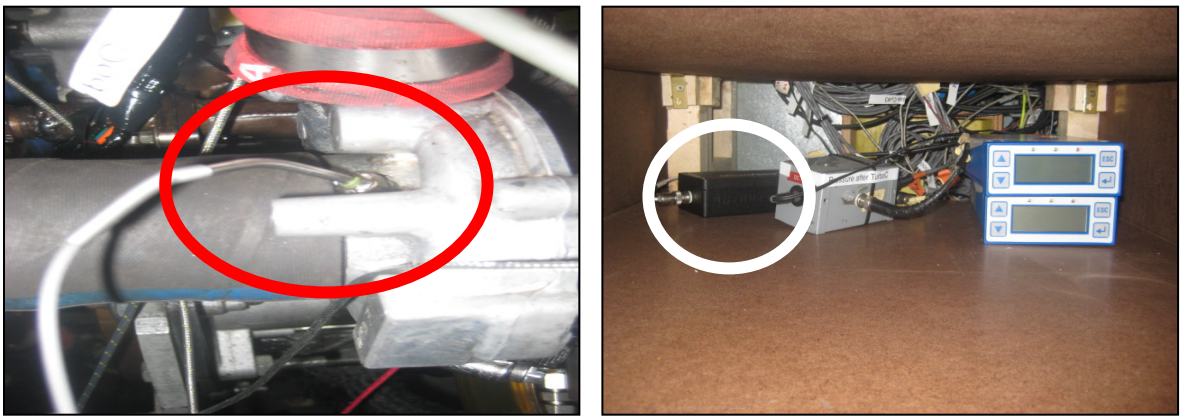

Figure 2.20 – Turbocharger speed sensor and its charge amplifier.

The following calibration equation is used to calculate the turbocharger speed as shown in figure 2.21: $\left(\frac{20000 * Signal}{100}\right)$ rpm

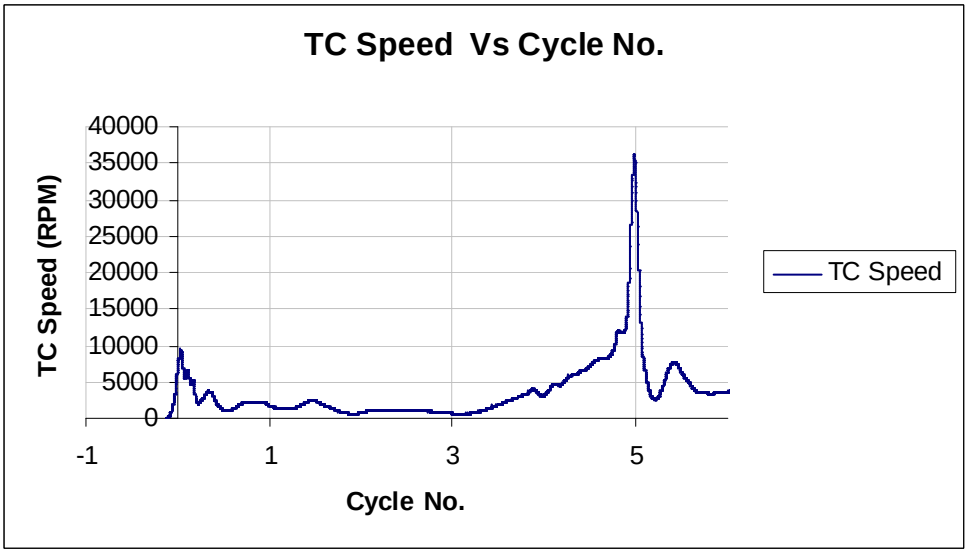

Figure 2.21 – turbocharger speed.

2.3.9 Engine RPM:

The speed of the processor of the mother board –used for collecting the data- is used to calculate the engine RPM as shown in figure 2.22.

The following methodology is used to calculate the rpm:

Calibration equation: $\left(\frac{1}{\left(\frac{6 * time}{6000000} \right)} \right)$ rpm

If cell-1<Cell-2

Time = Cell-2 - Cell-1

Else time = 65536+ Cell-2- Cell-1

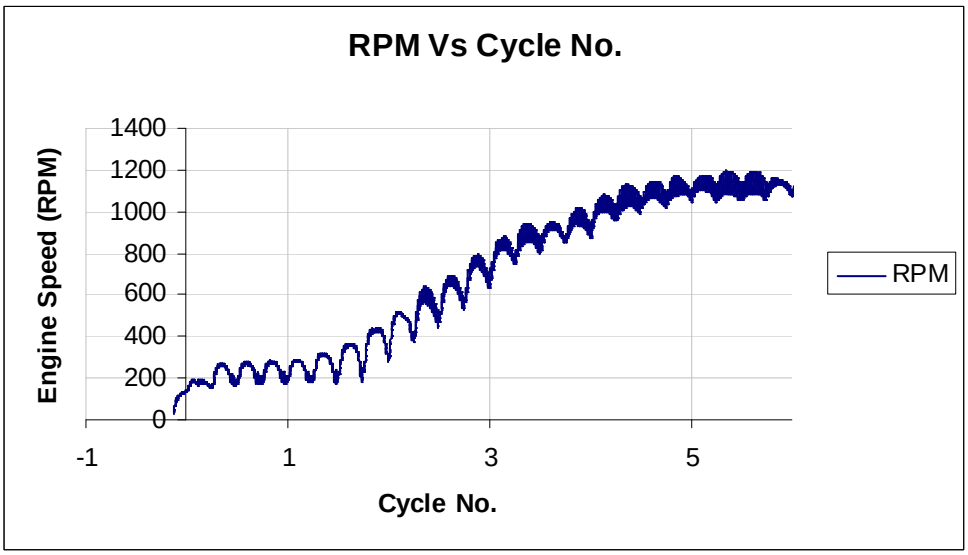

Figure 2.22 – Engine speed.

2.3.10 Unburnt Hydrocarbon Emissions:

A fast response Cambustion FID (Flame Ionization Detector) is used for real-time HC emissions measurements as shown in figure 2.23. A 15000 ppm sample gas and Zero air gas are used to calibrate the system.

Figure 2.23 – Fast response FID.

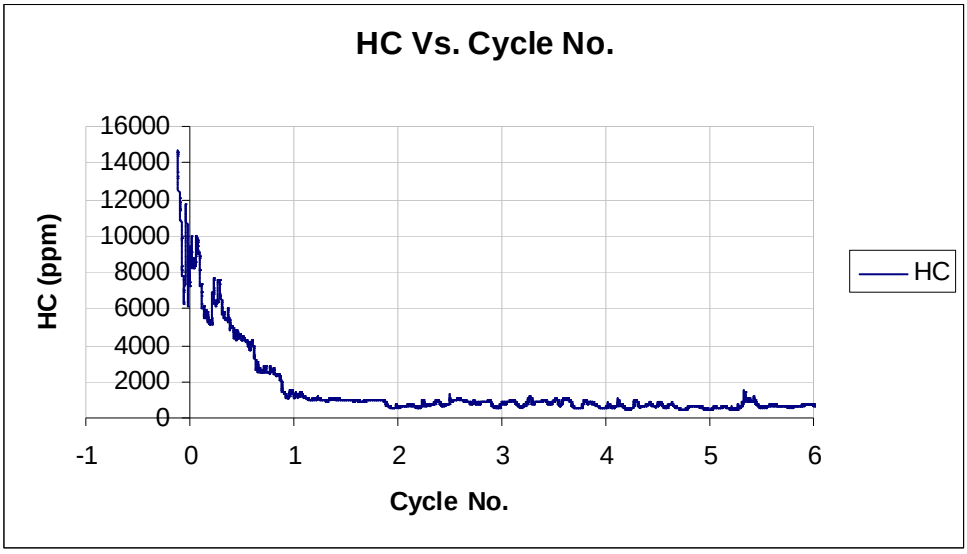

Figure 2.24 – Unburned hydrocarbons concentration.

To calculate the unburned hydrocarbons concentration, the following calibration equation is used as shown in figure 2.24:

(Signal * Calibration gas in ppm/ Calibrated Volt) ppm

2.3.11 NOx Emissions:

A Cambustion CLD (chemiluminescence detector) is used for real-time NO emissions measurements as shown in figure 2.25. A 962 ppm sample gas and Zero air gas are used to calibrate the system.

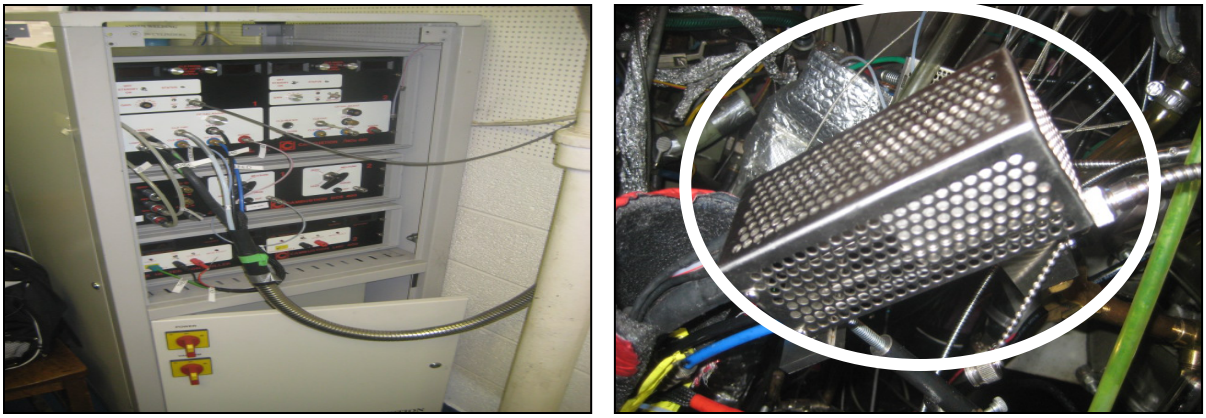

Figure 2.25 – Fast response Nox.

To calculate the unburned hydrocarbons concentration, the following calibration equation is used as shown in figure 2.26: (Signal * Calibration gas in ppm/ Calibrated Volt)

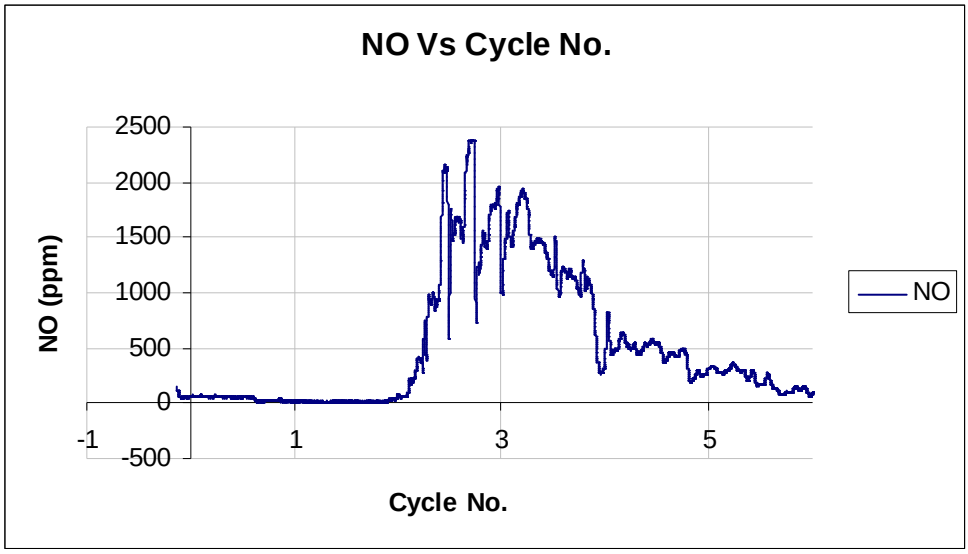

Figure 2.26 – No concentration.

2.3.12 Fuel consumption:

A FCI FlexCOR series mass flow meter with Coriolis measurement technology is used for the fuel consumption measurements as shown in figure 2.27.

Figure 2.27 – Fuel consumption, mass flow meter.

The following calibration equation is used for the fuel consumption calculation: ((13.116*Signal)-25.635) g/min

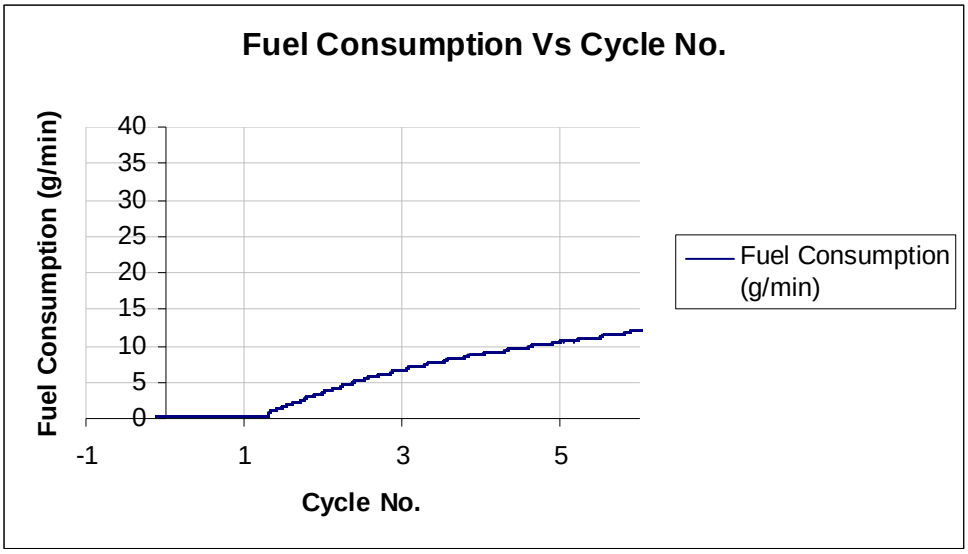

Figure 2.28 – Fuel consumption.

2.3.13 Air mass flow:

A 96FP series mass flow meter is used for the air flow mass measurements as shown in figure 2.29.

Figure 2.29 – Air mass flowmeter.

The following calibration equation is used for the air mass flow calculation as shown in figure 2.30 : $\left(10.787 * \left(\frac{Signal}{100}\right)^2\right) + \left(0.5754 * \left(\frac{Signal}{100}\right)\right) + 0.0337$ Kg/hr

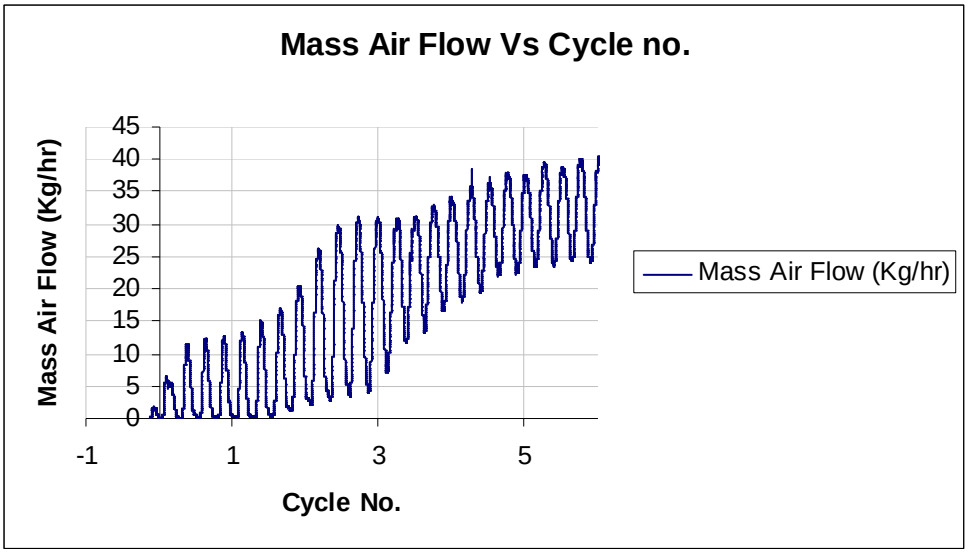

Figure 2.30 –Air Mass flow.

2.3.14 Blow-By flow:

A J-TEC flow meter with its respective filter is used for the Blow-By flow measurements as shown in figure 2.31.

Figure 2.31 – Blow-by flow meter and its filter.

The volumetric capacity of the blow-by is calculated using the following calibration equation as shown in figure 2.32: $\left(1.0128 * \frac{Signal}{100}\right) + 0.0027$ cu.ft/min

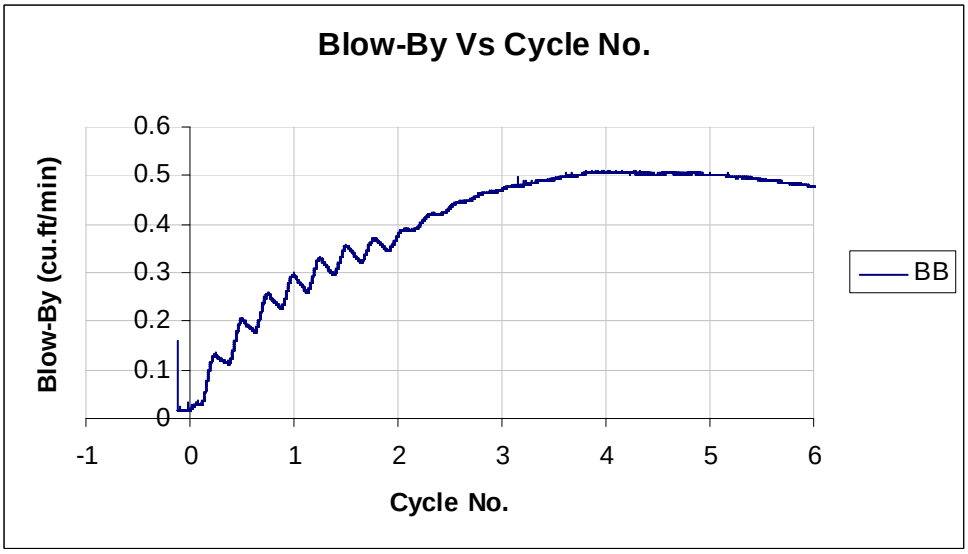

Figure 2.32 – Blow-by volumetric capacity.

2.4 Engine control

Some of the engine variables can be controlled and others can be only monitored as shown below.

2.4.1 Variables that can only be monitored:

- BE_ACT: Air Temperature (deg. C)
- BE_ECT: Coolant Temperature (deg. C)
- BE_MAF: Air Mass Sensor Reading, (kg/hr)
- BE_MAP: Intake Air Pressure, (kPa)

- BE_RPM: Engine Speed (rev/min)
- CRD_P_RAIL_FBK: Actual Fuel Rail Pressure, (bar)

2.4.2 Engine variables that can be controlled:

- Injection timing (for pilot and main injection)
- Injection pressure
- Injection quantity (for pilot and main injection)

These Variables (D)** can be controlled through **Parameters (**C)** and **Maps (**M) using GREDI software**:

1- **CRD_P_RAIL_DMD:** Desired Fuel Rail Pressure, (bar) controlled by Parameters: CRC_P_RAIL_DYNO_ADD & CRC_P_RAIL_DYNO_MUL And a Map: CRM_P_RAIL_MAX

2- **CRD_PLT_Q_DMD:** Desired Pilot Fuel Injection Quantity, (mg/stoke) controlled by Parameters: CRC_PLT_Q_DYNO_MUL & CRC_PLT_Q_DYNO_ADD

3- **CRD_PLT_TIM_DMD:** Desired Pilot Injection Timing, (deg. Before Main Inj. Start) controlled by Parameters: CRC_PLT_TIM_MUL & CRC_PLT_TIM_ADD

4- **FQD_FUEL_DMD:** Desired Main Fuel Quantity, (mg/stroke) Controlled by a Map: FQM_CR_CLD_ADD

5- **TID_DMD:** Desired Main Injection Timing, (deg. BTDC) controlled by Parameters: TIC_DYNO_ADDER & TIC_DYNO_MULT

2.5 Detailed Steps with illustrations for a complete single run

1- Disconnect both sides, engine side and sample head side (sample head connection and electrical connection) of the HC and NO probes.

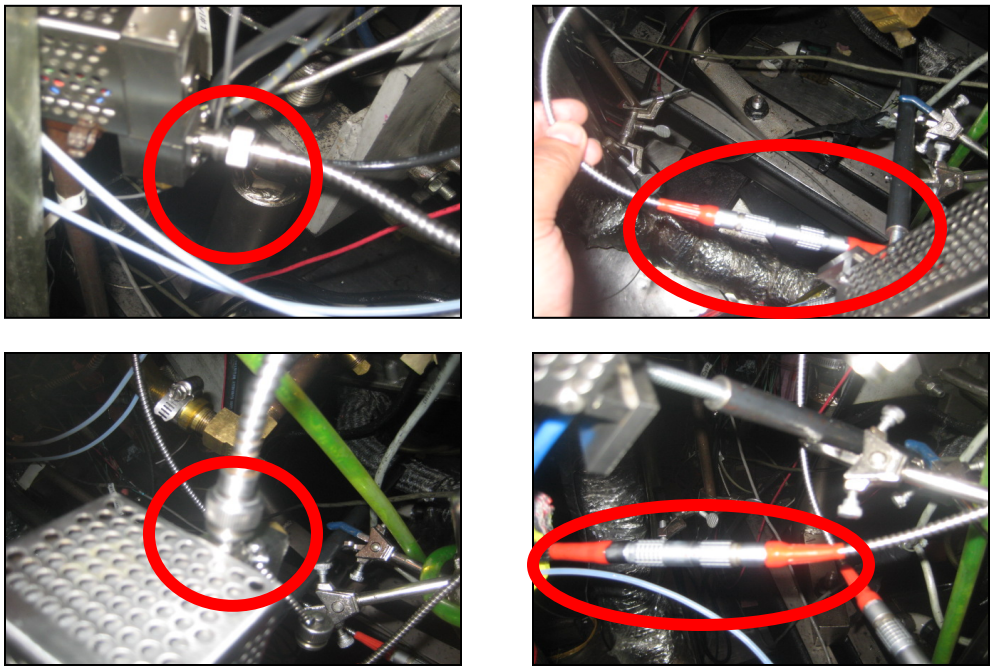

2- Clean the probes with a 0.022” wire.

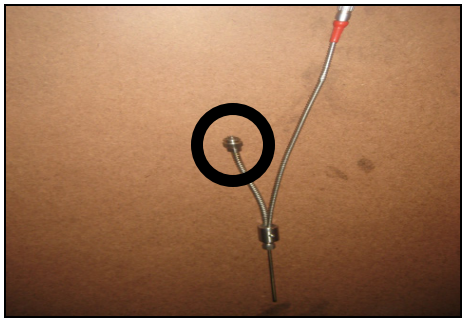

3- Clean the sample head with the yellow dot wire for the HC and the red red wire for the NO.

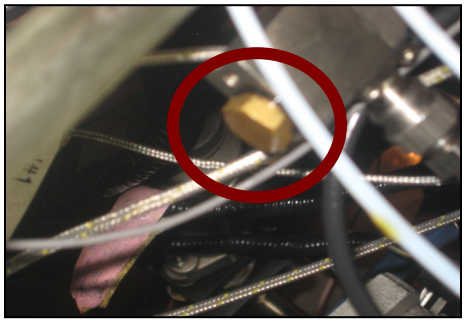

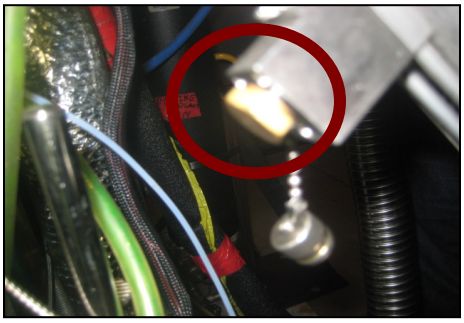

4- Connect the probes back

5- Turn on the main power for the cold room controller

6- Program the cold room for the required temperature.

For example, set the cold room for a -20 C and soak it for 8 hours

1) Go to the profile menu.

2) Enter create profile menu

3) Step 1 is going to be a Ramp time step, step does not wait, set time

for 1 second, set the set point to -20 C

4) Step 2 will be a Soak Step, Step waits for, Wait, -19 C, soak time set for 8 hours, PID 1, Guaranteed Soak No

5) Step 3 Set to End, All off.

N.B.: It can be adjusted to run automatically at a specified time by adding a step, start automatically and adjust the starting time, between step 2 and step 3 mentioned above.

7- Run the NOx machine

1) Open the knobs of the nitrogen cylinder with 960 ppm concentration and the zero air cylinders.

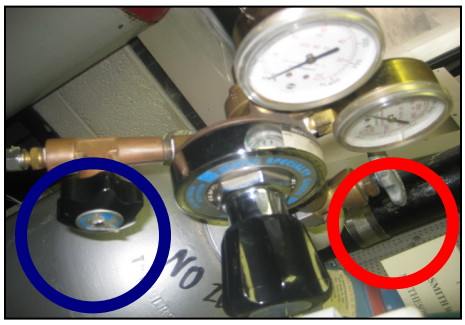

2) Switch on the machine (the two red switches)

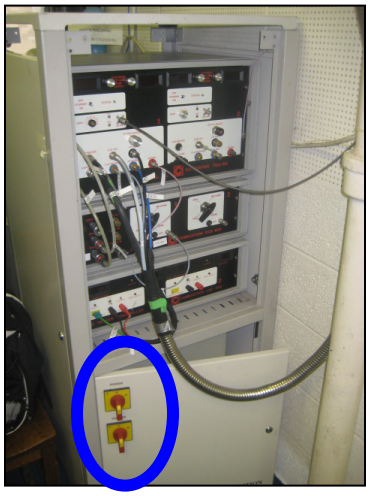

3) Leave it about 20 to 30 minutes till it stabilizes and the temperature reaches around 300 C

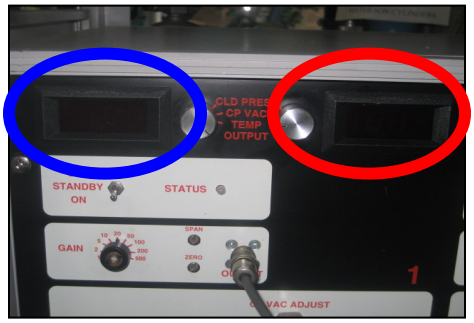

8- Run the HC machine

1) Open the knobs of the HC cylinder with 15000 ppm concentration, the zero air cylinder, the nitrogen cylinder and the hydrogen cylinder. Check the pressures

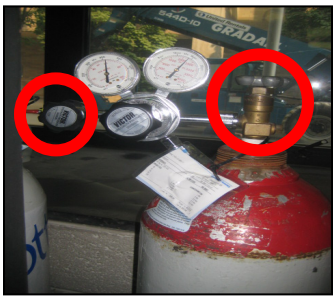

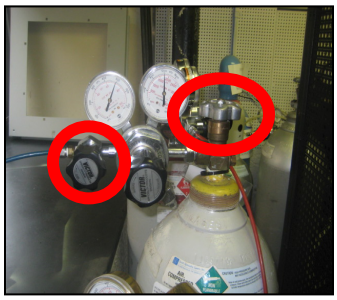

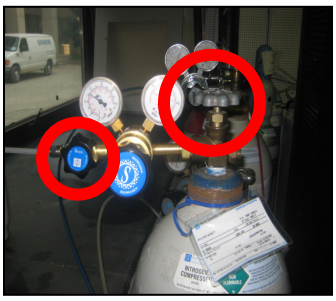

2) Hit the start button till the temperature start to rise automatically

3) Leave it about 20 to 30 minutes till it stabilizes and the temperature reaches around 300 C (±50)

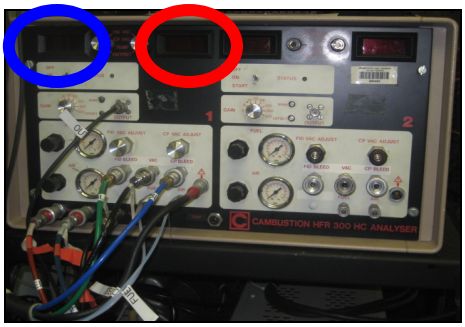

9- Turn on the main power switch

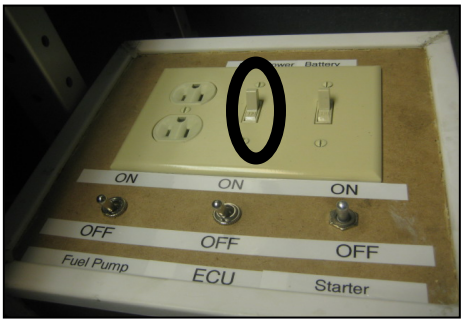

10-Turn on the two PCs

11-Switch the 4 cylinder pressure amplifiers to operate mode

12-Calibrate the NO machine

1) Switch the knob to ZERO position and adjust the ZERO adjustable bolt to zero

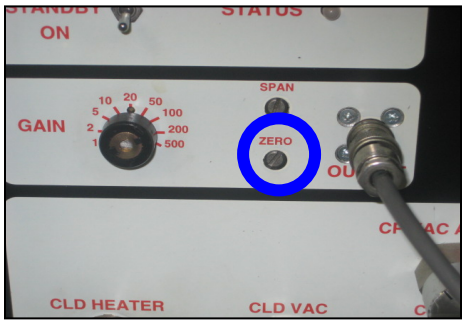

2) Switch the knob to SPAN position and adjust the SPAN adjustable bolt to 5

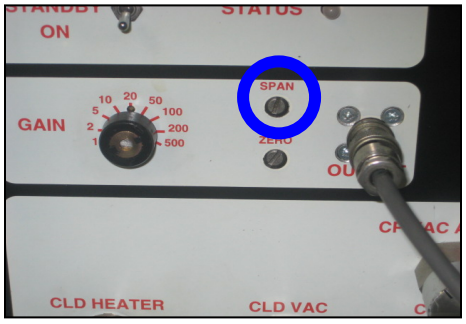

13-Calibrate the HC machine

1) Switch the knob to ZERO position and adjust the OFFSET adjustable bolt to zero

2) Switch the knob to SPAN position and adjust the SPAN adjustable bolt to 5

14- Switch-on the fuel pump

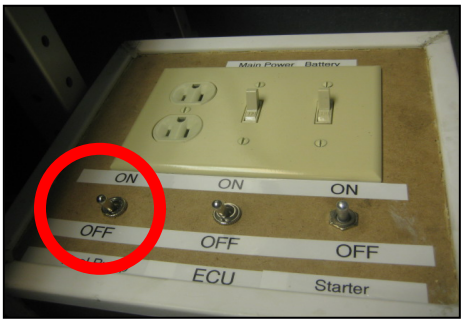

15-Open the GREDI software

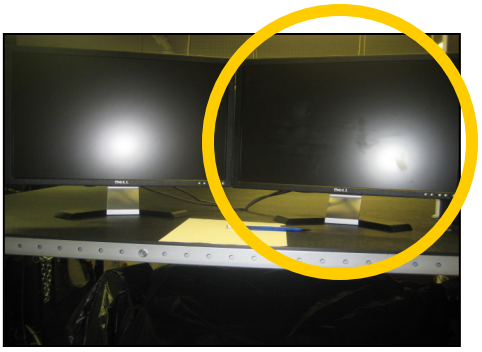

16-Switch-on the ECU switch

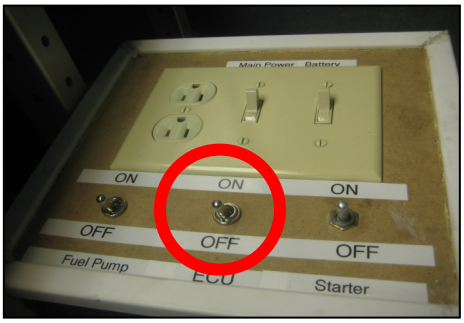

17-Connect the ECU online through the software at the same time while doing step 16

18-Open the RTcam software

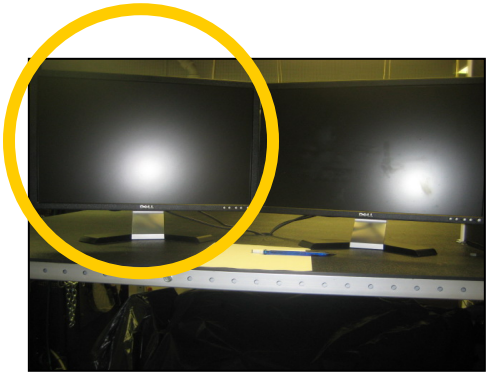

19-Switch on the battery switch

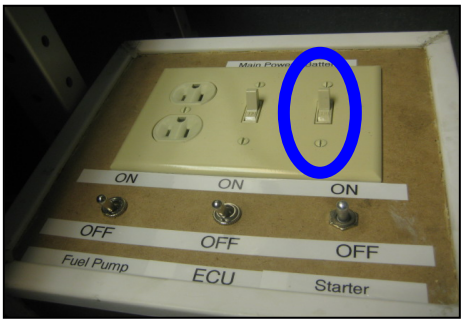

20-Hit the starter switch till the engine runs

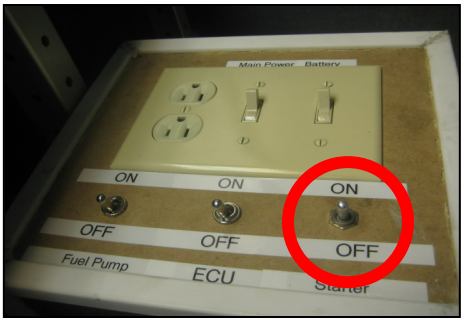

21-Leave the engine until it warms up and then turn off the ECU and the fuel pump switches.

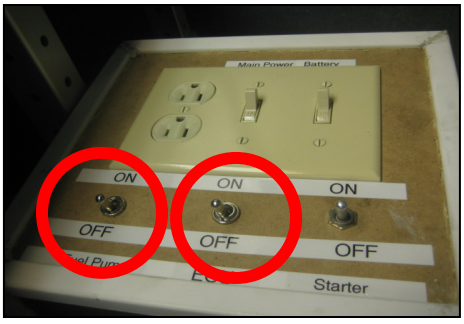

CHAPTER 3

EXPERIMENTAL RESULTS AND DISCUSSIONS

3.1 Introduction

Introducing a combination of HCs and HCHO into the intake manifold has been investigated experimentally by recirculating part of the exhaust gases to the intake manifold and checking the effect of different recirculated percentage on the cranking period, fuel consumption and the exhaust hydrocarbons.

3.2 Baseline Test

The baseline test was at an ambient temperature of 15°C and a fuel injection rate of 25 mg per stroke. Figures 3.1.a shows the instantaneous engine speed and the gas pressure in each of the four cylinders in the first 22 cycles (44 revolutions). Figure 3.1.b shows the mole fraction of the HC emissions. The details of these traces for the first five cycles are given in Figures 3.2.a and 3.2.b. The numbering of the cycles starts when the piston of cylinder 4 is at TDC, end of compression. The recording of the crankshaft rotation starts with its motion. Data before the zero point indicates that the crankshaft was not at TDC of cylinder 4. Figure 3.1.a shows the engine started with cylinder 3 in partial compression. This agrees with previous findings that gasoline and diesel engines stop rotation after shut down with one of the cylinders in the compression stroke. [44]. Cylinder 3 was followed by a sequence of cylinders 4, 2 and 1 in the first

two cycles. Cylinder 2 fired in the third cycle causing the engine speed to increase from 200 rpm to 400 rpm.

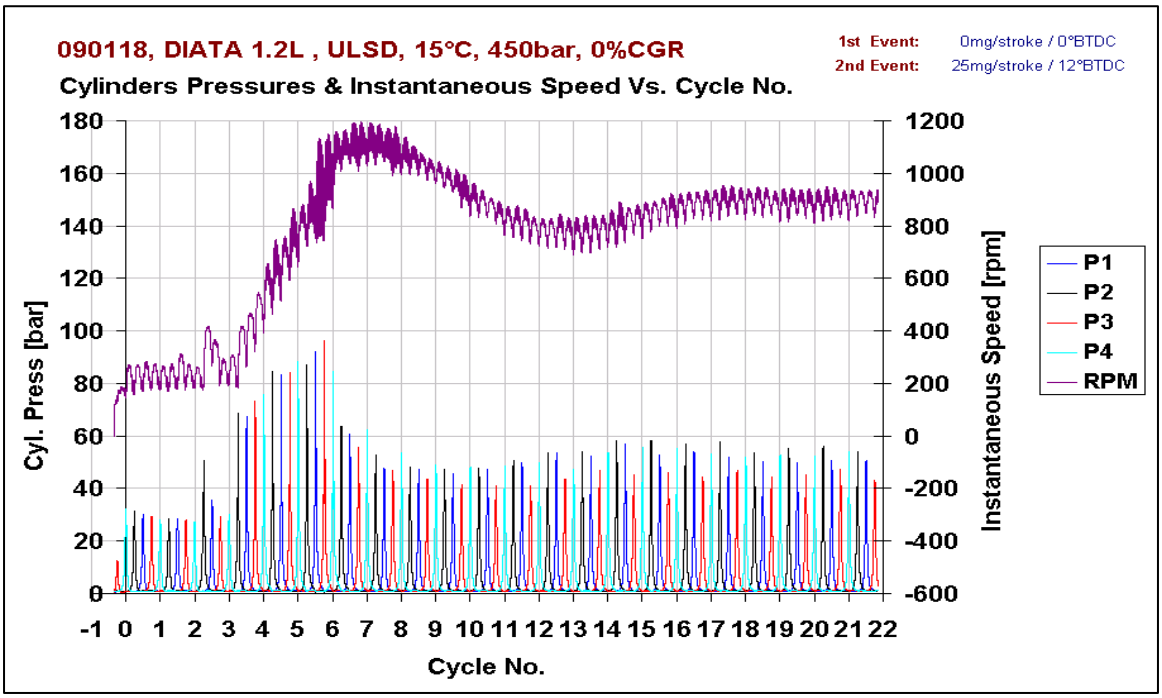

Figure 3.1.a - Gas pressure and instantaneous engine speed with 25 mg/stroke. SOI: 12°BTDC, T_{amb}:15℃, 0%CGR.

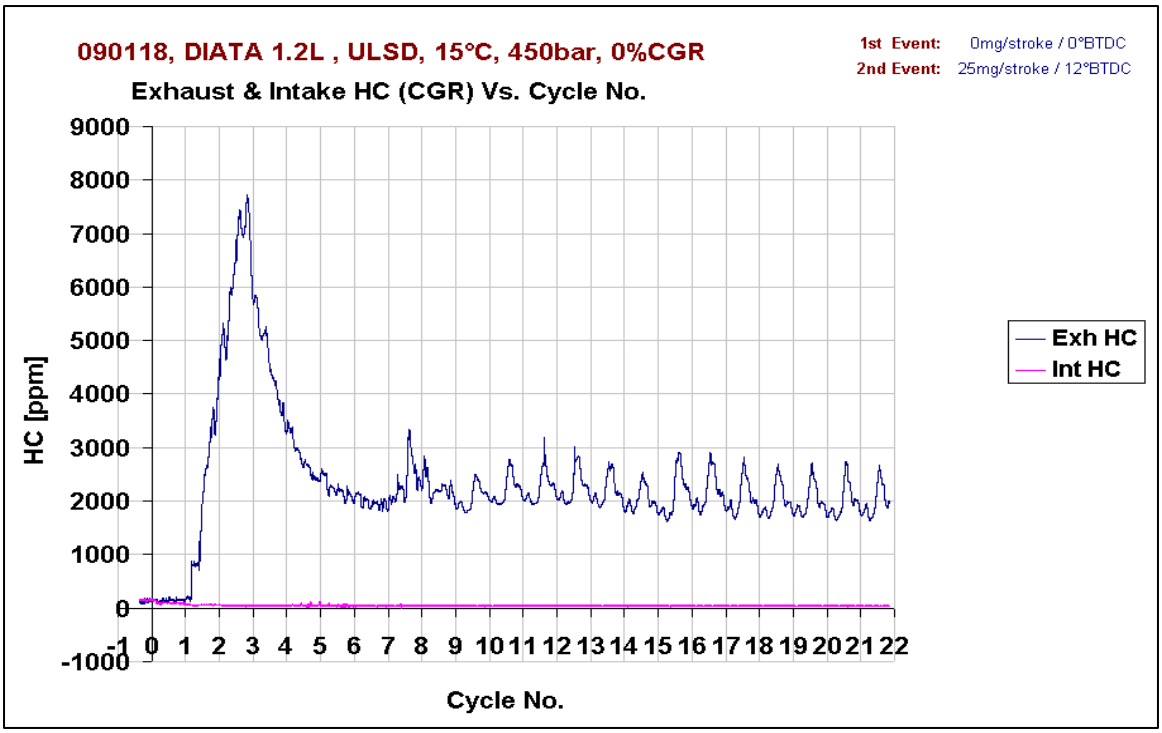

Figure 3.1.b - HCs emissions with 25 mg/stroke. SOI: 12°BTDC, T_{amb}:15℃, 0%CGR.

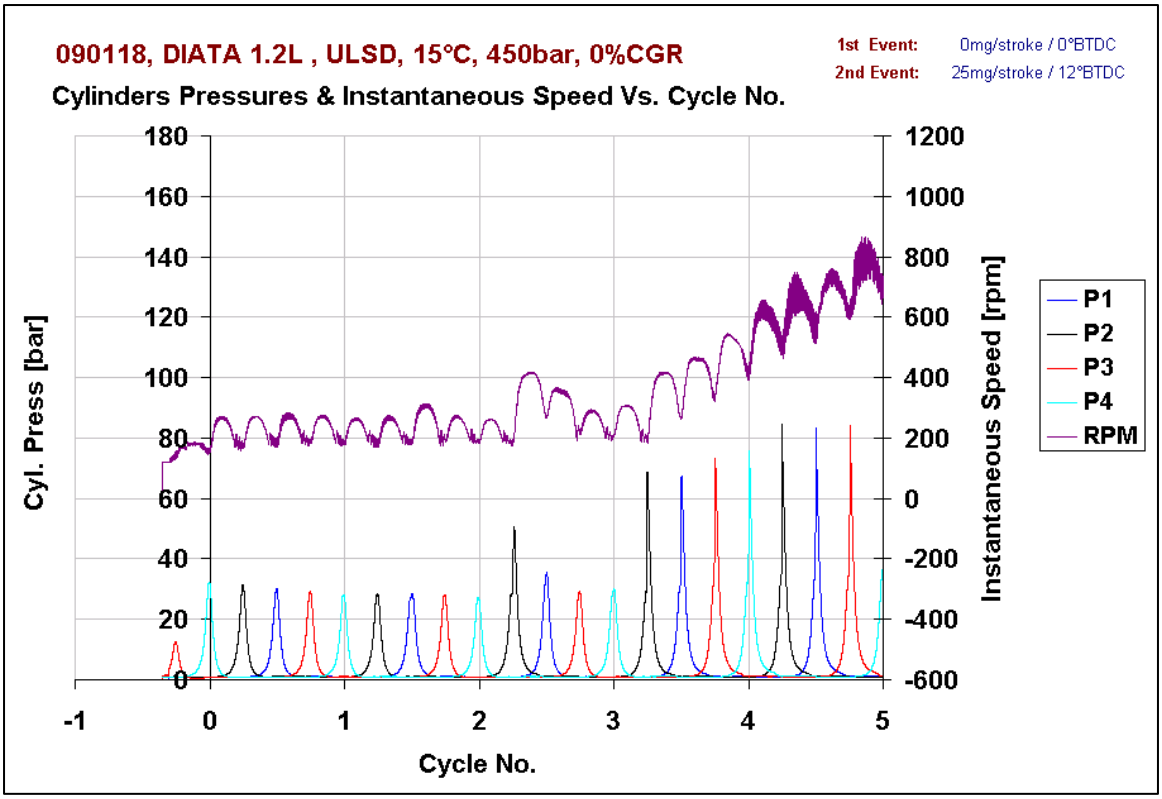

Figure 3.2.a - First 5 cycles of gas pressure and instantaneous engine speed with 25 mg/stroke. SOI: 12°BTDC, T_{amb}:15℃, 0%CGR.

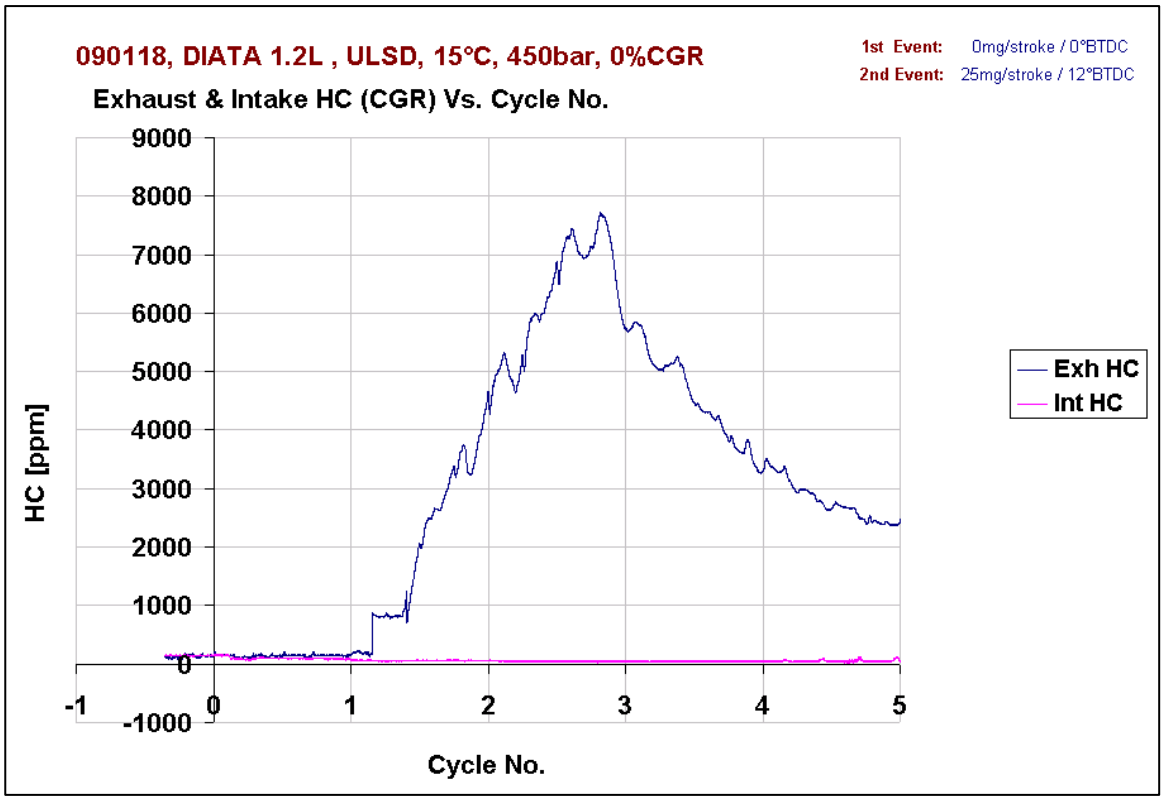

Figure 3.2.b - First 5 cycles of HCs emissions with 25 mg/stroke. SOI: 12° BTDC, T_{amb}:15℃, 0%CGR.

This was followed by partial combustion in cylinder 1 and complete misfire in cylinder 3. Cylinder 2 fired again in the fourth cycle and caused the engine to accelerate and reach 400 rpm, followed by continuous firing in the other three cylinders. The engine reached 1100 rpm during flare up and decelerated to the idle speed in cycle 17.

Figures 3.1.b and 3.2.b show the HC in the engine-out gases. HC increased from 900 ppm at the start of cycle number 2 to 4000 at the end of this cycle. HC increased to 7,800 ppm in cycle number 3, after which HC dropped, during engine acceleration, to 2,000 ppm at the end of cycle 7. The total mass of HC emitted after the first 22 cycles was 112.52 mg.

3.3 Effect of Low Rates of CGR on Cranking Period and Unburned HC Emissions

This set of experiments was conducted at an ambient temperature of 15℃ with 25 mg/stroke fuel injection and without any back pressure on the engine. The percentage of CGR was varied from 0% (Base line test) to 20%, 40%, 60%, 80% and 100% by using the GR valve during the starting process up to the 25^{th} cycle for this set of experiments.

Figure 3.3.a shows traces for the 100% GR valve opening with 25 mg/stroke fuel injection. Cylinder 2 was the first to fire in cycle number 2. Figure 3.3.b shows HC in the intake follow the same tend as the HC in the exhaust. HC emissions reached 4,600 ppm during acceleration and dropped to 1000 ppm during idling. During idling the HC followed the same pattern, where cylinder 3 had incomplete

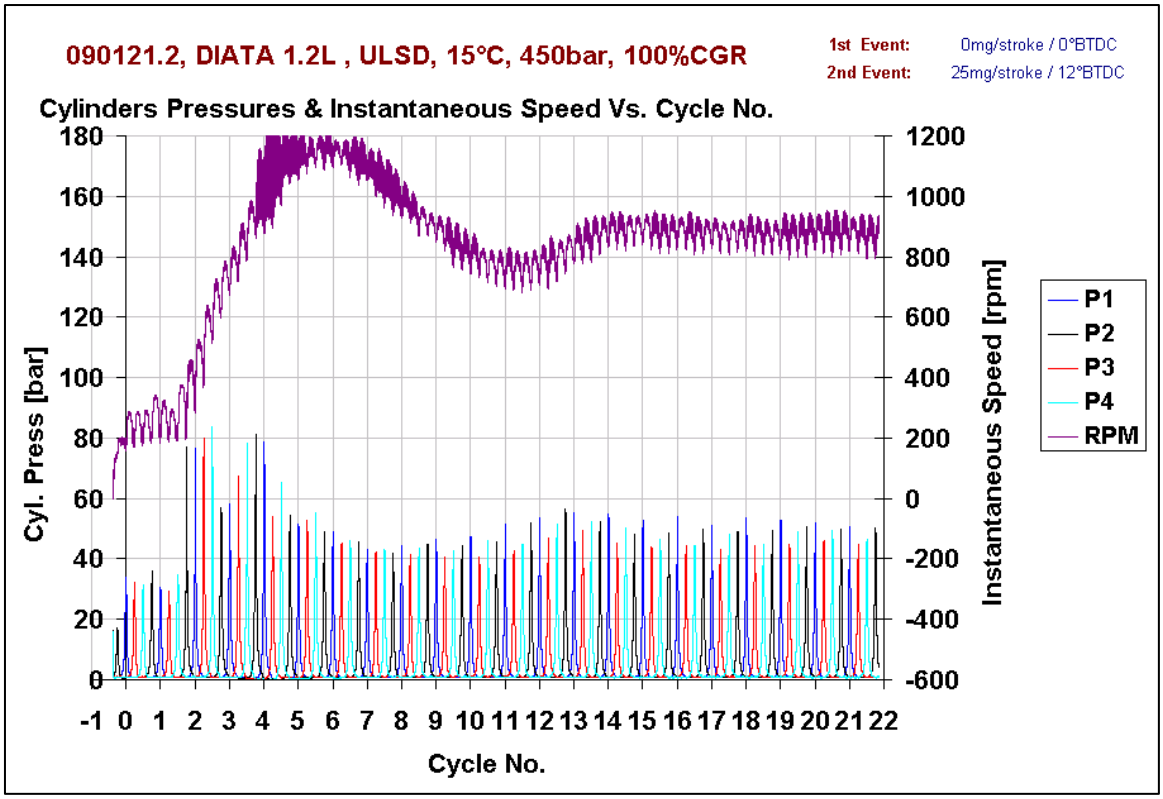

Figure 3.3.a - Gas pressure and instantaneous engine speed with 25 mg/stroke. SOI: 12°BTDC, T_{amb}:15℃, 100%CGR.

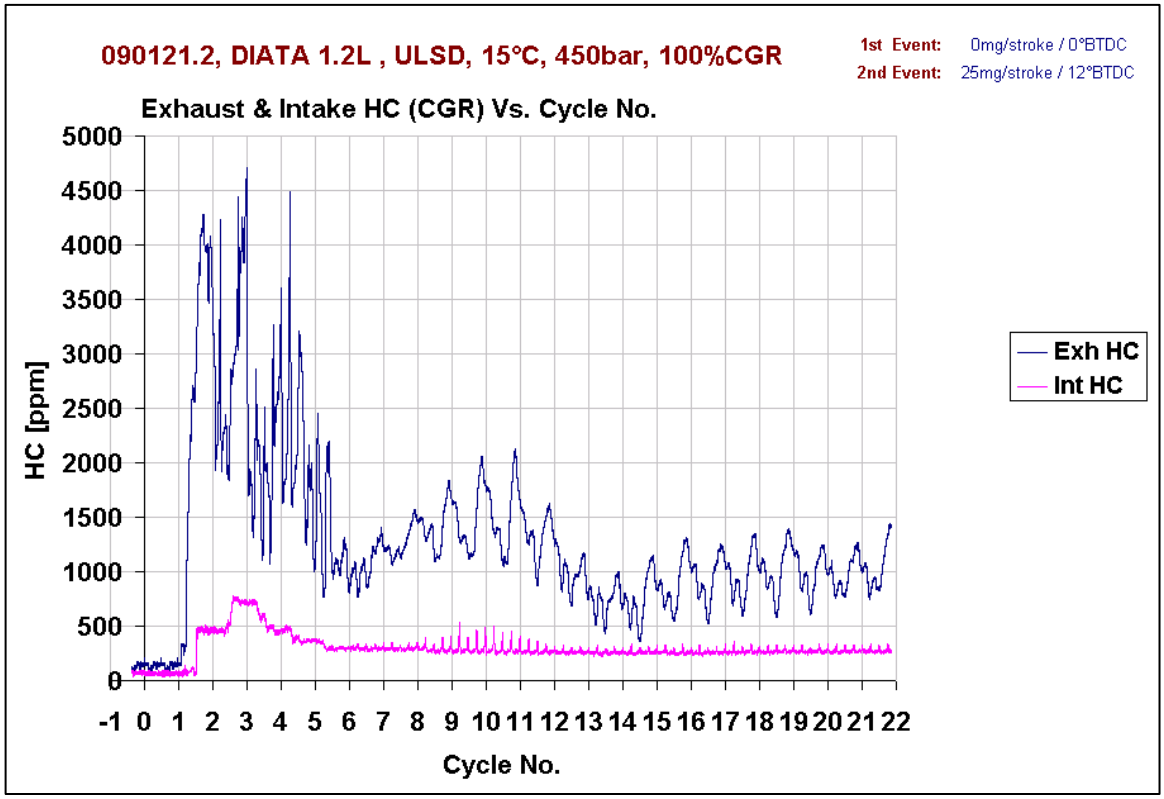

Figure 3.3.b - HCs emissions with 25 mg/stroke. SOI: 12°BTDC, T_{amb}:15℃, 100%CGR.

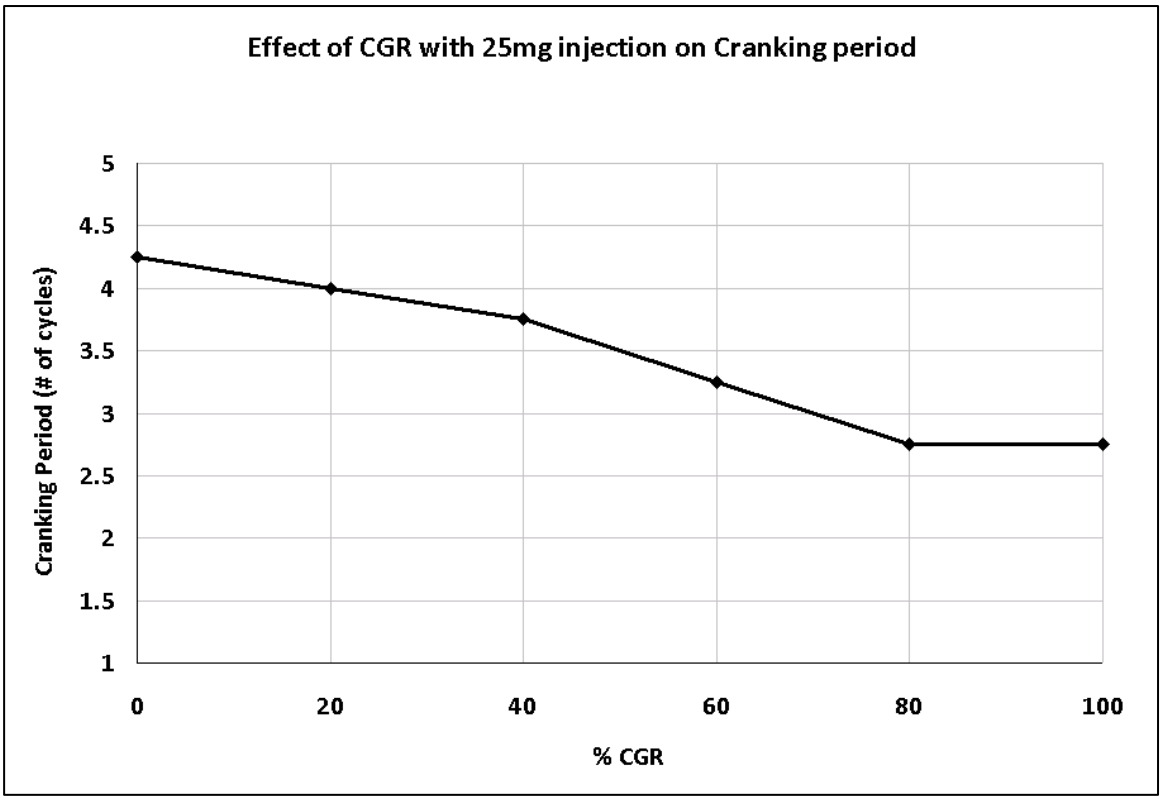

Figure 3.4.a - Effect of different CGR (0, 20, 40, 60, 80 and 100%) on Cranking Period with 25 mg/stroke. SOI: 12°BTDC, T_{amb}:15℃.

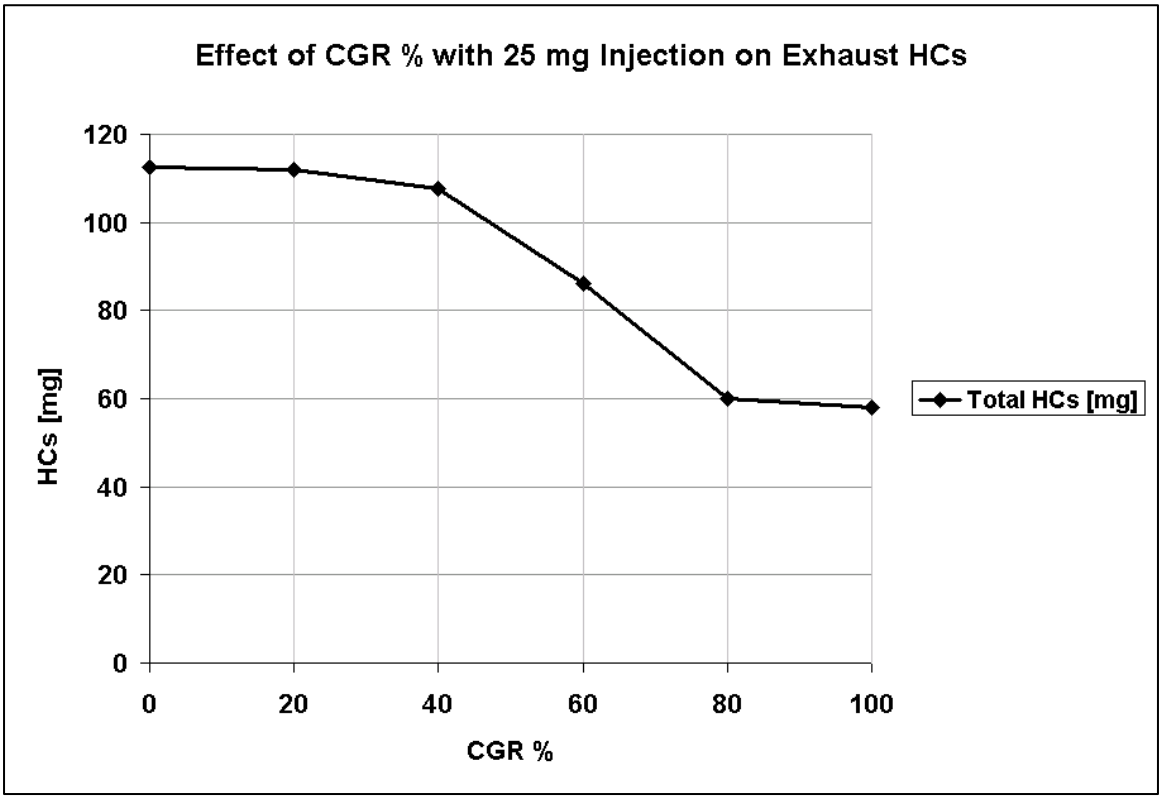

Figure 3.4.b - Effect of different CGR (0, 20, 40, 60, 80 and 100%) on HC at the Exhaust manifold with 25 mg/stroke. SOI: 12°BT DC, T_{amb}:15℃.

combustion and produced a sharp increase in HC emissions, followed by a drop as the other three cylinders fired. The intake HC reached 750 ppm during cranking and stabilized at 350 ppm during idling. The total HC emitted during the first 22 cycles was 58.12 mg.

In figure 3.4.a shows the effect of CGR on the cranking period with fuel injection rate of 25mg/stoke. The cranking period was reduced from 4 cycles without CGR to 2 cycles at 100%. Also, Figure 3.4.b shows HC emissions decreased from a total of 112.52 mg during the first 22 cycles without CGR to 58.12 mg with 100% GR valve opening.

3.4 Effect of High Rates of CRG on Cranking Period and Unburned HC Emissions at Reduced Fuel Injection

The following sets of experiments show the effect of different CGR% and BF valve opening on reducing fuel injection, cranking period and hydrocarbons.

3.4.1 Effect of applying the highest rates of CGR:

Initially, attempts were made to start the engine applying the highest CGR rate, at an ambient temperature of 16℃, delivering 25 mg/stroke of fuel. For this, the BF valve was completely closed and the GR valve was fully opened. The results given in figure 3.5.a show the engine completely failed to start after a few attempts. Figure 3.5.b shows a sharp increase in HC in the exhaust and intake. Exhaust HC reached 15000 ppm, the upper limit of the instrument after 7 cycles.

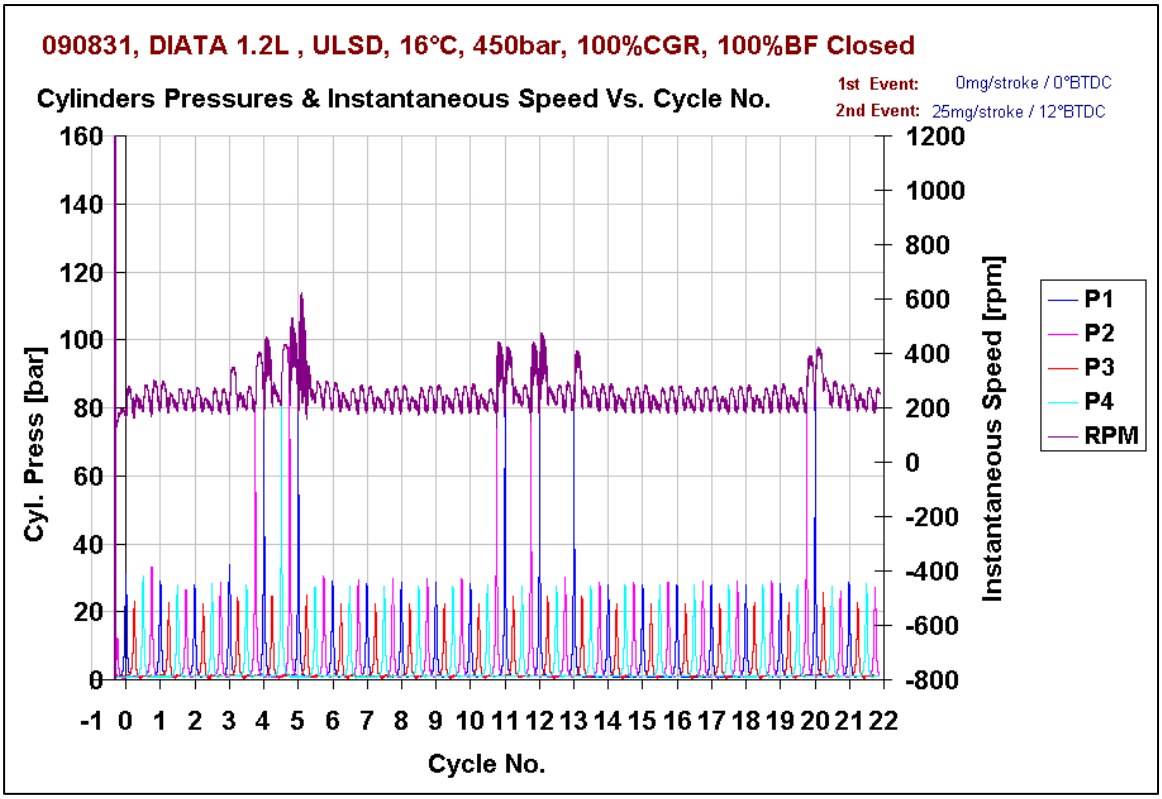

Figure 3.5.a - Gas pressure and instantaneous engine speed with 25 mg/stroke. SOI: 12°BTDC, T_{amb}:16℃, 100%CGR and 100% BF close.

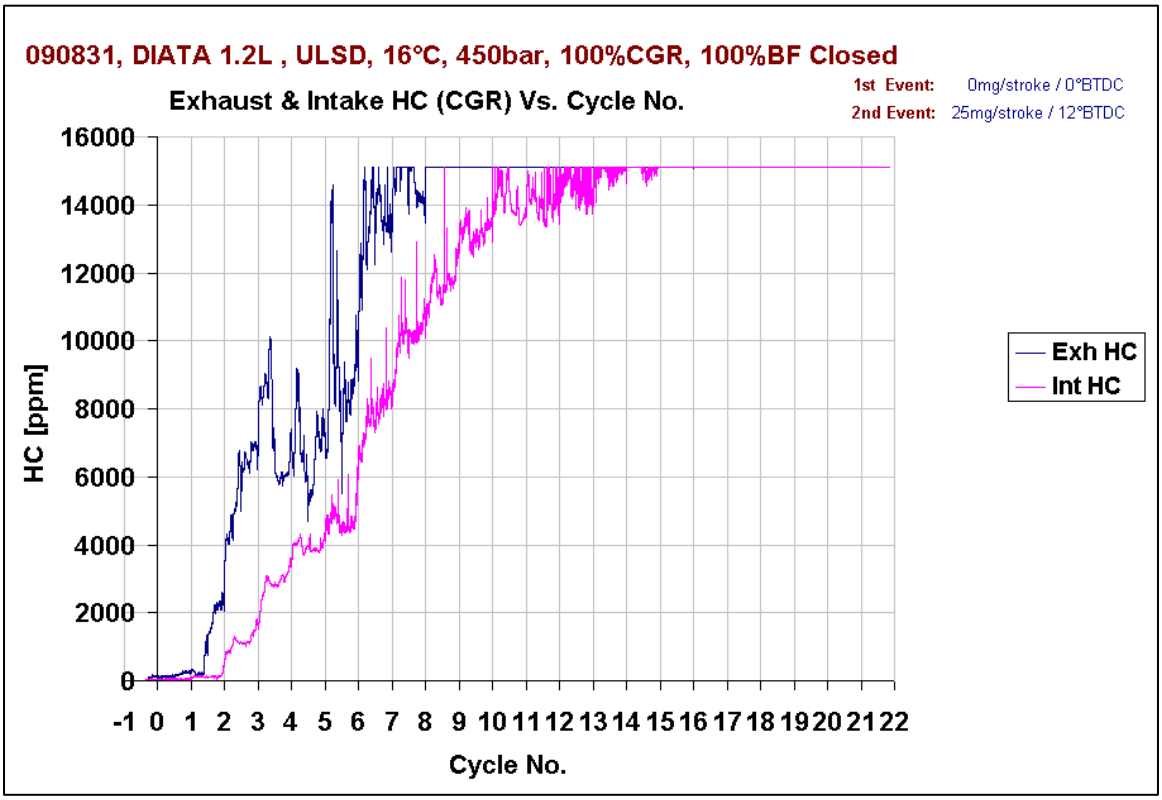

Figure 3.5.b - HCs emissions with 25 mg/stroke. SOI: 12°BTDC, T_{amb}:16℃, 100%CGR and 100% BF close.

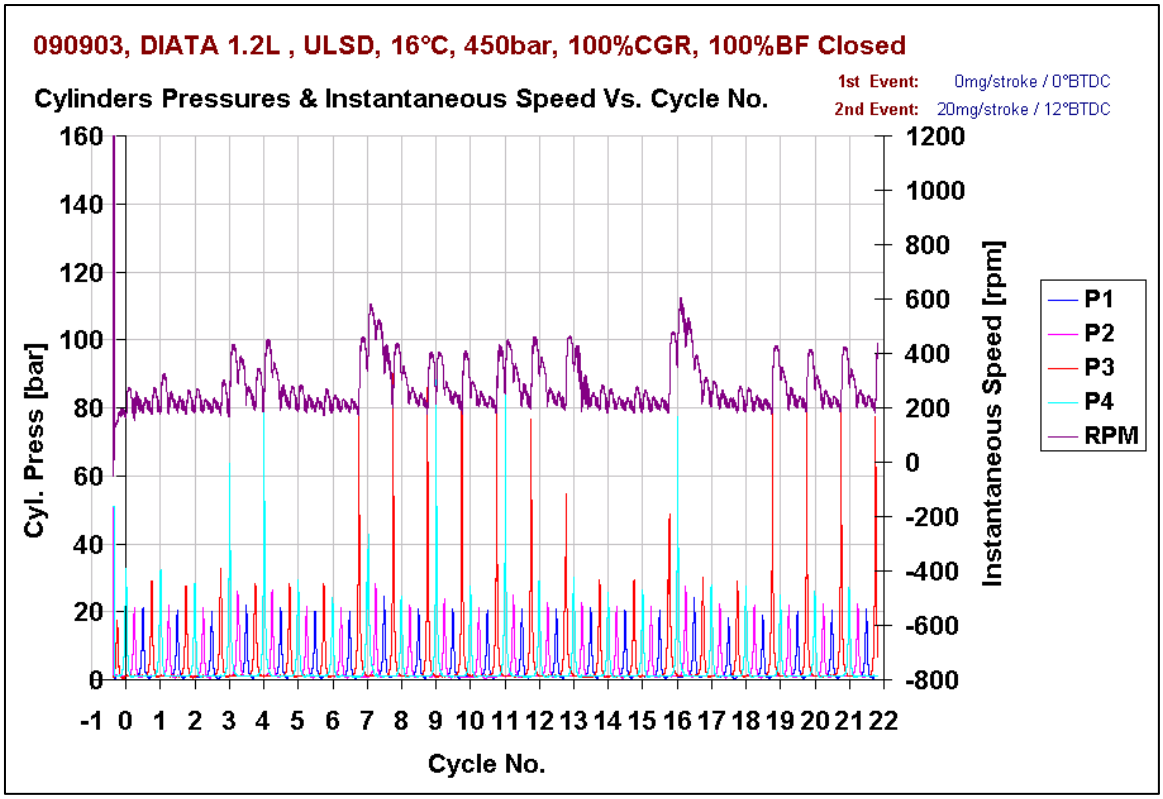

Figure 3.6.a - Gas pressure and instantaneous engine speed with 20 mg/stroke. SOI: 12°BTDC, T_{amb}:16℃, 100%CGR and 100% BF close.

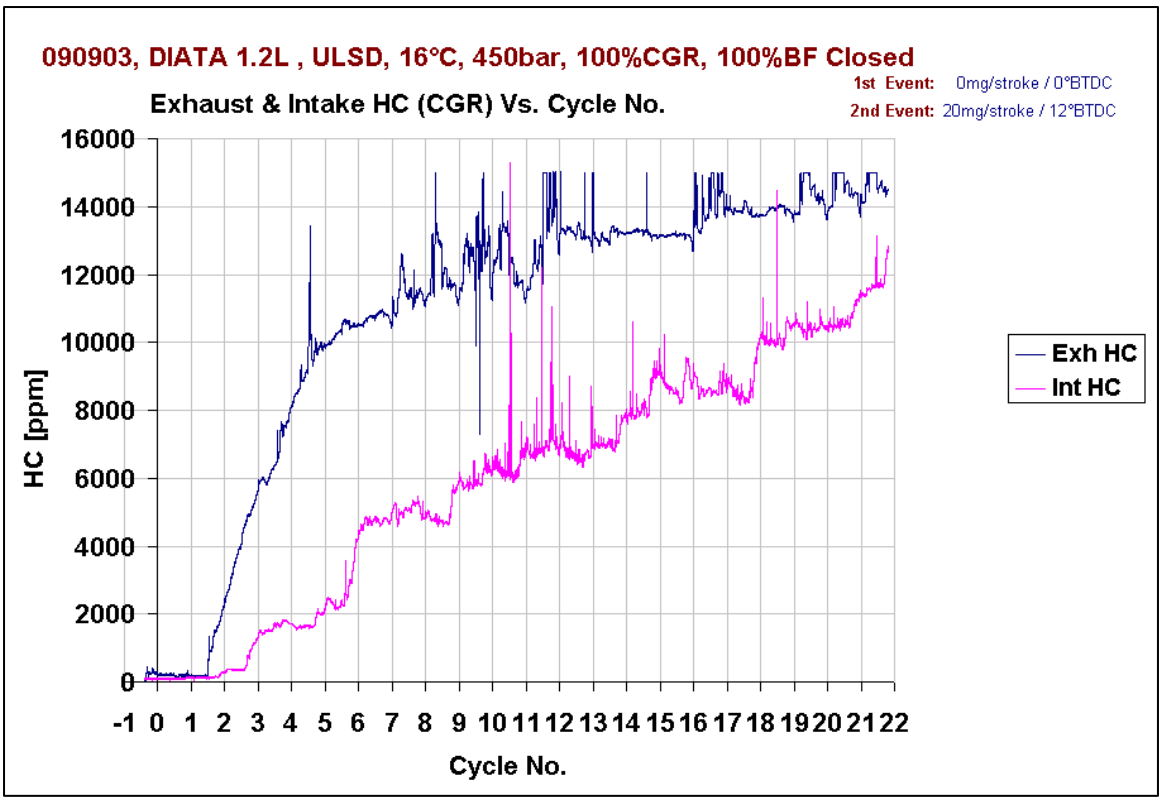

Figure 3.6.b - HCs emissions with 20 mg/stroke. SOI: 12°BTDC, T_{amb}:16℃, 100%CGR and 100% BF close.

The mass of HC emitted during 22 cycles was 635.96 mg, or 28.9% of the fuel delivered.

Figure 3.6.a shows the results after reducing the fuel injection from 25 mg/stroke to 20 mg/stroke. It is noticed that the attempts to fire increased, indicating that the mixture in the previous run was very rich, and reducing the fuel injection produced a better ignitable mixture. Figure 3.6.b shows exhaust HC reached the instrument limit of 15000 ppm after 19 cycles. The mass of HC emitted in the 22 cycles was 581.296 mg, or 26.42 % of the delivered fuel.

3.4.2 Effect of applying controlled rates of CGR at 3 ℃ ambient temperature:

After observing the results at 16℃ ambient temperature, experiments were conducted at 3 ℃ ambient temperature and 25 mg/stroke. Without any CGR the engine failed to start, even by increasing fuel injection up to 40 mg/stroke.

But by opening the GR valve 40% and BF valve 50% the engine fired in cycle number 14 as shown in figure 3.7.a. Figure 3.7.b shows the HC reached 11,900 ppm before firing in cycle 14, after which HC dropped to 3500 ppm during idling. The total HC emitted after 22 cycles amounted to 301.88 mg.

Increasing the GR valve opening to 60% while the BF valve was kept 50% closed, reduced the cranking period to 5 cycles and the HC reached 4500 ppm at the end of the cranking period, as shown in figures 3.8.a and 3.8.b. The total HC emitted amounted to 120.24 mg during the first 22 cycles.

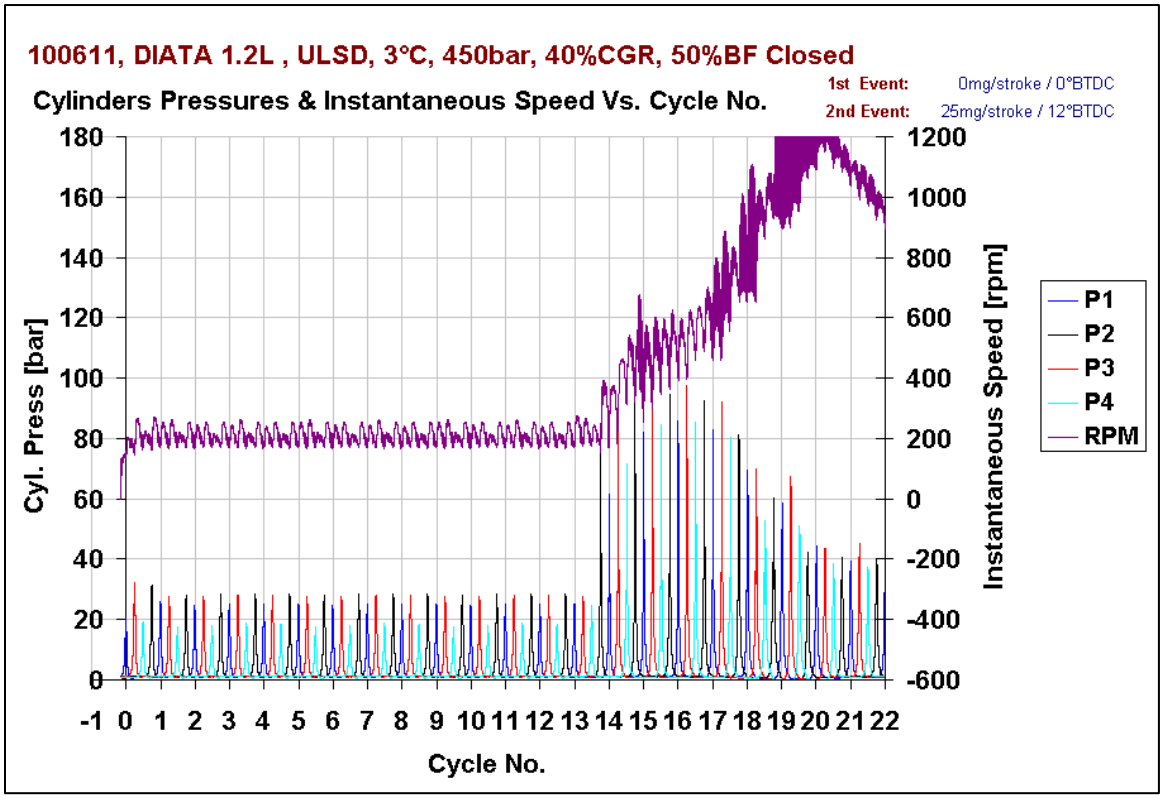

Figure 3.7.a - Gas pressure and instantaneous engine speed with 25 mg/stroke. SOI: 12°BTDC, T_{amb}:3℃, 40%GR valve and 50% BF valve.

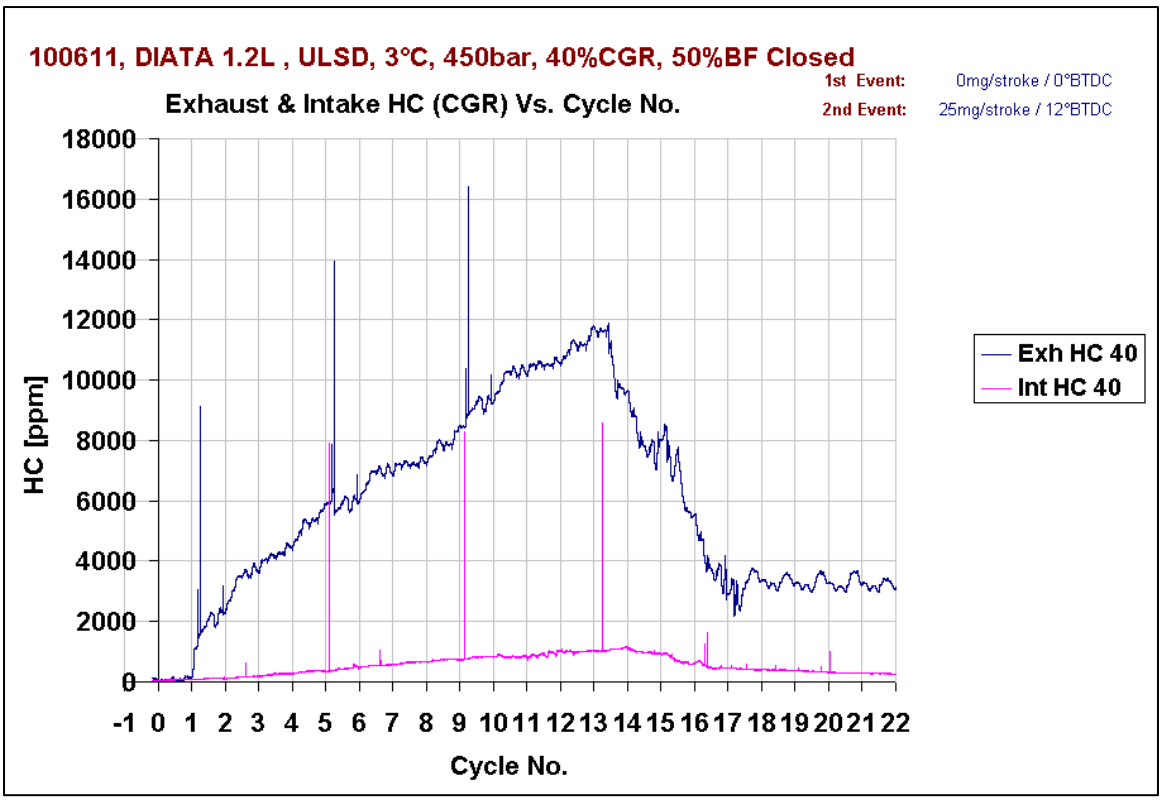

Figure 3.7.b - HCs emissions with 25 mg/stroke. SOI: 12°BTDC, T_{amb}:3℃, 40%GR valve and 50% BF valve.

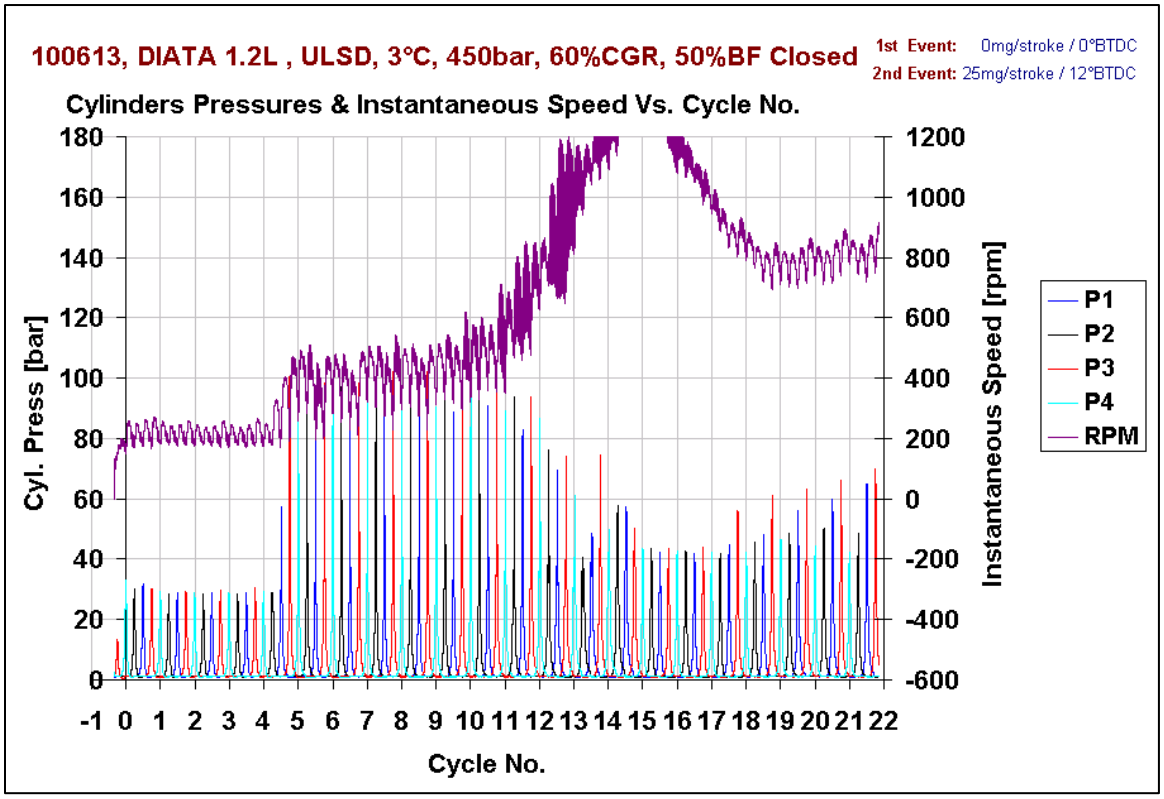

Figure 3.8.a - Gas pressure and instantaneous engine speed with 25 mg/stroke. SOI: 12°BTDC, T_{amb}:3℃, 60%GR valve and 50% BF valve.

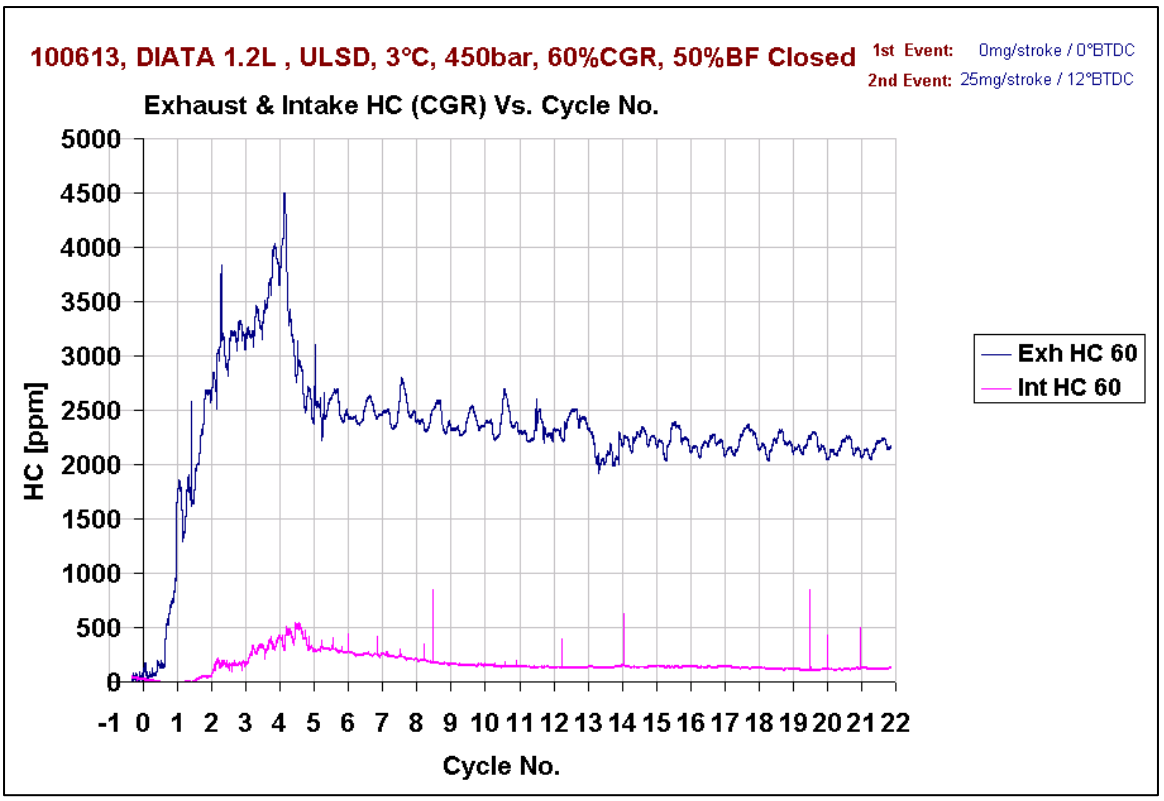

Figure 3.8.b - HCs emissions with 25 mg/stroke. SOI: 12°BTDC, T_{amb}:3℃, 60%GR valve and 50% BF valve.

Further increases in the GR valve opening produced opposite effects till the engine completely misfired.

3.4.3 Effect of applying controlled rates of CGR at -3 ℃ ambient temperature:

More experiments were conducted at a lower temperature of -3 ℃. Again the engine failed to start even by increasing the fuel injection up to 50 mg/stroke at 0% CGR.

As shown in figure 3.9.a. the engine fires successfully at cycle number 24 by opening the GR valve 80% and BF valve 50%. Figure 3.9.b shows the HC reached 11,920 ppm before firing in cycle 24, after which HC dropped again during idling. The total HC emitted after 22 cycles amounted to 359.92 mg.

The engine failed to fire during the first attempt at all other GCR valve openings.

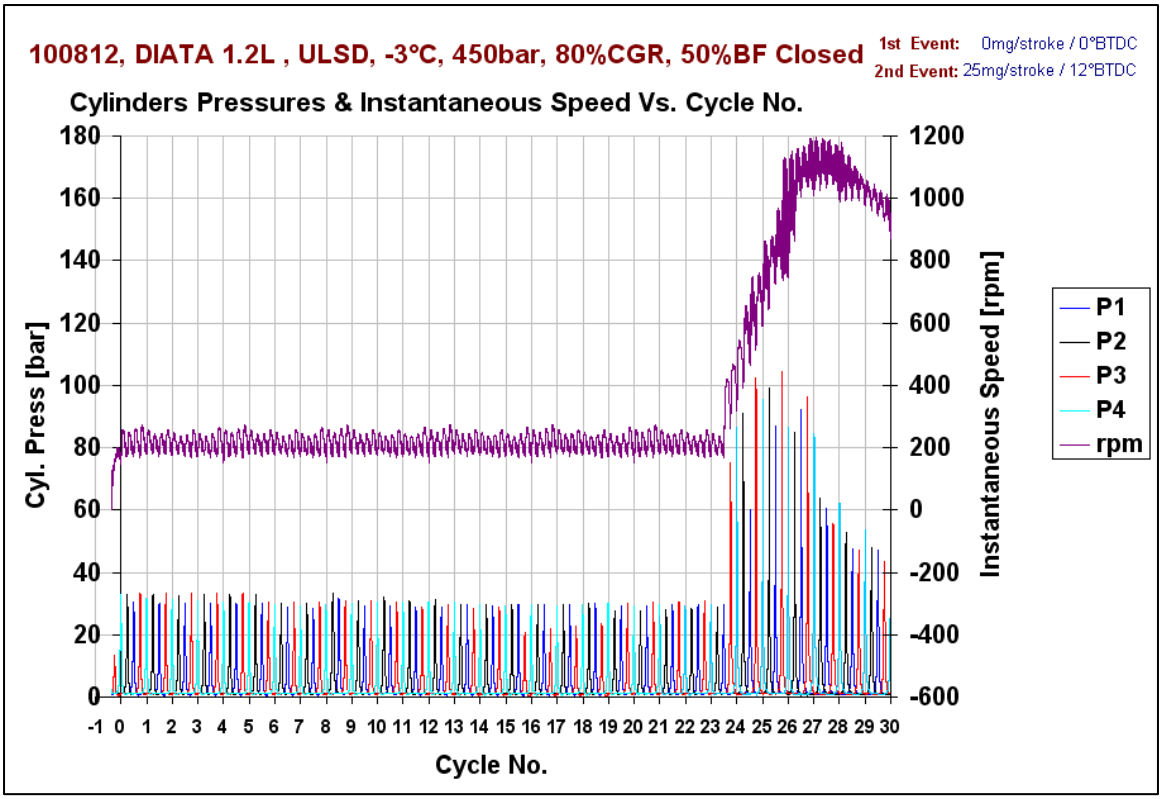

Figure 3.9.a - Gas pressure and instantaneous engine speed with 25 mg/stroke. SOI: 12°BTDC, T_{amb}: -3℃, 80%GR valve and 50% BF valve.

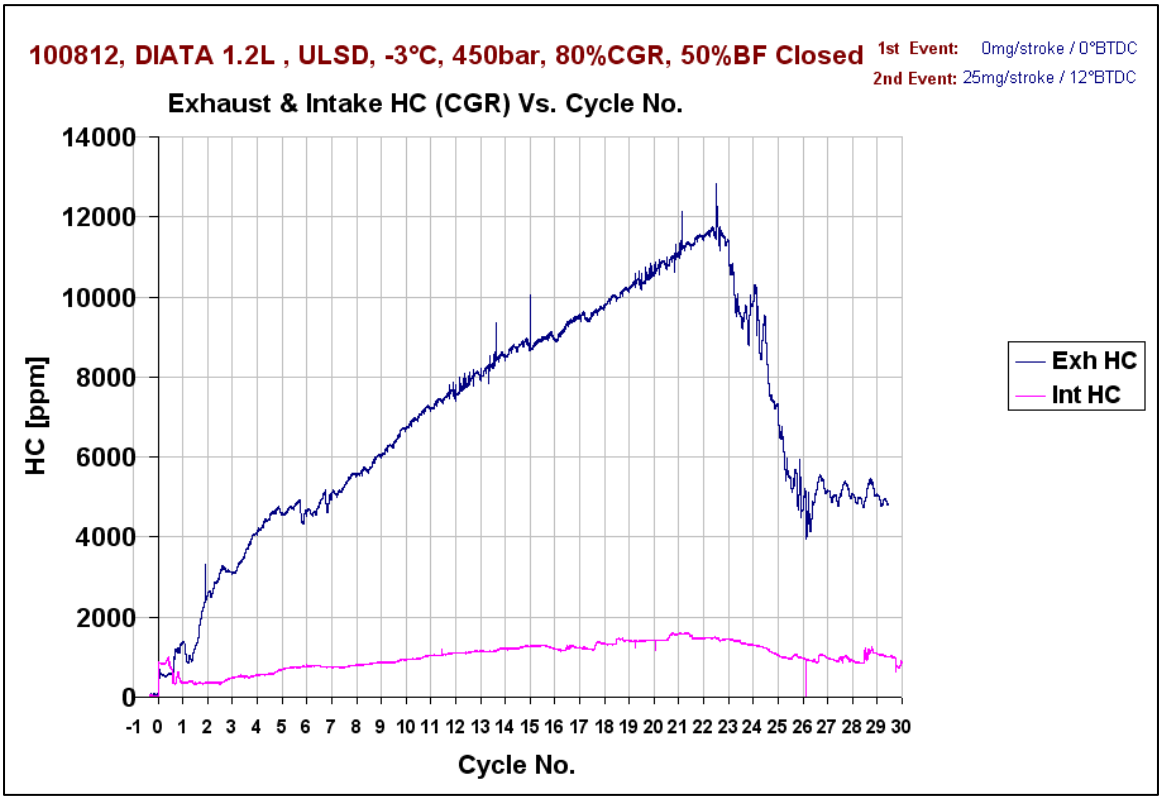

Figure 3.9.b - HCs emissions with 25 mg/stroke. SOI: 12°BTDC, T_{amb}: -3℃, 80%GR valve and 50% BF valve.

3.4.4 Effect of varying fuel injection rate at a constant CGR rate

These run were conducted to find out the fuel savings that can be achieved by applying CGR. The exhaust BF valve was kept 50% closed to raise the back pressure and the GR valve was 60% opened. Figures 3.10.a and 3.10.b show increasing the fuel injection from 20 mg/stoke to 21 mg/stoke reduced the cranking period from 20 revolutions to 9 revolutions and the HC dropped from 287.43 mg in the first 22 cycles to 128.8 gm. An increase to 22 mg/stoke reduced the cranking period by 2 revolutions, and HC by 29.08 mgs. A further increase to 23 mg/stoke caused the cranking period to increase by 2 revolutions as well as the HC emissions to increase from 99.72 mg to 130.44 mg during the first 22 cycles.

From the above experimental investigation, there is an optimum opening for the recirculation valves at which the cranking period and HC emissions are minimum; any further increase in the amount of gases recirculated has an opposite effect. Since the fuel vapor in CGR is expected to enhance the autoignition process, it became important to find out the role of the partial oxidation products at different rates of fuel injection on autoignition and combustion. This has been achieved by diesel cycle simulation.

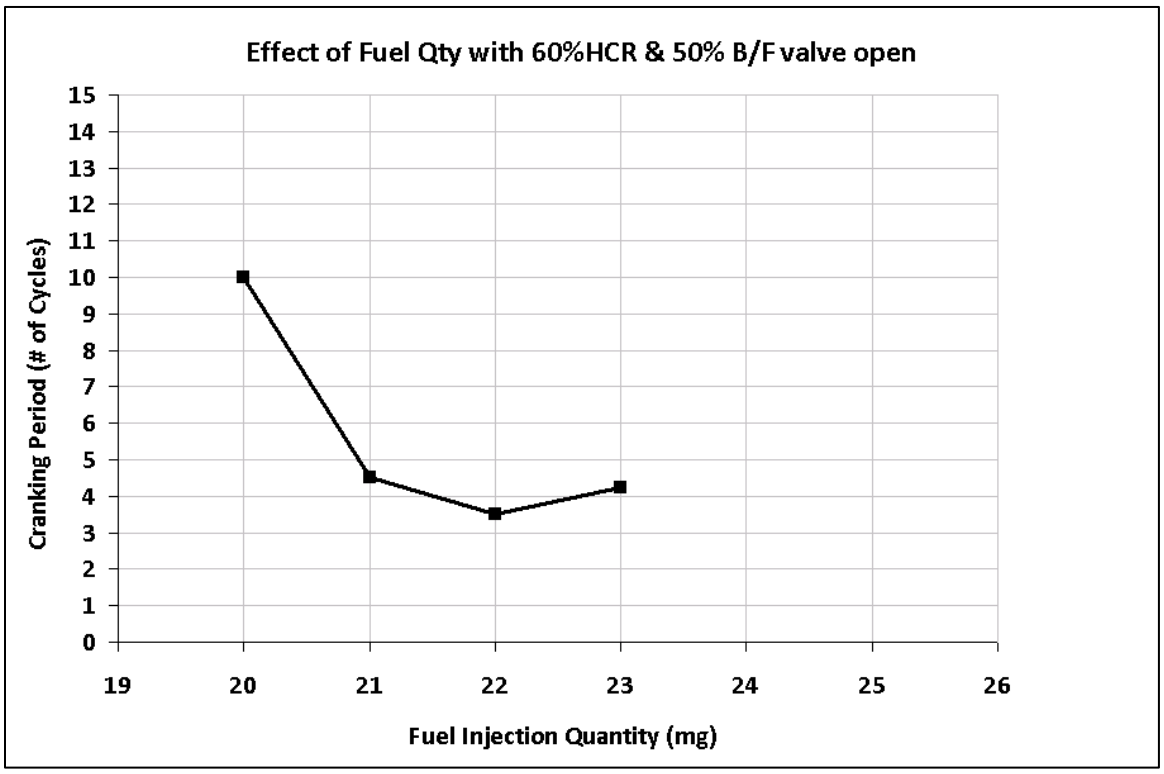

Figure 3.10.a - Effect of different fuel quantity (20, 21, 22, 23 & 24 mg/stroke/ 12°BTDC) on cranking period with 60% CGR and 50% BF valve close during cold start. T_{amb}:16 °C.

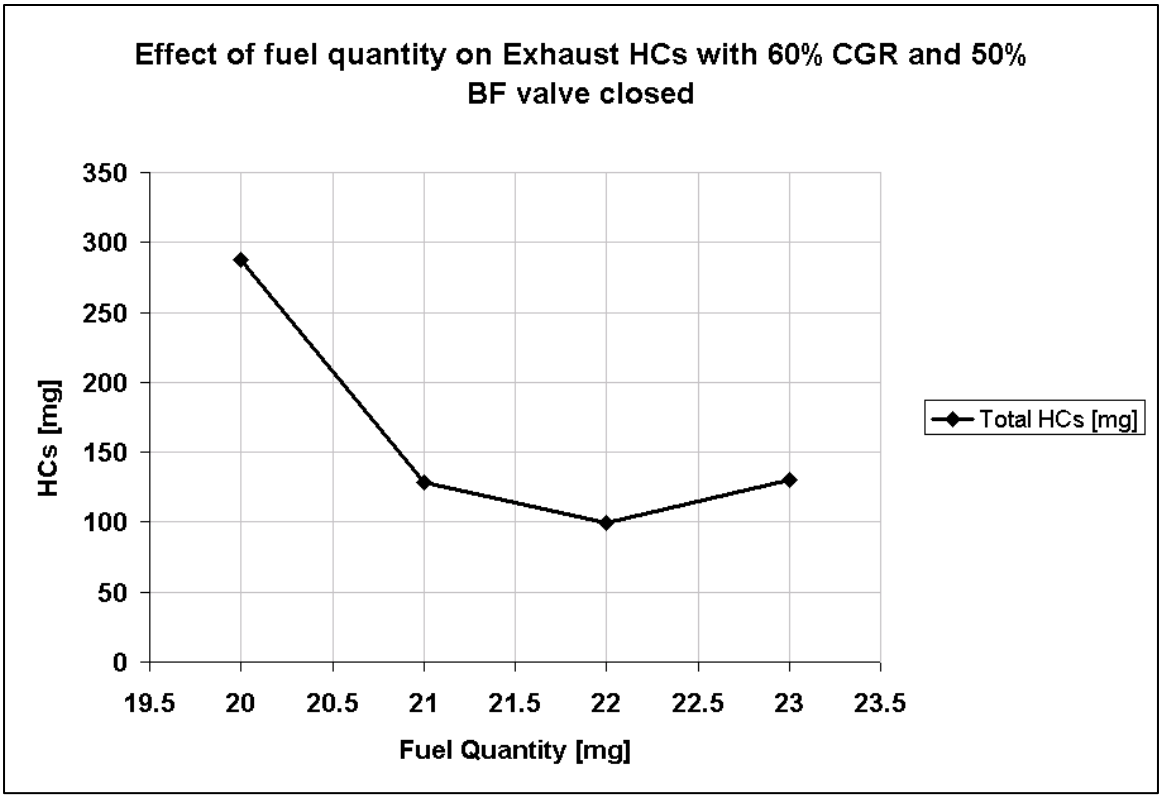

Figure 3.10.b - Effect of different fuel quantity (20, 21, 22, 23 & 24 mg/stroke/ 12°BTDC) on HC with 60% CGR and 50% BF valve close during cold start. T_{amb}:16 °C.

CHAPTER 4

SIMULATION RESULTS AND DISCUSSIONS

4.1 Introduction

In order to understand the behavior of recirculated gases, two approaches are taken to simulate the effect of adding hydrocarbons species and formaldehyde (HCHO) gases to the fresh charge on the ignition delay and combustion during starting of the DIATA direct injection diesel engine. In the first one the charge is heterogeneous and homogeneous in the second one. The study has been carried at different equivalence ratios and concentrations.

Table 4.1 shows the specifications of the DIATA diesel engine.

Table 4.1 – DIATA engine specifications:

No. of Cylinders	4
Working Cycle	Four Stroke Diesel
Firing Order	1-3-4-2
No. of Valves	16
Displacement	1.2 liters
Bore x Stroke	70 x 78 mm
Max BMEP	16 Bar
Compression Ratio	19.5 : 1
Fuel system	Direct Injected Common
Air system	Inter cooled, EGR, VGT
Configuration	Injectors centered
Piston Bowl Shape	Mexican Hat
Number of Spray Holes	6
Spray Hole Diameter (mm)	0.124
Cone Angle	150°

4.2 Heterogeneous Charge

A preliminary study of the effect of some HCs species and HCHO with different mole fractions on ignition delay at 25 mg/stroke has been investigated using a CFD code combined with a chemical kinetic model. This cycle simulation is closer to the real engine conditions than the model which will be explained in the next section of this dissertation. The CFD model using STAR-CD's pro-STAR and es-ice coupled with chemical kinetics model using DARS-CFD is used in the cycle simulation of DIATA engine. The Mexican hat bowl shape, no swirl and the 6 holes injector with 0.124mm hole diameter and 150 degrees cone angle were taken into consideration as mentioned in table 4.1.

"es-ice" is designed to facilitate moving-grid, transient analysis of internal combustion engines and is used in conjunction with STAR-CD's pro-STAR. After the model and solution control parameter set-up is completed in pro-STAR, the CFD calculations are performed by the STAR solver and the results displayed and analyzed via pro-STAR.

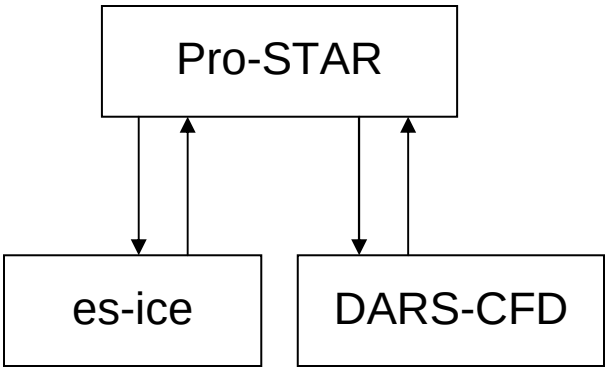

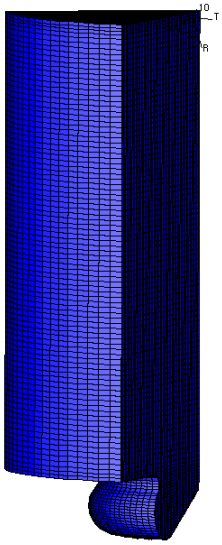

The following assumptions and approaches have been used for the CFD model:

1- 33 species reduced n-Heptane mechanism for the chemical kinetic model

2- No blow-by.

3- Reitz model for droplet break-up

4- Bai model for droplet-wall interaction

5- Huh model for atomization

6- The temperatures of the combustion dome regions, piston crown regions and cylinder wall regions are assumed constants

4.2.1 Effect of adding three different concentrations of HCHO to the intake charge on ignition delay at 25 mg/stroke fuel injected using CFD simulation.

Three different HCHO concentrations have been studied. Figure 4.1 shows the retarding effect on autoignition from 8 CAD to 20 CAD caused by increasing the HCHO concentration from 0 to 150. The increase in ignition delay can help in explaining the longer cranking period that happens with increasing the CGR%.

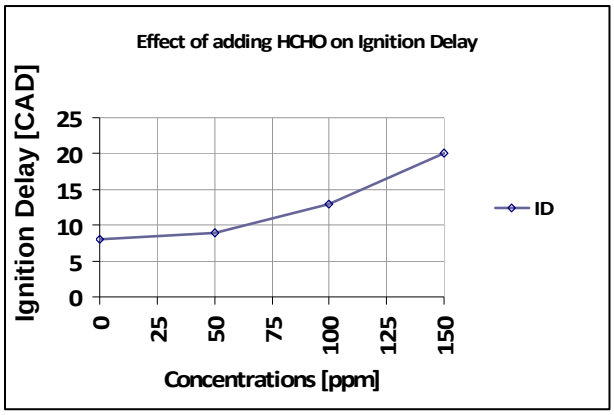

Figure 4.1- Effect of adding HCHO on ignition delay at 25 mg/stroke injection.

4.2.2 Effect of adding different HCs with different concentrations to the intake charge on ignition delay at 25 mg/stroke fuel injected using CFD simulation.

Also some HCs species have been added to check their effects on ignition delay. Since each run takes from seven to ten days using two processors computer, a few cycle simulations were conducted to show the effects of different hydrocarbons on ID.

Table 4.2 shows that adding CH2 has an enhancing effect on the autoignition process. The ignition delay decreases from 8 to 6 CAD as the CH2 mole fraction increases from 0 to 150 ppm. Meanwhile C2H4 has a retarding effect on autoignition where ID increased by 2 CAD as its mole fraction increased from 0 to 150 ppm.

The results of adding C3H4, given in table 4.3, show adding 150 ppm to 1000 ppm of C3H4 has no effect on ignition delay. An additional 500 ppm of C3H4

increased ID by three CADs. Table 3 shows that some of the HCs species have no effect on ignition delay at low concentrations but a retarding effect at higher concentrations which agrees with the chemical kinetic model explained later in this dissertation.

Tables 4.2 and 4.3 show some HCs species and the effect of increasing their mole fractions on ignition delay, knowing that the base line ignition delay without any additives is 8 CAD.

Table 4.2 – Effect of adding 150 ppm HC species concentration on ignition delay.

HC specie	**Ignition Delay with 150 ppm**
No-additives	8 CAD
CH2	6 CAD
CH3	7 CAD
CH4	8 CAD
C2H4	10 CAD
C3H6	8 CAD
C3H7	8.7 CAD

Table 4.3 – Effect of adding 150, 1000 and 1500 ppm HC species concentration on ignition delay.

HC specie	**Ignition Delay with adding**			
	0 ppm	**150 ppm**	**1000 ppm**	**1500 ppm**
C3H4	8 CAD	8 CAD	8 CAD	11 CAD
C3H5	8 CAD	8 CAD	8 CAD	10 CAD

The detailed simulation results show that some species have an enhancing effect on autoignition while others have a retarding effect.

Due to the long processing time for each run, switching to faster software is necessary. The results of the faster software will be compared with trends found in the CFD model.

4.3 Homogeneous Charge

A Zero-D model is used in this simulation and does not account for variations in thermodynamics properties of the contents of the combustion chamber. The model with Chemkin was used just to investigate the chemical kinetic effects of

formaldehyde (HCHO) and some HCs species on the autoignition process during cold starting of the engine.

An HCCI model with DIATA dimensions is used for this simulation, assuming that all the fuel is injected in a vapor form. Woschni correlation is used for the heat transfer calculations with the walls at 300K. N-Heptane is used as the fuel and its widely accepted autoignition mechanism is applied [62]. During compression at 12° BTDC, n-heptane and HCHO are instantaneously added in an idealized injection, evaporation and mixing process. The gas kinetics calculations start at a cylinder gas pressure of 28 bar and temperature of 617K. The engine speed is kept at 200 rpm.

Clearly, such a model overlooks wall temperature distribution, spray evaporation, and the kinetic effects of fuel components other than n-heptane. Results from such a model may not reasonably be used to simulate conditions inside an engine. Nevertheless, the model provides useful insight to the effect of some HCs species and formaldehyde on autoignition and combustion and help in explaining some of the observations made during the cold start experiments in which the CGR (Cranking Gases Recirculation) technique was applied.

The calculation domain covered three equivalence ratios 0.8, 1.0 and 1.2 and a range of 0 to 900 ppm of the HCs and the HCHO species.

4.3.1 Effect of adding 0 to 900 ppm HCHO to the intake charge on ignition delay using Chemkin at different equivalence ratios.

The simulation covered a wide range of formaldehyde concentrations and their effects on the ignition delay at different equivalence ratios (0.8, 1 and 1.2) at 200 rpm were determined.

Figure 4.2 shows the effect of different equivalence (0.8, 1.0 and 1.2) ratios on ignition delay while adding different amounts of HCHO to the intake charge. It is obvious that for the same amount of HCHO added, the ignition delay increases as the equivalence ratio increases.

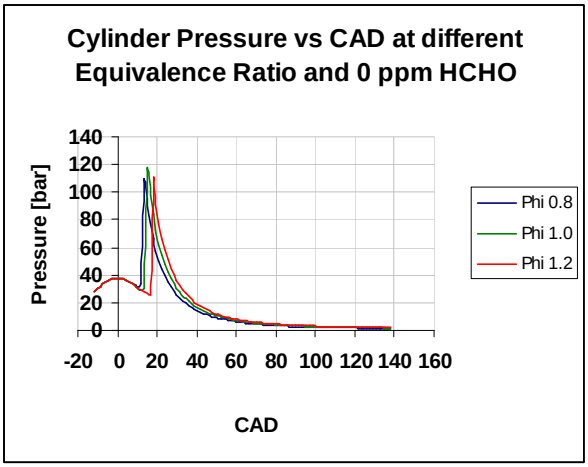

Figure 4.2.a - Gas pressure vs CAD at different equivalence ratios (0.8, 1.0 and 1.2) without adding HCHO.

The longer ignition delay trend is consistent while increasing the HCHO concentration to 100 ppm to the intake charge as shown in figure 4.2.b. As the equivalence ratio increases the ignition delay increases. Also by comparing

figure 4.2.b with 4.2.a it can be noticed that for the same equivalence ratio, the ignition delay increases as the amount of HCHO increases.

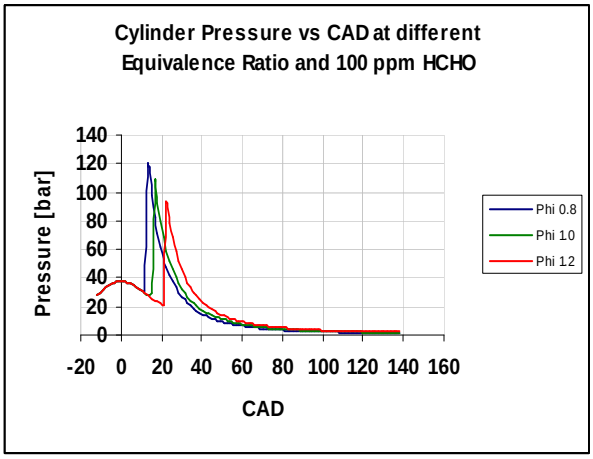

Figure 4.2.b - Gas pressure vs CAD at different equivalence ratios (0.8, 1.0 and 1.2) with adding 100ppm HCHO.

Figure 4.2.c shows that by increasing the HCHO up top 250, the combustion failed at equivalence ratio of 1.2. By increasing the amount of HCHO more to 300 ppm, the combustion failed at equivalence ratio of 1.0 as shown in figure 4.2.d.

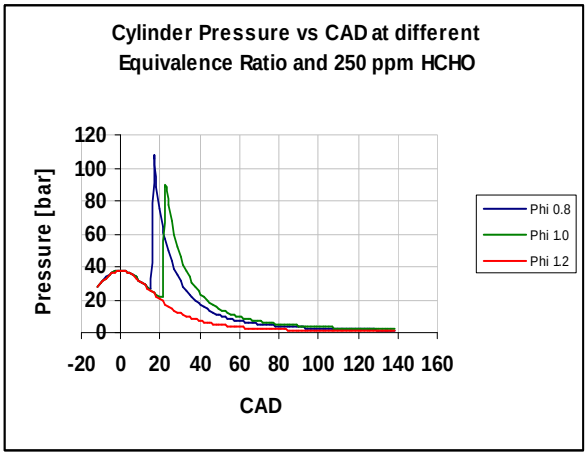

Figure 4.2.c - Gas pressure vs CAD at different equivalence ratios (0.8, 1.0 and 1.2) with adding 250ppm HCHO.

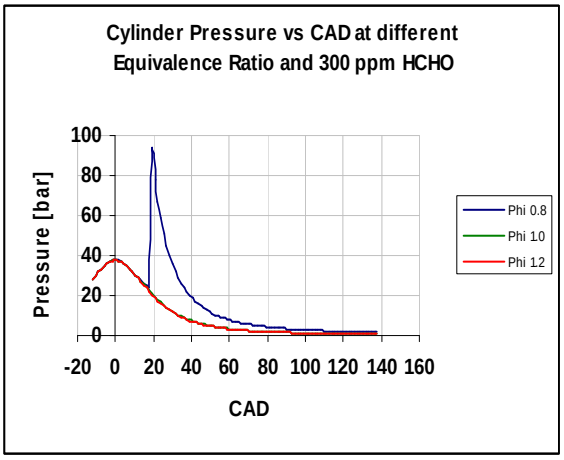

Figure 4.2.d - Gas pressure vs CAD at different equivalence ratios (0.8, 1.0 and 1.2) with adding 300ppm HCHO.

And finally the combustion failed at all equivalence ratios when the HCHO concentration reached 350 ppm as shown in figure 4.3.

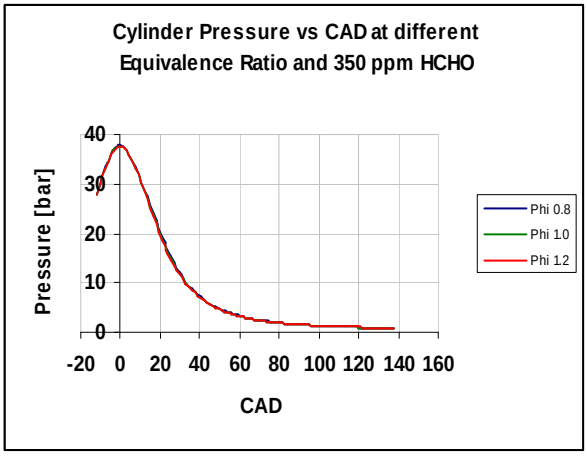

Figure 4.3 - Gas pressure vs CAD at different equivalence ratios (0.8, 1.0 and 1.2) with adding 350ppm HCHO.

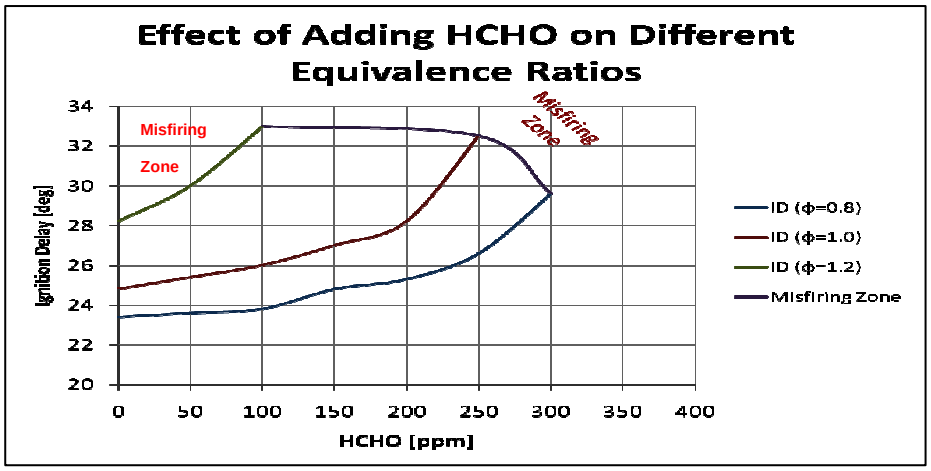

Figure 4.4 - Effect of adding HCHO on ignition delay at equivalence ratios of 0.8, 1.0 and 1.2.

Figure 4.4 shows the interrelationship between the equivalence ratio and HCHO mole fraction and their combined effect on the ignition delay period. At any HCHO mole fraction, increasing the equivalence ratio from 0.8 to1.2 increases the ignition delay period. At richer mixtures, misfiring occurs because combustion starts late in the expansion stroke. It is interesting to notice that leaner mixtures tolerate higher mole fractions of HCHO before misfiring takes place. It can be concluded from figure 4.4 that there is a trade off between the amount of HCHO added, which represent the rates of CGR, and fuel injection for minimum ignition delay.

The above results suggest that autoignition reactions are affected by the mole fractions of both the fuel vapor and aldehydes in the recirculated gases during cranking. This explains the trend shown in figure 6 where ID decreased as the

fuel delivery increased from 20 mg/stroke to 22 mg/stroke, after which ID increased again with fuel delivery of 23 mg/stroke.

4.3.2 Effect of adding 0 to 900 ppm of different species of HCs to the intake charge on ignition delay at different equivalence ratios.

The effects of the following HCs species on ignition delay have been studied. The HCs species are: C2H, C2H2, C2H3, C2H4, C2H5, C2H6, C3H2, C3H3, C3H6, C3H8, C4H10, C4H6, CH2, CH3, CH4 and C3H7.

Depending on the HCs species mole fractions, their effects on ignition delay can be categorized into 3 categories. First category contains HCs species that have enhancing effect on autoignition. Second category contains HCs species that have retarding effect on autignition. While the third category contains HCs species that have no effect on ignition delay.

Figure 4.5 shows the effect of increasing the mole fraction of C3H6 on the ignition delay. Increasing the C3H6 mole fraction from 0 to 400 ppm, caused the ignition delay to decrease from 25 CAD to 21 CAD at equivalence ratio of 1. A further increase to 900 ppm had no effect on the ignition delay at the three equivalence ratios. Also, the increase in equivalence ratio at any mole fraction of C3H6 causes ignition delay to increase. For instance the ignition delay increases from 20.5 to 22.5 as the equivalence ratio increases from 0.8 to 1.2 at 300 ppm C3H6. This might explain the experimental observations described earlier about the effect of low rates of CGR on reducing the cranking period by enhancing the autoignition reactions. At the same time, the longer cranking

periods observed at higher rates of CGR could be explained by the higher mole fractions of species such as C3H6 introduced at the higher rates of CGR.

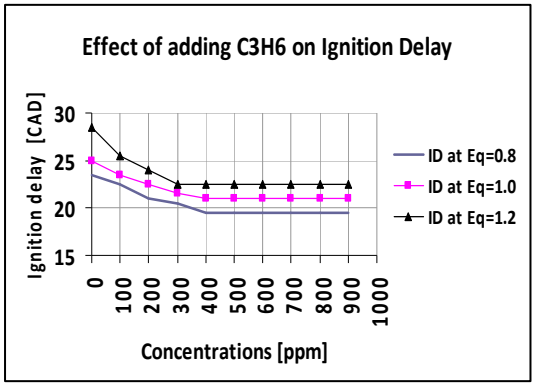

Figure 4.5 - Effect of adding C3H6 on ignition delay at equivalence ratios of 0.8, 1.0 and 1.2.

Figure 4.6 shows the effect of adding C2H6 on the ignition delay. The ignition delay increases from 25 CAD to 30 CAD as C2H6 increased from 0 to 900 ppm at equivalence ratio of 1. Also it can be noticed that alt lower concentrations, down to 300 ppm, there is no effect on ignition delay which can explain the experimental observation about the increase in the cranking period at the high flow rates of GCR. Figure 4.6 shows the increase in the equivalence ratio from 0.8 to 1.2 at any mole fraction of C3H6 increases the ignition delay period.

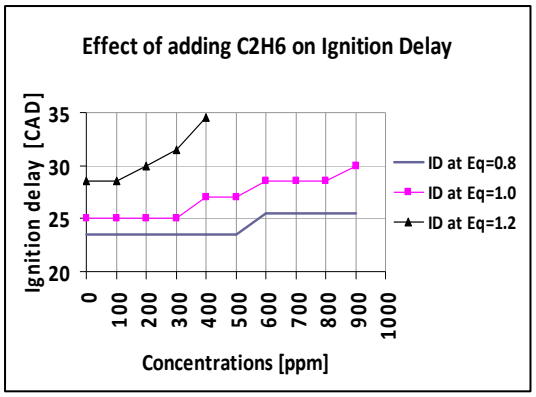

Figure 4.6 - Effect of adding C2H6 on ignition delay at equivalence ratios of 0.8, 1.0 and 1.2.

The results of adding C2H5, given in figure 4.7, show adding 100 ppm C2H5 reduced ID from 25 CAD to 11 CAD. An additional 100 ppm of C2H6 reduced ID by two CADs. Further increase in C3H6 has no effect on ID. Figure 4.7 shows that changing the equivalence ratio from 0.8 to 1.2 has a very minimal effect or almost no effect on ignition delay.

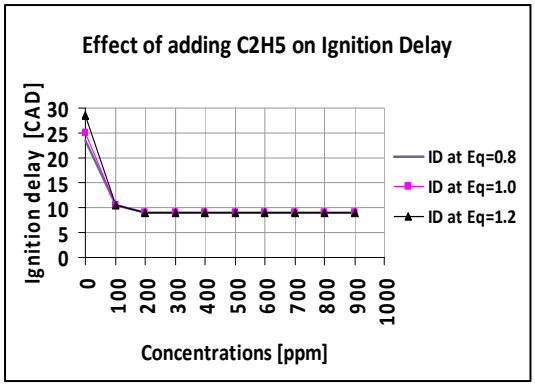

Figure 4.7 - Effect of adding C2H5 on ignition delay at equivalence ratios of 0.8, 1.0 and 1.2.

The effect of adding the following hydrocarbon species to the charge is shown in figure 4.8 at three equivalence ratios: C2H, C2H2, C2H3, C3H2, C3H3, CH2, CH3 and C3H7. It is noticed that these hydrocarbons enhance the autoignition reactions as evidenced for the shorter ID periods

Figure 4.9 shows the retarding effect and no effect on ignition delay of the following hydrocarbons at three equivalence ratios: C2H4, C3H8, C4H10, C4H6 and CH4.

The simulation results indicate that autoignition reactions are affected by the mole fractions of both the fuel vapor and aldehydes in the recirculated gases during cranking. At low concentrations the enhancing effect of HCs on ignition delay dominate over the retarding effect. But at higher concentrations most of the HCs species had no effect on ID, but some hydrocarbons slow down the autoignition reactions and increase ID. This in addition to the retarding effect of HCHO would have an impact on the autoignition reactions during the cranking period.

The simulation results explain the effect of increasing the equivalence ratio on the ignition delay period and the effect of injecting large amounts of fuels during cranking.

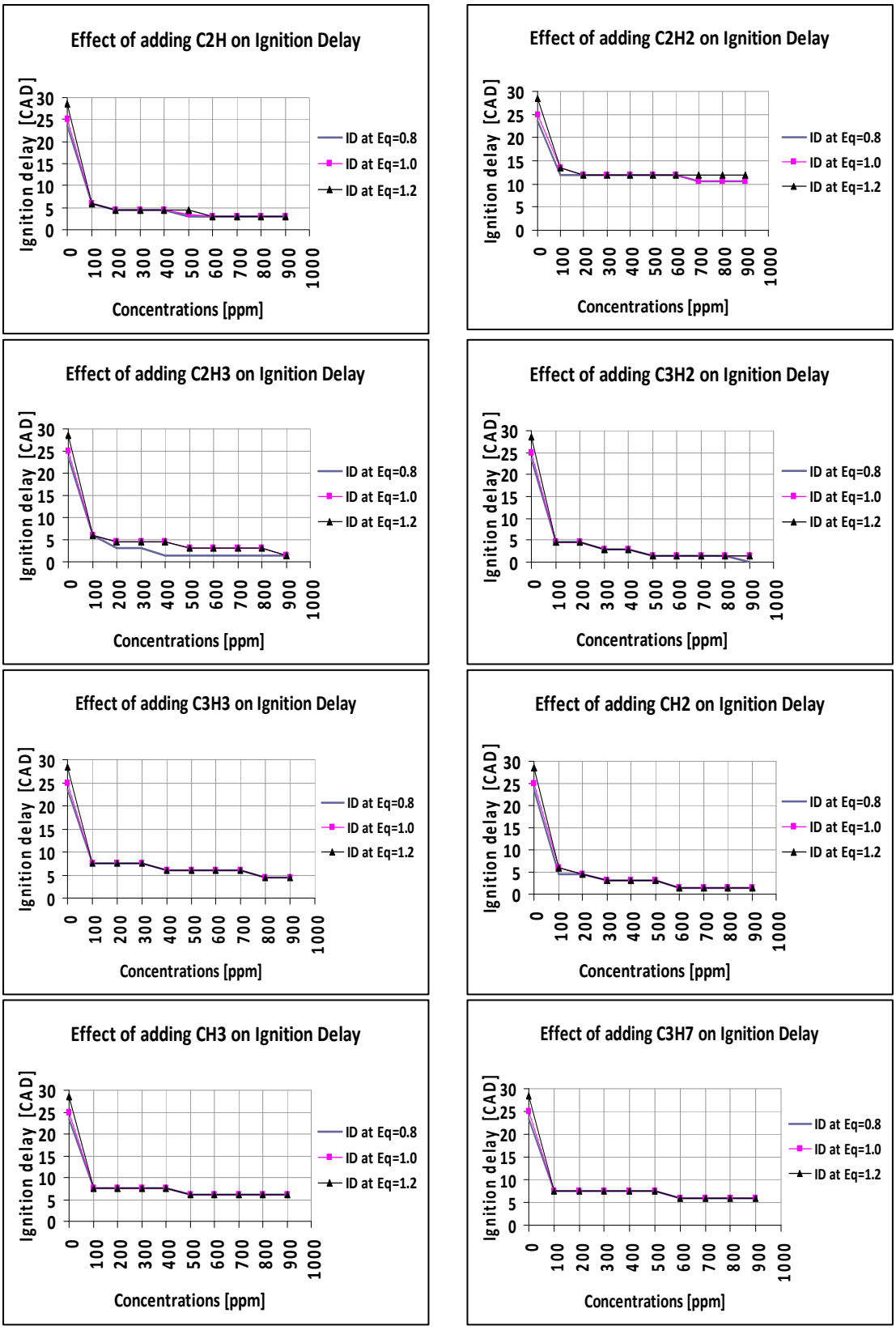

***Figure 4.8 - Effect of adding C2H, C2H2, C2H3, C3H2, C3H3, CH2, CH3 and C3H7 on ignition delay at equivalence* ratios of 0.8, 1.0 and 1.2.**

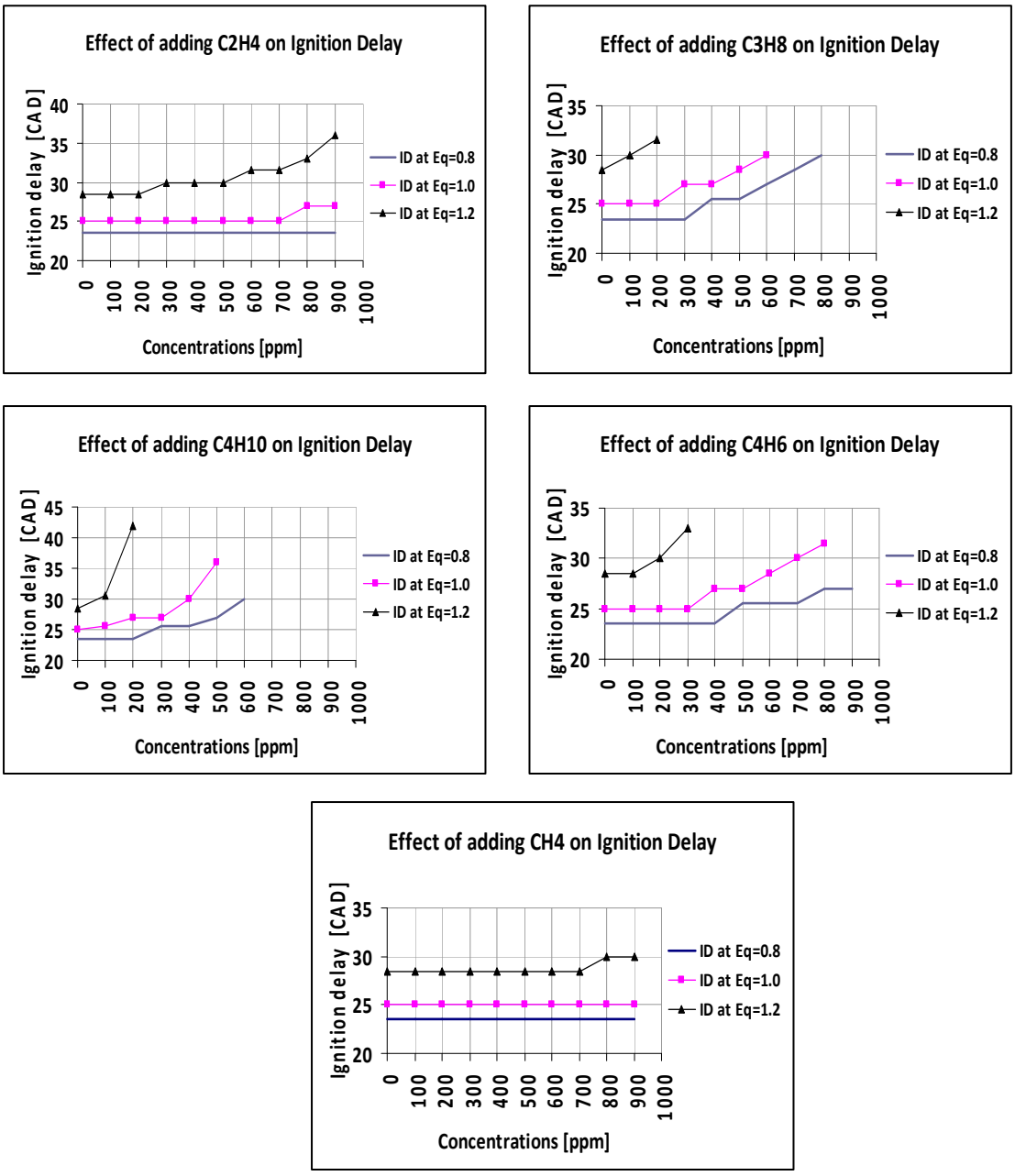

Figure 4.9 - Effect of adding C2H4, C3H8, C4H10, C4H6 and CH4 on ignition delay at equivalence ratios of 0.8, 1.0 and 1.2.

The results of the two levels of sophistication in diesel cycle simulation can explain the following experimental observations: a) at low species concentrations

which means low CGR% the enhancing effect on autoignition dominates and b) a higher species concentrations which means at higher CGR%, the retarding effect on autoignition dominates. This explains the trend shown in figure 5 where ID decreased as the CGR opening % increased from 0% to 20%, after which ID increased again with CGR opening percentage 40% and up.

4.4 Investigation of Ignition Delay.

The aim of this study is to a- determine the effect of temperature on ignition delay, b- determine the species that affect combustion the most, c- develop a new technique to determine if the engine will fire or misfire in a certain cycle, based on the concentration of some species at a certain time, d- investigation of the effect of added species to the intake on ignition delay and check the applicability of this new technique on it.

4.4.1 Effect of temperature on ignition delay.

During cold start of diesel engine, the temperature is one of the most important factors affecting the ignition delay. Figure 4.10 shows the pressure traces versus time as the cylinder gas temperatures at SOI at -12 BTDC decreased from 346 ℃ to 342 ℃. It is obvious that the ignition delay increased as the temperature decreased till the engine misfired at 343 ℃.

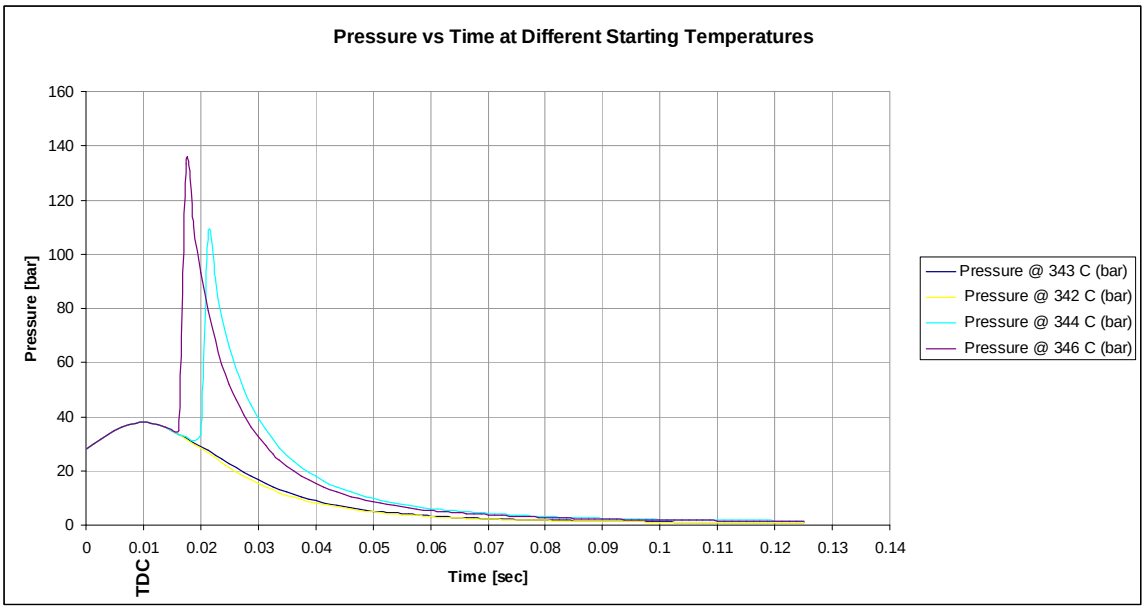

Figure 4.10 – Effect of different cylinder gas temperatures at SOI on ignition delay

4.4.2 Species that affect the start of combustion.

By examining the species that affect the start of combustion, two species were found to play a major role in whether the engine will fire or misfire. These species are H2O2 and HCHO. Figure 4.11.a and 4.11.b show the mole fractions of these two species at 344℃ at 343℃ respectively. By comparing figure 4.11.a and 4.11.b, it is clear that OH only appeared at 344 when the engine fired. It can also be noticed that in case of firing, H2O2 reached a much higher mole fractions earlier than in the case of misfiring. In the firing cycle, HCHO increased to a level higher than in the misfiring cycle, but decayed very quickly as H2O2 started to increase. In the firing cycle, as HCHO started to drop down to zero level, H2O2 dropped but OH started to rise at sharp rate. This is not the case in the misfiring

cycle, where HCHO reached a high level plateau while H2O2 increased at a very slow rate without forming OH as explained earlier.

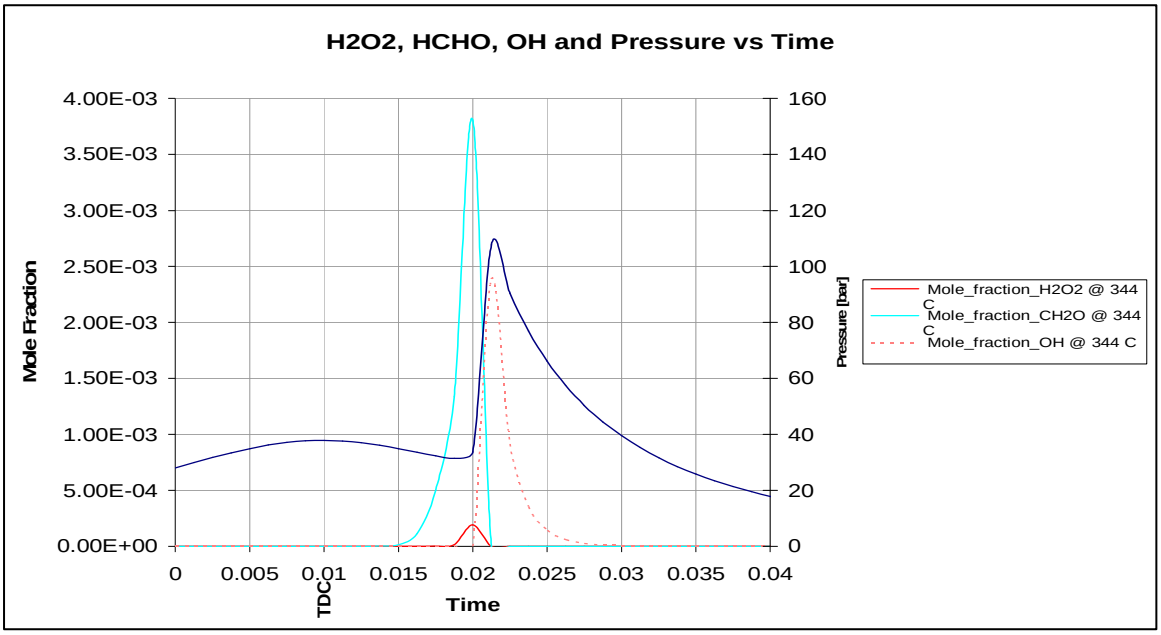

Figure 4.11.a – In-Cylinder pressure and the corresponding H2O2, HCHO, OH vs time at SOI temperature of 344 ℃

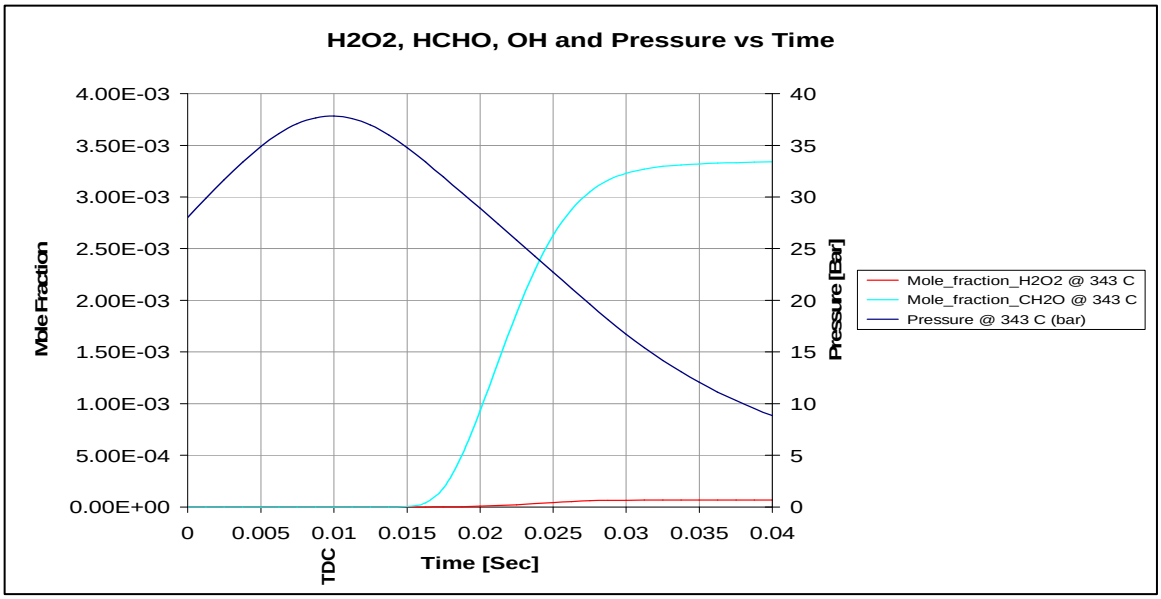

Figure 4.11.b – In-Cylinder pressure and the corresponding H2O2, HCHO, OH vs time at starting temperature of 343 ℃

The study of the H2O2 was necessary to show its variation with the cylinder gas temperature at SOI.

a) At 344℃ SOI temperature:

Using Chemkin reaction path analyzer, it was observed that the reaction most responsible for the production of H2O2 is H2O2+O2 <==> 2HO2, as shown in figure 4.12. The overall reaction moves in the backward direction to produce H2O2.

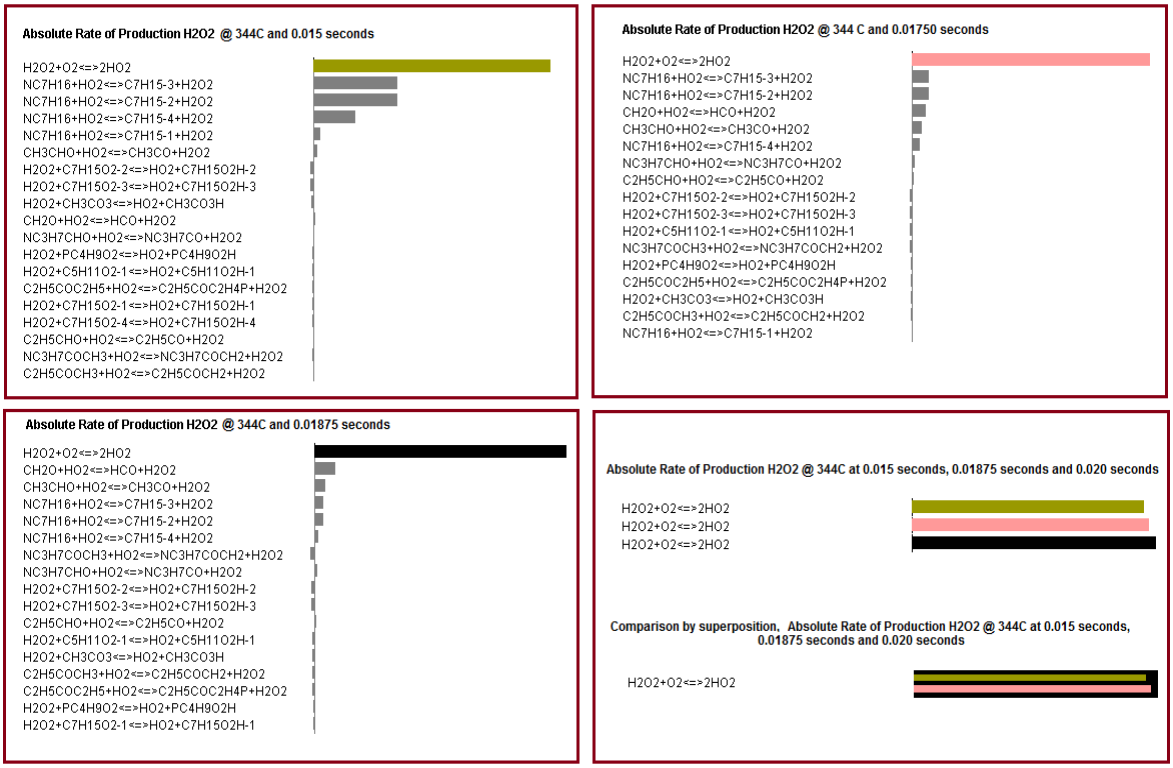

Figure 4.12 – Absolute rate of the reaction of H2O2 at starting temperature of 344 ℃

The calculated values of the rate of the reaction for this reaction at times 0.015 seconds, 0.01750 second and 0.01875 second are tabulated below. It should be noted that at 344C SOI temperature, combustion occurs at 0.01875 second.

Reaction : H2O2 + O2 <==> 2HO2		Rate of Forward Reaction	Rate of Backward Reaction	Absolute Rate of Production of H2O2
Starting Temperature	Time	Rf = Kf [H2O2] * [O2]	Rb = 2 Kb *[HO2]^2	Rb-Rf
344 C	0.015 sec	2.76E-14	2.21E-07	2.21E-07
	0.0175 sec	1.68E-13	3.92E-06	3.92E-06
	0.01875 sec	8.51E-13	1.63E-05	1.63E-05

b) At 343.5°C SOI temperature:

Considering the reaction H2O2+O2 <==> 2HO2, the calculated values of the rate of the reaction for this reaction at time 0.015second, 0.01750 second, 0.01875 second and 0.02125 second are tabulated below. At SOI temperature of 343.5C combustion occurs at 0.02125 second.

Reaction : H2O2 + O2 <==> 2HO2		Rate of Forward Reaction	Rate of Backward Reaction	Absolute Rate of Production of H2O2
Starting Temperature	Time	Rf = Kf [H2O2] * [O2]	Rb = 2 Kb *[HO2]^2	Rb-Rf
343.5 C	0.015 seconds	2.19E-14	1.65E-07	1.65E-07
	0.0175 seconds	8.00E-14	1.92E-06	1.92E-06
	0.01875 seconds	2.21E-13	5.30E-06	5.30E-06
	0.02125 seconds	5.98526E-12	8.06692E-05	8.0662E-05

c) At 343°C SOI Temperature

Considering the reaction H2O2+O2 <==> 2HO2, the calculated values of the rate of the reaction for this reaction at time 0.015 second, 0.01750 second, 0.01875 second, 0.02125 second and 0.03 second are tabulated below. At 343° C SOI temperature, the engine does not fire.

Reaction : H2O2 + O2 <==> 2HO2		Rate of Forward Reaction	Rate of Backward Reaction	Absolute Rate of Production of H2O2
Intake Temperature	Time	Rf = Kf [H2O2] * [O2]	Rb = 2 Kb *[HO2]^2	Rb-Rf
343	0.015 seconds	1.74856E-14	1.29222E-07	1.29E-07
	0.0175 seconds	4.22392E-14	9.61431E-07	9.61E-07
	0.01875 seconds	8.16253E-14	2.22266E-06	2.22E-06
	0.02125 seconds	2.20992E-13	5.22401E-06	5.22E-06
	0.03 seconds	4.60626E-14	1.18055E-06	1.18E-06

The change in temperature with time is shown in the figure 4.13.a. It is evident that the rise in temperature due to combustion is earlier as the SOI temperature is increased.

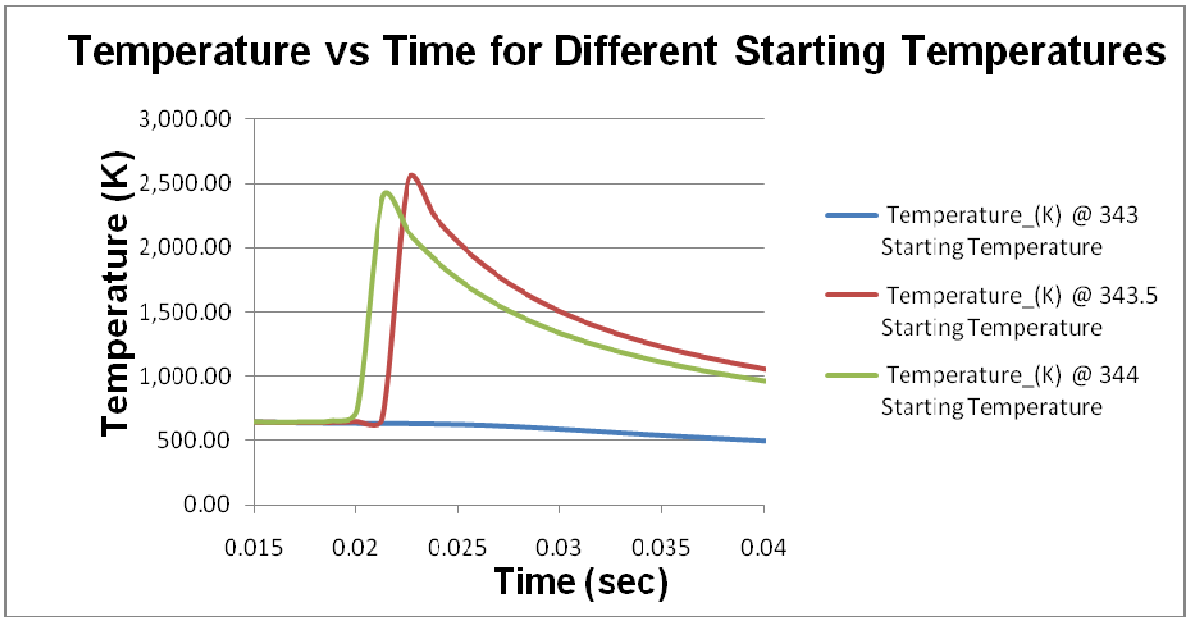

Figure 4.13.a -Temperature vs time at different SOI temperatures.

The change in pressure with time is shown in figure 4.13.b. It is evident that the rise in pressure due to combustion is earlier as the SOI temperature is increased.

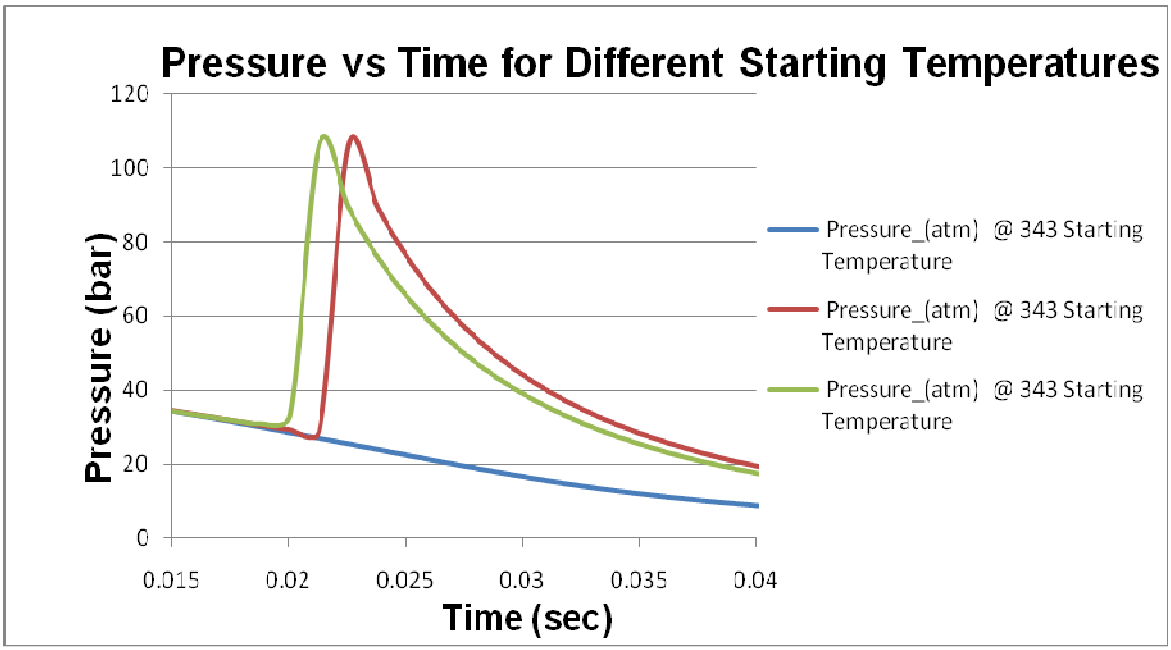

Figure 4.13.b - Pressure vs time at different SOI temperatures.

4.4.3 A new parameter to indicate if firing will occur in a cycle based on the ratio between HCHO and H2O2 mole fractions.

By taking a close look on these two species, it was found that the ratio of HCHO to H2O2 with the corresponding piston position is a parameter that can indicate whether the engine will fire or misfire. Figure 4.14 shows the pressure trace with the corresponding HCHO to H2O2 ratio at 344 ℃ when the engine fired. Figure 4.15 shows the ratio at 343 ℃ when the engine misfir ed.

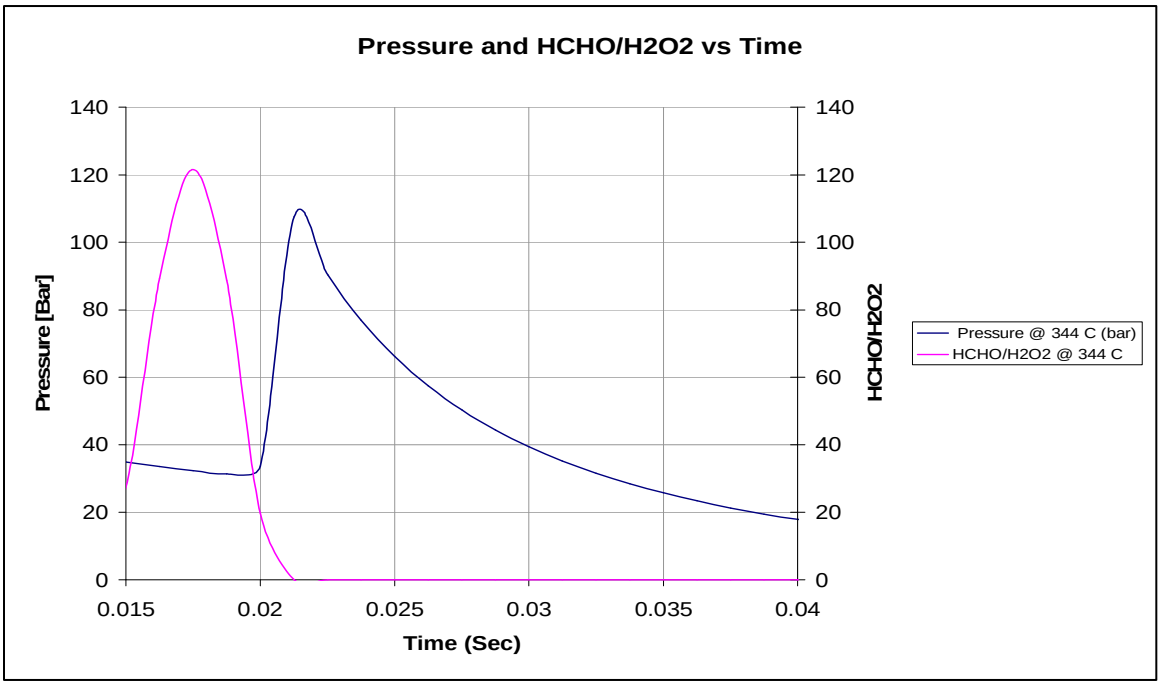

Figure 4.14 – In-Cylinder pressure and the corresponding HCHO/H2O2 vs time at SOI temperature of 344 ℃

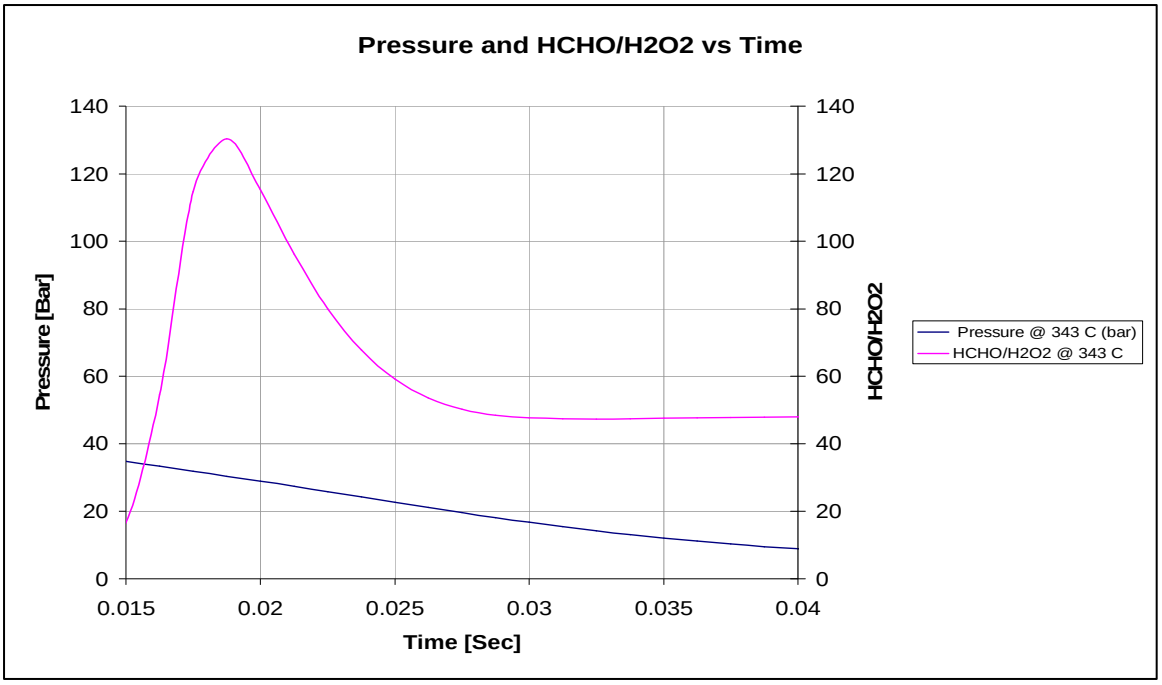

Figure 4.15 – In-Cylinder pressure and the corresponding HCHO/H2O2 vs time at SOI temperature of 343 ℃

It is clear that the ratio of HCHO to H2O2 is higher in the case of misfiring and lower in the case of firing. For instance, at time 0.02 sec the ratio of HCHO to H2O2 is 115.29 in the case of misfiring at 343 ℃ and the ratio is 20 in the case of firing at 344 ℃. By applying the same concept, it was found that as the temperature decreased from 344℃ to 343℃, the igniti on delay increased and the ratio of HCHO to H2O2 increased as shown in figure 4.16 for time 0.02 s. The same trend is observed at different times.

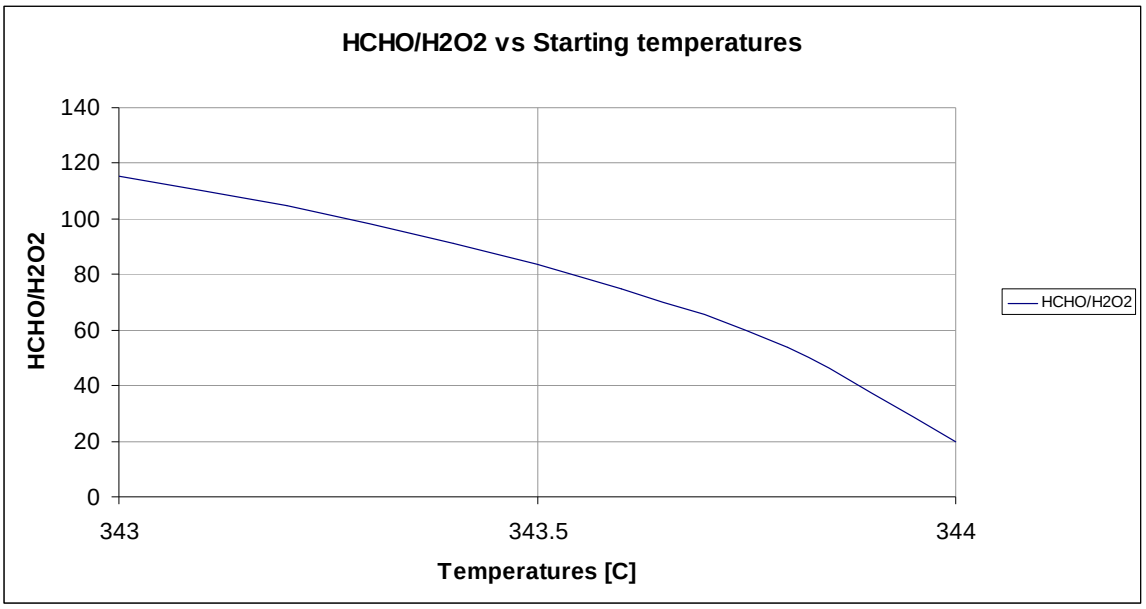

Figure 4.16 – Comparison between the HCHO/H2O2 at different SOI temperatures varying from 343 ℃ to 344 ℃

4.4.4 Effect of adding hydrocarbon species on ignition delay and applying the HCHO/H2O2 parameter to indicate if firing will occur.

For this investigation, two species Propane (C3H8) and Propene (C3H6) were chosen as two different cases as both these species were found to have opposite effects on ignition delay. This study was also based on the ratio of HCHO to H2O2 as discussed in section 4.4.3.

4.4.4.1 Effect of adding Propene (C3H6) on ID

It is observed that with the increase in mole fraction of C3H6 addition, the ratio of HCHO to H2O2 parameter decreases along with a reduction in the ignition delay as shown in figure 4.17.a and 4.17.b.

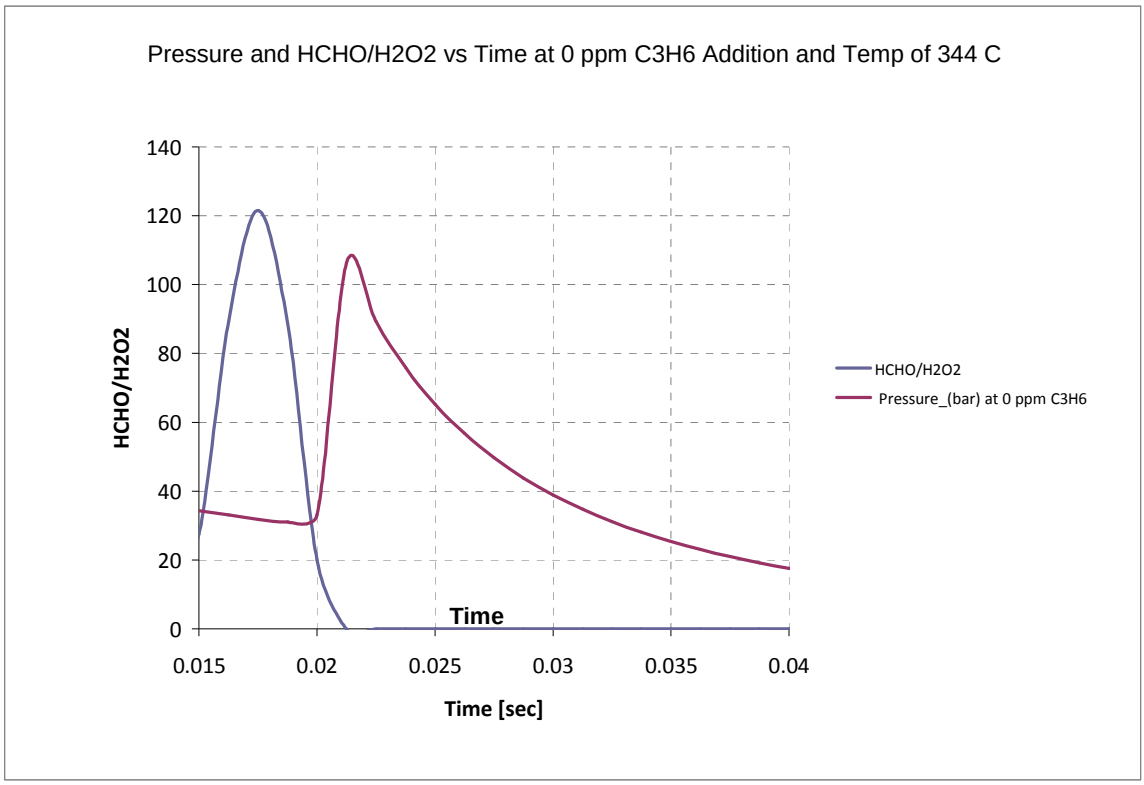

Figure 4.17.a - HCHO/H2O2 vs time without C3H6 addition.

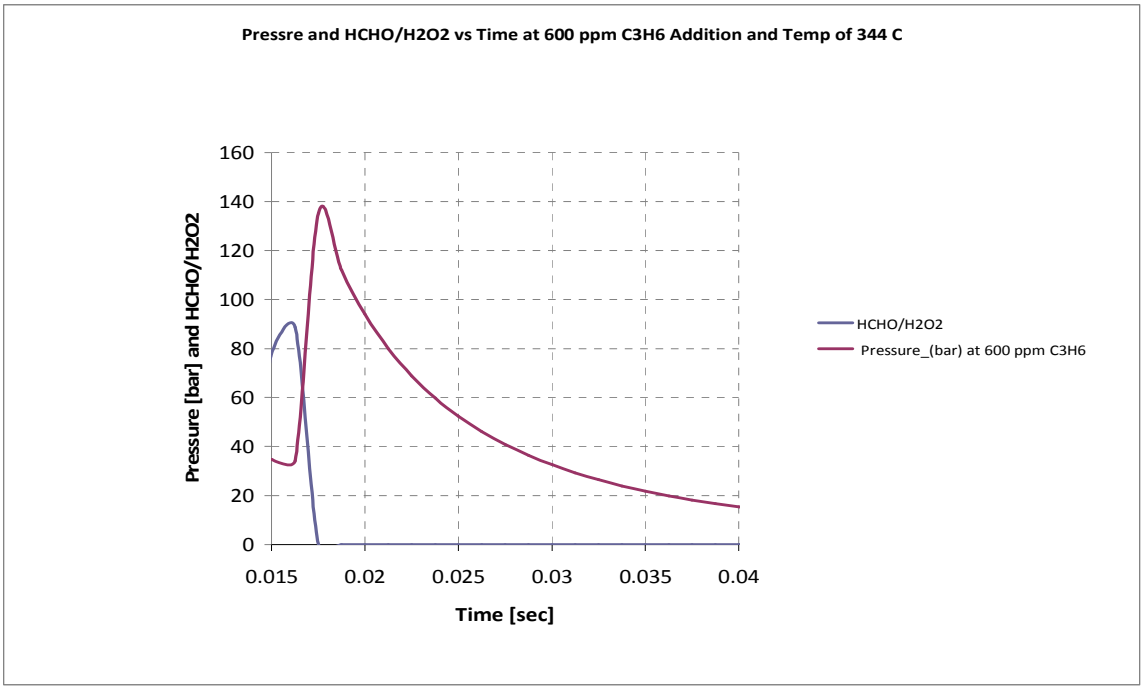

Figure 4.17.b - HCHO/H2O2 vs time with the addition of 600 ppm C3H6

Figure 4.18 shows the change in HCHO to H2O2 ratio with the addition of different Propene mole fractions. It can be noticed that the higher C3H6 addition, the lower HCHO/H2O2 at a certain time.

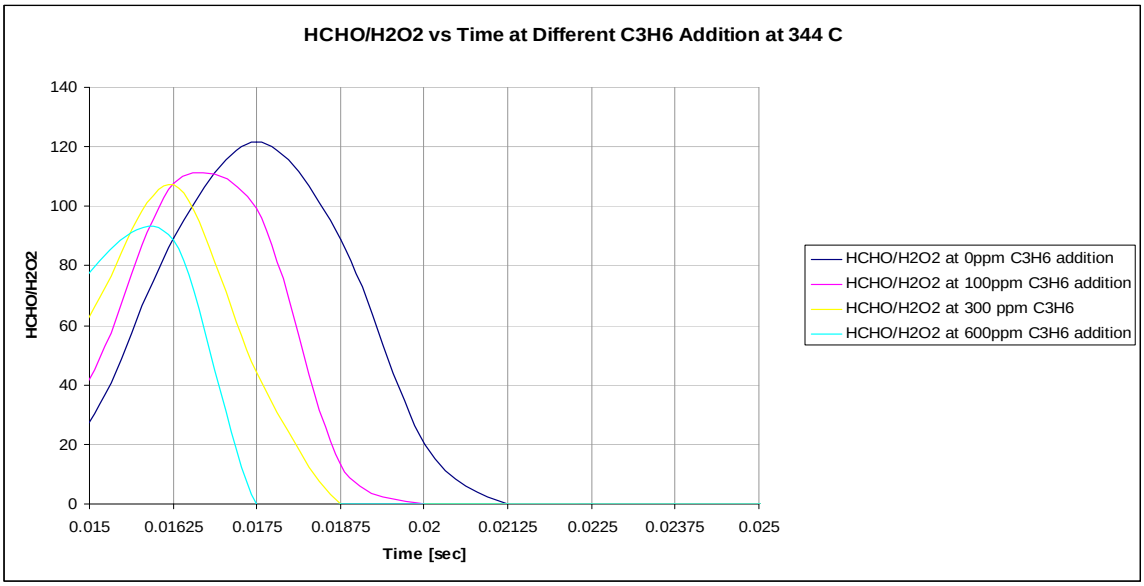

Figure 4.18 - Ratio of HCHO to H2O2 vs time at different C3H6 addition.

4.4.4.2 Effect of adding Propane (C3H8) on ID

From figure 4.19 and referring to figure 4.9 (C3H8 addition), it was evident that the addition of propane increases the ignition delay. With Zero ppm of propane, the ignition started at about 10.5 CAD ATDC. Increasing propane to 300ppm did not have a noticeable effect on ignition delay. At 400 ppm of propane addition, the ignition was retarded by 1.5 CAD. With 600ppm for propane addition, the ignition was further retarded by 1.5 CAD. Adding 900 ppm and higher ppm of propane caused the engine to misfire.

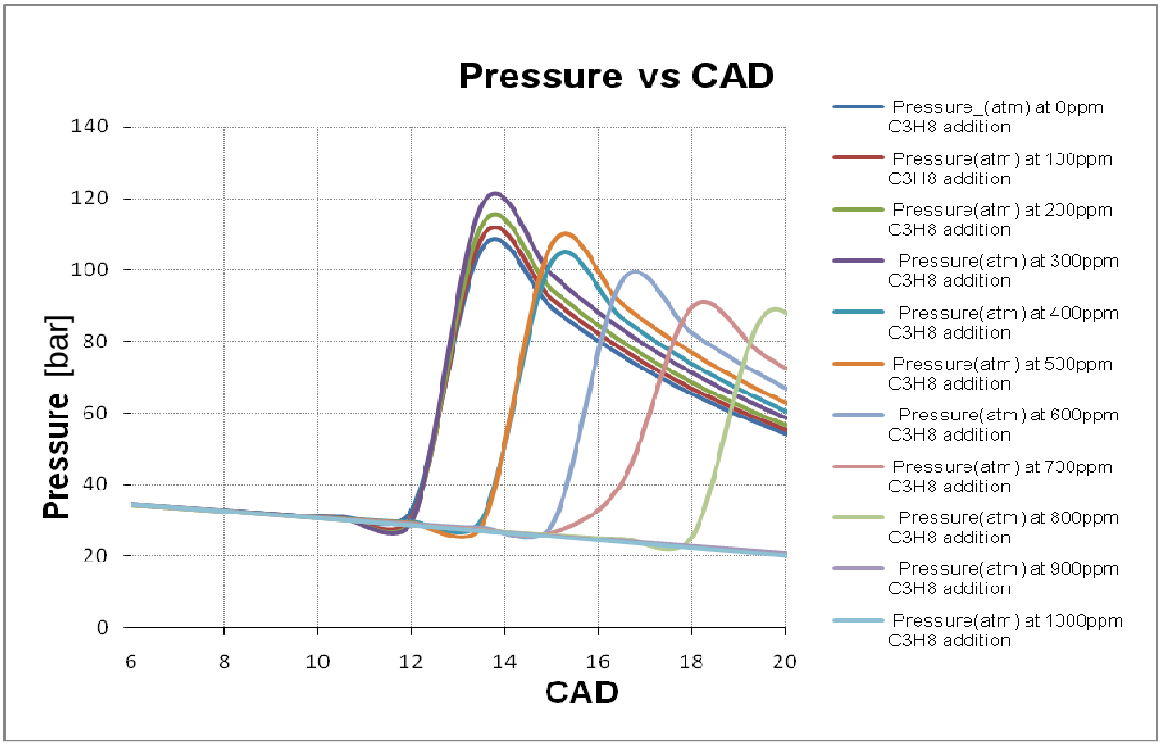

Figure 4.19 - Effect of Propane addition on Ignition Delay at Equivalence Ratio 1.0

Considering the ratio between HCHO and H2O2, figure 4.20.a, figure 4.20.b and figure 4.20.c show an increase in ratio of HCHO to H2O2 with the increase in the propane mole fraction. This follows the trend described in the case of propane addition and explains the increase in ignition delay observed in figure 4.9.

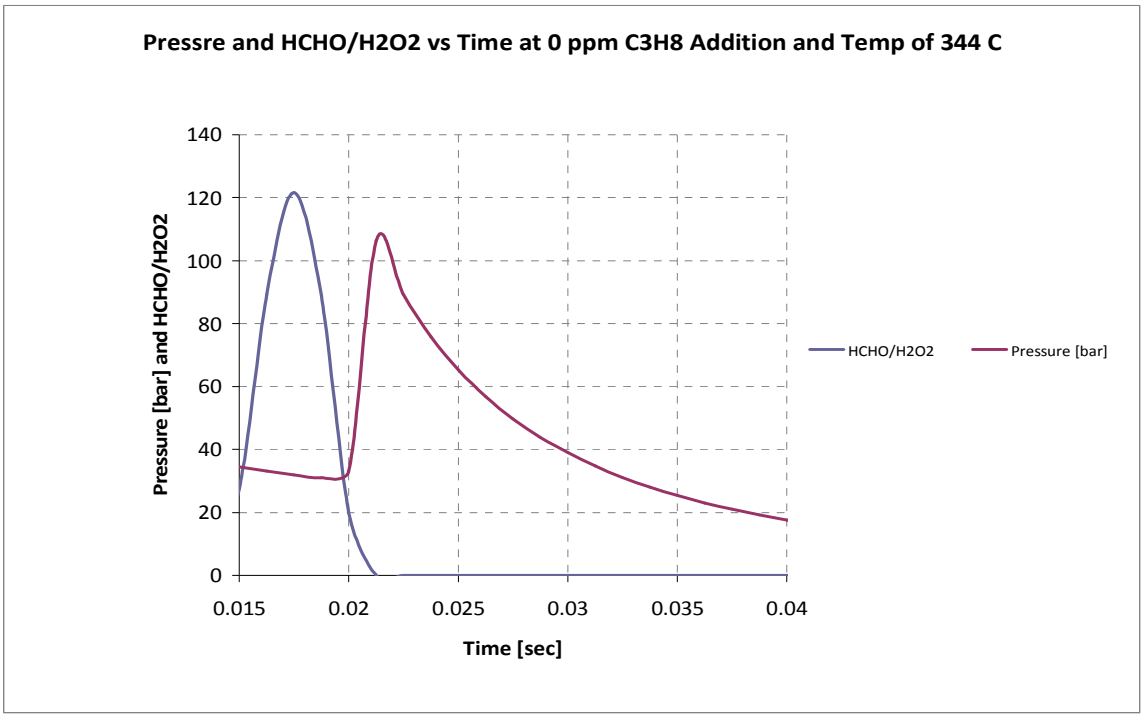

Figure 4.20.a - Ratio of HCHO to H2O2 vs time at 0 ppm C3H8 addition.

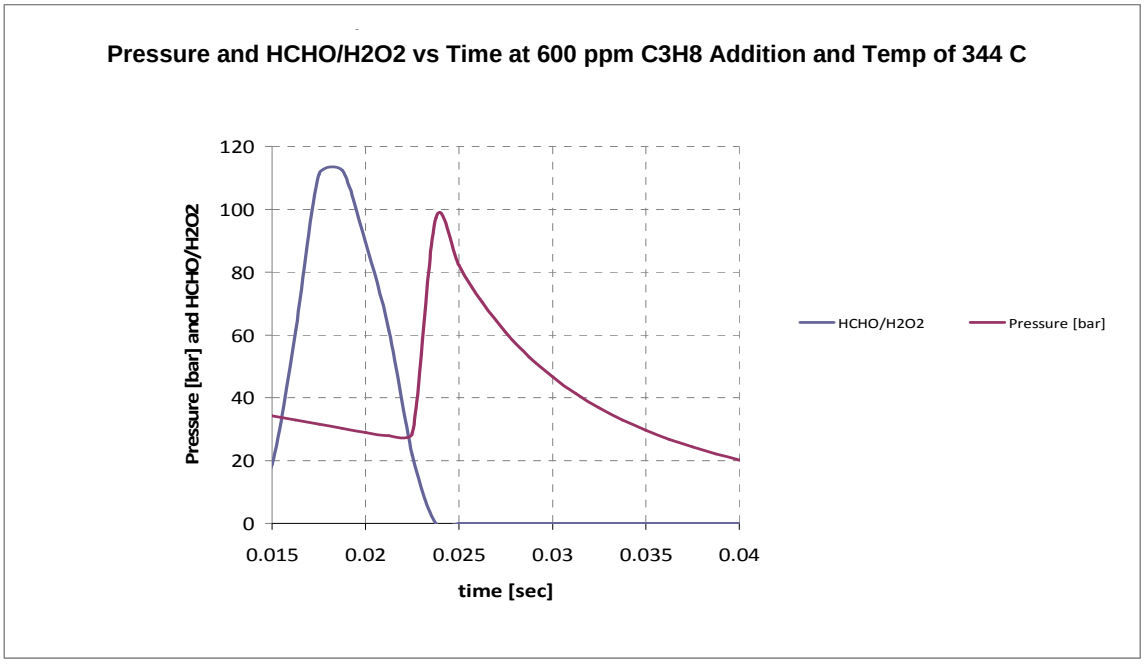

Figure 4.20.b - Ratio of HCHO to H2O2 vs time at 600 ppm C3H8 addition.

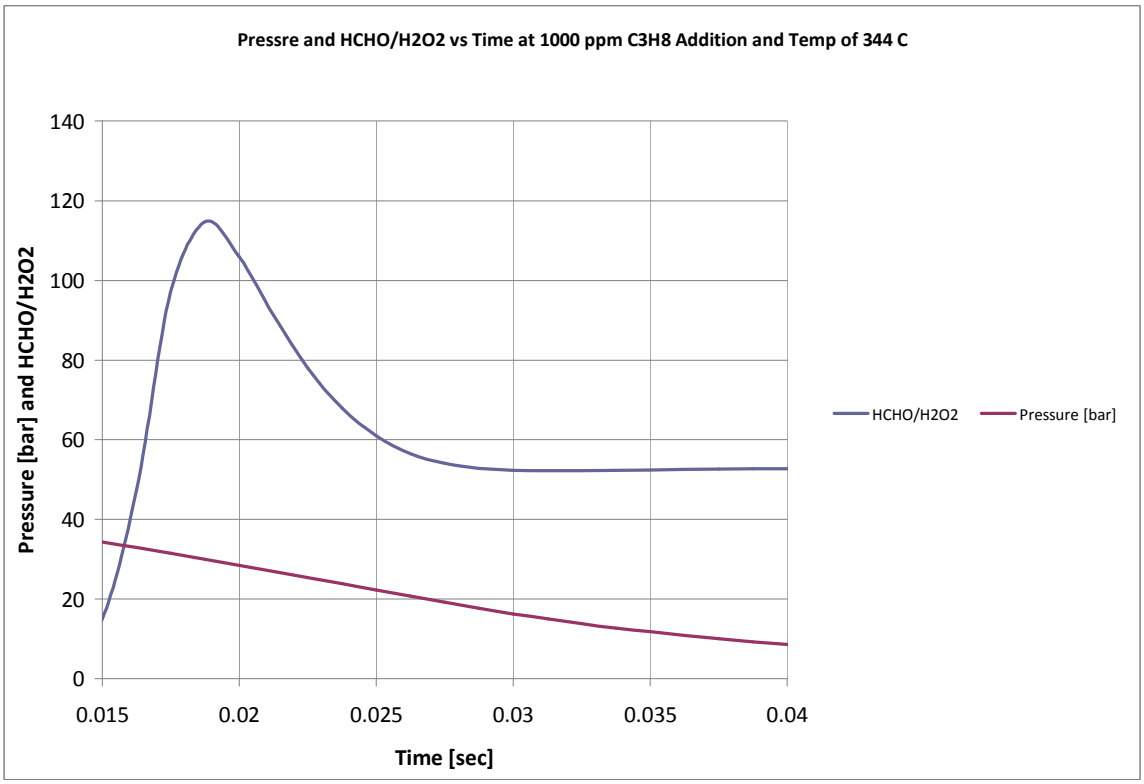

Figure 4.20.c - Ratio of HCHO to H2O2 vs time at 1000 ppm C3H8 addition.

4.4.5 Summary and conclusions

The above investigation indicates that the HCHO to H2O2 ratio is a useful parameter to predict whether the engine will fire or misfire. By analyzing the data of hundreds runs at different temperatures and mole fractions of added species it was found that the ratio of HCHO to H2O2 can be a useful parameter to detect if firing will occur. This parameter varies with time (or CAD) after injection. Figure 4.21 shows the firing and misfiring zones at different times with the corresponding CAD. The area above the curve represents the misfiring zone and the area below the curve represents the firing zone.

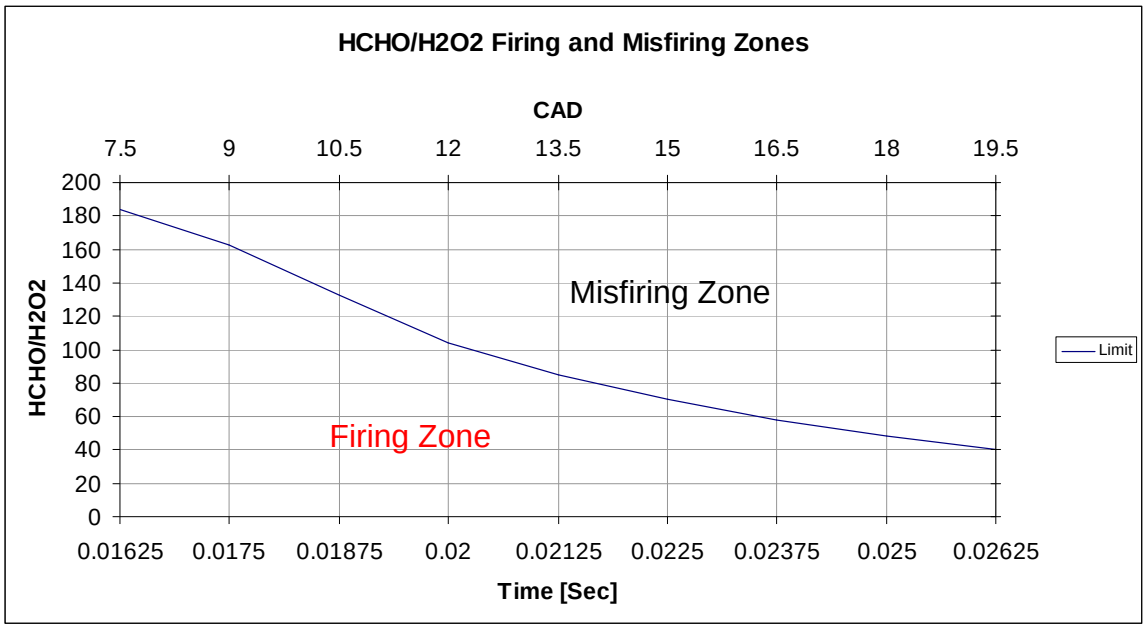

Figure 4.21 – Firing and Misfiring zones based on [HCHO / H2O2] parameter.

It should be noted that the HCHO/H2O2 ratio increases after the SOI, reaches a peak value, and drops back, whether the engine is firing or misfiring. The analysis of many cycles indicated that the engine never fires when the rate of

formation of HCHO is higher than the rate of formation of H2O2, causing their ratio to increase till it reaches the peak. Accordingly, the curve in figure 4.21 applies only to the time (CAD) when HCHO/H2O2 drops after its peak.

4.4.5.1 Check the applicability of firing and misfiring zones of HCHO/H2O2 graph on the cases of different concentrations of formaldehyde addition.

a) Without HCHO addition when the engine fired.

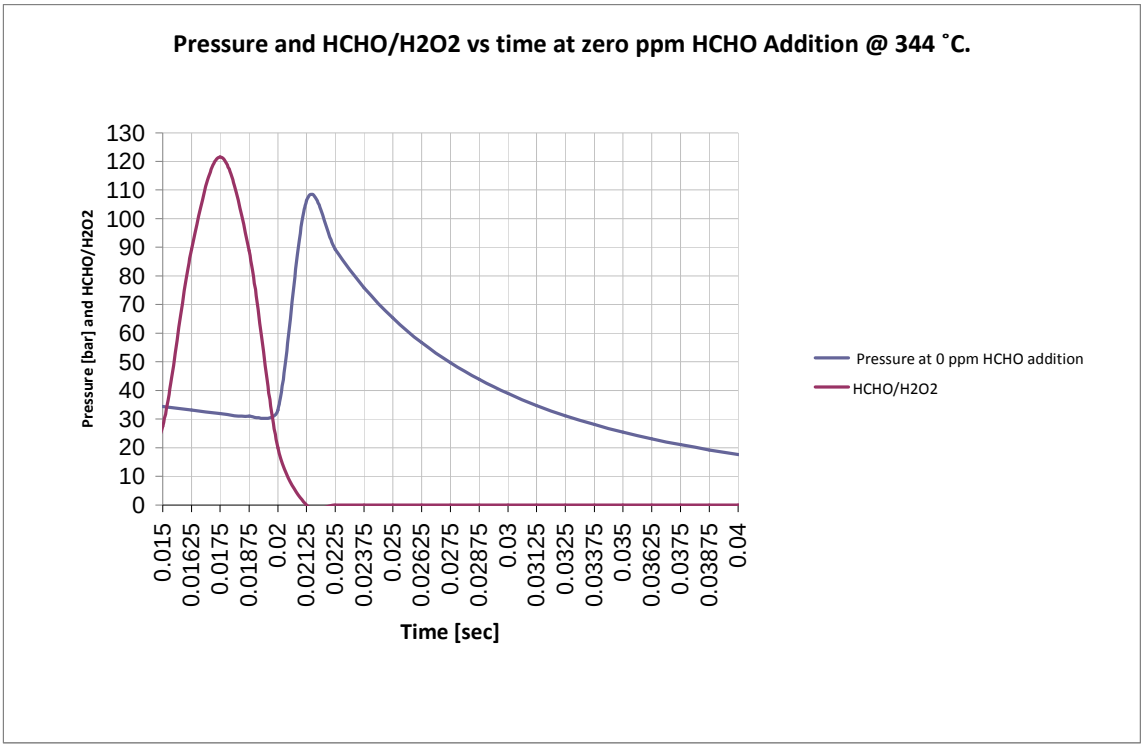

Figure 4.22 - Ratio of HCHO to H2O2 vs time at 0 ppm HCHO addition.

Figure 4.22 shows the HCHO/H2O2 and the pressure curve versus time in case of no formaldehyde addition.

For example: The value of HCHO/H2O2 at time 0.01875 is 88.8, this value is located in the firing zone of graph 4.21.

b) With 300 ppm HCHO addition when the engine fired.

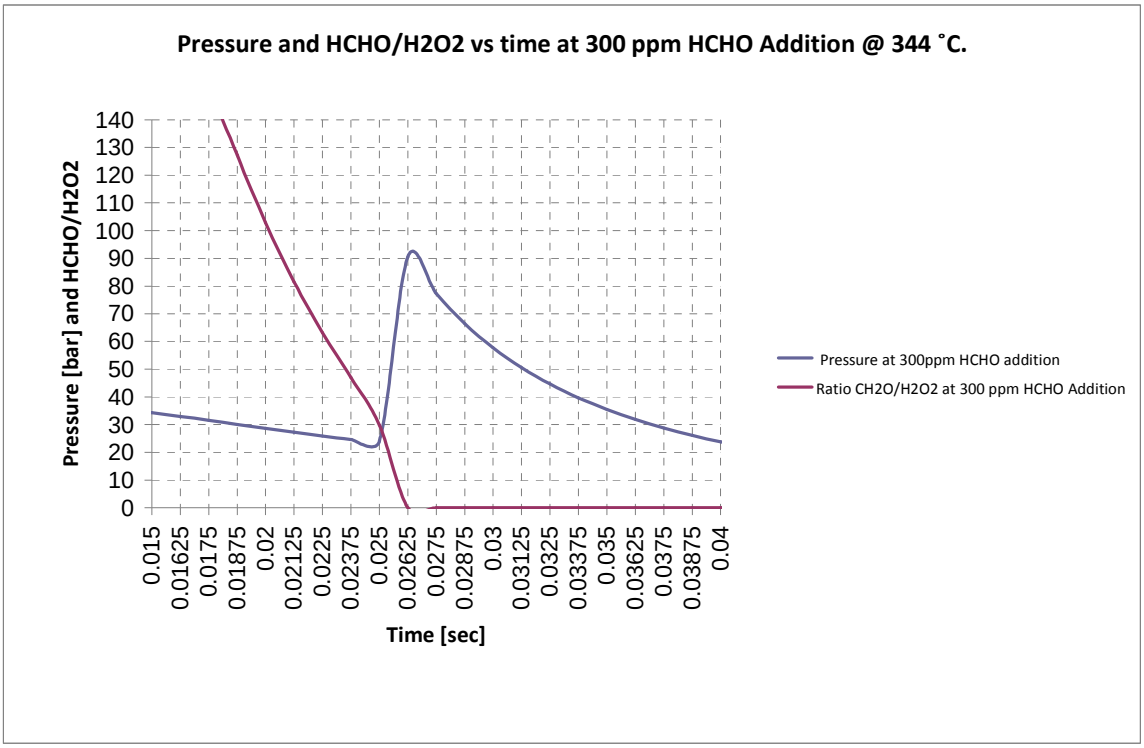

Figure 4.23 - Ratio of HCHO to H2O2 vs time at 300 ppm HCHO addition.

Figure 4.23 shows the HCHO/H2O2 ratio and the pressure trace versus time in case of 300 ppm formaldehyde addition.

The value of HCHO/H2O2 at time 0.02 is 103, which is located in the firing zone of graph 4.21 indicating engine firing

c) With 500 ppm HCHO addition when the engine misfired.

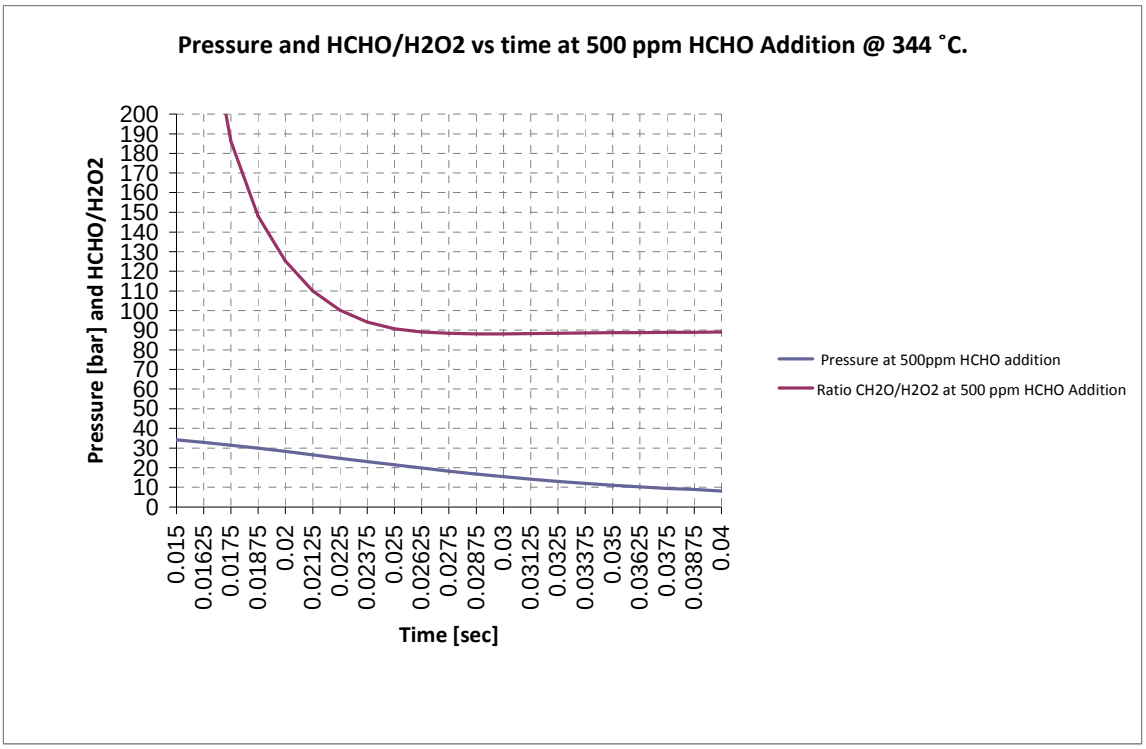

Figure 4.24 - Ratio of HCHO to H2O2 vs time at 500 ppm HCHO addition.

Figure 4.24 shows the HCHO/H2O2 ratio and the pressure trace versus time in case of 500 ppm formaldehyde addition.

The value of HCHO/H2O2 at time 0.0175 is 186, which is located in the misfiring zone of graph 4.21 indicating engine misfire.

From the above three cases, it can be concluded that the firing and misfiring zones of HCHO/H2O2 shown in figure 4.21 can be applied to a wide range to predict if the engine will fire or misfire.

4.5 Reaction Path Analysis for OH Formation and Ignition Delay with Formaldehyde addition:

This study was conducted to determine the effect of formaldehyde addition on the ignition delay. Ignition delay is defined as the time from the start of injection to the start of combustion. During the cold start of a diesel engine, ignition delay becomes a critical parameter in determining whether the engine will fire and accelerate to the idling speed or fail to start. Based on how low the ambient temperatures are, the engine take different cranking periods during the cold start to fire stably. During these cranking cycles, engine may misfire or completely fail to start. The exhaust at this stage mainly consists of fuel vapor and partially oxidized products such as formaldehyde. This leads to the production of white smoke emissions in addition to fuel wastage. Therefore, it is very important to understand the effect of different parameters on ignition delay in order to reduce the problems associated with start of diesel engines at low ambient temperatures. This work utilizes cycle simulation to investigate the effect of formaldehyde content of the recirculated gases on the ignition delay considering n-Heptane combustion mechanisms.

In a mixture of fuel (NC7H16) and air, HCHO was added successively in quantities of 100 ppm at each run. The values of pressure and temperature at SOI were kept constant at 28 bar and 344° C respectively, based on the experimental data. The DIATA engine specs are input to the program as shown in figure 4.25

The studies were conducted using the Chemical Kinetics Simulations by Chemkin Pro Release 15092.

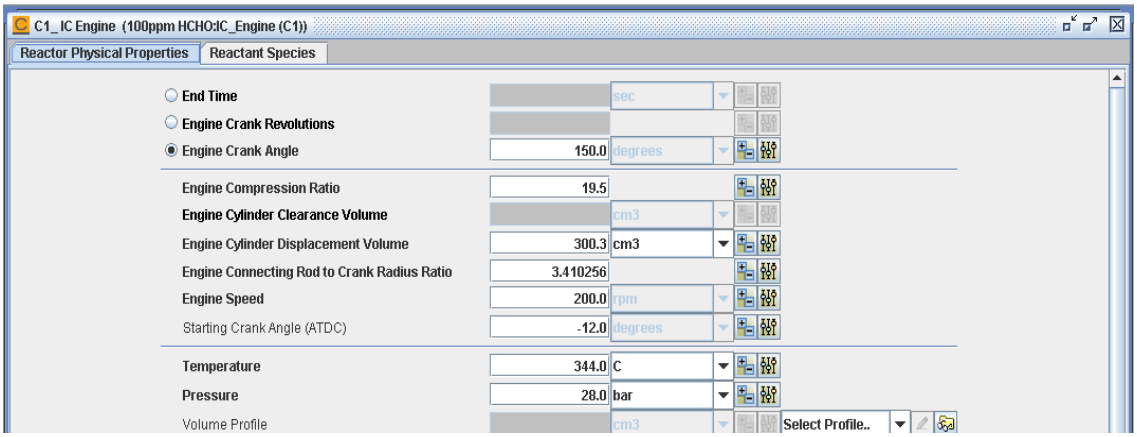

Figure 4.25 - DIATA Engine Specs

It was observed through reaction path analysis that fuel has maximum interaction with the OH radical. The rate of the reactions between fuel NC7H16 and the OH radical is much higher than the reaction between the fuel and any other species. The same is depicted in figure 4.26 below indicated by the length of the colored bars representing all OH and NC7H16 reactions. The direction of the colored bars representing fuel and OH reactions is towards the left of the reference line indicating the OH consumption and thus a forward reaction causing the fuel to breakdown to the species NC7H15-1, NC7H15-2, NC7H15-3 and NC7H15-4.

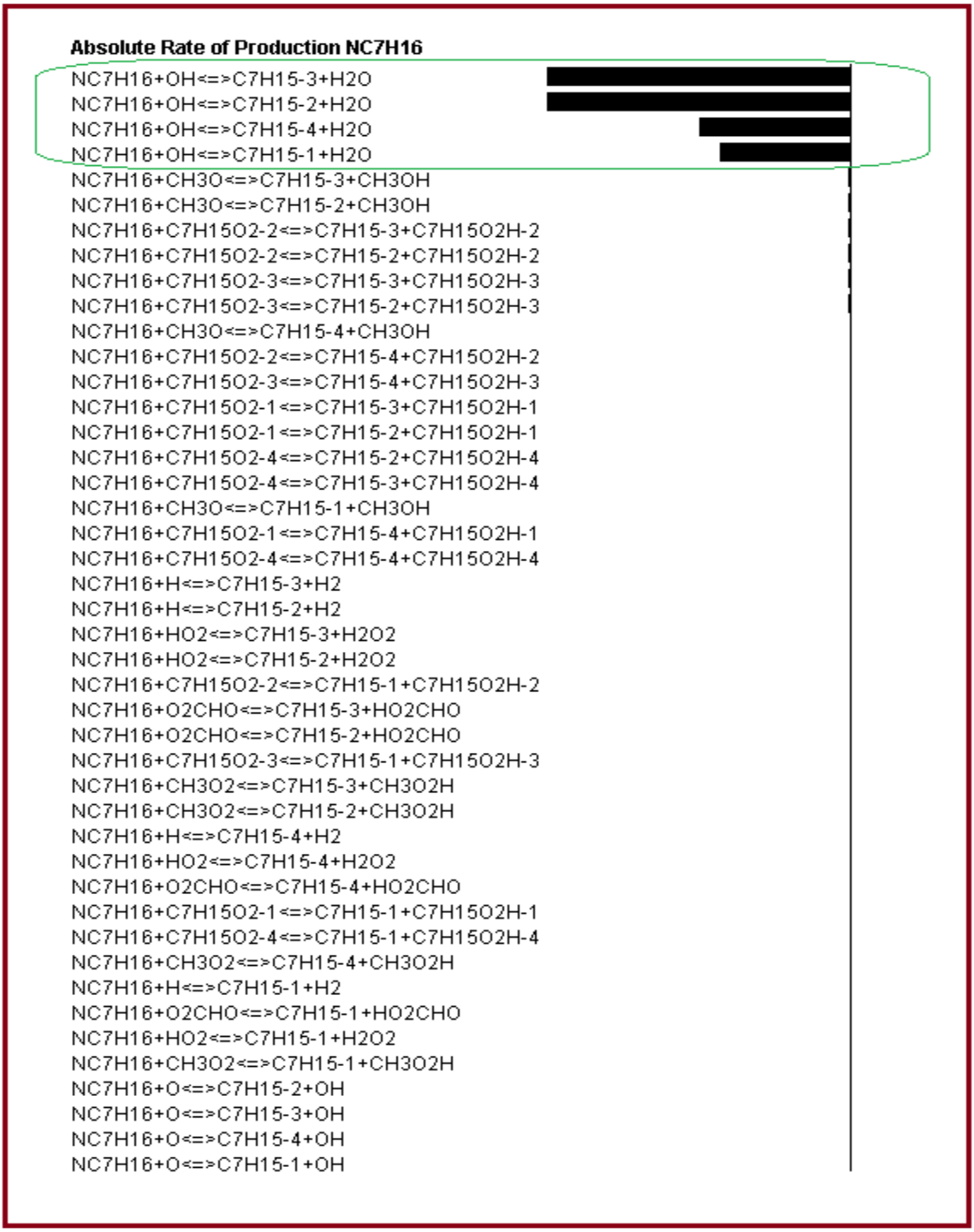

Figure 4.26- Reactions involving NC7H16.

The rate of consumption of the fuel by OH can be described by the following four reactions:

I. NC7H16 + OH <==> NC7H15-1 + H2O

II. NC7H16 + OH <==> NC7H15-2 + H2O
III. NC7H16 + OH <==> NC7H15-3 + H2O
IV. NC7H16 + OH <==> NC7H15-4 + H2O

Assuming Kf1, Kf2, Kf3 and Kf4 to be the forward reaction rate constants and Kb1, Kb2, Kb3 and Kb4 to be the backward reaction rate constants for reactions I, II, III, IV respectively. The rate of consumption of fuel by OH radical can be given by:

$$\frac{d[NC7H16]}{dt} = -\{K_{f1}[NC7H16][OH] + K_{f2}[NC7H16][OH] + K_{f3}[NC7H16][OH] + K_{f4}[NC7H16][OH]\} + \{K_{b1}[NC7H15\text{-}1][H2O] + K_{b2}[NC7H15\text{-}2][H2O] + K_{b3}[NC7H15\text{-}3][H2O] + K_{b4}[NC7H15\text{-}4][H2O]\}$$

Addition of formaldehyde was parameterized with an increment of 100 ppm in each successive run starting from 0 ppm to 1000 ppm.

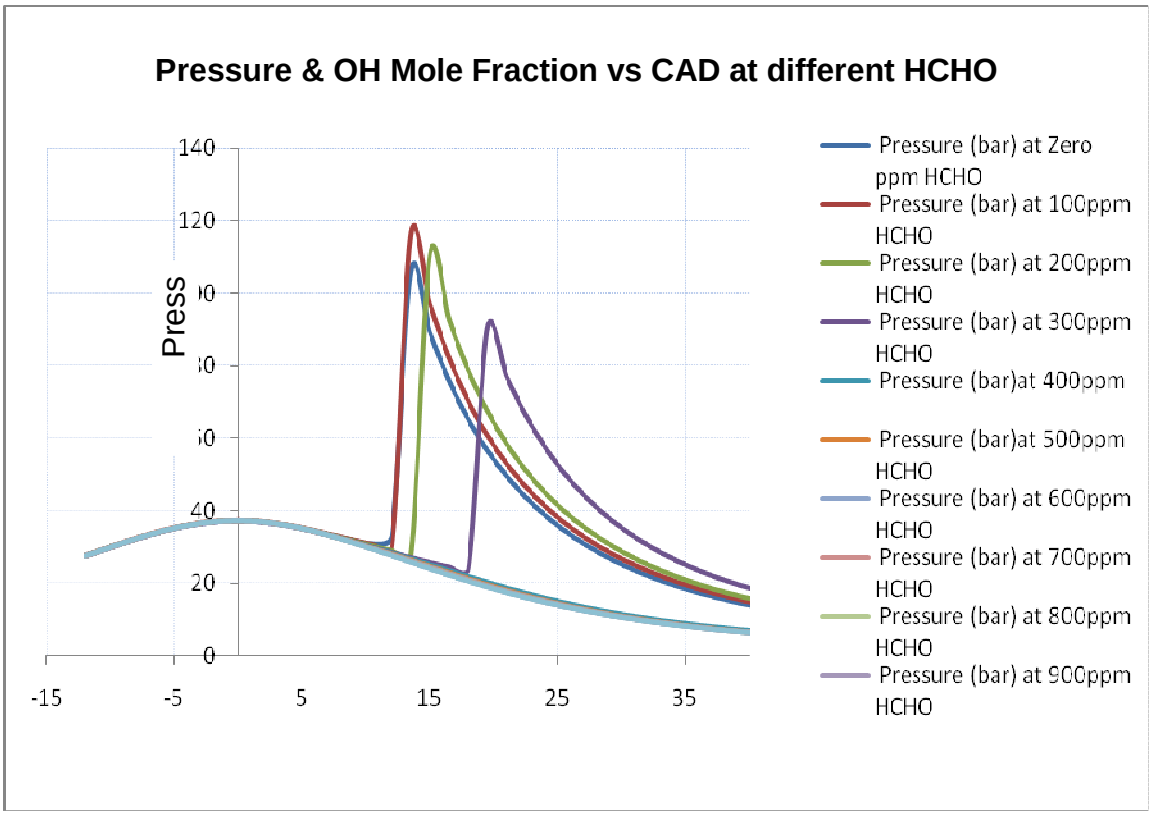

Figure 4.27- Effect of HCHO addition on Ignition Delay at Equivalence Ratio 1.0

From Figure 4.27, it is evident that the addition of formaldehyde increases the ignition delay. With Zero ppm of formaldehyde, the ignition starts at about 12 CAD ATDC. With addition of 100 ppm of formaldehyde, start of ignition is not greatly affected and combustion starts nears 12CAD ATDC. With the addition of another 100 ppm, the ignition is retarded to 13.5 CAD. Adding another 100 ppm, to a total of 300 ppm retarded ignition by 5 CAD to 18CAD ATDC. At 400 ppm of formaldehyde, the engine fails to fire.

4.5.1 Investigation of the delay in ignition caused by adding folmaldehyde

Plots for pressure and OH concentrations are shown in figure 4.28 and figure 4.29. It is interesting to notice that the rise in pressure due to combustion is accompanied by the rise in OH concentration. The plot below shows that OH concentration follows almost the exact pattern of the pressure.

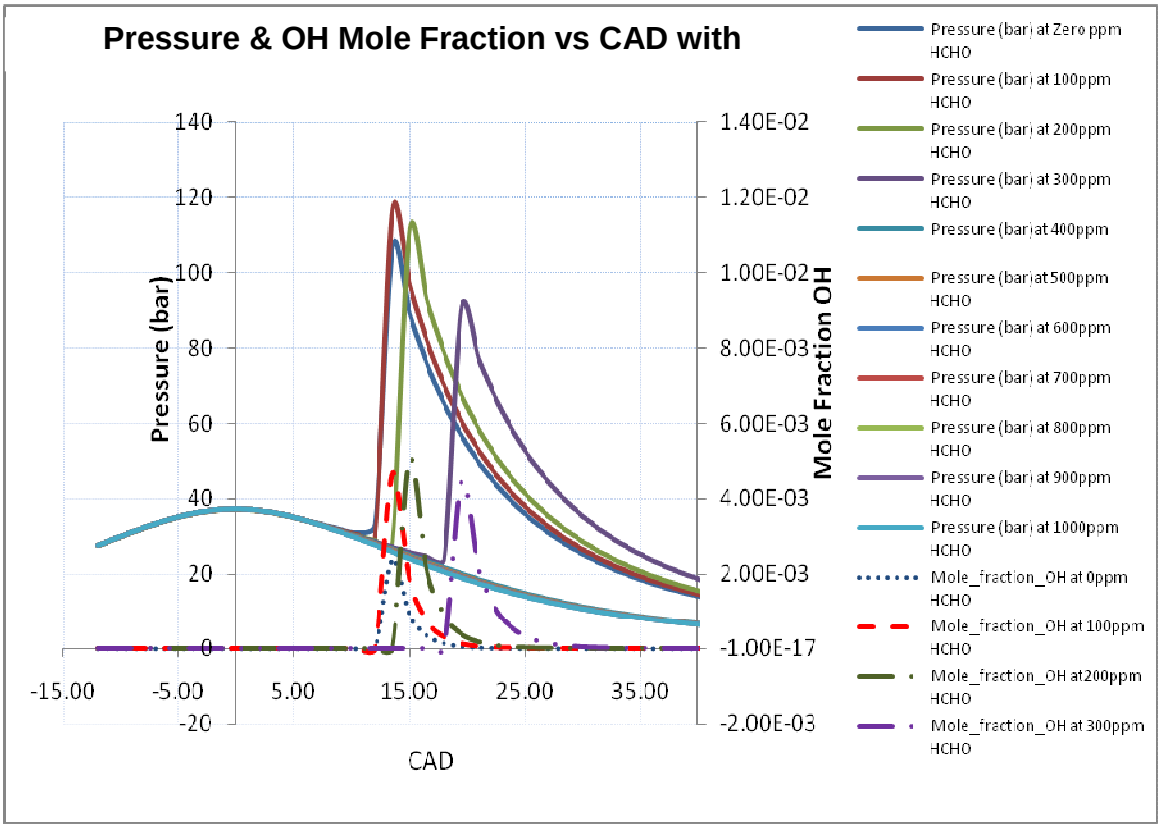

Figure 4.28 - In-cylinder Pressure and OH mole fractions at different HCHO concentrations versus CAD

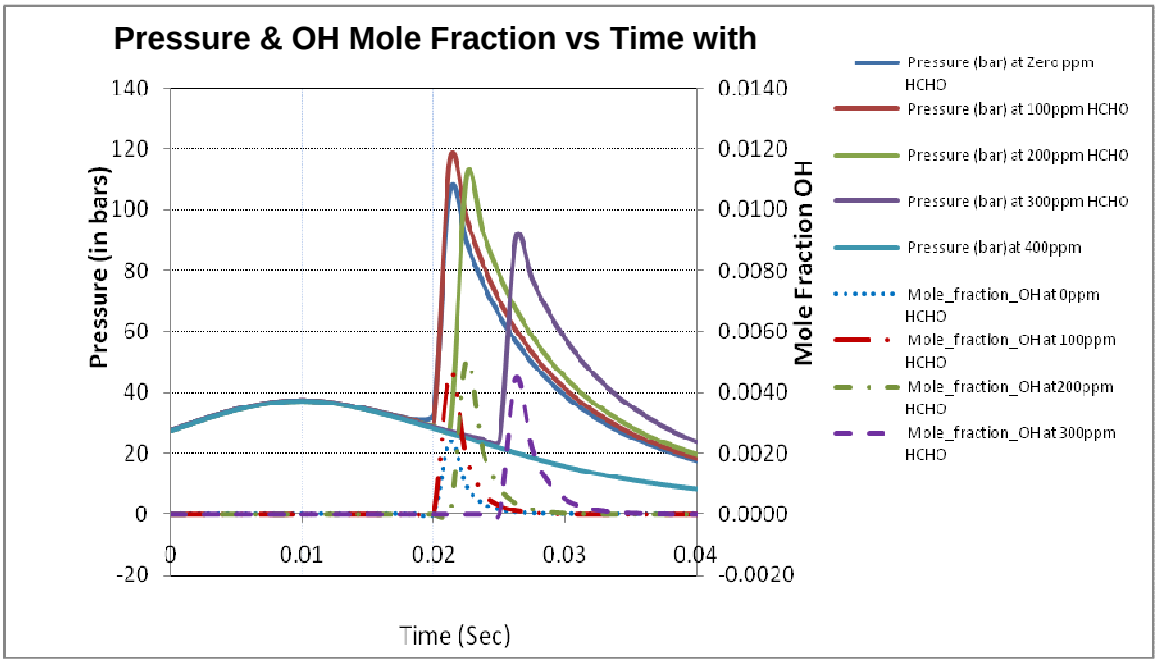

Figure 4.29 - In-cylinder Pressure and OH mole fractions at different HCHO concentrations versus Time

From figures 4.28 and 4.29, it can be concluded that addition of formaldehyde has a direct effect on OH formation. Since OH is a main contributor to the start of combustion, the effects of formldehyde on OH formation needs to be examined.

Considering two cases, no formaldehyde added in the first case while 200 ppm formaldehyde added in the second case. The comparison of these two different conditions can help in understanding the effect of adding HCHO in retarding the ignition process..

4.5.2 Investigation using Reaction Path Analysis:

In any detailed chemistry model, understanding of the dominant reaction paths can be helpful in the analysis of the kinetic model results.

Applying the CHEMKIN-PRO Reaction Path Analyzer (RPA) to the results provides a visual representation of the reaction paths that form or deplete chemical species.

There are many interactive visualization options within the RPA that allow to drill down into the information provided. Reaction path analysis can be used to look in the reactions involving a species at a particular interval of time.

This approach is used in this work, recognizing the effect on the reaction occurrence of the addition of 200 ppm HCHO. The study was performed at time intervals 0.01750 sec, 0.018750 sec and 0.020 sec from the start of injection of NC7H16. Using reaction path analysis, the process was studied in details. Simulation results indicated that combustion occurred at 0.01875 seconds. Therefore, the time intervals were selected as one before and one after 0.01875 second.

The objective was to compare between the reactions with and without HCHO at two times.

The comparison between the two cases shows a bright picture of the kinetics of the reactions. Although, most of the reactions were common for both cases, the rates of the reactions were different at the given interval of time for the case

without formaldehyde and the case with 200 ppm formaldehyde. The formation or consumption of the species are explained in the following sections.

4.5.2.1 At 0.01750 seconds:

Figure 4.30.a shows the rate of formation of OH at 0.01750 seconds with zero and 200 ppm HCHO while figure 4.30.b gives the comparison by superposition for the two cases of HCHO addition. According to Chemkin code the most important reactions for OH are as follows:

- CH2CHO + 02 ==> CH2O + CO + OH ------ (a)
- CH2O + OH <==> HCO + H2O ------ (b)
- HOCH2O <==> CH2O + OH ------ (c)

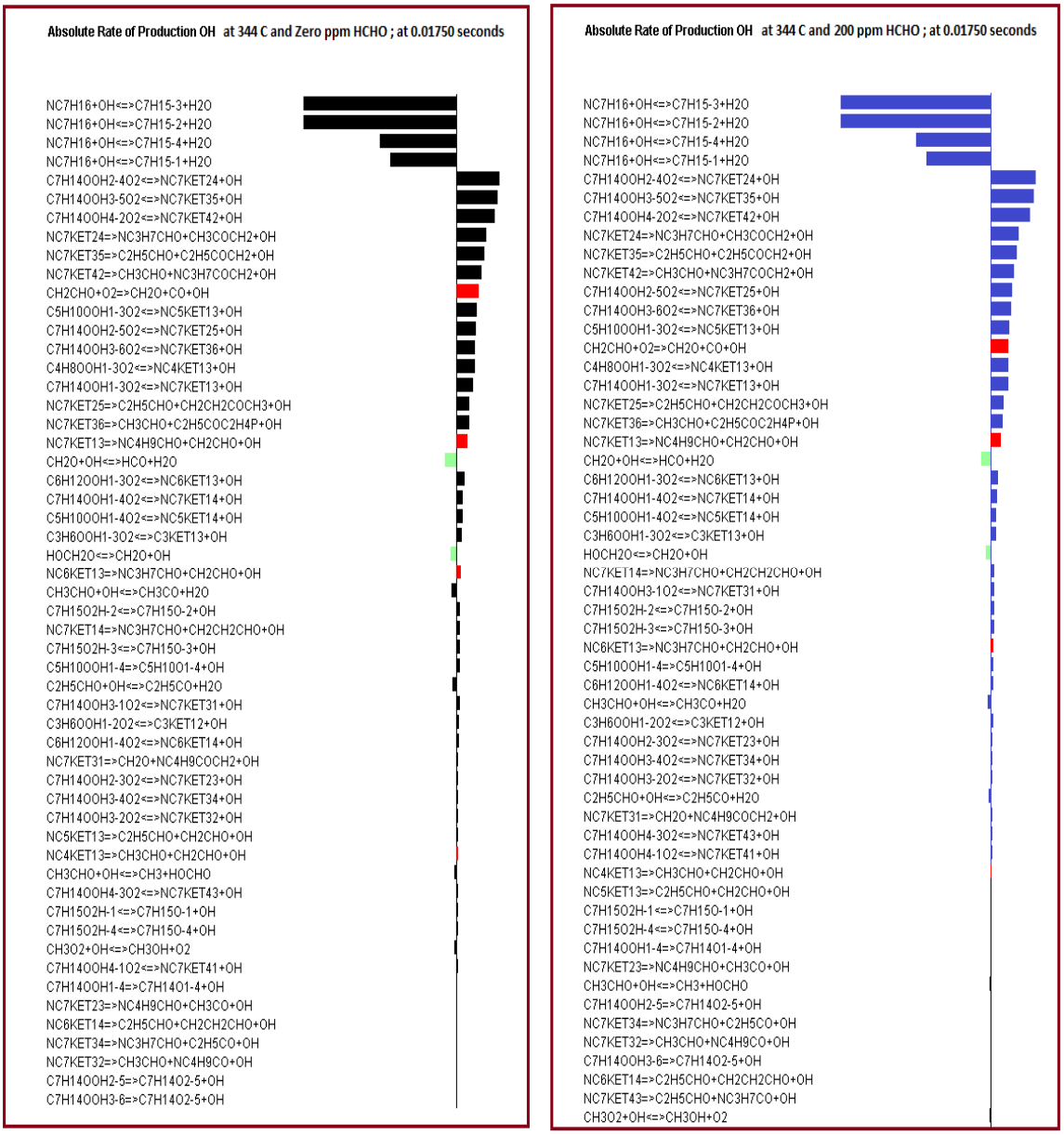

Figure 4.30.a - Rate of formation of OH at 0.01750 seconds with zero and 200ppm HCHO

Color code was used in order to easily identify the reactions involving a particular species. The color black was chosen for the reactions involving no formaldehyde addition and blue for reactions involving 200ppm formaldehyde addition. Within

this black and blue color code, the color red was chosen to easily identify the reactions involving the specie CH2CHO and the color green to identify the reactions involving HCHO for both the cases. In any diagram, the colored bars towards the left of the reference line indicate the reactions involved in consumption of a specie while those towards right of the reference line indicate the reactions involved in production of that specie.

For the diagram involving the superposition of the two cases, the color code blue for the reactions involving 200ppm formaldehyde addition was changed to pink in order to show a better recognizable difference among the length of the colored bars for both the cases. Larger the length of the colored bars towards left of the reference line, more is the absolute rate of consumption of the OH radical whereas larger the length of the color bars towards right of the reference line, more is the absolute rate of production of OH by any given reaction.

Figure 4.30.b - Comparison using superposition between the rate of formation of OH at 0.01750 seconds with zero and 200ppm HCHO

The change in temperature in two cases is shown in the tabular format below.

Time	Temperature (K) at 0 ppm HCHO	Temperature (K) at 200 ppm HCHO
0.0175	648.53 K	642.92 K

With the addition of Formaldehyde, both the compression pressure and the compression temperature decreases as a result of higher specific heat. This later explains why the temperature at a specific time with formaldehyde addition is lower than the temperature without formaldehyde addition. Figure 4.31 depicts the reduction in pressure and temperature with the formaldehyde addition.

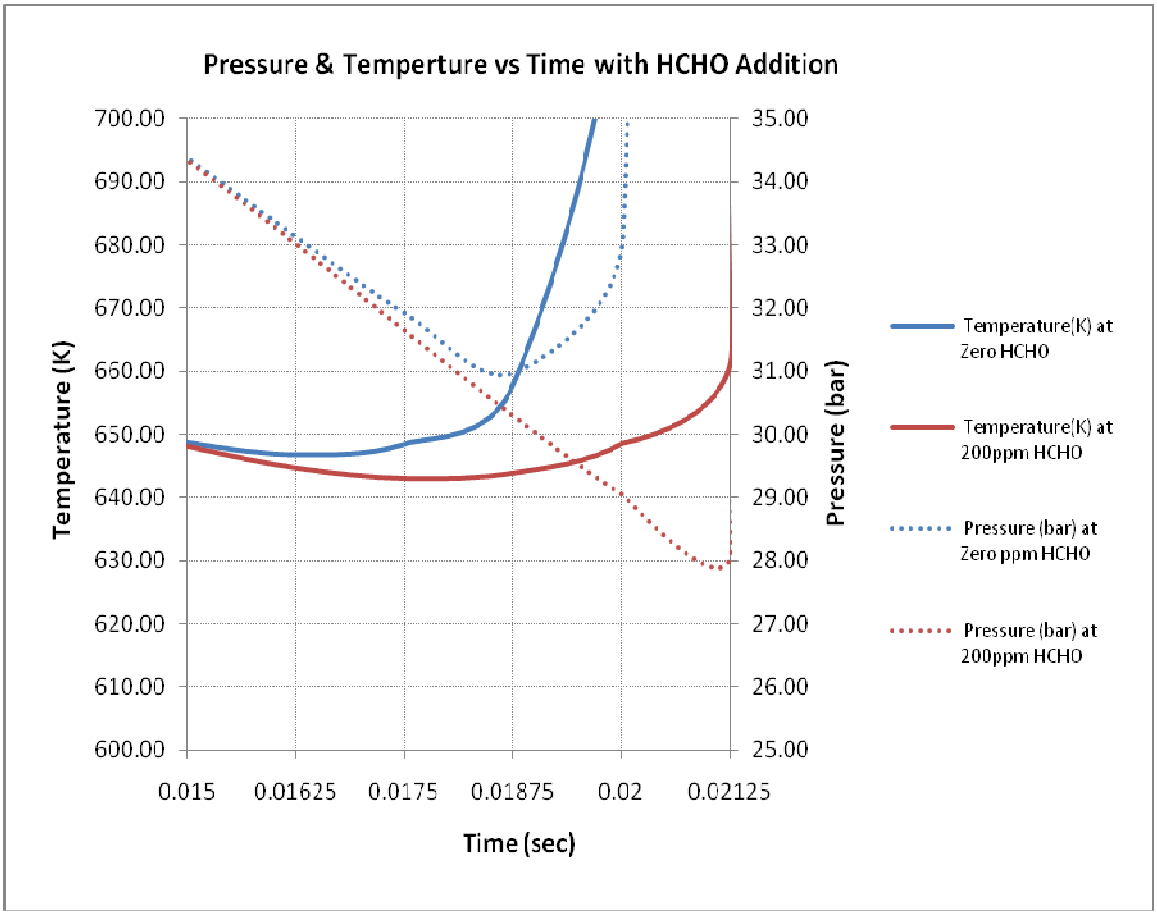

Figure 4.31 – Effect of HCHO addition on the pressure and temperature

Temperature at start of combustion for no formaldehyde addition, i.e. at 0.01875 seconds is 658K whereas the temperature at start of combustion for 200ppm formaldehyde addition, i.e. at 0.02125 seconds is 663K.

The reaction (a), **CH2CHO + 02 ==> CH2O + CO + OH**, goes only in forward direction. This forward reaction favors the formation of OH. By considering the rate of the reaction for both the cases, the following rate of formation of OH is obtained through this reaction.

Time	At 0 ppm HCHO and 0.0175 seconds; Rf : CH2CHO + 02 ==> CH2O + CO + OH	At 200 ppm HCHO and 0.0175 seconds; Rf : CH2CHO + 02 ==> CH2O + CO + OH
0.0175	1.94E-05 units	1.06E-05 units

The value for the rate of the reaction can also be calculated using the species concentrations and the Arrhenius equation. The value of the reaction rate constant K can be calculated using the Arrhenius Equation as follows:

$$K = A T^{n} \exp [-E / (RT)]$$

The values of the constants A, n and E can be obtained from the mechanism file available online at Lawrence Livermore National Laboratory website.

Considering the reaction CH2CHO + O2 ==> CH2O + CO + OH , the values of A, n, and E for the forward reaction are tabulated below. The value of Kf for the above reaction calculated at 0.0175 seconds is 6.95E08 cubic cm/ mol sec. The temperature value considered for the calculations is 648.53 K.

Reaction	A	n	E
CH2CHO + O2 ==> CH2O + CO + OH	8.95E+13	-0.6	10120

The mole fraction of CH2CHO and O2 can be obtained from the Chemkin data export option. The values for mole fraction of CH2CHO and O2 at the time interval 0.01750 seconds with no formaldehyde addition is shown in the table below.

Time	Species	Mole Fraction
0.0175	CH3CHO	3.70E-07
	O2	2.04E-01

The value for the concentration of a species can be obtained by multiplying its mole fraction with the total concentration. The total concentration can be calculated as:

$$[i] = \frac{P}{RT}$$

where [i] is the total concentration, P is the Pressure and T is the temperature. Considering the value of pressure and temperature at 0.0175 seconds, the total concentration is calculated as 5.99 E-04 mol/cubic cm.

Time	Species	Concentration (mol/cubic cm)
0.0175	CH3CHO	2.16E-10
	O2	1.22E-04

The rate of reaction is calculated as Rf = Kf [CH2CHO] [O2]. The calculated value of Rf equals 1.9E-06 mol/cubic cm sec. This value is in accordance with the value obtained from the Chemkin Reaction Path Analyzer.

Considering the same reaction for the case of 200ppm formaldehyde addition, the values of A, n and E remains the same but he temperature changes to 642.92 K. Following the calculations performed in the case of no formaldehyde addition, the rate of the forward reaction CH2CHO + O2 => CH2O + CO + OH is calculated as 1.03E-06 which is very close to the value obtained from the RPA.

The above results were obtained from Reaction Path Analyzer. It is evident that the rate of formation of OH with HCHO is lower than without HCHO.

Now considering reaction (b), **CH2O + OH <==> HCO + H2O**, the forward reaction decreases the amount of OH formed and the backward reaction favors the OH formation. Therefore from equation (b), the rate of formation of OH can be described as

$$\frac{d[OH]}{dt} = -K_f[CH_2O][OH] + K_b[HCO][H_2O]$$

From the equation above, it is evident that any increase in the quantity of formaldehyde will decrease the rate of formation of OH. Hence, the formation of OH is lower in the case of formaldehyde addition. The rates of reactions obtained from Reaction Path analysis are:

Time	At 0 ppm HCHO and 0.0175 seconds; R_f : CH2O + OH <==> HCO + H2O	At 200 ppm HCHO and 0.0175 seconds; R_f : CH2O + OH <==> HCO + H2O
0.0175	9.74E-06 mol/cubic cm	5.56E-06 mol/cubic cm

Time	At 0 ppm HCHO and 0.0175 seconds; R_b : CH2O + OH <==> HCO + H2O	At 200 ppm HCHO and 0.0175 seconds; R_b : CH2O + OH <==> HCO + H2O
0.0175	-2.22E-18 mol/cubic cm	-7.03E-19 mol/cubic cm

The values for reaction rate constants were calculated:

Time	At 0 ppm HCHO and 0.0175 seconds; K_f : CH2O + OH <==> HCO + H2O	At 200 ppm HCHO and 0.0175 seconds; K_f : CH2O + OH <==> HCO + H2O
0.0175	6.81501E+12	6.76752E+12

Time	At 0 ppm HCHO and 0.0175 seconds; K_b : CH2O + OH <==> HCO + H2O	At 200 ppm HCHO and 0.0175 seconds; K_b : CH2O + OH <==> HCO + H2O
0.0175	92.03468997	74.3782223

From the table above, it is quite evident that the rate of forward reaction for 0 ppm formaldehyde is higher than the rate of forward reaction with 200 ppm formaldehyde. The rates of backward reaction are very small for comparison.

Now with the formaldehyde addition, the mass average temperature dropped to 643K from 648K. This drop in temperature caused a change in the value of reaction rate constant K.

Now considering reaction (c), **HOCH2O <==> CH2O + OH,** the forward reaction favors the OH formation while the backward reaction reduces the OH concentration. Also, any increase in the quantity of formaldehyde increases the

rate of backward reaction. Hence, OH formation is reduced with the presence of 200 ppm of formaldehyde when compared to 0 ppm formaldehyde.

From the reaction path analysis:

Time	At 0 ppm HCHO and 0.0175 seconds;	At 200 ppm HCHO and 0.0175 seconds;
	R_f : HOCH2O <==> CH2O + OH	R_f : HOCH2O <==> CH2O + OH
0.0175	6.47E-09 mol/cubic cm	3.56E-09 mol/cubic cm

Time	At 0 ppm HCHO and 0.0175 seconds;	At 200 ppm HCHO and 0.0175 seconds;
	R_b : HOCH2O <==> CH2O + OH	R_b : HOCH2O <==> CH2O + OH
0.0175	-5.21E-06 mol/cubic cm	-3.20E-06 mol/cubic cm

By adding the forward and the backward rate of reactions, the result is still a negative number symbolizing that the overall reaction moves in the backward direction, i.e. net rate of backward reaction for formaldehyde addition is lower as compared to no formaldehyde addition. (-0.00000520353; -0.00000319644 respectively, negative sign only symbolizes the backward reaction.).

The total OH mole fraction at time 0.01750 seconds is:

Time	**Mole_fraction_OH at 0ppm HCHO**	**Mole_fraction_OH at200ppm HCHO**
0.01750	7.99E-09	5.12E-09

In figure 4.32, solid lines with black color represent reactions with 0 ppm formaldehyde, the red and the green solid lines represent reactions with 200 ppm formaldehyde addition. Now, with 200 ppm formaldehyde addition, reaction (a)

proposes less OH formation, reaction (b) proposes comparatively less OH consumption and reaction (c) proposes comparatively less OH consumption.

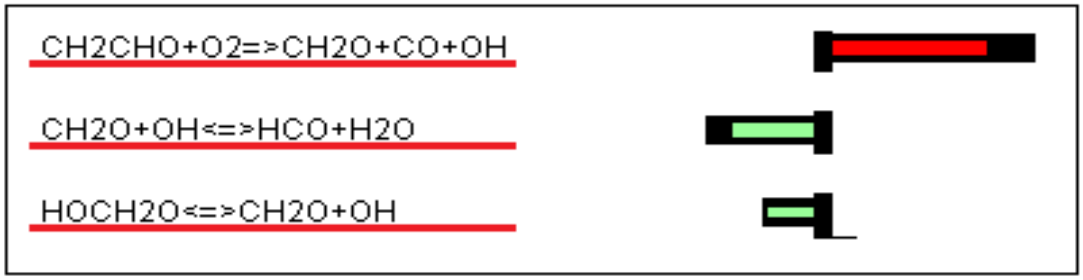

Figure 4.32 - Comparison of Net rate of OH production at zero and 200ppm HCHO and by 3 major reactions at 0.01750 seconds

Since, the net OH mole fraction is lower in case of formaldehyde addition at 0.01750 seconds, and from the above results, it is evident that the effect of reaction (a) is dominating at this time interval.

4.5.2.2 At 0.01875 seconds:

Figure 4.33.a shows the rate of formation of OH at 0.018750 seconds with zero and 200 ppm HCHO while figure 4.33.b represents the comparison by superposition for the two cases of HCHO addition. There are three main reactions involving Formaldehyde and OH. These 3 reactions are:

- CH2CHO + 02 ==> CH2O + CO + OH ------ (a)
- CH2O + OH <==> HCO + H2O ------ (b)
- HOCH2O <==> CH2O + OH ------ (c)

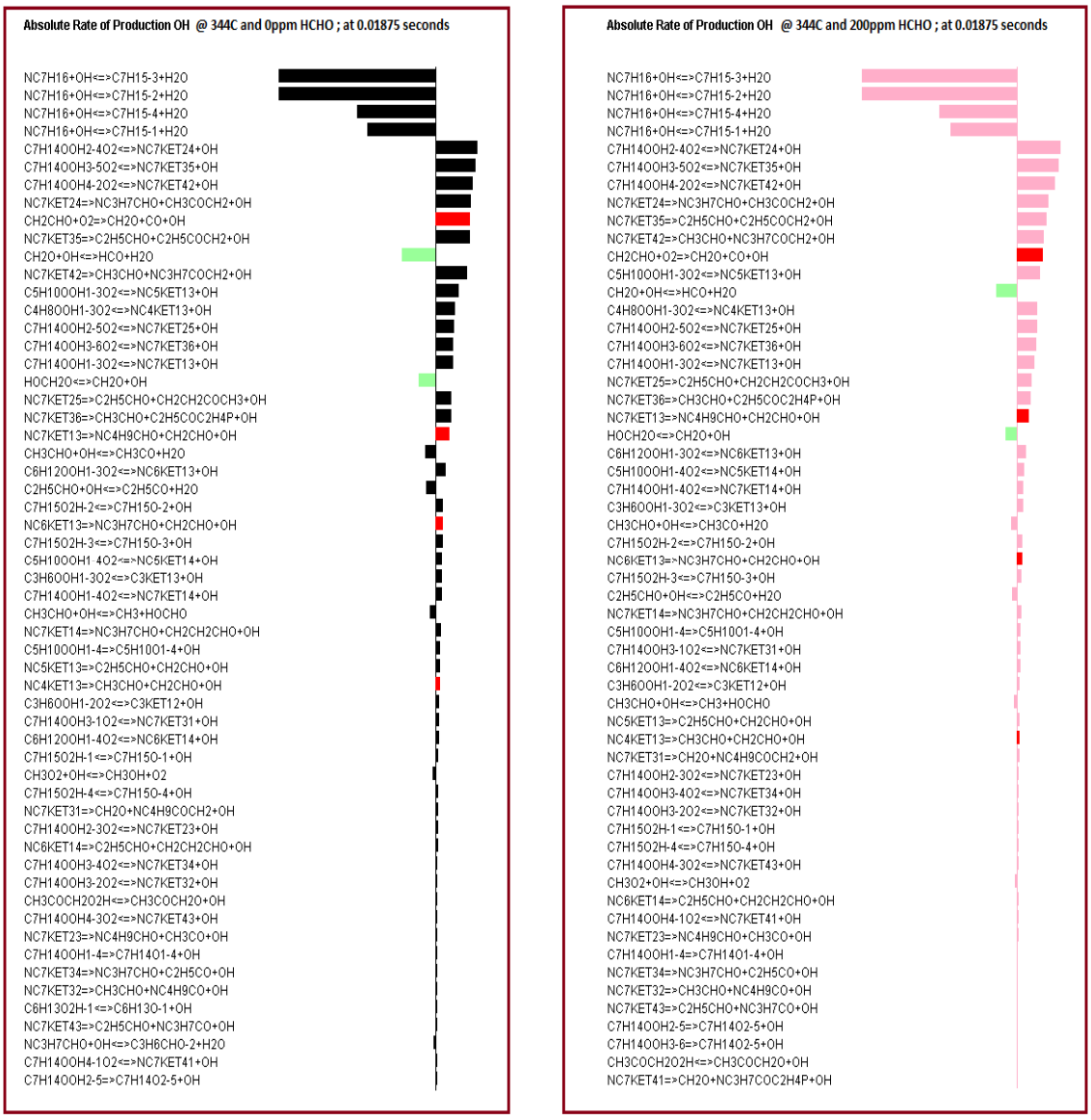

Figure 4.33.a - Rate of formation of OH at 0.018750 seconds with zero and 200ppm HCHO

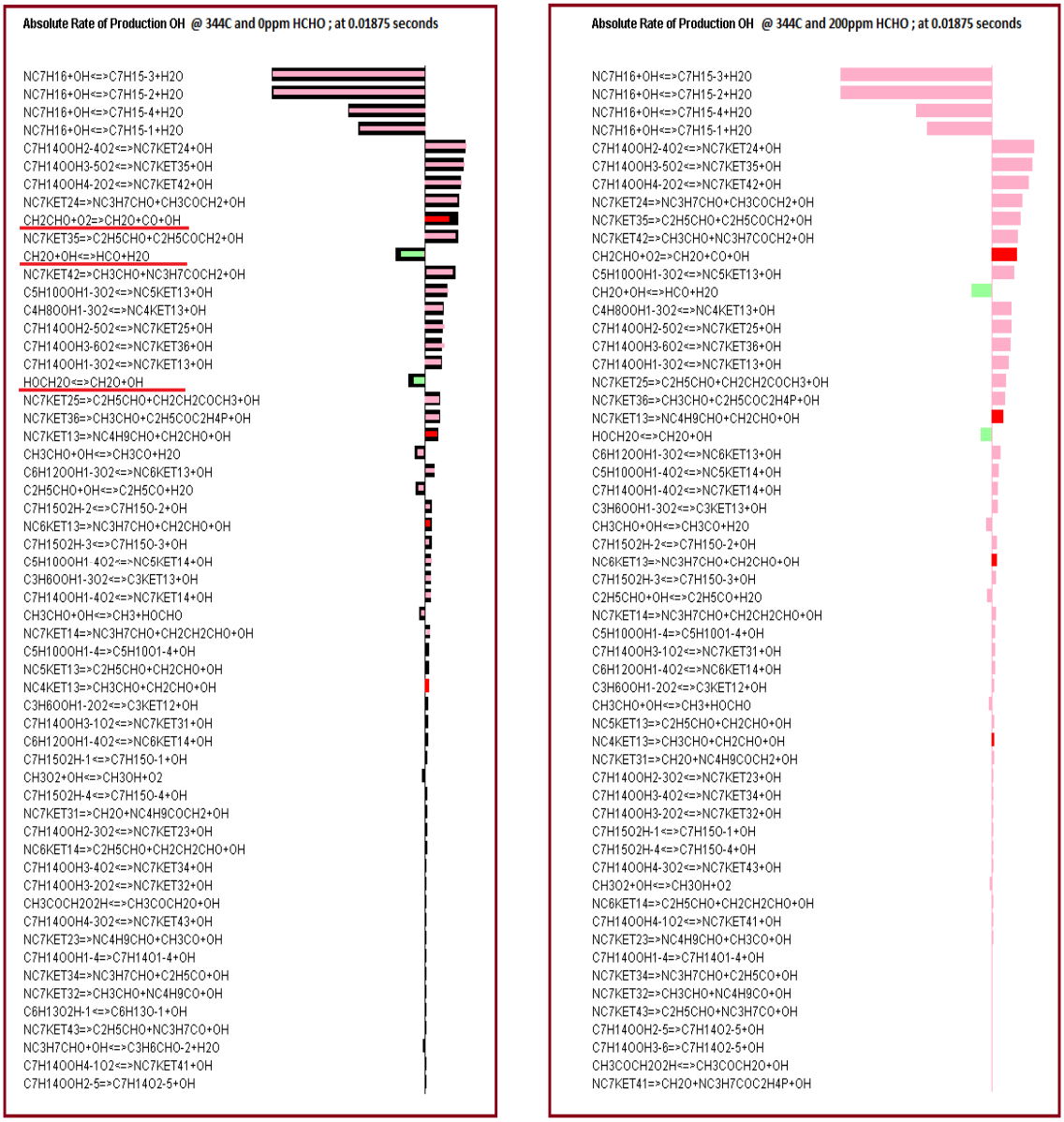

Figure 4.33.b - Comparison using superposition between the rate of formation of OH at 0.018750 seconds with zero and 200ppm HCHO

The reaction (a), **CH2CHO + 02 ==> CH2O + CO + OH**, goes only in forward direction. This forward reaction favors the formation of OH. By considering the rate of the reaction for both cases, the following rate of OH formation is given by

Time	At 0 ppm HCHO and 0.01875 seconds; Rf : CH2CHO + 02 <==> CH2O + CO + OH	At 200 ppm HCHO and 0.01875 seconds; Rf : CH2CHO + 02 <==> CH2O + CO + OH
0.0185	5.21E-05	1.86E-05

The above results were obtained from Reaction Path Analyzer. It is quite evident that the rate of formation of OH is less in case of formaldehyde addition.

Considering reaction (b), **CH2O + OH <==> HCO + H2O**

The rate of reactions obtained from Reaction Path analysis are :

Time	At 0 ppm HCHO and 0.01875 seconds; R_f : CH2O + OH <==> HCO + H2O	At 200 ppm HCHO and 0.01875 seconds; R_f : CH2O + OH <==> HCO + H2O
0.01875	4.98E-05	1.49E-05

Time	At 0 ppm HCHO and 0.01875 seconds; R_b : CH2O + OH <==> HCO + H2O	At 200 ppm HCHO and 0.01875 seconds; R_b : CH2O + OH <==> HCO + H2O
0.01875	-2.69E-17	-3.15E-18

From the table above, it is quite evident that the rate of forward reaction for 0 ppm formaldehyde is higher than the rate of forward reaction with 200 ppm formaldehyde. The rates of backward reaction are very small for comparison. This indicates that rate of the consumption of OH is higher in the case of no formaldehyde addition.

Now considering reaction (c), **HOCH2O <==> CH2O + OH,** the forward reaction favors the OH formation while the backward reaction red OH concentration.

Time	At 0 ppm HCHO and 0.01875 seconds;	At 200 ppm HCHO and 0.01875 seconds;
	R_f : HOCH2O <==> CH2O + OH	R_f : HOCH2O <==> CH2O + OH
0.01875	3.52E-08	9.57E-09

Time	At 0 ppm HCHO and 0.01875 seconds;	At 200 ppm HCHO and 0.01875 seconds;
	R_b : HOCH2O <==> CH2O + OH	R_b : HOCH2O <==> CH2O + OH
0.01875	-2.95E-05	-8.06E-06

By adding the forward and the backward rate of reactions, the result is still a negative number symbolizing that the overall reaction moves in the backward direction, i.e. net rate of backward reaction for formaldehyde addition is lower as compared to no formaldehyde addition. The total OH mole fraction at time 0.018750 seconds is:

Time	**Mole_fraction_OH at 0ppm HCHO**	**Mole_fraction_OH at 200ppm HCHO**
0.01875	1.65E-08	1.07E-08

Also formaldehyde addition reduces the overall temperature by 14.47C

Time	**Temperature (K) at 0ppm HCHO**	**Temperature (K) at 200ppm HCHO**
0.01875	658.2793 K	643.8068 K

In figure 4.34, solid lines with black color represent reactions with 0 ppm formaldehyde, the red and the green solid lines represent reactions with 200 ppm formaldehyde addition. Now with 200 ppm formaldehyde addition, reaction (a)

proposes less OH formation, reaction (b) proposes comparatively less OH consumption and reaction (c) proposes lesser OH consumption.

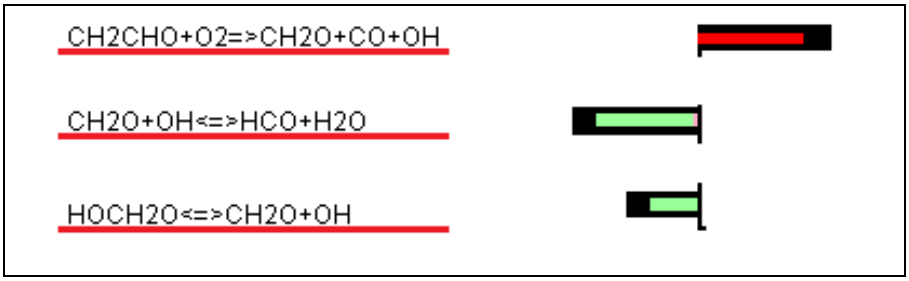

Figure 4.34 - Comparison of Net rate of OH production at zero and 200ppm HCHO and by 3 major reactions at 0.018750 seconds

Since, the net OH mole fraction is lower in case of formaldehyde addition at 0.018750 seconds; it is evident that the effect of reaction (a) is dominating at this time interval.

It is observed from the data that the combustion starts at about 0.01875 seconds for 0ppm formaldehyde addition along with the fuel. For any analysis after time 0.01875 seconds, it should be kept into consideration that ignition has already started in case of 0ppm formaldehyde addition.

4.5.2.3 At 0.0200 Seconds:

Figure 4.35.a shows the rate of formation of OH at 0.018750 seconds with zero and 200ppm HCHO while figure 4.35.b represent the comparison by superposition for the two cases of HCHO addition and it can observed that there are three main reactions involving Formaldehyde and OH. These 3 reactions are:

- CH2CHO + 02 ==> CH2O + CO + OH ------ (a)

- CH2O + OH <==> HCO + H2O ------ (b)
- HOCH2O <==> CH2O + OH ------ (c)

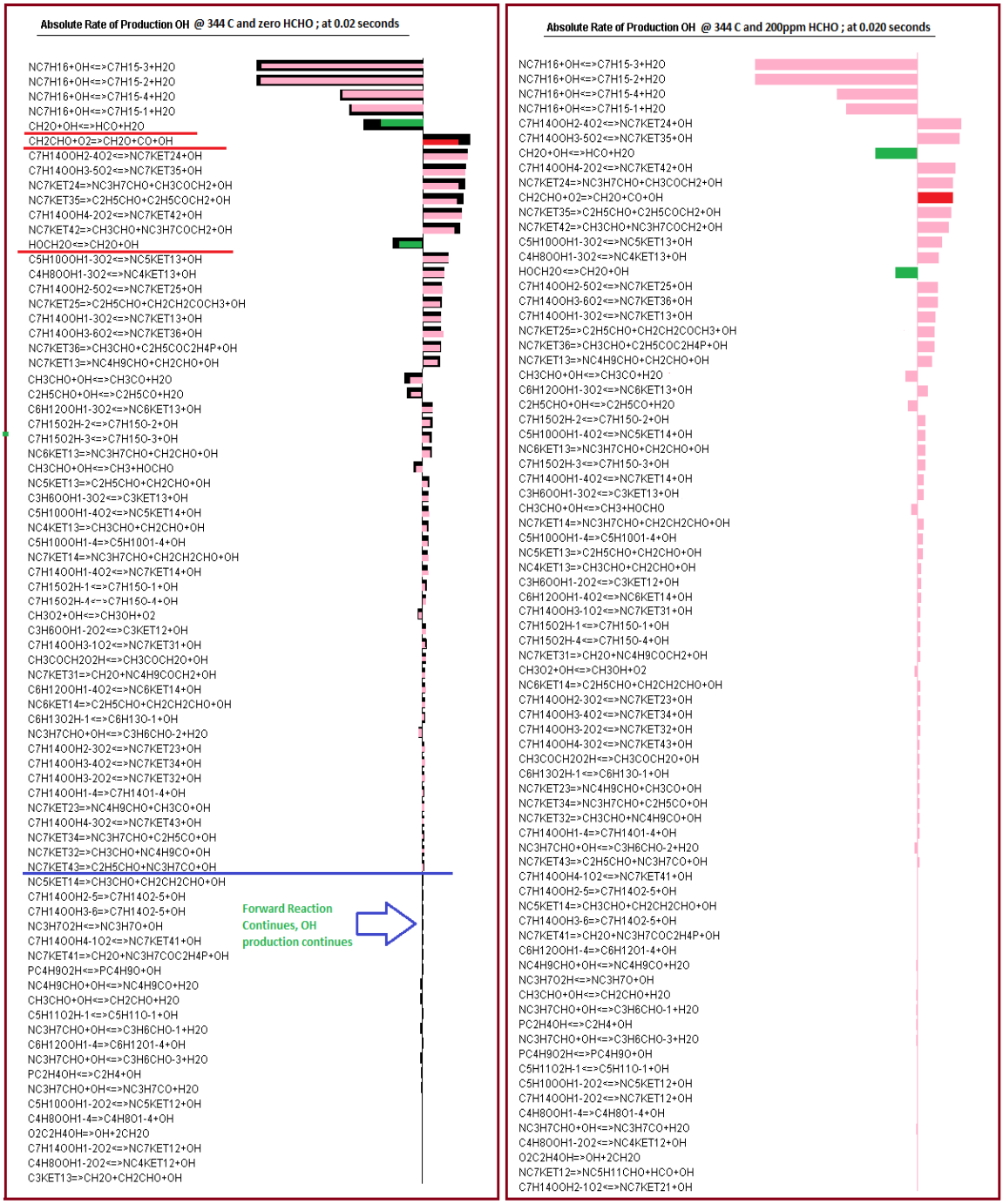

Figure 4.35.a - Rate of formation of OH at 0.020 seconds with zero and 200ppm HCHO

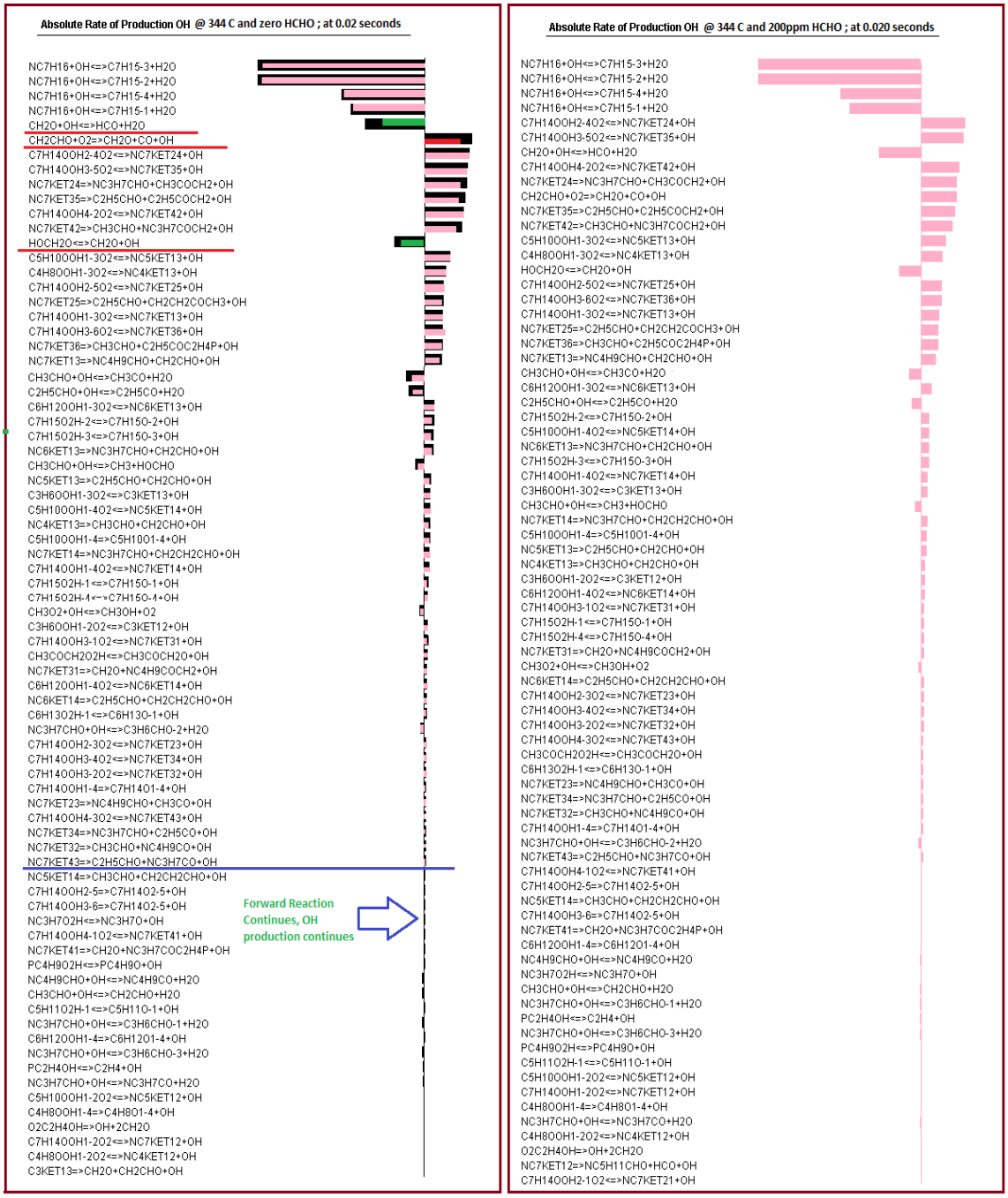

Figure 4.35.b - Comparison using superposition between the rate of formation of OH at 0.020 seconds with zero and 200ppm HCHO

Again, the reaction (a), **CH2CHO + 02 ==> CH2O + CO + OH**, goes only in forward direction. This forward reaction favors the formation of OH. Comparing the Rate of the Reaction for both the cases, the OH formation can be obtained through this reaction.

Time	At 0 ppm HCHO and 0.02 seconds; Rf : CH2CHO + 02 <==> CH2O + CO + OH	At 200 ppm HCHO and 0.02 seconds; Rf : CH2CHO + 02 <==> CH2O + CO + OH
0.02	1.77E-03	3.31E-05

The above results were obtained from Reaction Path Analyzer. It is quite evident that the rate formation of OH is lower in case of f ormaldehyde addition.

Now considering reaction (b), **CH2O + OH <==> HCO + H2O**

The rate of reaction obtained from Reaction Path analysis are :

Time	At 0 ppm HCHO and 0.02 seconds;	At 200 ppm HCHO and 0.02 seconds;
	R_f : CH2O + OH <==> HCO + H2O	R_f : CH2O + OH <==> HCO + H2O
0.02	2.58E-03	3.65E-05

Time	At 0 ppm HCHO and 0.02 seconds;	At 200 ppm HCHO and 0.02 seconds;
	R_b : CH2O + OH <==> HCO + H2O	R_b : CH2O + OH <==> HCO + H2O
0.02	-5.05E-14	-1.4E-17

From the table above, it is quite evident that the rate of forward reaction for 0 ppm formaldehyde is higher than the rate of forward reaction with 200ppm

Formaldehyde. The rates of backward reaction are very small for comparison. This indicates that the rate of consumption of OH is higher in the case of no Formaldehyde addition. This can be related with higher rate of OH formation by reaction (a).

Now considering reaction (c), **HOCH2O <==> CH2O + OH,** the forward reaction favors the OH formation while the backward reaction reduces the OH concentration.

Time	At 0 ppm HCHO and 0.02 seconds;	At 200 ppm HCHO and 0.02 seconds;
	R_f : HOCH2O <==> CH2O + OH	R_f : HOCH2O <==> CH2O + OH
0.02	2.71E-06 mol/cubic cm	2.43E-08 mol/cubic cm

Time	At 0 ppm HCHO and 0.02 seconds;	At 200 ppm HCHO and 0.02 seconds;
	R_b : HOCH2O <==> CH2O + OH	R_b : HOCH2O <==> CH2O + OH
0.02	-1.07E-03 mol/cubic cm	-1.95E-05 mol/cubic cm

By adding the forward and the backward rate of reactions, the result is still a negative number symbolizing that the overall reaction moves in the backward direction, i.e. net rate of backward reaction for formaldehyde addition is lower as compared to no formaldehyde addition.

The total OH mole fraction at time 0.020 seconds is:

Time	**Mole_fraction_OH at 0 ppm HCHO**	**Mole_fraction_OH at 200 ppm HCHO**
0.01875	2.99E-07	1.18E-08

Also the Formaldehyde addition reduces the overall temperature by **14.47C**

Time	Temperature (K) at 0ppm HCHO	Temperature (K) at 200ppm HCHO
0.01875	737.5097 K	648.5343 K

In figure 4.36, solid lines with black color represent reactions with 0ppm Formaldehyde, the red and the green solid lines represent reactions with 200ppm formaldehyde addition It is evident that with 200ppm Formaldehyde addition, reaction (a) proposes less OH formation, reaction (b) proposes comparatively less OH consumption and reaction (c) proposes lesser OH consumption. Also, it is observed that there are some other reactions that occur in case of no formaldehyde addition. This can be explained as the increase in the temperature that is evident in both the cases.

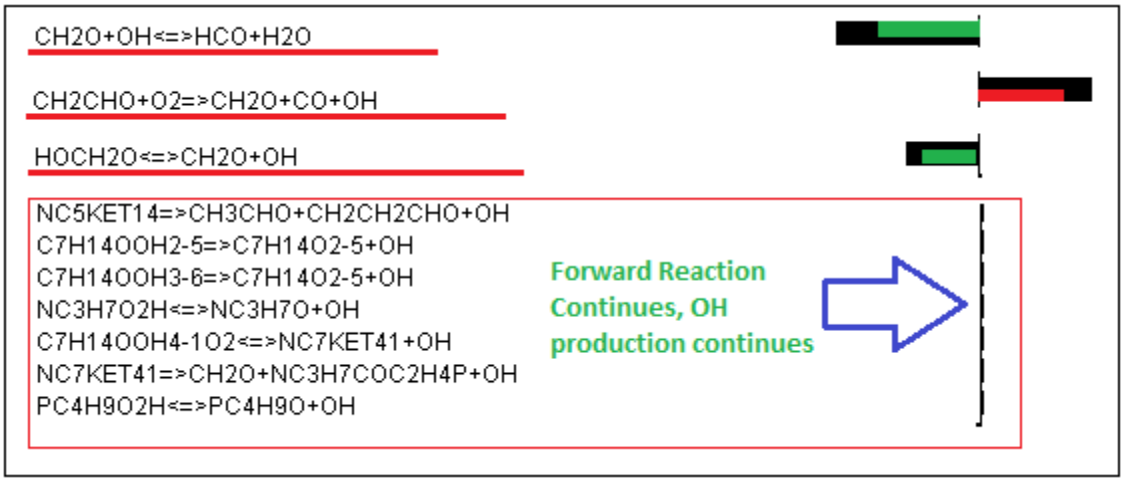

Figure 4.36 - Comparison using superposition between the rate of formation of OH at 0.02175 seconds with zero and 200ppm HCHO and some other reactions contributing towards OH formation.

Since, the net OH mole fraction is lower in case of Formaldehyde addition at 0.01750 seconds, it can be said that the effect of reaction (a) along with reaction set shown above is dominating the reactions (b) and (c).

4.5.3 Summary:

- It is evident that the start of combustion is retarded by formaldehyde addition. Therefore ignition delay is increased.
- OH production rate is also retarded with the formaldehyde addition.
- Using Chemical Kinetics, it can be inferred that the three reaction (a), (b), (c) together decide the total OH mole fraction and formaldehyde interaction at a given interval of time. {Are these the only reactions for the formation and disappearance of OH?
- Reaction CH2CHO + 02 ==> CH2O + CO + OH, is the major contributor in the OH formation for all the three equations discussed in this thesis. The rate of this reaction is reduced with formaldehyde addition and hence OH formation is affected.
- The addition of Formaldehyde lowers the average mass temperature. Therefore, a change in the value of reaction rate constant and the reaction rate is evident.

4.6 Reaction Path Analysis for OH Formation and Ignition Delay with Propene addition:

This study was conducted to determine the effect of propene addition on the ignition delay. Fuel was N-Heptane (NC7H16). Addition of propene was parameterized with an increment of 100 ppm in each successive run starting from 0 ppm to 1000 ppm.

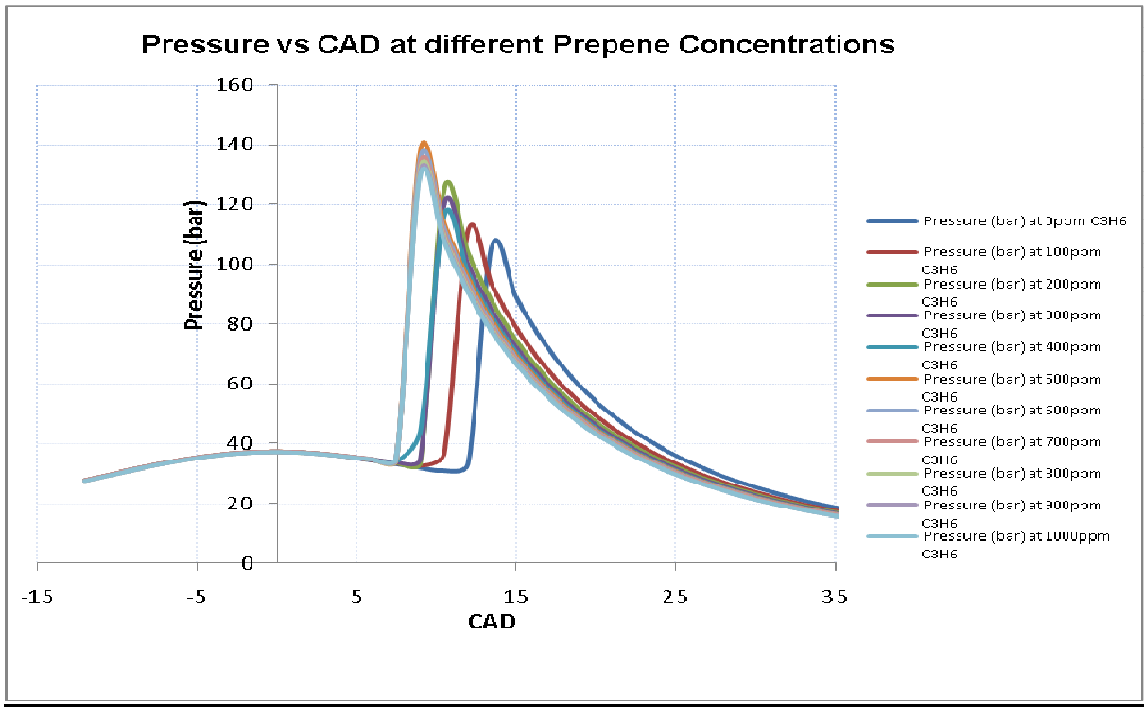

Figure 4.37 - Effect of C3H6 addition on Ignition Delay at Equivalence Ratio 1.0

From figure 4.37, it is evident that the addition of propene decreases the ignition delay. With Zero ppm of propene, the ignition starts at about 12 CAD ATDC. With successive addition of 100ppm of propene, start of ignition is advanced by 1.5 CAD and the ignition starts at about 10.5 CAD ATDC. With the addition of

another 100ppm, the ignition is further advanced and finally with a total of 1000ppm addition of propene, the start of ignition is advanced by 4.5 CAD with the start of ignition occurring at 7.5 CAD ATDC.

4.6.1 Investigation of Ignition delay Retard:

Various plots were made for pressure and OH concentrations as shown in figures 4.38 and 4.39. It was interesting to find that the rise in pressure due to combustion is accompanied by the rise in OH concentration. Figure 4.38 and 4.39 show that OH concentration follows almost the same pattern of the pressure. The plot was made for two different concentrations of propene which are 0 ppm propene and 200ppm propene.

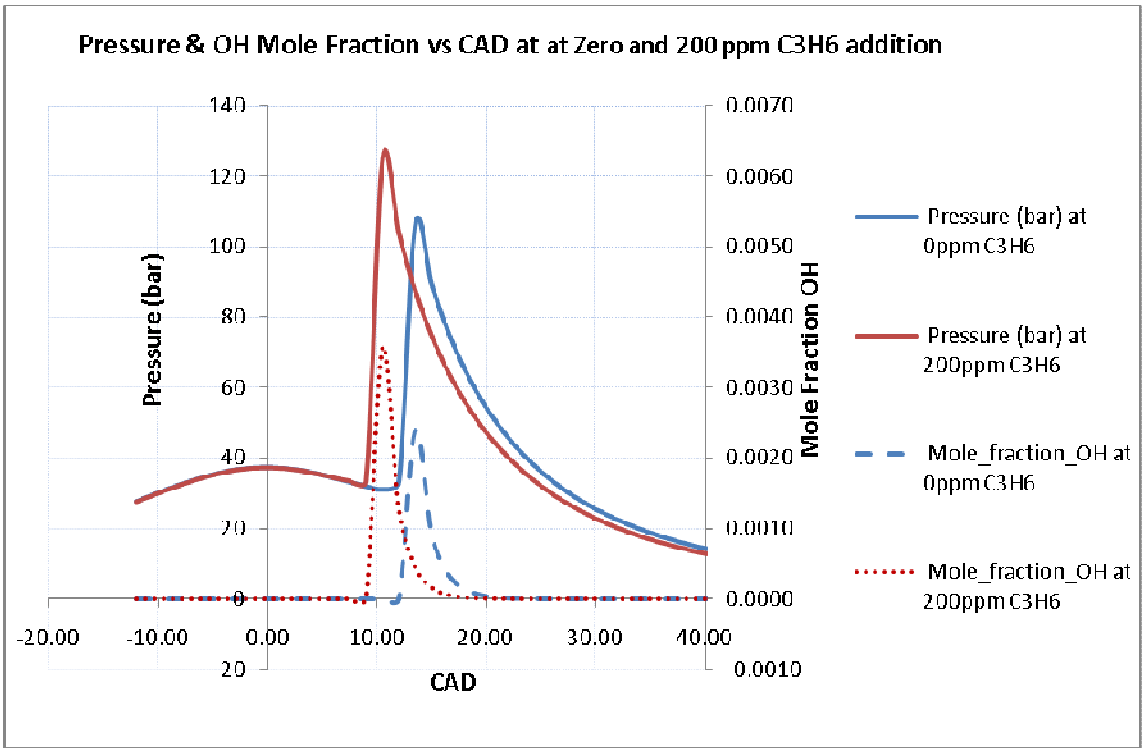

Figure 4.38 - In-cylinder Pressure and OH mole fractions at different C3H6 concentrations versus CAD

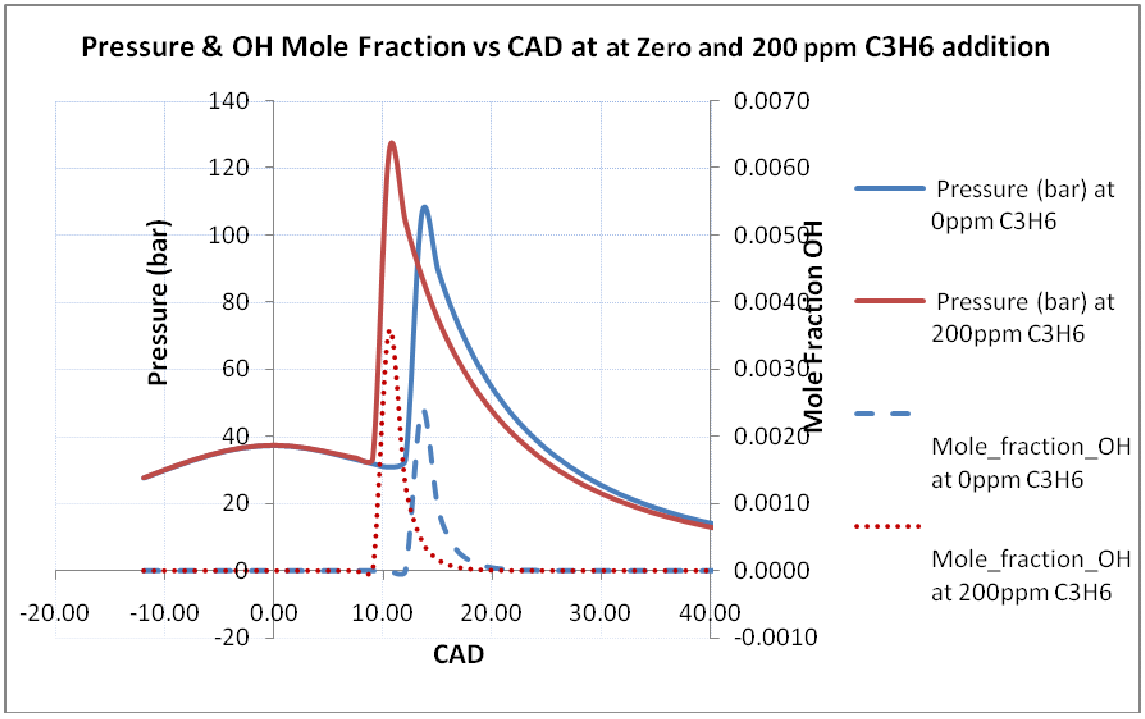

Figure 4.39 - In-cylinder Pressure and OH mole fractions at different C3H6 mole fractions versus crank angle degrees

From the figures 4.38 and 4.39, it can be concluded that addition of propene has a direct effect on OH concentration. OH being a main contributor to the start of combustion, the effects of propene on OH needs to be examined.

Considering the two cases, no propene added in the first case while 200 ppm propene added in the second case. The comparison between these two conditions can help in understanding the effect of adding C3H6 in reducing the ignition delay.

4.6.2 Investigation using Reaction Path Analysis:

The RPA approach is used in this work, recognizing the effect on the reaction occurrence with the addition of zero and 200 ppm C3H6. The study was performed at time intervals 0.01750 sec, 0.018750 sec and 0.02 sec from the start of injection of the fuel NC7H16.

Using reaction path analysis, the process was studied in details. It was observed that the start of combustion occurred at 0.01875 seconds. Therefore, the time intervals were selected as one before this period and one after this period. The approach was to compare the reactions involved in each of the case, i.e., zero propene and 200 ppm propene at various time intervals. The comparison of the two cases shows a very bright picture that involves the kinetics of the reactions. Although, most of the reactions were common for both the cases, the rates of the reactions were different at the given interval of time for zero Propene and 200ppm Propene. Therefore, formation or consumption of the species involved in the reaction varied greatly.

Locating the start of combustion and the rise in pressure helps in identifying the duration of ignition delay. From the figure 4.38 and 4.39, it is quite evident that the start of combustion occurs earlier in case of Propene addition. Following tables describes the pressure and OH mole Fractions at different time Intervals.

Time (sec)	CAD	Pressure (bar) (0ppm C3H6)	Pressure (bar) (200ppm C3H6)	Mole fraction OH (0ppm C3H6)	Mole fraction OH (200ppm C3H6)
0.0175	9.00	3.19E+01	3.33E+01	7.99E-09	3.16E-08
0.01875	10.50	3.10E+01	1.25E+02	1.65E-08	3.58E-03
0.02	12.00	3.31E+01	1.04E+02	2.99E-07	1.27E-03

It is very clear that the pressure difference at time 0.0175 seconds between 0ppm Propene and 200ppm Propene is much lower than the pressure difference at time 0.01875 seconds. Also, rise in pressure is very high for 200ppm Propene from 0.01750 seconds to 0.01875 seconds. At 0.01875 seconds, the fuel and 200ppm Propene mixture attains peak pressure, therefore, comparison of 0ppm Propene and 200ppm Propene, along with the fuel, is more vital between the time interval 0.01750 seconds and 0.01875 seconds.

Considering the OH mole fractions, at all time intervals in the table above, OH mole fraction is higher for 200ppm Propene addition with fuel. Therefore, Propene addition favors the OH formation. With the Propene addition, the mass average temperature increased to 675.74 K from 648.53 K. This difference in temperature caused a change in the value of reaction rate constant K. The temperature change is shown in the tabular format below.

Time	**Temperature (K) at 0ppm C3H6**	**Temperature (K) at 200ppm C3H6**
0.0175	648.53 K	675.74 K

Following section describes the reason of higher OH mole fraction with 200ppm Propene using Reaction Path Analyzer.

4.6.2.1 At 0.01750 Seconds:

At the time 0.01750 seconds, the main reactions involving C3H6 are:

1. C3H6 + OH <==> C3H5 -T + H2O
2. C3H6 + OH <==> C3H5 -A + H2O
3. C3H6 + OH <==> C3H5 -S + H2O
4. C3H6OH <==> C3H6 + OH

Following these reactions:

1. C3H6 + OH <==> C3H5 -T + H2O

Time	At 0 ppm C3H6 and 0.0175 seconds; R_f: C3H6 + OH <==> C3H5 -T + H2O	At 200 ppm C3H6 and 0.0175 seconds; R_f: C3H6 + OH <==> C3H5 -T + H2O
0.0175	2.65 E-09 mol/cubic cm	4.04 E-07 mol/cubic cm

Time	At 0 ppm C3H6 and 0.0175 seconds; R_b: C3H6 + OH <==> C3H5 -T + H2O	At 200 ppm C3H6 and 0.0175 seconds; R_b: C3H6 + OH <==> C3H5 -T + H2O
0.0175	-1.35 E-16 mol/cubic cm	-7.2 E-14 mol/cubic cm

2. C3H6 + OH <==> C3H5 -A + H2O

Time	At 0 ppm C3H6 and 0.0175 seconds; R_f: C3H6 + OH <==> C3H5 -A + H2O	At 200 ppm C3H6 and 0.0175 seconds; R_f: C3H6 + OH <==> C3H5 -A + H2O
0.0175	2.9 E-08 mol/cubic cm	4.17E-6 mol/cubic cm

Time	At 0 ppm C3H6 and 0.0175 seconds; R_b: C3H6 + OH <==> C3H5 -A + H2O	At 200 ppm C3H6 and 0.0175 seconds; R_b: C3H6 + OH <==> C3H5 -A + H2O
0.0175	-3.34E-17 mol/cubic cm	-5.98E-15 mol/cubic cm

3. C3H6 + OH <==> C3H5 -S + H2O

Time	At 0 ppm C3H6 and 0.0175 seconds; R_f: C3H6 + OH <==> C3H5 -S + H2O	At 200 ppm C3H6 and 0.0175 seconds; R_f: C3H6 + OH <==> C3H5 -S + H2O
0.0175	1.89 E-09 mol/cubic cm	2.86 E-07 mol/cubic cm
Time	At 0 ppm C3H6 and 0.0175 seconds; R_b: C3H6 + OH <==> C3H5 -S + H2O	At 200 ppm C3H6 and 0.0175 seconds; R_b: C3H6 + OH <==> C3H5 -S + H2O
0.0175	-4.53 E-16 mol/cubic cm	-1.24 E-13 mol/cubic cm

4. C3H6OH <==> C3H6 + OH

Time	At 0 ppm C3H6 and 0.0175 seconds; R_f: C3H6OH <==> C3H6 + OH	At 200 ppm C3H6 and 0.0175 seconds; R_f: C3H6OH <==> C3H6 + OH
0.0175	1.05 E-11 mol/cubic cm	3.45 E-11 mol/cubic cm

Time	At 0 ppm C3H6 and 0.0175 seconds; R_b : C3H6OH <==> C3H6 + OH	At 200 ppm C3H6 and 0.0175 seconds; R_b : C3H6OH <==> C3H6 + OH
0.0175	-3.66E-08 mol/cubic cm	-4.76E-6 mol/cubic cm

From all of the above four reactions, the rate of backward reaction for reaction 4 is highest. Following this reaction, there are some other chain reactions that occur with the C3H6OH presence. These reactions are described in figure 4.40.

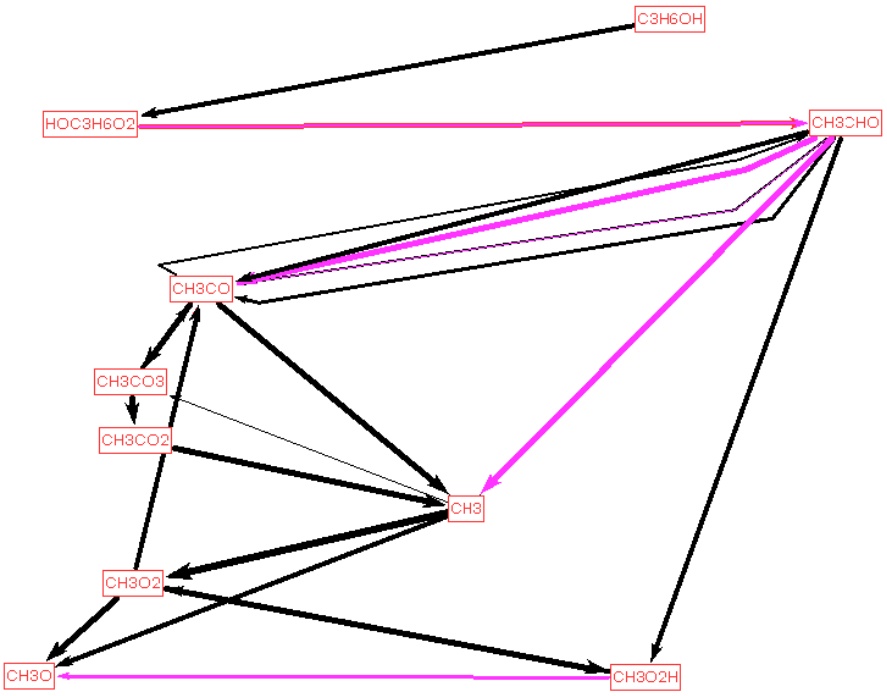

Figure 4.40 - Reaction Path diagram for C3H6OH

Figure 4.40 shows the Reaction path for the specie C3H6OH. Details of each reaction in the path are given below.

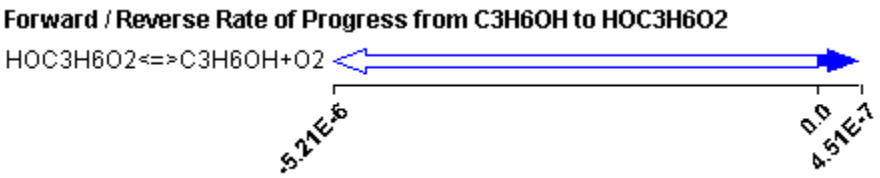

In the above reaction, rate of backward reaction is higher than the rate of the forward reaction. Therefore, the overall reaction moves in the backward direction.

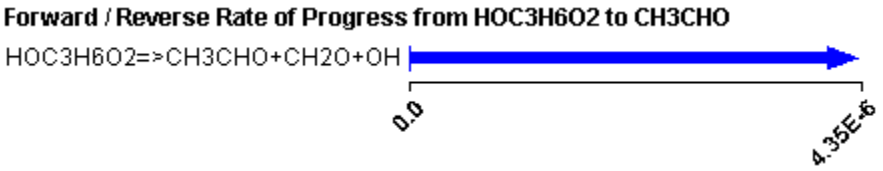

The reaction above moves only in the forward direction at this time interval. This reaction contributes to the OH formation.

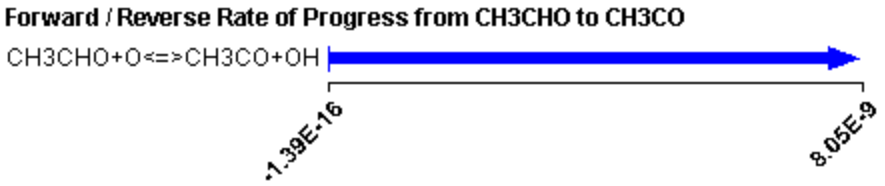

Again, for the reaction above, the rate of forward reaction is higher than the backward reaction. Therefore overall reaction moves in the forward direction. This reaction also contributes to the OH formation.

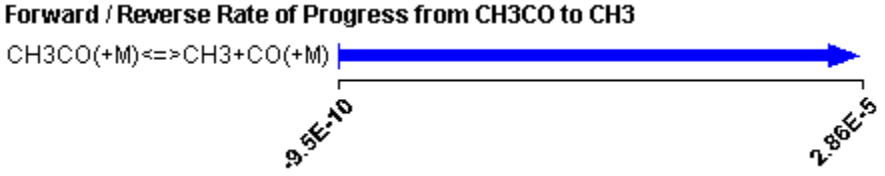

Again, for the reaction above, the rate of forward reaction is higher than the backward reaction. Also, the reaction produces two radicals.

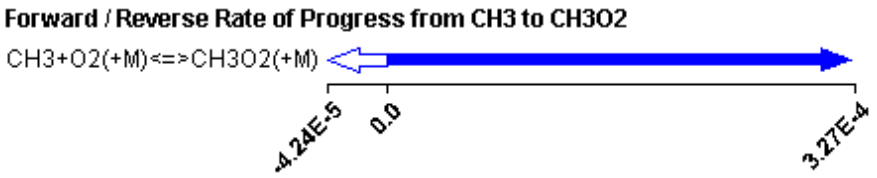

Again, for the reaction above, the rate of forward reaction is higher than the backward reaction. Therefore overall reaction moves in the forward direction.

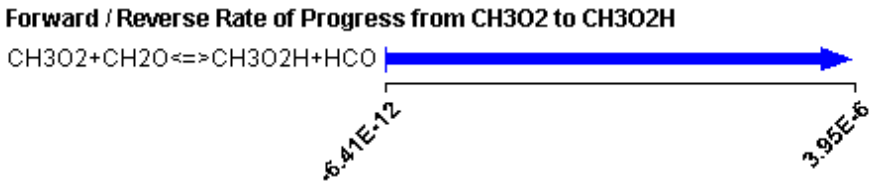

Above reaction also moves in the forward direction.

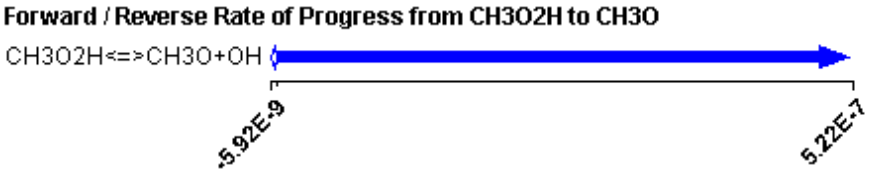

Again, for the reaction above, the rate of forward reaction is higher than the backward reaction. Therefore overall reaction moves in the forward direction. This reaction also contributes to the OH formation.

Therefore, the formation of C3H6OH causes chain reactions that produce OH at various steps in the chain. Therefore, OH mole fraction increases as per the set of reactions mentioned above.

Figure 4.41.a shows the rate of formation of OH at 0.01750 seconds with zero and 200ppm C3H6 while figure 4.41.b represent the comparison by superposition for the two cases of C3H6 addition and it can observed that there are three main reactions involving OH formation and consumption. These 3 reactions are:

- CH2CHO + 02 <==> CH2O + CO + OH ------ (a)
- CH2O + OH <==> HCO + H2O ------ (b)
- HOCH2O <==> CH2O + OH ------ (c)

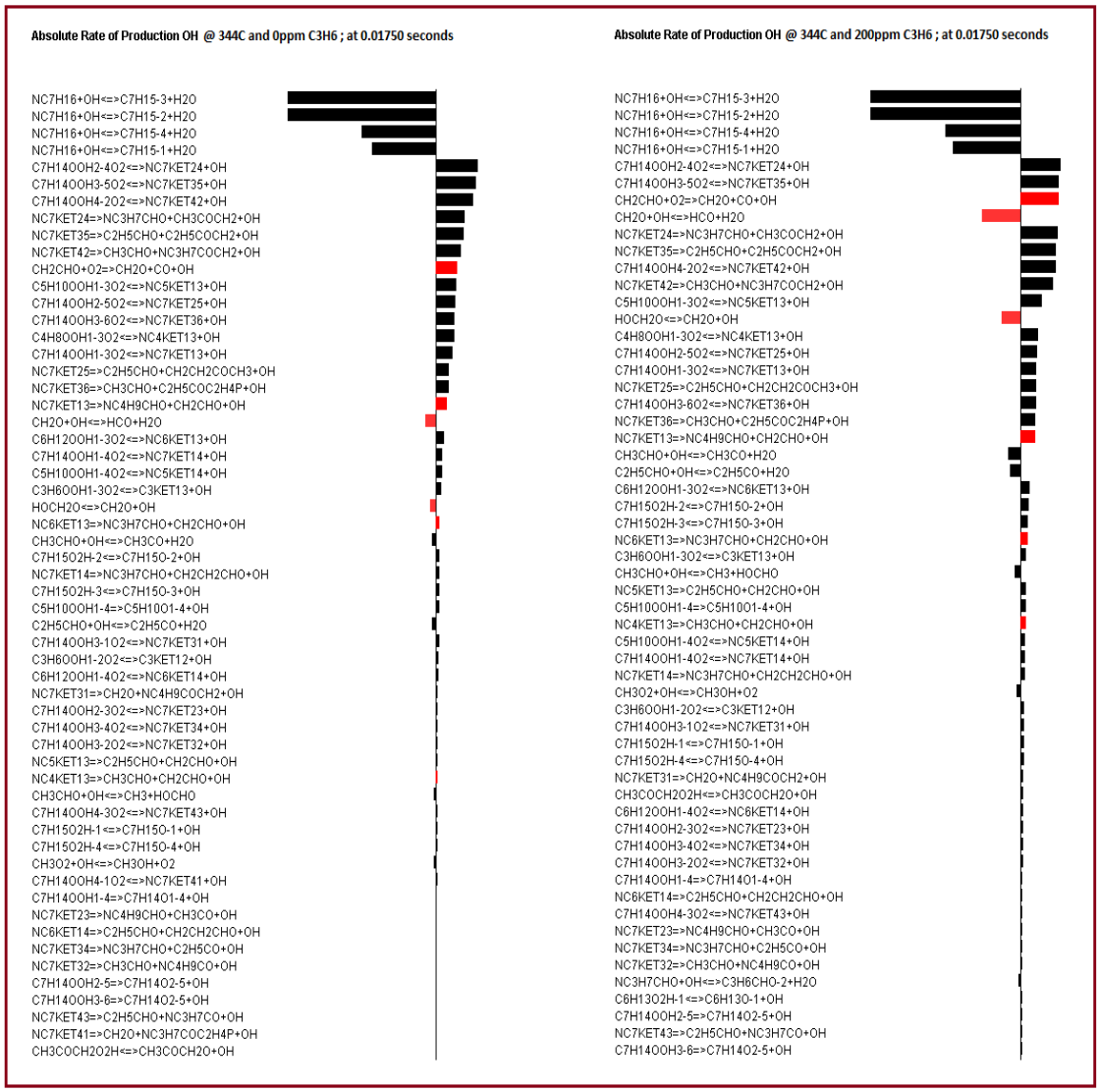

Figure 4.41.a - Rate of formation of OH at 0.01750 seconds with zero and 200ppm C3H6

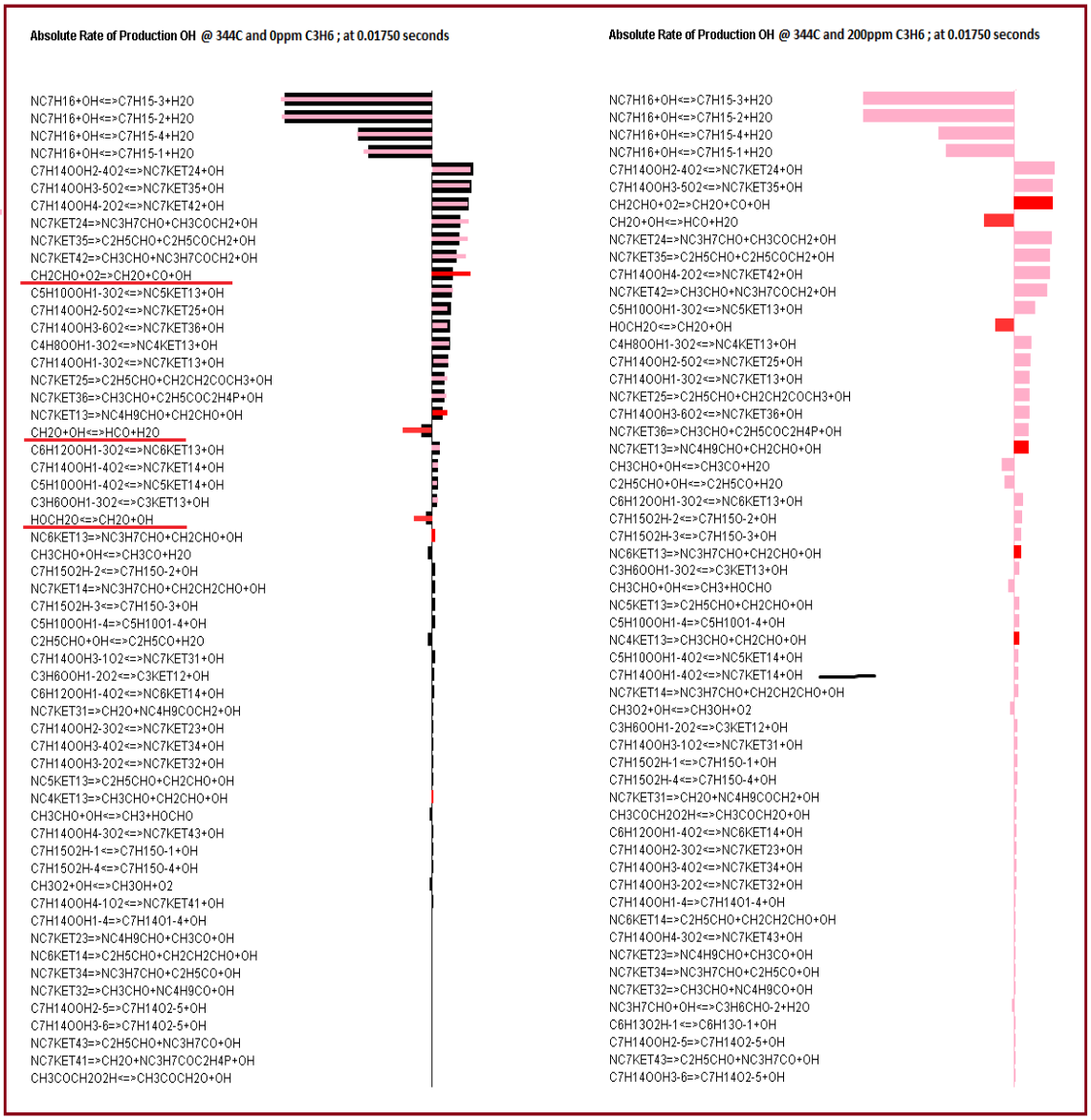

Figure 4.41.b - Comparison using superposition between the rate of formation of OH at 0.01750 seconds with zero and 200ppm C3H6

The reaction (a), **CH2CHO + 02 ==> CH2O + CO + OH**, goes only in forward direction. This forward reaction favors the formation of OH. By considering the Rate of the Reaction for both the cases, the OH formation can be obtained through this reaction.

Time	At 0 ppm C3H6 and 0.0175 seconds; Rf : CH2CHO + 02 <==> CH2O + CO + OH	At 200 ppm C3H6 and 0.0175 seconds; Rf : CH2CHO + 02 <==> CH2O + CO + OH
0.0175	1.94E-05	1.26E-04

Now considering reaction (b), **CH2O + OH <==> HCO + H2O,**

The rate of reaction obtained from Reaction Path analysis are :

Time	At 0 ppm C3H6 and 0.0175 seconds; R_f : CH2O + OH <==> HCO + H2O	At 200 ppm C3H6 and 0.0175 seconds; R_f : CH2O + OH <==> HCO + H2O
0.0175	9.74E-06	1.25E-04

Time	At 0 ppm C3H6 and 0.0175 seconds; R_b : CH2O + OH <==> HCO + H2O	At 200 ppm C3H6 and 0.0175 seconds; R_b : CH2O + OH <==> HCO + H2O
0.0175	-2.22E-18	-1.44E-16

From the table above, it is quite evident that the rate of forward reaction for 0ppm Propene is higher than the rate of forward reaction with 200ppm Propene. The rates of backward reaction are very small for comparison.

Now considering reaction (c), **HOCH2O <==> CH2O + OH,** the forward reaction favors the OH formation while the Backward Reaction Reduces the OH concentration

From the reaction path analysis:

Time	At 0 ppm C3H6 and 0.0175 seconds;	At 200 ppm C3H6 and 0.0175 seconds;
	R_f : HOCH2O <==> CH2O + OH	R_f : HOCH2O <==> CH2O + OH
0.0175	6.47E-09	9.8E-08

Time	At 0 ppm C3H6 and 0.0175 seconds;	At 200 ppm C3H6 and 0.0175 seconds;
	R_b : HOCH2O <==> CH2O + OH	R_b : HOCH2O <==> CH2O + OH
0.0175	-5.21E-06	-6.19E-05

The total OH mole fraction at time 0.01750 seconds is:

Time	Mole_fraction_OH at 0ppm C3H6	Mole_fraction_OH at 200ppm C3H6
0.01750	7.99E-09	3.16E-08

It is evident that with 200ppm Propene addition, reaction (a) proposes higher OH formation, reaction (b) proposes comparatively higher OH consumption and reaction (c) proposes comparatively higher OH consumption. since the mole fraction of OH is higher in the case of 200ppm Propene addition, it can be concluded that reaction (a) along with the chain reaction shown in figure 4.40 dominate at this time interval and OH concentration is higher as compared to no Propene addition.

4.6.2.2 At 0.01875 Seconds:

Absolute rate of Formation of OH at 0.018750 seconds with Zero ppm C3H6 and 200ppm C3H6 respectively.

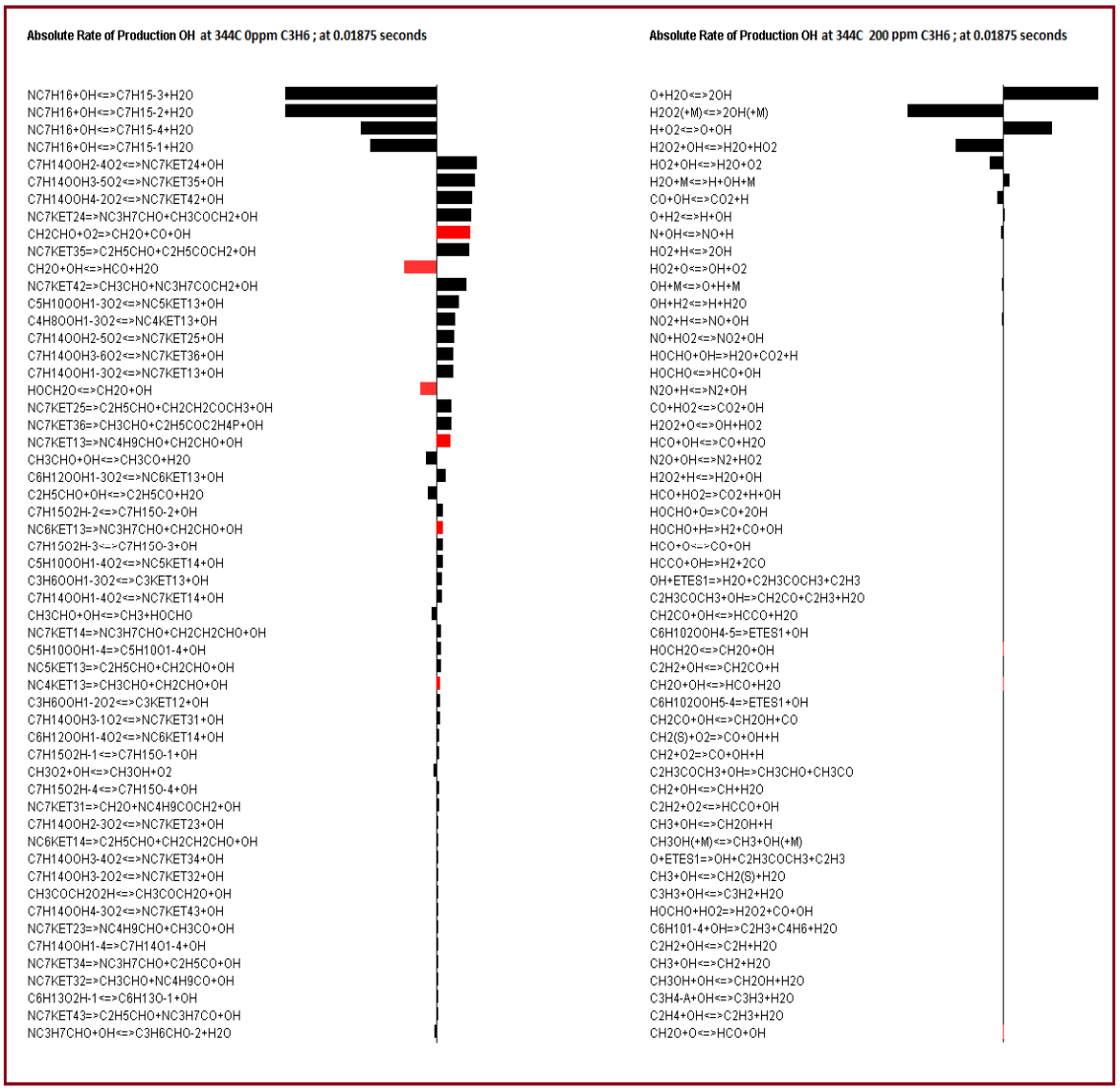

Figure 4.42 - Rate of formation of OH at 0.018750 seconds with zero and 200ppm C3H6

From figure 4.42, it is evident that the combustion of fuel is still in process for the case of no Propene addition. On the other side, the combustion process has almost finished for the fuel mixed with 200ppm Propene. Therefore the comparison of the reactions is not of much help in this time interval.

4.6.3 Summary:

- It is evident that the start of combustion is advanced by Propene addition indicating a decrease in ID.
- OH production rate is also advanced with the Propene addition.
- Using Chemical Kinetics, it can be inferred that the three reactions (a), (b) and (c) together with the C3H6OH chain reaction decide the total OH mole fraction.
    - The addition of Propene increases the average mass temperature and reaction rate constant.
    - More case studies for different Hydrocarbon species are given in appendix C and appendix D.

CHAPTER 5

CONCLUSIONS AND RECOMMENDATIONS

5.1 Conclusions

In the dissertation a new concept has been investigated and a control strategy has been developed for gases recirculation strategy of a diesel engine with common rail fuel injection system to improve diesel engine cold startability, and to reduce fuel delivery per cycle, cranking periods and HC emissions (or white smoke) during cold starting. These conclusions are based on an experimental investigation on a 1.2 liter, 4 cylinders diesel engine equipped with a common rail injection system in a cold room to determine the effects of the fuel injection and cranking gas recirculation (CGR) on the cranking period, fuel consumption and HC emissions. The experiments were conducted at ambient room temperatures of 16℃ and 3℃.

1. CGR is a viable approach, that at certain rates, can reduce the cranking period, fuel consumption and HC emissions (white smoke) during cold start without any external aid (unaided cold start).

2. Low rates of CGR enhance the autoignition process, reduce the cranking period, fuel injection and engine-out hydrocarbons that appear as white smoke during cranking.

3. CGR at higher rates, produced by increasing the back pressure, hinders the autoignition reactions and increases the cranking period, fuel injection and hydrocarbons emissions.

4. There is an optimum CGR valve opening beyond which the CGR percentage in the fresh charge increases and causes an increase in the cranking period.

5. For the same amount of fuel injected, the lower the temperature the higher the CGR opening required to reduce the cranking periods.

The simulation results explained many observations made from the experimental work.

1. The diesel cycle simulation showed clearly the effect of the increase in HCHO mole fraction on slowing the autoignition reactions till misfiring while the increase of some HCs species have an enhancing effect on autoignition.

2. At low mole fractions, some HCs species enhance the autoignition process while others have no effect or little retarding effects. Accordingly, low rates of CGR reduce the cranking period in addition to lowering the demand on fuel delivery during cranking. This is due to the increase in the fuel vapor concentration by the CGR, in spite of the presence of a low concentration of HCHO.

3. Some HCs species have small or no effect on enhancing the autoignition reactions. Meanwhile, other HCs have retarding effects. The high mole fractions of these species in addition to the effect of HCHO at high rates of CGR dominate over the enhancing effects of other species and increase the cranking period at the same fuel delivery. {Rafik: Can you summarize all the findings regarding which HC enhance autignition reactions and which hinder …}

4. HCHO/H2O2 is a powerful parameter that can predict whether the engine increase will fire or misfire. .

5.2 Recommendations

1. Extend the experiments and the simulation to lower ambient temperatures and different fuels and determine the optimum fuel delivery rate.
2. Develop an electronically controlled CGR valve for a better control of the rate of recirculated gases.
3. Determine the effect of the partial closing of the CGR valve on the charge temperature and pressure.
4. Extend the simulation to investigate the effect of different HCs and HCHO combinations on ignition delay.
5. Investigate in more details the effect of recirculated gases on changing the compression temperature as it is one of the main factors affecting the cold start of diesel engines.

APPENDIX A

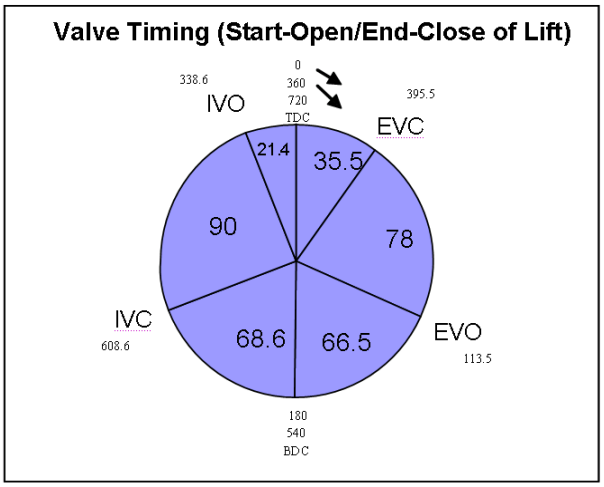

Figure A.1-Valve Timing (Start of Lift)

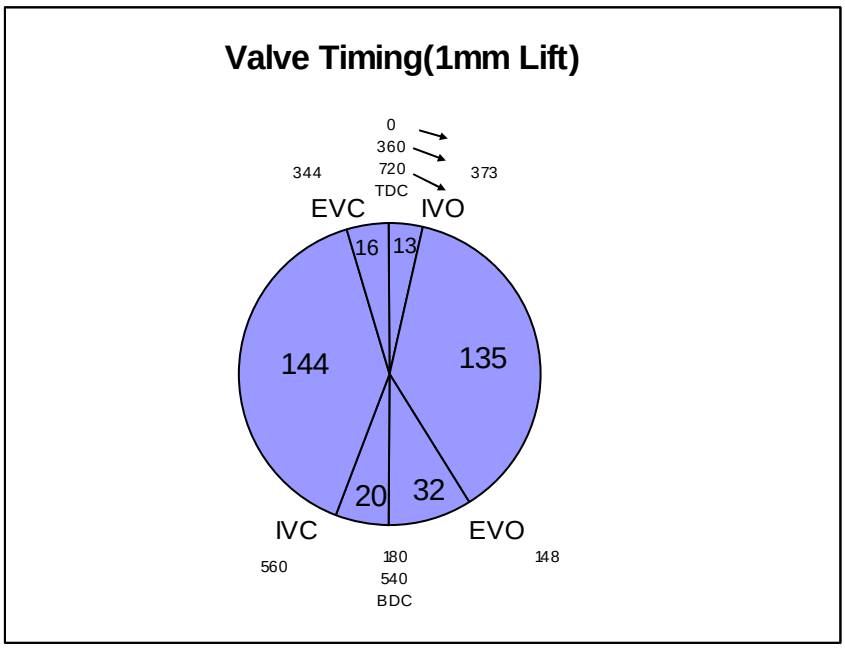

Figure A.2-Valve Timing (1mm Lift)

APPENDIX B

Cylinder Capacity	300 cc
Number of Spray Holes	6
Spray Hole Diameter [mm]	0.124
Hydr. Flow Rate [cm^3/30 s] at 100 bar	250
Cone Angle	150°
Medium Hole Roundness [%]	7
Needle Guide	single
Needle Length [mm]	31.07

Figure B.1 - Injectors Nozzle geometry details

APPENDIX C

C.1 Reaction Path Analysis for OH Formation and Ignition Delay with Ethane addition:

This study was conducted to study the effect of Ethane addition on the ignition delay. Fuel was N-Heptane (NC7H16). Addition of Ethane was parameterized with an increment of 100 ppm in each successive run starting from 0 ppm to 1000 ppm.

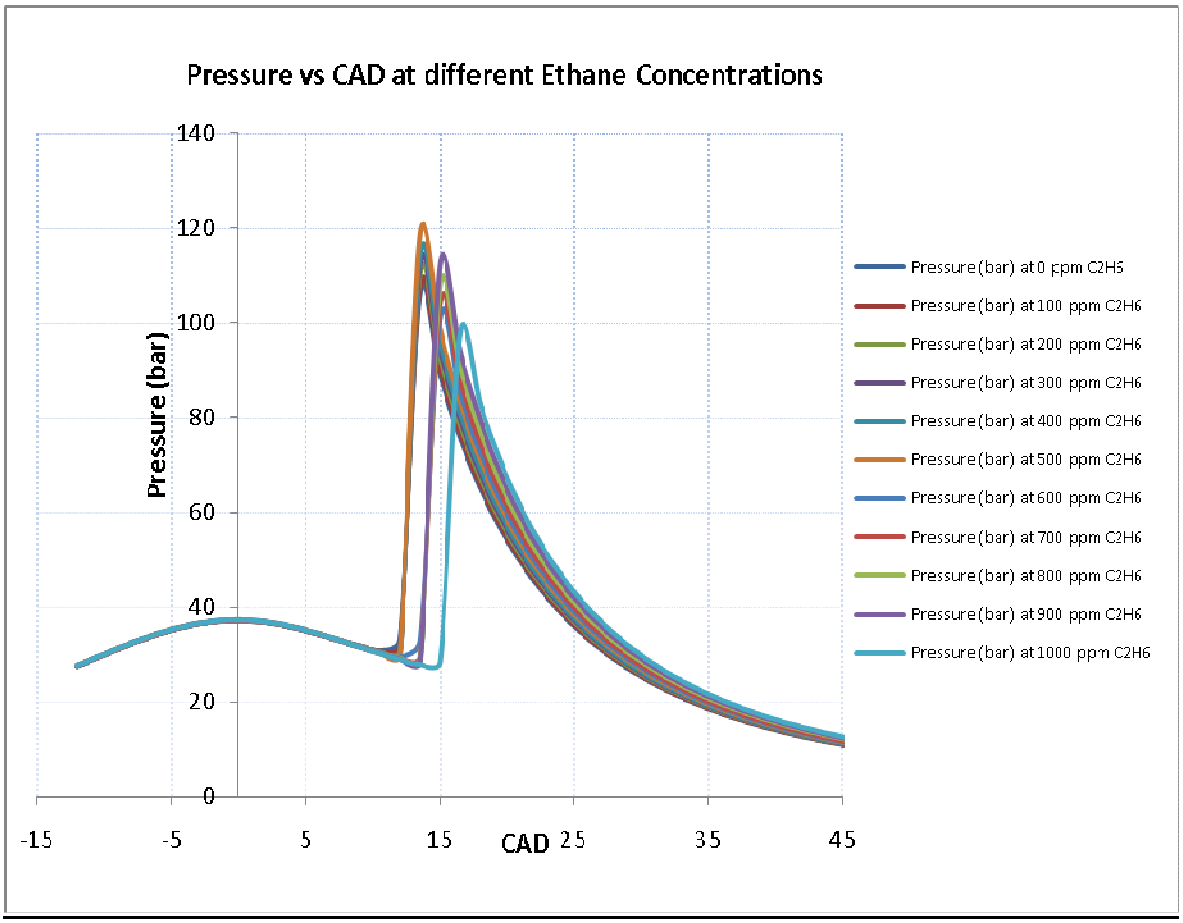

Figure C.1 - Effect of C2H6 addition on Ignition Delay at Equivalence Ratio 1.0

From Figure C.1, it is evident that the addition of ethane increases the ignition delay. Up to 500 ppm, the start of ignition occurs near 12 CAD ATDC. Increasing the ethane mole fraction above 500 ppm, increases ID, retarding the start of ignition from 12 to 13.5 CAD ATDC (500ppm to 900ppm). At 1000pmm, ignition delay is increased to 15 CAD.

C.1.1 Investigation of Ignition Retard:

Various plots were made for pressure and OH concentrations as shown in figure C.2 and C.3. It was interesting to find that the rise in pressure due to combustion is accompanied by the rise in OH concentration. The plot below shows that OH mole fraction follows almost the same pattern as the pressure.

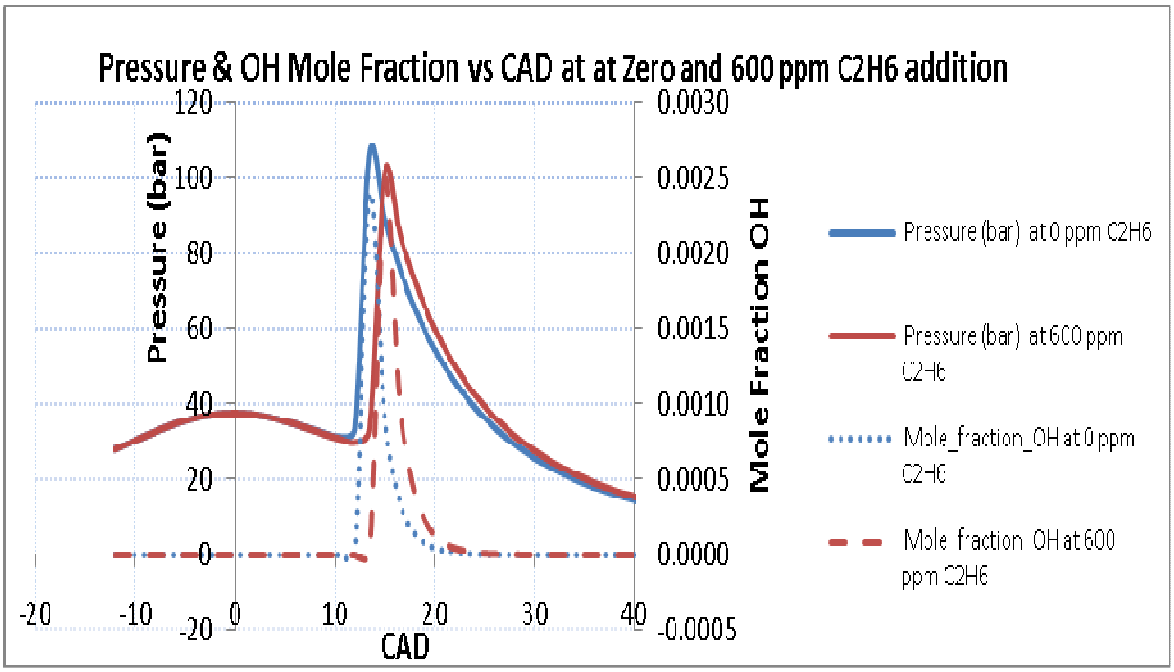

Figure C.2 - In-cylinder Pressure and OH mole fractions at zero and 600ppm C2H6 addition versus CAD

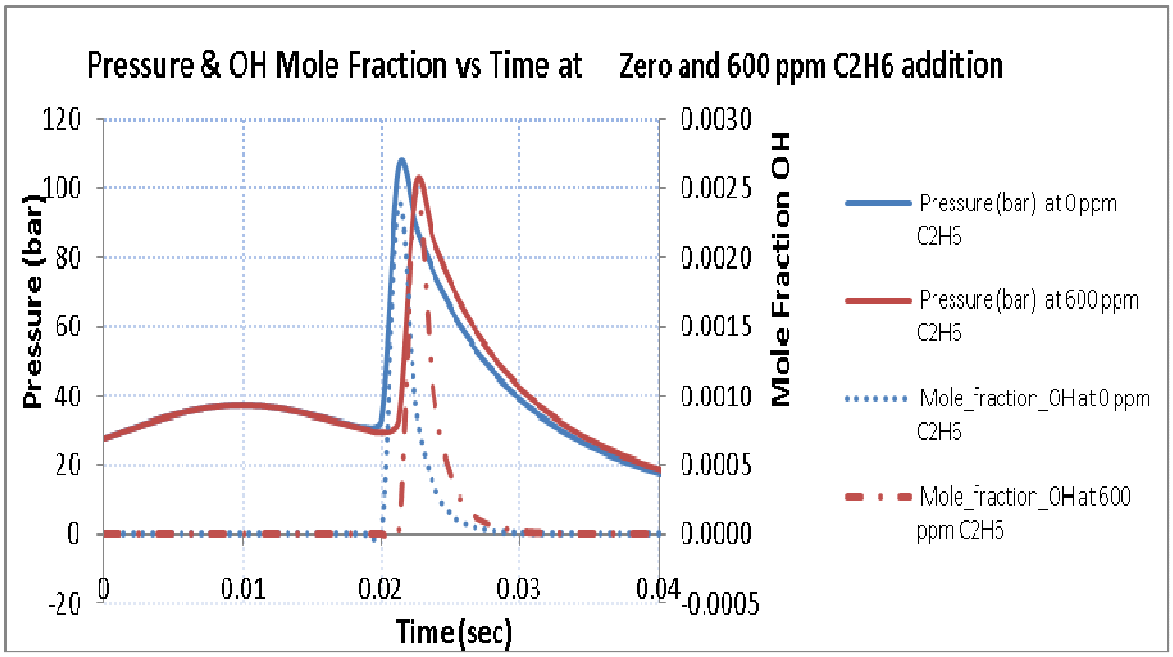

Figure C.3 - In-cylinder Pressure and OH mole fractions at zero and 600ppm C2H6 addition versus Time

From figures C.2 and C.3, it can be concluded that addition of ethane has a direct effect on the OH concentration. OH being a main contributor to the start of combustion, the effects of ethane on OH need to be examined.

Considering two cases, no Ethane added in the first case while 600ppm Ethane added in the second case. The comparison between these two conditions can help in understanding the effect of adding C2H6 on retarding the ignition.

C.1.2 Investigation using Reaction Path Analysis:

The RPA approach is used in this work, recognizing the effect on the reaction occurrence with the addition of zero C2H6 and 600ppm C2H6. The study was performed at the time intervals 0.018750 seconds, 0.020 seconds and 0.02175 seconds from the start of injection of the fuel NC7H16. It was observed that the combustion occurred at about 0.01875 seconds.

The approach was to compare the reactions involved in each of the two cases at the various time intervals.

The comparison of the two cases shows a very bright picture that involves the kinetics of the reactions. Although, most of the reactions were common for both the cases, the rates of the reactions were different at the given interval of time for zero Ethane and 600ppm Ethane. Therefore, formation or consumption of the species involved in the reaction varied greatly. Following are the results for comparisons of the two different ethane mole fractions.

C.1.2.1 At Time 0.01875 Seconds

Absolute rate of Formation of OH at 0.01875 seconds with Zero ppm C2H6 and 600ppm C2H6 respectively.

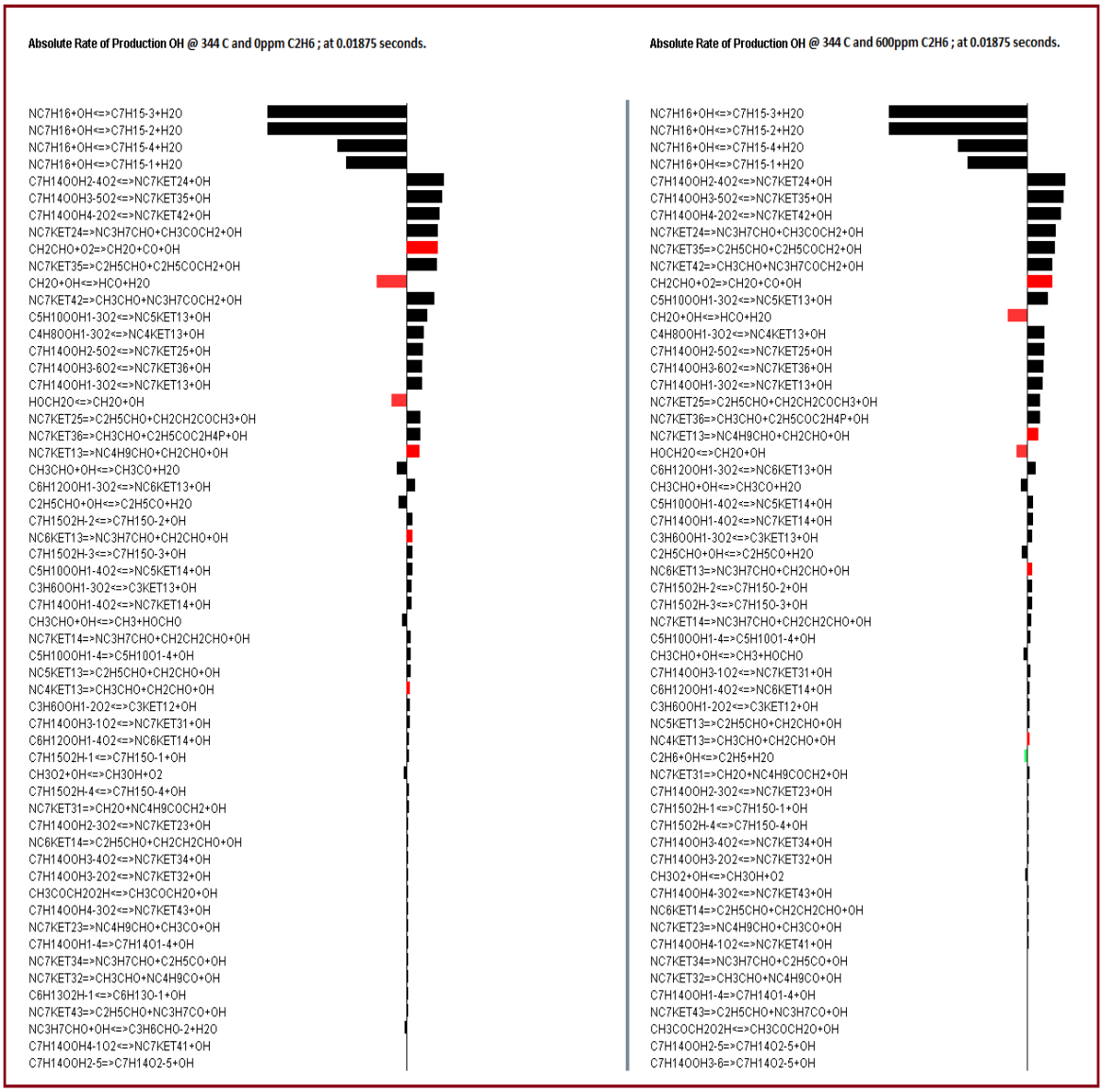

Figure C.4.a - Rate of formation of OH at 0.01875 seconds with zero and 600ppm C2H6

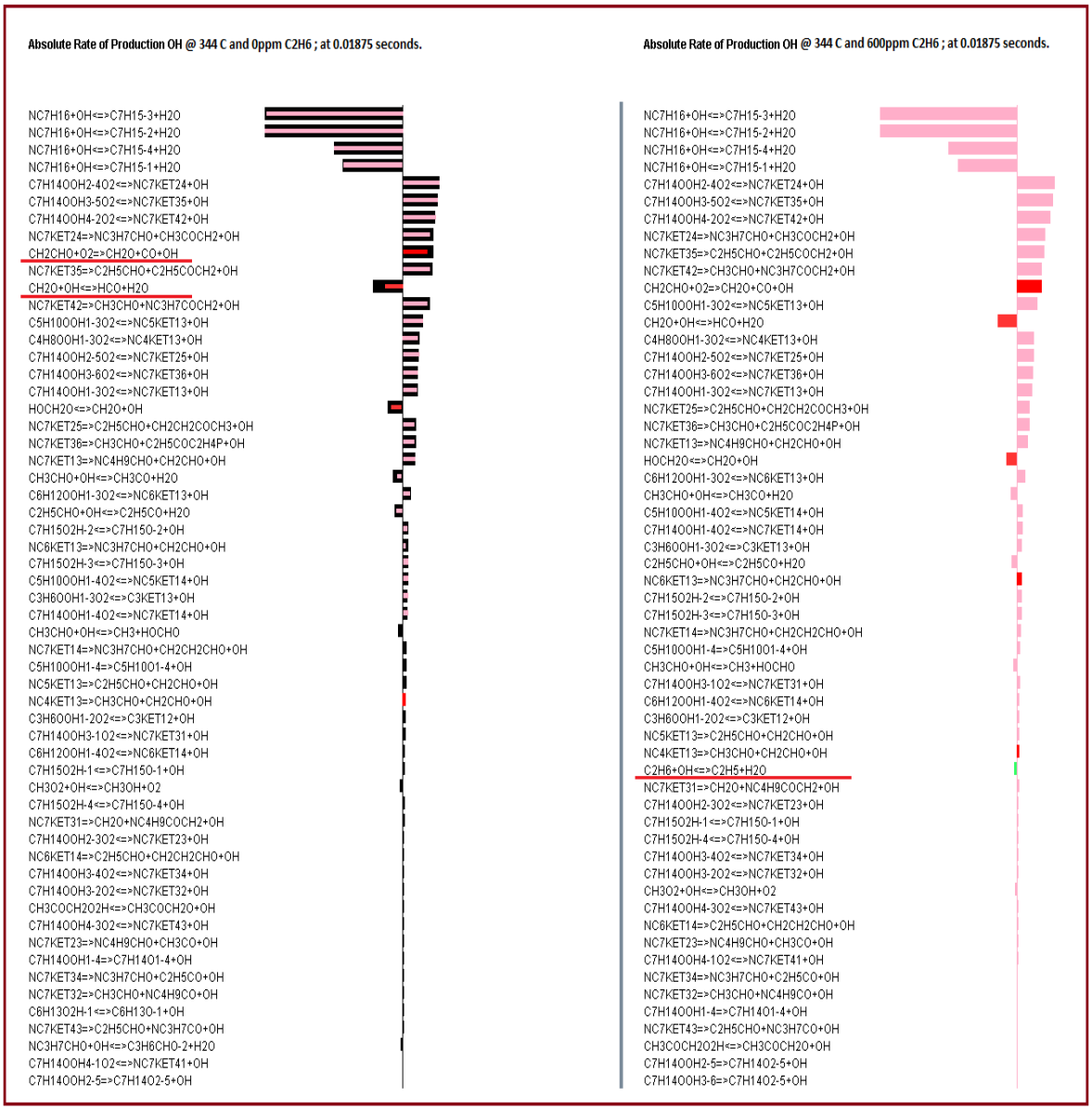

Figure C.4.b - Comparison using superposition between the rate of formation of OH at 0.018750 seconds with zero and 600ppm C2H6

Figure C.4.a shows the rate of formation of OH at 0.018750 seconds with zero and 600ppm C2H6 while figure C.4.b represents the comparison by superposition for the two cases of C2H6 addition. It can be observed that main reactions involving OH and C2H6 are:

- CH2CHO + 02 ==> CH2O + CO + OH ------ (a)
- CH2O + OH <==> HCO + H2O ------ (b)
- C2H6 + OH <==> C2H5 + H2O ------ (c)
- C2H6 + 02 <==> C2H5 + HO2 ------- (d)

Now with the Ethane addition, the mass average temperature dropped to 647.8K from 658.3 K. This change in temperature is shown in the tabular format below.

Time	Temperature at 0ppm C2H6	Temperature at 600ppm C2H6
0.01875	658.279	647.835

This drop in temperature caused a change in the value of reaction rate constant K. This can be shown by the Arrhenius Equation as follows:

$$K = A \exp\left(\frac{-E}{RT}\right)$$

Now, reaction (a), **CH2CHO + 02 ==> CH2O + CO + OH**, goes only in forward direction. This forward reaction favors the formation of OH. Considering the rate of the reaction for both the cases, the OH formation can be observed through this reaction.

Time	At 0 ppm C2H6 and 0.01875 seconds; Rf : CH2CHO + 02 <==> CH2O + CO + OH	At 600 ppm C2H6 and 0.01875 seconds; Rf : CH2CHO + 02 <==> CH2O + CO + OH
0.01875	5.21E-05	2.55E-05

The above results were obtained from Reaction Path Analyzer. It is evident that the formation of OH is lower in case of Ethane addition. It can be due to change in the temperature or the availability of O2 atom.

Considering reaction (b), **CH2O + OH <==> HCO + H2O**,

Time	At 0 ppm C2H6 and 0.01875 seconds; R_f : CH2O + OH <==> HCO + H2O	At 600 ppm C2H6 and 0.01875 seconds; R_f : CH2O + OH <==> HCO + H2O
0.01875	4.98 E-05	1.96 E-05

Time	At 0 ppm C2H6 and 0.01875 seconds; R_b : CH2O + OH <==> HCO + H2O	At 600 ppm C2H6 and 0.01875 seconds; R_b : CH2O + OH <==> HCO + H2O
0.01875	-2.69 E-17	-5.72 E-18

From the table above, it is evident that the rate of forward reaction for 0 ppm Ethane is higher than the rate of forward reaction with 600 ppm Ethane. The rates of backward reaction are very small for comparison. Now the forward reaction consumes OH radical. Therefore, OH consumption is lower according to this equation in case of C2H6 addition. This can be explained in the following manner. The rate of reaction (a) is much higher for no Ethane addition. Therefore, the products of the reaction (a) are higher in concentration for the case of 0ppm Ethane addition. Reaction (a) produces formaldehyde which is one of the reactant in reaction (b). Thus, higher the quantity of formaldehyde, higher is the rate of forward reaction of reaction (b).

Now considering reaction (c), **C2H6 + OH <==> C2H5 + H2O,** the forward reaction consumes the OH radical. Therefore any increase in the quantity of Ethane increases the rate of forward reaction with all other parameters

remaining constant. Hence, OH consumption increases with the presence of 600 ppm of Ethane when compared to 0 ppm Ethane.

From the reaction path analysis, the net rate of the reaction

Time	At 0 ppm C2H6 and 0.01875 seconds;	At 600 ppm C2H6 and 0.01875 seconds;
	Rf : C2H6 + OH <==> C2H5 + H2O	Rf : C2H6 + OH <==> C2H5 + H2O
0.01875	**6.1E-11**	**2.88E-06**

Time	At 0 ppm C2H6 and 0.01875 seconds;	At 600 ppm C2H6 and 0.01875 seconds;
	Rb : C2H6 + OH <==> C2H5 + H2O	Rb : C2H6 + OH <==> C2H5 + H2O
0.01875	-2.76E-13	-8.4E-14

There is a remarkable difference between the rates of the forward reaction in the two cases of ethane addition. There is a difference of the magnitude of E05 in the reaction rates. Therefore, the Ethane addition reduces the net OH radical mole fraction as per the above reaction.

Now considering reaction (d), **C2H6 + 02 <==> C2H5 + HO2,** the forward reaction consumes the available oxygen inside the combustion chamber. It is interesting to see that this reaction does not occur at 600 ppm Ethane at 0.01875 second. This can be due to reduction in temperature caused by Ethane addition. For no ethane addition, the reaction occurs but the rate is very small.

From the reaction path analysis, the net rate of the reaction

Time	At 0 ppm C2H6 and 0.01875 seconds;	At 600 ppm C2H6 and 00.01875 seconds;
	R_{net}: C2H6 + 02 <==> C2H5 + HO2	R_{net} : C2H6 + 02 <==> C2H5 + HO2
0.01875	2.22E-09	Reaction not occurring at these conditions.

The total OH mole fraction at time 0.01875 seconds is:

Time	Mole fraction OH at 0ppm C2H6	Mole fraction OH at 600ppm C2H6
0.01875	1.65E-08	9.59E-09

It is evident that with 600 ppm Ethane addition, reaction (a) results in less OH formation, reaction (b) results in comparatively less OH consumption and reaction (c) results in higher OH consumption. Other than that, some other reactions also contribute to the OH formation; rates of these are higher in case of 0 ppm Ethane. These reactions are shown in figure C.5. Solid lines with black color represent reactions with 0 ppm Ethane, the pink lines and the red lines represent reactions with 600ppm Ethane addition

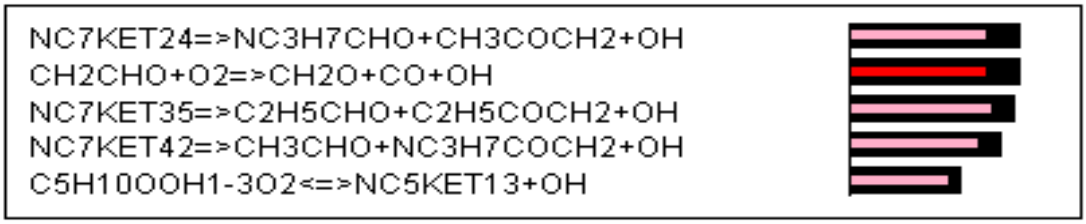

Figure C.5 - Comparison of Absolute rate of OH formation by some other reactions for zero and 600ppm Ethane addition at 0.01875 seconds.

Since, the net OH mole fraction is lower in case of Ethane addition at 0.01875 second, and from the above results, it is evident that the effect of reaction (a) and (c) is dominating at this time interval. There is not much reduction in the OH interaction with the fuel at this time.

C.1.2.2 At 0.020 Seconds:

Absolute rate of Formation of OH at 0.020 seconds with Zero ppm C2H6 and 600 ppm C2H6 respectively.

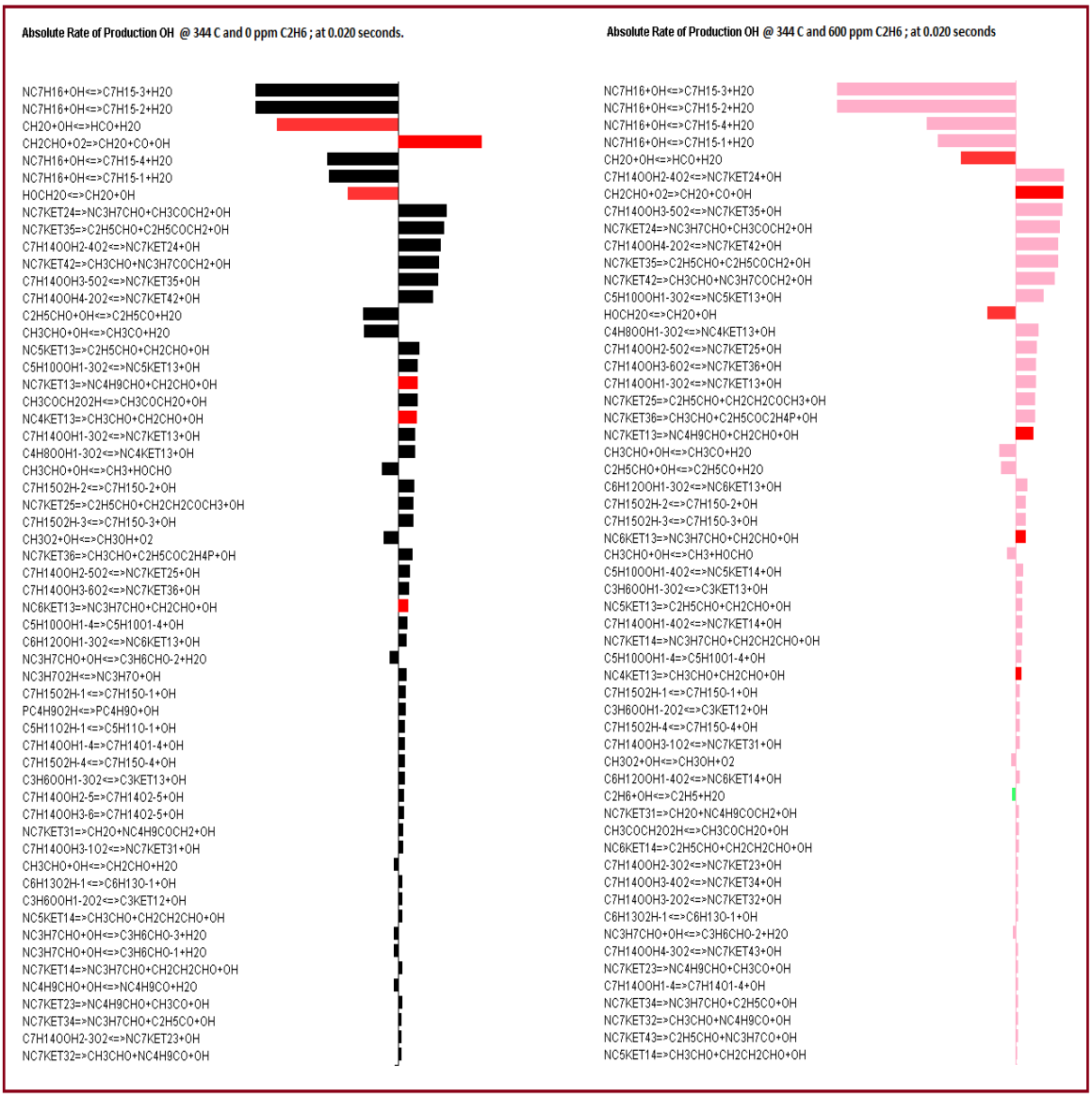

Figure C.7.a - Comparison using superposition between the rate of formation of OH at 0.020 seconds with zero and 600ppm C2H6

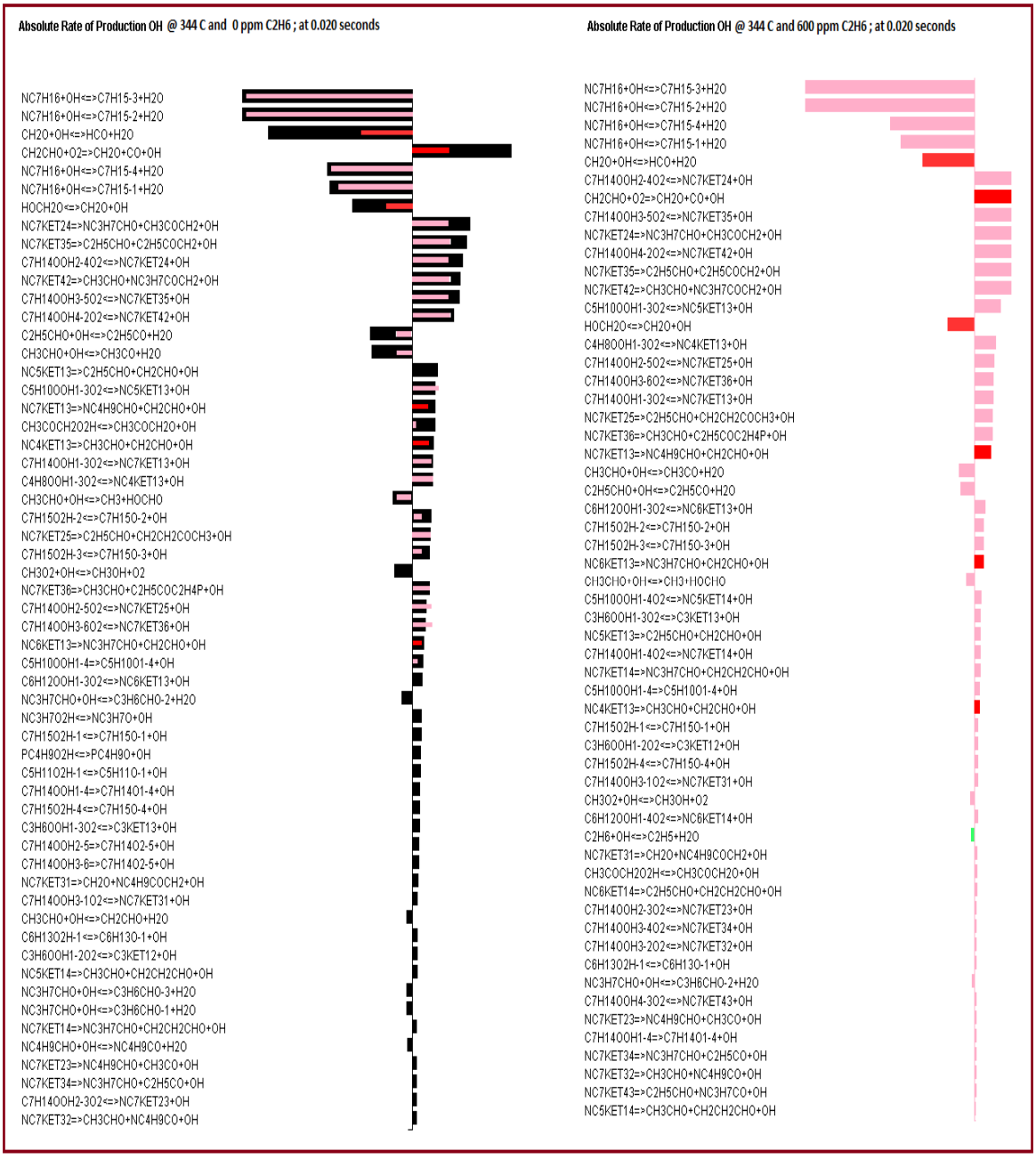

Figure C.7.b - Comparison using superposition between the rate of formation of OH at 0.020 seconds with zero and 600ppm C2H6

Figure C.7.a shows the rate of formation of OH at 0.020 seconds with zero and 600 ppm C2H6 while figure C.7.b represents the comparison by superposition

for the two cases of C2H6 addition. The main reactions involving OH and C2H6 are:

- CH2CHO + 02 ==> CH2O + CO + OH ------ (a)
- CH2O + OH <==> HCO + H2O ------ (b)
- C2H6 + OH <==> C2H5 + H2O ------ (c)
- C2H6 + 02 <==> C2H5 + HO2 ------- (d)

Now with the Ethane addition, the mass average temperature dropped to 659.K from 737.5K. This change is shown in the tabular format below.

{ Rafik: Temperature to forth digit is not reasonable to write even if the program prints it} If I were you, I would fix in all the previous cases}

Time	Temperature at 0ppm C2H6	Temperature at 600ppm C2H6
0.02	737.5097	659.026

Now reaction (a), **CH2CHO + 02 ==> CH2O + CO + OH**, goes only in forward direction. This forward reaction favors the formation of OH. Considering the Rate of the Reaction for both the cases, the OH formation can be obtained through this reaction.

Time	At 0 ppm C2H6 and 0.0200 seconds; Rf : CH2CHO + 02 <==> CH2O + CO + OH	At 600 ppm C2H6 and 0.0200 seconds; Rf : CH2CHO + 02 <==> CH2O + CO + OH
0.0200	**1.77 E-03**	**6.16 E-05**

The above results were obtained from Reaction Path Analyzer. It is quite evident that the formation of OH is lesser in case of Ethane addition. It can be due to change in the temperature or the availability of O2 atom.

Now considering reaction (b), **CH2O + OH <==> HCO + H2O**,

The rate of reaction obtained from Reaction Path analysis is:

Time	At 0 ppm C2H6 and 0.0200 seconds; R_f : CH2O + OH <==> HCO + H2O	At 600 ppm C2H6 and 0.0200 seconds; R_f : CH2O + OH <==> HCO + H2O
0.0200	2.58 E-03	7.09 E-05

Time	At 0 ppm C2H6 and 0.0200 seconds; R_b : CH2O + OH <==> HCO + H2O	At 600 ppm C2H6 and 0.0200 seconds; R_b : CH2O + OH <==> HCO + H2O
0.0200	-5.05 E-14	-4.92 E-17

From the table above, it is evident that the rate of forward reaction for 0ppm Ethane is higher than the rate of forward reaction with 600ppm Ethane. The rates of backward reaction are very small for comparison.

Now considering reaction (c), **C2H6 + OH <==> C2H5 + H2O,** the forward reaction consumes the OH radical. From the reaction path analysis, the net rate of the reaction

Time	At 0 ppm C2H6 and 0.0200 seconds;	At 600 ppm C2H6 and 0.0200 seconds;
	Rf : C2H6 + OH <==> C2H5 + H2O	Rf : C2H6 + OH <==> C2H5 + H2O
0.0200	**4.3E-08**	**5.31E-06**

Time	At 0 ppm C2H6 and 0.0200 seconds;	At 600 ppm C2H6 and 0.0200 seconds;
	Rb : C2H6 + OH <==> C2H5 + H2O	Rb : C2H6 + OH <==> C2H5 + H2O
0.0200	-2.26E-10	-3.03E-09

Therefore, the Ethane addition reduces the OH radical concentration as per the above reaction.

Now considering reaction (d), **C2H6 + 02 <==> C2H5 + HO2,** the forward reaction consumes the available oxygen inside the combustion chamber. It is interesting to see that this reaction does not occur at 600 ppm Ethane at 0.020 seconds. This can be due to reduction in temperature because of Ethane addition.

From the reaction path analysis, the net rate of the reaction

Time	At 0 ppm C2H6 and 0.0200 seconds;	At 600 ppm C2H6 and 0.0200 seconds;
	R_{net}: C2H6 + 02 <==> C2H5 + HO2	R_{net} : C2H6 + 02 <==> C2H5 + HO2
0.0200	9.46E-07	Reaction not occurring at these conditions.

The total OH mole fraction at time 0.02000 seconds is:

Time	Mole fraction OH at 0ppm C2H6	Mole fraction OH at600ppm C2H6
0.02000	2.99E-07	1.89E-08

It is evident that with 600 ppm Ethane addition, reaction (a) results in less OH formation, reaction (b) results in comparatively less OH consumption and reaction (c) results in comparatively more OH consumption. Other than that, some other reactions also contribute to the OH formation; rates of these are higher in case of 0 ppm Ethane. Figure C.8 shows some of these reactions. Solid

lines with black color represent reactions with 0 ppm Ethane, the pink lines represent reactions with 600 ppm Ethane addition.

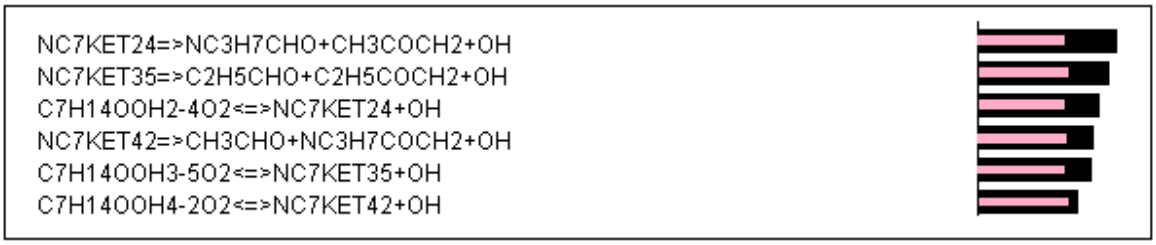

Figure C.8 - Comparison of Absolute rate of OH formation by some other reactions for zero and 600ppm Ethane addition at 0.020 seconds.

Since, the net OH mole fraction is lower in case of Ethane addition at 0.02000 second, and from the above results, it is evident that the effect of reaction (a) and (c) is dominating at this time interval. Also, with Ethane addition, the OH interaction with the fuel is reduced at this time.

C.1.2.3 At 0.02175 seconds:

Absolute rate of formation of OH at 0.02175 seconds with Zero ppm C2H6 and 600 ppm C2H6 respectively.

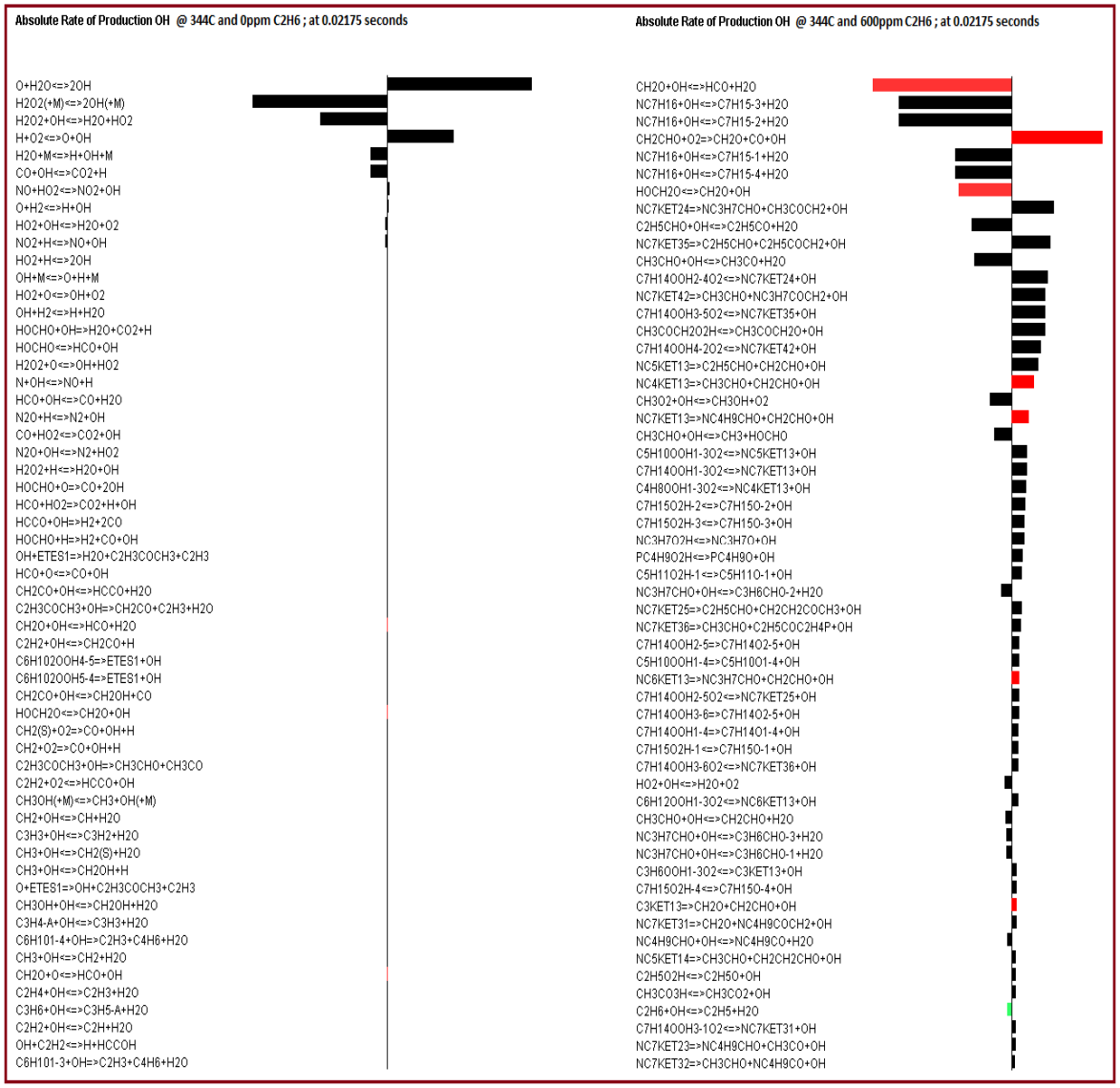

Figure C.9 - Comparison using superposition between the rate of formation of OH at 0.02175 seconds with zero and 600ppm C2H6

Figure C.9 represent the comparison by superposition, the rate of formation of OH at 0.021750 second with zero and 600 ppm C2H6 addition. Since most of the combustion process has finished for the case of zero ppm Ethane addition, the comparison of reactions at this stage is not greatly helpful in determining OH mole fraction. From figure C.9, there are very few reactions that involve the OH radical for the case of no Ethane addition. On the other side, in case for 600 ppm Ethane, the combustion process has just started and therefore a lot of reactions involving the OH radical occur.

C.1.3 Summary:

- It is evident that the start of combustion is retarded by Ethane addition. Therefore ignition delay increased.
- OH production rate is also retarded with the Ethane addition.
- The addition of Ethane decreases the average mass temperature. Therefore, a change in the reaction rate constant and the reaction rate is evident.

APENDIX D

D.1 Reaction Path Analysis for OH Formation and Ignition Delay with Methane addition:

This study was conducted to study the effect of Methane addition on the ignition delay. Fuel was N-Heptane (NC7H16). Addition of Methane was parameterized with an increment of 100ppm in each successive run starting from 0ppm to 1000ppm.

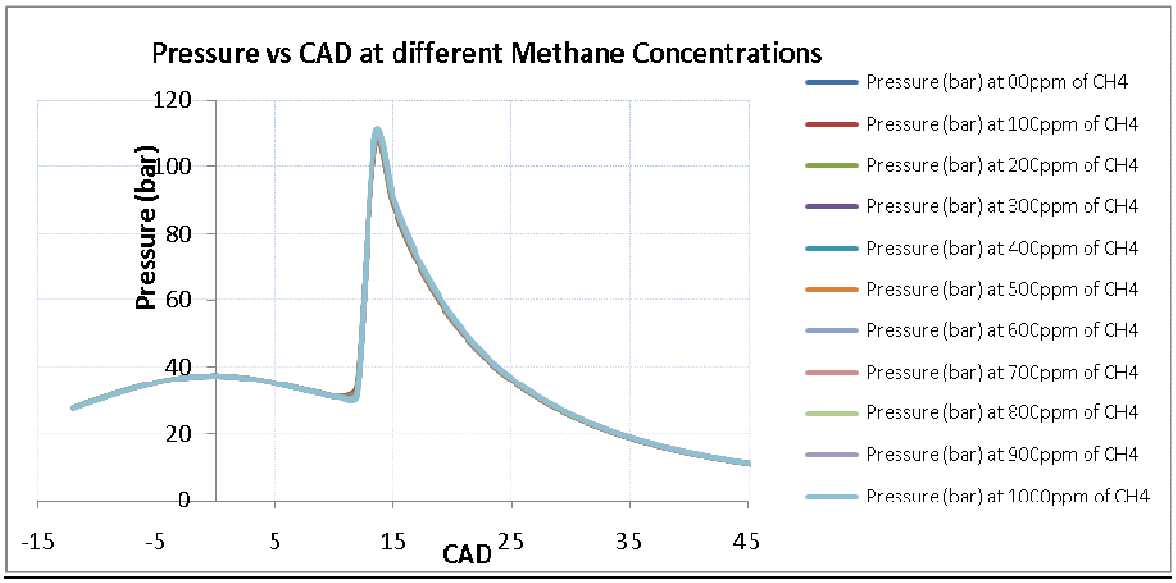

Figure D.1- Effect of CH4 addition on Ignition Delay at Equivalence Ratio 1.0

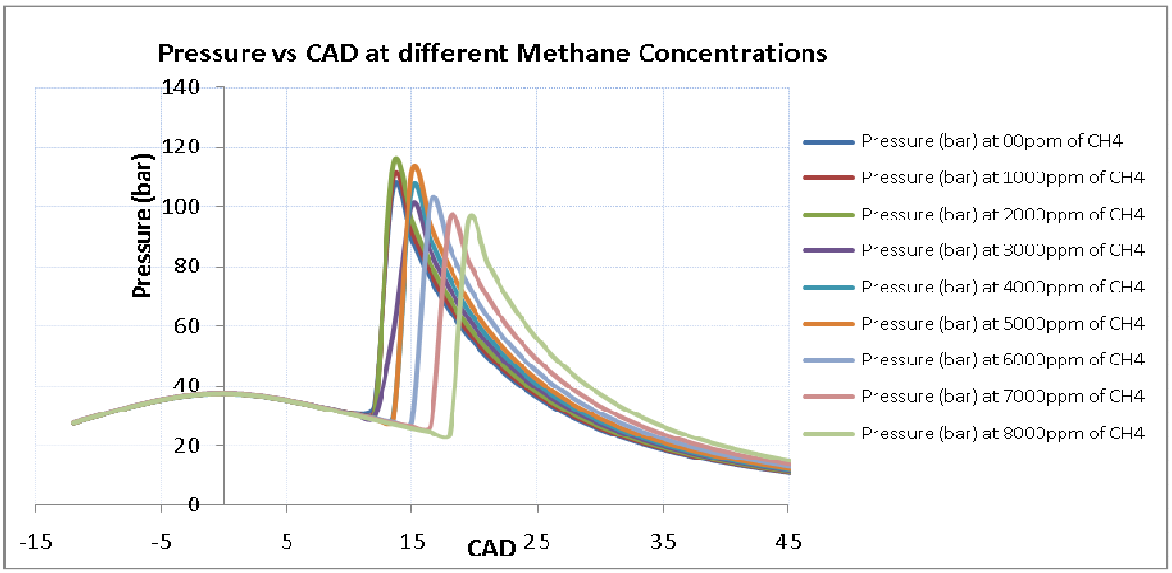

Figure D.2 - Effect of CH4 addition on Ignition Delay at Equivalence Ratio 1.0

From the figure D.1, it is evident that up to 1000ppm, Methane has almost no significant effect on ignition delay. Therefore, Methane was added in steps of 1000ppm, starting from 0ppm to 8000ppm as shown in figure D.2. Now addition of 2000ppm of Methane increases the ignition delay. Up to 3000ppm, the start of ignition occurs near 12CAD ATDC, After 3000 ppm to up to 5000ppm of methane addition, the start of combustion is retarded from 12 to 13.5 CAD. Further addition of Methane retards the start of combustion and at 8000ppm, the mixture ignites at 18 CAD ATDC.

D.1.1 Investigation of Ignition Retard:

Various plots were made for pressure and OH concentrations as shown in figure D.3 and D.4. It was interesting to find that the rise in pressure due to combustion is accompanied by the rise in OH concentration. Figures D.3 and D.4 show that OH concentration follows almost the exact pattern as of the Pressure.

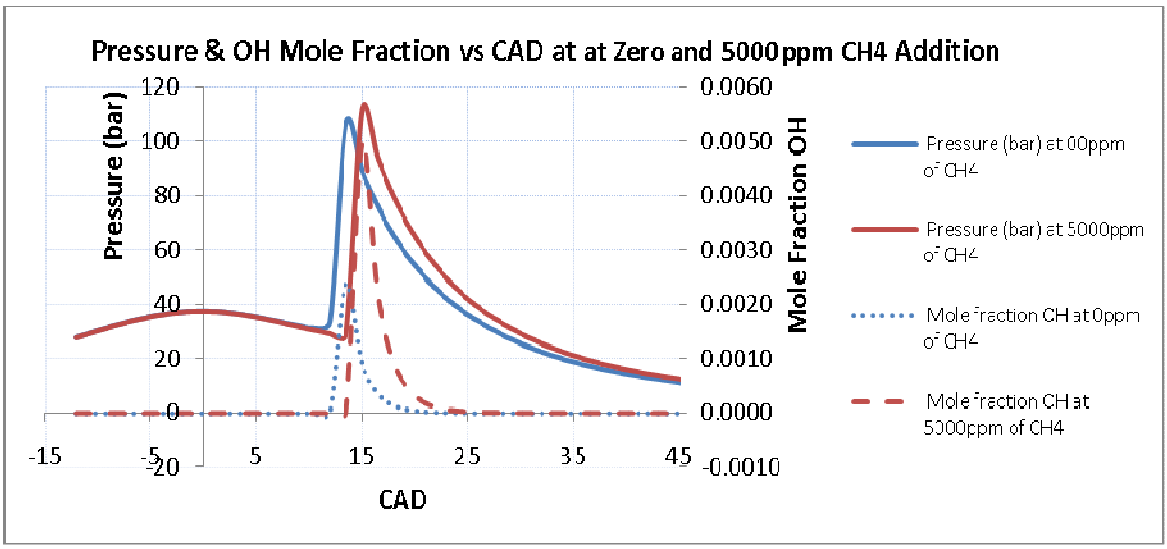

Figure D.3 - In-cylinder Pressure and OH mole fractions at zero and 5000ppm CH4 addition versus CAD

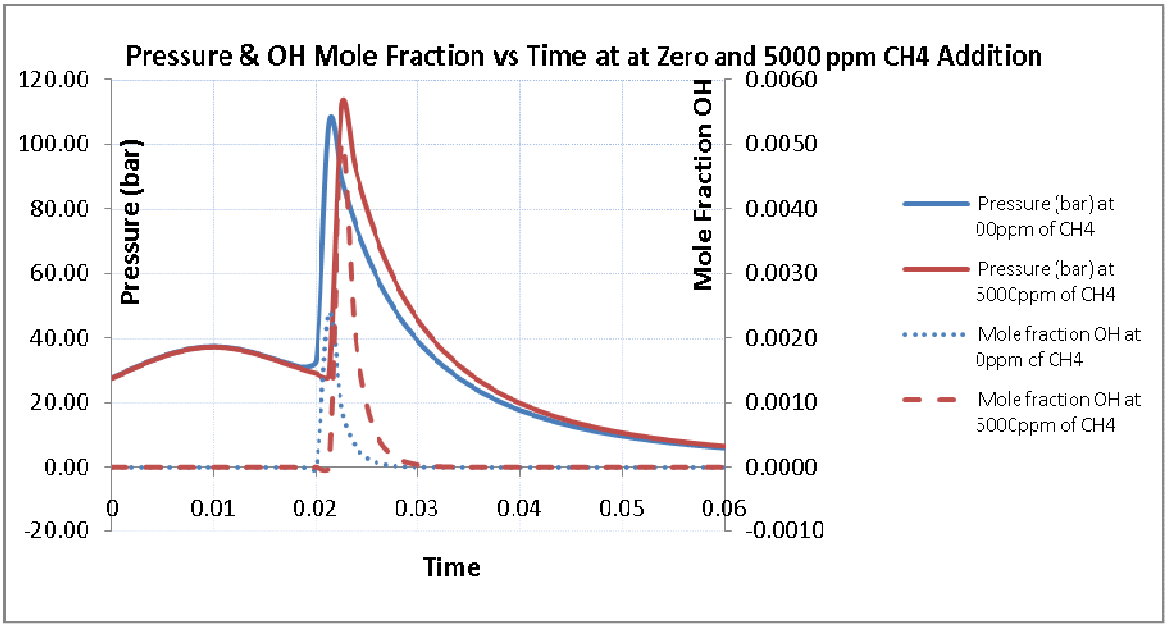

Figure D.4 - In-cylinder Pressure and OH mole fractions at zero and 5000ppm CH4 addition versus CAD

From figures D.3 and D.4, it can be concluded that addition of Methane has a direct effect on the OH concentration. OH being a main contributor to the start of combustion, the effects of Methane on OH needs to be examined.

D.1.2 Investigation using Reaction Path Analysis:

The RPA approach is used in this work, recognizing the effect on the reaction occurrence with the addition of zero CH4 and 5000ppm CH4. The study was performed at the time intervals 0.020 sec and 0.02175 sec from the start of injection of the fuel NC7H16. Using reaction path analysis, the process was studied in details. It was observed that the start of combustion occurred at 0.01875 seconds.

The approach was to compare the reactions involved in each of the two cases at the various time intervals.

The comparison of the two cases shows a very bright picture that involves the kinetics of the reactions. Although, most of the reactions were common for both the cases, the rates of the reactions were different at the given interval of time for zero Methane and 5000ppm Methane. Therefore, formation or consumption of the species involved in the reaction varied greatly. Following are the results for comparisons of the two different Methane concentrations.

Locating the start of combustion and the rise in pressure helps in identifying the duration of ignition delay. From the figure D.3 and D.4, it is quite evident that the

start of combustion occurs earlier in case of no methane addition. Following table describes the Pressure and OH mole Fractions at different time Intervals.

Time (sec)	CAD	Pressure (bar) (0ppm CH4)	Pressure (bar) (5000ppm CH4)	Mole fraction OH (0ppm CH4)	Mole fraction OH (0ppm CH4)
0.02	12.00	33.14132	29.12251	2.99E-07	1.27E-08
0.02125	13.50	106.2382	28.42922	2.39E-03	3.08E-08
0.0225	15.00	89.24704	111.5528	9.15E-04	4.99E-03

The Pressure difference at time 0.020 second between 0ppm Methane and 5000 ppm Methane is much lower than the pressure difference at time 0.02125 seconds. Also, rise in pressure is very high for 0ppm Methane from 0.020 seconds to 0.02125 second. In addition to this, at 0.02125 second, the fuel with 0ppm Methane mixture attains peak pressure, therefore, comparison of 0ppm Methane and 5000ppm Methane, along with the fuel, is more vital between the time interval 0.0200 second and 0.02125 second.

Considering the OH mole fractions, at all time intervals in the table above, OH mole fraction is higher for 0 pmm Methane addition with fuel. Therefore, Methane addition retards the OH formation rate.

Now with the Methane addition, the mass average temperature dropped at the time intervals 0.020 seconds and 0.02125 seconds. This drop in temperature caused a change in the value of reaction rates. This change in temperature is shown in the tabular format below.

Time (sec)	Temperature at 0ppm CH4 (T1)	Temperature at 5000ppm CH4 (T6)	T1-T6
0.02	737.5097 K	650.1334	87.376
0.02175	2390.927 K	668.63	1722.297

Following part describes the reason of lower OH mole fraction with 5000ppm Methane using Reaction Path Analyzer.

D.1.2.1 At 0.020 Seconds:

Considering the reactions involving CH4, following main reactions are evident:

1) CH4 + OH <==> CH3 + H2O

2) CH3 + O2 (+M) <==> CH3O2

3) CH3CHO <==> CH3 +HCO

4) CH3CHO +OH <==> CH3 + HOCHO

Above reactions are part of a chain mechanism that starts from reaction (1). Reaction (1) and reaction (4) involve the OH radical. Reaction 2 involves the oxygen atom. The reaction path for this chain reaction is described in figure D.5.

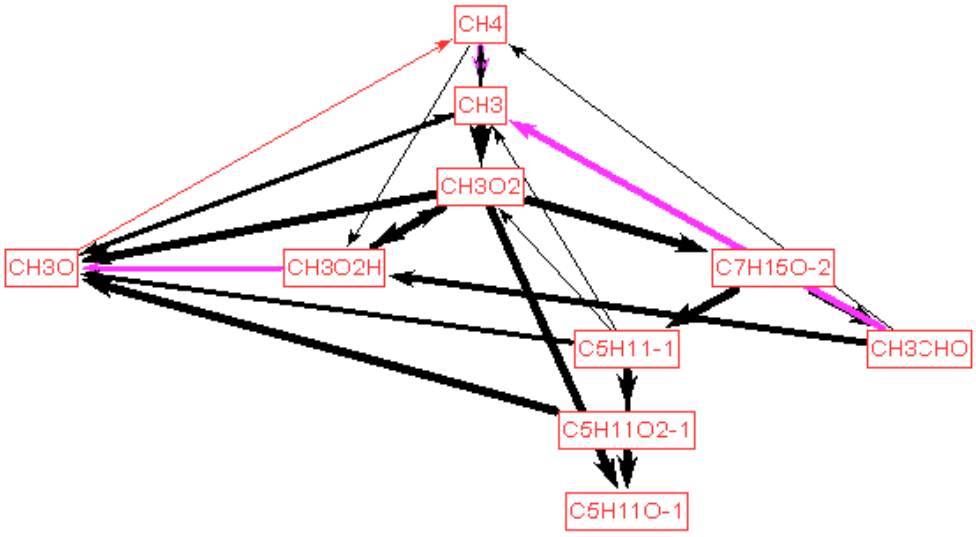

Figure D.5- Reaction Path diagram for CH4

Starting with reaction 1:

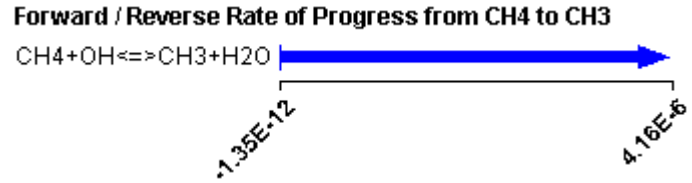

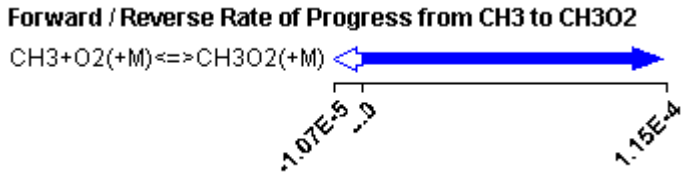

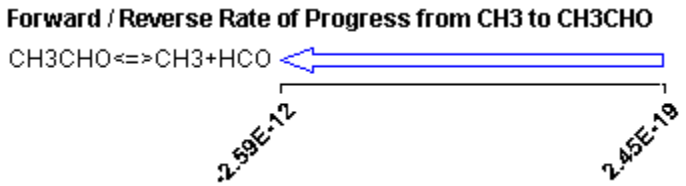

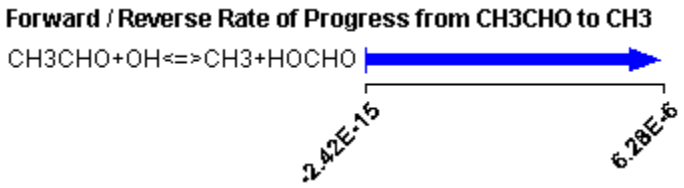

Now reaction number (2), CH3 + O2 (+M) <==> CH3O2, the species CH3O2 again forms a chain, shown in figure D.6, and finally produce HCHO according to the following process:

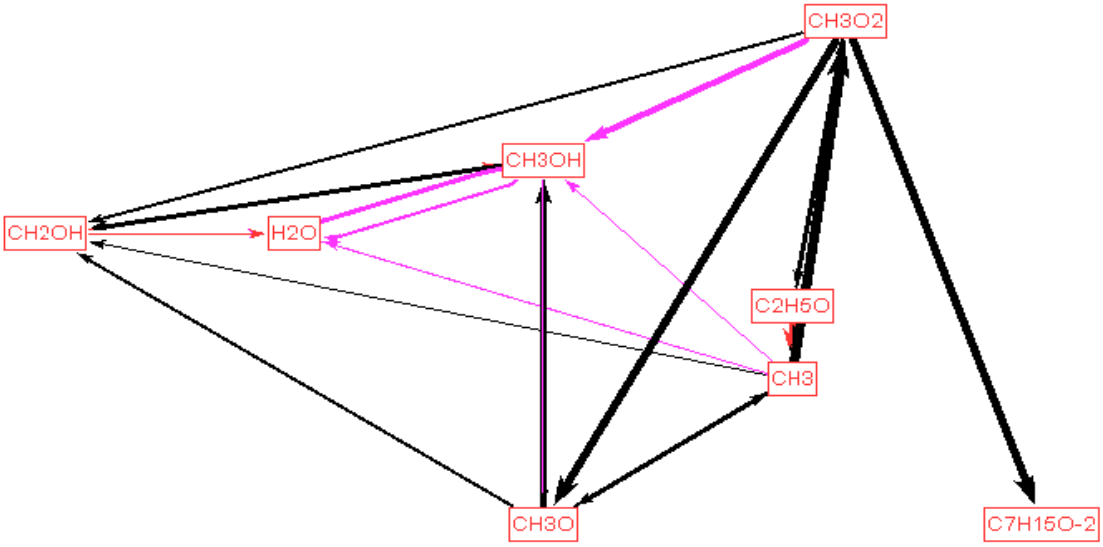

Figure D.6 - Reaction Path diagram for CH3O2

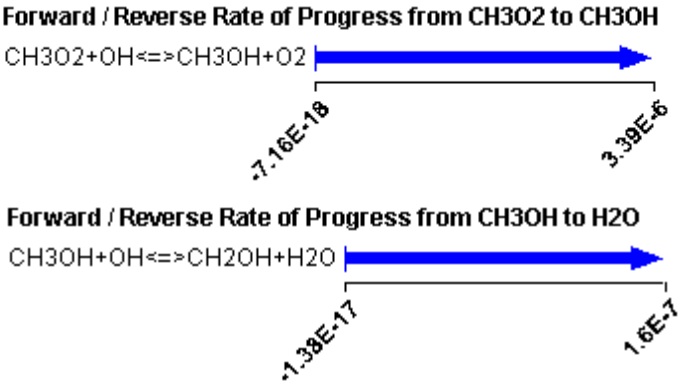

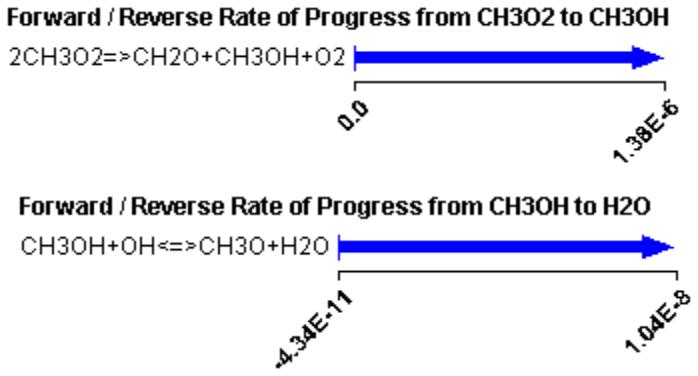

By following the reaction path for the reaction 1, **CH4 + OH <==> CH3 + H2O** , it is observed that there are some other reactions (chain reactions, shown in figure D.6) that involve the consumption of OH radical, all of these reactions occurring due to presence of methane. Therefore, more the quantity of methane, more will be the OH consumption due to these reactions.

Absolute rate of Formation of OH at 0.020 seconds with Zero ppm CH4 and 5000ppm CH4 respectively.

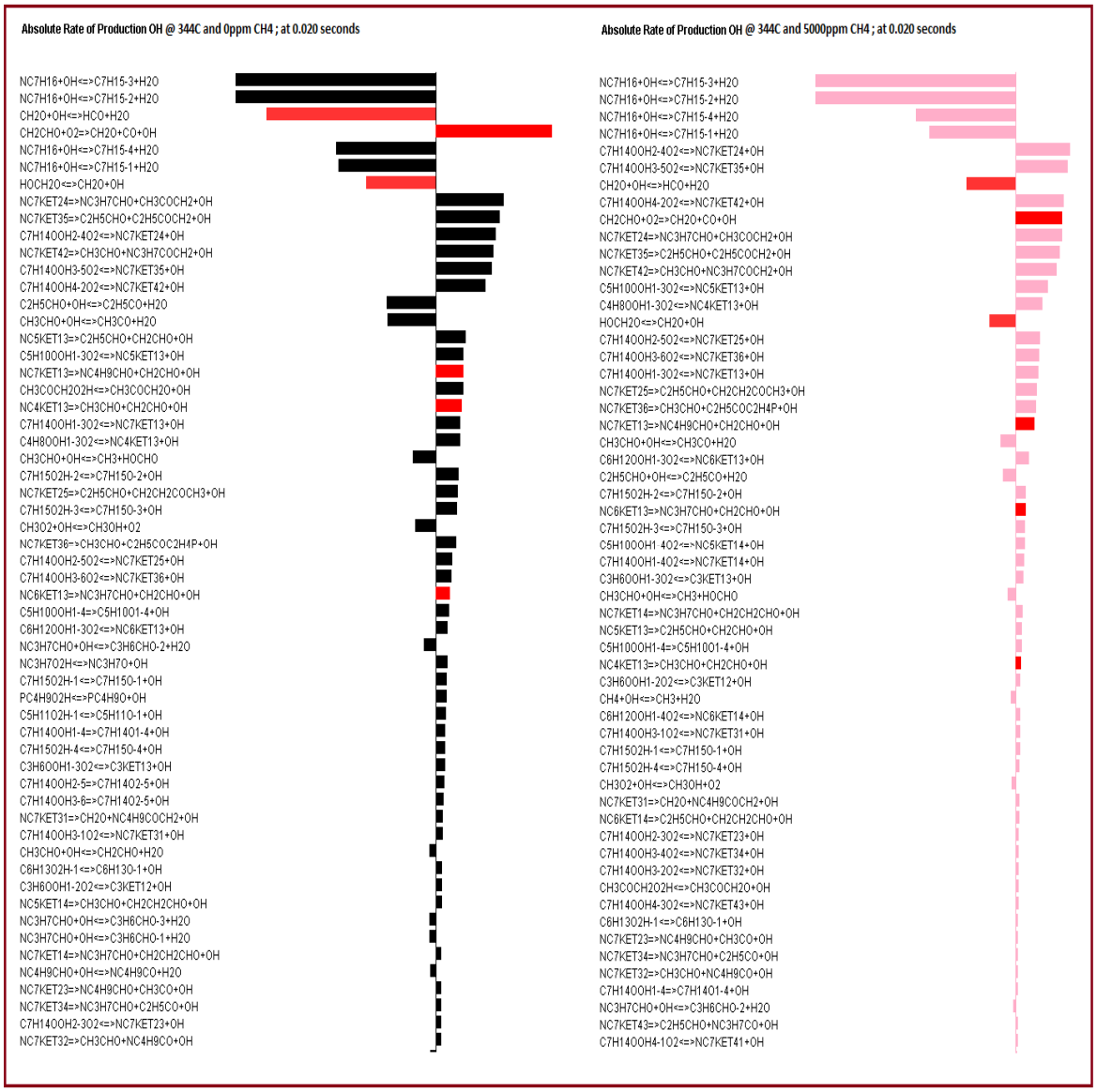

Figure D.7.a - Rate of formation of OH at 0.020 seconds with zero and 5000ppm CH4

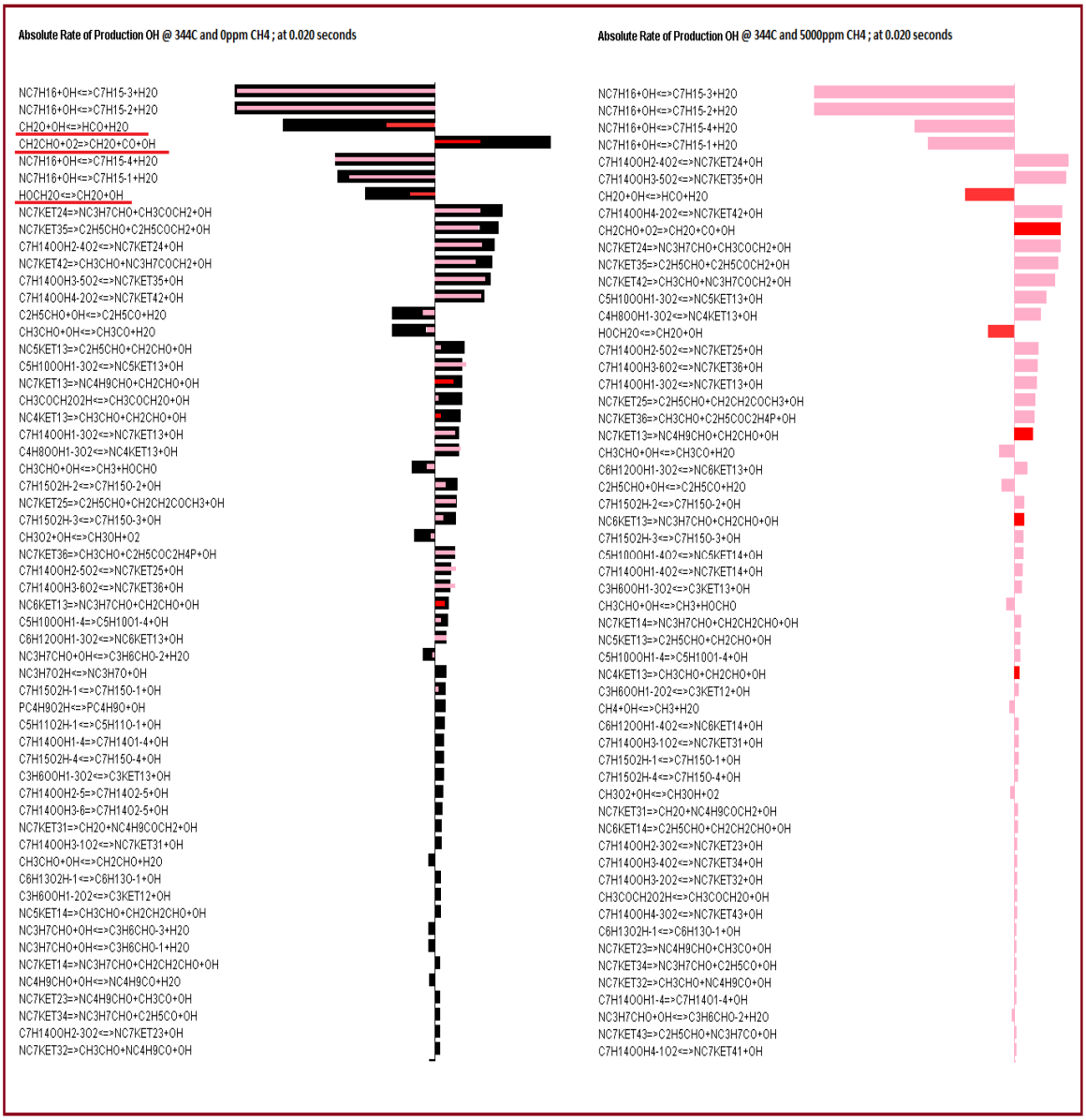

Figure D.7.b - Comparison using superposition between the rate of formation of OH at 0.020 seconds with zero and 5000ppm CH4

Figure D.7.a shows the rate of formation of OH at 0.020 seconds with zero and 5000ppm CH4 while figure D.7.b represent the comparison by superposition for the two cases of CH4 addition and it can observed that main reactions involving OH are:

- CH2CHO + 02 <==> CH2O + CO + OH ------ (a)
- CH2O + OH <==> HCO + H2O ------ (b)
- HOCH2O <==> CH2O + OH ------ (c)

Now reaction (a), **CH2CHO + 02 ==> CH2O + CO + OH**, goes only in forward direction. This forward reaction favors the formation of OH. Considering the rate of the reaction for both the cases, the OH formation through this reaction can be obtained.

Time	At 0 ppm CH4 and 0.020 seconds; Rf : CH2CHO + 02 <==> CH2O + CO + OH	At 5000ppm CH4 and 0.020 seconds; Rf : CH2CHO + 02 <==> CH2O + CO + OH
0.020	1.94E-05	3.66E-05

Now considering reaction (b), **CH2O + OH <==> HCO + H2O** the rate of reaction obtained from Reaction Path analysis are :

Time	At 0 ppm CH4 and 0.020 seconds; R_f : CH2O + OH <==> HCO + H2O	At 5000 ppm CH4 and 0.020 seconds; R_f : CH2O + OH <==> HCO + H2O
0.020	9.74E-06	3.83E-05

Time	At 0 ppm CH4 and 0.020 seconds; R_b : CH2O + OH <==> HCO + H2O	At 5000 ppm CH4 and 0.020 seconds; R_b : CH2O + OH <==> HCO + H2O
0.020	-2.22E-18	-1.65E-17

From the table above, it is quite evident that the rate of forward reaction for 0ppm Methane is lesser than the rate of forward reaction with 5000ppm Methane. The rates of backward reaction are very small for comparison.

Now considering reaction (c), **HOCH2O <==> CH2O + OH,** the forward reaction favors the OH formation while the Backward Reaction Reduces the OH concentration

From the reaction path analysis:

Time	At 0 ppm CH4 and 0.020 seconds;	At 5000ppm CH4 and 0.020 seconds;
	R_f : HOCH2O <==> CH2O + OH	R_f : HOCH2O <==> CH2O + OH
0.020	6.47E-09	2.57E-08

Time	At 0 ppm CH4 and 0.020 seconds;	At 5000ppm CH4 and 0.020 seconds;
	R_b : HOCH2O <==> CH2O + OH	R_b : HOCH2O <==> CH2O + OH
0.020	-5.21E-06	-2.04E-05

The total OH mole fraction at time 0.0200 seconds is:

Time	Mole fraction OH at 0ppm CH4	Mole fraction OH at5000ppm CH4
0.0200	2.99E-07	1.27E-08

With 5000ppm Methane addition, reaction (a) proposes higher OH formation, reaction (b) proposes comparatively higher OH consumption and reaction (c) proposes comparatively higher OH consumption.

Therefore, it can be inferred that the reactions shown in the figure D.5 and D.6 along with the reactions (a), (b) and (c) result in lower OH concentration with Methane addition.

D.1.3 Summary:

- It is evident that the start of combustion is retarded by Methane addition. Therefore Ignition delay is increased.
- OH production rate is also retarded with the Methane addition.
- The addition of Methane decreases the average mass temperature. Therefore, a change in the value of reaction rate constant and the reaction rate is evident.

REFERENCES

1. Liu, H., Henein, N. A. and Bryzik, W., "Simulation of diesel engines cold-start". SAE 2003-01-0080, 2003.

2. Bielaczyc, P., Merkisz, J. and Pielecha, J., "Investigation of exhaust emissions from DI diesel engine during cold and warm start". SAE 2001-01-1260, 2001.

3. Raihan, K. A., Takimoto, F., Ogawa, H. and Miyamoto, N.,, "Time-Resolved Behavior of Unburned Hydrocarbon Components in Diesel Exhaust under Transient Operations". SAE 2001-01-1259, 2001.

4. Ogawa, H., Raihan, K. A., Iizuka, K. and Miyamoto, N., "Cycle-to-cycle Transient Characteristics of Diesel Emissions during Starting". SAE 1999-01-3495,1999.

5. Bielaczyc, P. and Merkisz, J., "Cold-Start Emissions Investigation at Different Ambient Temperature Conditions". SAE 980401, 1998.

6. Han, Z., Henein, N. A., Nitu, B. and Bryzik, W., "Diesel Engine Cold Start Combustion Instability and Control Strategy". SAE 2001- 01-1237, 2001.

7. Han, Z., Henein, N. A. and Bryzik, W., "A New Ignition Delay Formulation Applied to Predict Misfiring During Cold Starting of Diesel Engines". SAE 2000-01-1184, 2000.

8. Henein, N. A., Zahdeh, A. R., Yassine, M. K. and Bryzik, W., "Diesel Engine Cold Starting: Combustion Instability". SAE 920005, 1992.

9. Zahdeh, A., Henein, N. and Bryzik, W., "Diesel Cold Starting: Actual Cycle Analysis under Border- Line Conditions". SAE 900441, 1990.

10. Weilenmann, M., Soltic, P., Saxer, C., Forss, A. and Heeb, N., "Regulated and non regulated diesel and gasoline cold start emissions at different temperatures". Atmospheric Environment, 2005; 39: 2433-2441

11. Phatak, R. and Nakamura, T., " Cold Startability of Open-Chamber Direct-Injection Diesel Engines-Part I: Measurement Technique and Effects of Compression Ratio" SAE 831335, 1983.

12. Mohr, H. and Urlaub, A., "Improvement of the Cold Start Qualities of Diesel Engines with Swirl Chambers". SAE 940075, 1994.

13. Tsunemoto, H., Yamada, T. and Ishitani, H., "Behavior of Adhering Fuel on Cold Combustion Chamber Wall in Direct Injection Diesel Engines" SAE 920117, 1992.

14. Heywood, J. B., Internal Combustion Engine Fundamentals, McGraw-Hill, New York, 1988.

15. Hara, Hi.,, Itoh, Y., Henein, N. A. and Bryzik, W., "Effect of Cetane Number with and without Additive on Cold Startability and White Smoke Emissions in a Diesel Engine". SAE 1999-01-1476, 1999.

16. Clerc, J.C., "Cetane Number Requirements of Light-Duty Diesel Engines at Low Temperatures" SAE 860529, 1986.

17. Austen, W. and Lyn, W., "Some Investigations on Cold Starting Phenomena in Diesel Engines" SAE paper no. 5 1959-60.

18. Chang, J., Filipi, Z., Assanis, D., Kuo, T., Najt, P. and Rask, R., "Characterizing the Thermal Sensitivity of a Gasoline Homogeneous Charge Compression Ignition Engine with Measurements of Instantaneous Wall Temperature and Heat Flux", International Journal of Engine Research, **6**, pg. 289-309, 2005.

19. Dec, J. E., "A Computational Study of the Effects of Low Fuel Loading and EGR on Heat Release Rates and Combustion Limits in HCCI Engines", SAE 2002-01-1309, 2002.

20. Dec, J. E. and Sjöberg, M., "Isolating the Effects of Fuel Chemistry on Combustion Phasing in an HCCI Engine and the Potential of Fuel Stratification for Ignition Control", SAE 2004-01-0557, 2004.

21. Sjöberg, M. and Dec, J. E., "Smoothing HCCI Heat-Release Rates Using Partial Fuel Stratification with Two-Stage Ignition Fuels", SAE 2006-01-0629, 2006.

22. Aceves, S. M., Flowers, D. L., Westbrook, C. K., Smith, J. R., Pitz, W., Dibble, R., Christensen, M. and Johansson, B., "A Multi-Zone Model for Prediction of HCCI Combustion and Emissions", SAE 2000-01-0327, 2000.

23. Babajimopoulos, A., Assanis, N. and Fiveland, S. B., "An Approach for Modeling the Effects of Gas Exchange Processes on HCCI Combustion and Its Application in Evaluating Variable Valve Timing Control Strategies", SAE 2002-01-2829, 2002.

24. Babajimopoulos, A., Lavoie, G. A. and Assanis, D. N., "Modeling HCCI Combustion with High Levels of Residual Gas Fraction - a Comparison of Two VVA Strategies", SAE 2003-01-3220, 2003.

25. Chang, J., Guralp, O., Filipi, Z. S., Assanis, D. N., Kuo, T., Najt, P. and Rask, R., "New Heat Transfer Correlation for an HCCI Engine Derived from Measurements of Instantaneous Surface Heat Flux", SAE 2004-01-2996, 2004.

26. Kashdan, J. T. and Papagni, J., "LIF Imaging of Auto-Ignition and Combustion in a Direct-Injection, Diesel-Fuelled HCCI Engine", SAE 2005-01-3739, 2005.

27. Ladommatos, N., Abdelhalim, S. M., Zhao, H. and Hu, Z., "The Dilution, Chemical and Thermal Effects of Exhaust Gas Recirculation on Diesel Engine Emissions - Part 4: Effects of Carbon Dioxide and Water Vapor", SAE 971660, 1997.

28. Maiboom, A., Tauzia, X., Hetet, J, Cormerais, M., Tounsi, M., Jaine, T. and Blanchin, S., "Various Effects of EGR on Combustion and Emissions on an

Automotive DI Diesel Engine: Numerical and Experimental Study", SAE 2007-01-1834, 2007.

29. Nakano, M., Mandokoro, Y., Kubo, S. and Yamazaki, S., "Effects of Exhaust Gas Recirculation in Homogeneous Charge Compression Ignition Engines", International Journal of Engine Research, **1** (3), pg. 269-279, 2000.

30. Sjöberg, M. and Dec, J. E., "EGR and Intake Boost for Managing HCCI Low-Temperature Heat Release over Wide Ranges of Engine Speed", SAE 2007-01-0051, 2007.

31. Sjöberg, M. and Dec, J. E., "Comparing Late-Cycle Autoignition Stability for Single and Two-Stage Ignition Fuels in HCCI Engines", Proceedings of the Combustion Institute, **31**, pg. 2895-2902, 2007.

32. Sjöberg, M., Dec, J. E. and Hwang, W., "Thermodynamic and Chemical Effects of EGR and Its Constituents on HCCI Autoignitionn", SAE 2007-01-0207, 2007.

33. Urushihara, T., Hiraya, K., Kakuhou, A. and Itoh, T., "Expansion of HCCI Operating Region by the Combination of Direct Fuel Injection, Negative Valve Overlap and Internal Fuel Reformation", SAE 2003-01-0749, 2003.

34. Willand, J., Nieberding, R., Vent, G. and Enderle, C., "The Knocking Syndrome - Its Cure and Its Potential", SAE 982483, 1998.

35. Liu, Z. and Karim, G. A., "An Examination of the Role of Residual Gases in the Combustion Processes of Motored Engines Fueled with Gaseous Fuels", SAE 961081, 1996.

36. Olsson, J., Tunestal, P., Johansson, B., Fiveland, S., Agama, R., Willi, M. and Assanis, D., "Compression Ratio Influence on Maximum Load of a Natural Gas Fueled HCCI Engine", SAE 2002-01-0111, 2002.

37. Sjöberg, M., Dec, J. E., Babjimopoulos, A. and Assanis, D., "Comparing Enhanced Natural Thermal Stratification against Retarded Combustion Phasing for Smoothing of HCCI Heat-Release Rates", SAE 2004-01-2994, 2004.

38. Subramanian, G. and Pirez Da Cruz, A., "Chemical Impact of CO and H2 Addition on the Auto-Ignition Delay of Homogeneous NHeptane/Air Mixtures", Combustion Science and Technology, 179, pg. 1937-1962, 2007.

39. Yamaya, Y., Furutani, M. and Ohta, Y., "Premixed Compression Ignition of Formaldehyde-Doped Lean Butane/Air Mixtures in a Wide Range of Temperature", SAE 2004-01-1977, 2004.

40. Jansons, M., Florea, R., Zha, K., Estefanous, F., Florea, E., Taraza, D., Henein, N. A. and Bryzik, W., "Optical and Numerical Investigation of Pre-Injection Reactions and Their Effect on the Starting of a Diesel Engine". SAE 2009-01-0648, 2009.

41. Zahdeh, A., Henein, N. A. and Bryzik, W., “Diesel Cold Starting: Actual Cycle Analysis Under Border-Line Conditions”, SAE 900441, 1990.

42. Gonzalez, M. A., “A Computational Study of In-Cylinder Cold Starting Processes in a Diesel Engine,” Master Thesis, University of Wisconsin-Madison,1990.

43. Phatak, R. and Nakamura, T., " Cold Startability of Open-Chamber Direct-Injection Diesel Engines-Part II: Combustion Chamber Design and Additional Air and Glow Plug as a Starting Aid" SAE 831396, 1983.

44. Matsui, Y. and Sugihara, K., "Sources of Hydrocarbon Emissions from a Small Direct Injection Diesel Engine", SAE 871613, 1987.

45. Kato et al, " The Influence of Fuel Qualities on White Smoke Emissions from a Light-Duty Diesel Engine", SAE 870341, 1987.

46. Greeves, G. and Khan, I. M., " Origins of Hydrocarbon Emissions from a Diesel Engine", SAE 770259, 1977.

47. Yu, R. C., Wong, V. W. and Shahed, S. M., "Sources of the hydrocarbon Emissions from a DI Diesel Engine", SAE 800048, 1980.

48. Keppeler, S. and Schulte, H., (1998), “The Technical Ramifications of Downsizing HSDI Diesel Technology to the 300 cc Displacement Class” SAE 981916, 1998.

49. Osuka, I., Nishimura, M., Tanaka, Y. and Miyaki, M., "Benefits of new fuel injection system technology on cold startability of diesel engines". SAE 940586, 1994.

50. Bosch, Diesel Engine Management, 3e, 2000.

51. Karim, G. A, Mohan, K., and Burn, K., "Engine Exhaust Emissions under Very Low Ambient Temperature Conditions." Proceedings of the International Clean Air Conference, Brisbane, Australia, May 15-19, 1978.

52. Campbell, J., Scholl, J., Hibbler, F., Bagley, S., Leddy, D., Abata, D. and Johnson, J., "The effect of fuel Injection and Timing on the Physical, chemical and Biological Character of Particulate emissions from a DI Diesel Engine", SAE 810996, 1981.

53. Nakakita, K., et al, "Effects of high Pressure Fuel Injection on the Combustion and Exhaust Emissions of a High Speed DI Diesel Engine.", JSAE Review Vol. 12 no.1, Jan 1991.

54. Komoda, T. and Kawase, H., " Effect of Fuel Injection system Improvement on white Smoke Reduction in Small diesel Engines with Swirl Chamber", SAE 911256, 1991.

55. Woermann, R. J., Theuerkauf, H. J. and Heinrich, A., “A Real-Time Model of a Common Rail Diesel Engine”, SAE 1999-01-0862, 1999.

56. Roy, M. M. and Tsunemoto, H., “Effect of Injection Pressure and Split Injection on Exhaust Odor and Engine Noise in DI Diesel Engines” SAE 2002-01-2874, 2002.

57. Henein, N. A., "Starting of Diesel Engines: Uncontrolled Fuel Injection Problems," SAE 860253, 1986.

58. Bielaczyc, P., Merkisz, J. and Pielecha, J., "A Method of Reducing the Exhaust Emissions from DI Diesel Engines by the Introduction of a Fuel Cut Off System During Cold Start". SAE 2001-01-3283, 2001.

59. Lindl, B. and Schmitz, H. G., “Cold Start Equipment for Diesel Direct Injection Engines” SAE Paper 1999-01-1244, 1999.

60. Girotra, M., Henein, N. A., Zhong, L. and Bryzik, W., "Split Injection strategy for Prompt Cold Starting and Low White Smoke Emissions, " ASME ICE 2005 Spring Technical Conference, ICES2005-1100, 2005.

61. Gruenewald, S., "Effects of Hydrocarbon Recycling (HCR) and Varied Transient Strategies on Cold Starting of Direct Injection Common Rail Diesel Engine," M.S. Thesis, Wayne State University, 2006.

62. Seiser, H. H., Pitsch, K., Seshadri, W. J., and Curran, H. J., "Extinction and Autoignition of n-Heptane in Counterflow Configuration," Proceedings of the Combustion Institute **28**, p. 2029-2037, 2000.

ABSTRACT

OPPOSING EFFECTS OF RECIRCULATED GASES DURING CRANKING ON COLD START OF DIESEL ENGINES

by

RAFIK ROFAIL

August 2011

Advisor: Dr. Naeim Henein

Major: Mechanical Engineering

Degree: Doctor of Philosophy

Enhancing cold start of DI diesel engines is the motivation behind this study. A new control strategy is proposed to reduce the cranking period and the white smoke emissions. In the strategy, the gases leaving the cylinder during the cranking period are recycled back into the intake manifold using two different methods. In the first method the engine-out gases during cranking are recirculated into the intake manifold and their rate is controlled by a CGR (Cranking Gases Recirculation) valve, without applying any back pressure on the engine. In the second method a butterfly valve is installed in the exhaust system after the turbocharger to increase the back pressure and the rate of recirculated gases. Since there is no combustion during cranking, these gases contain evaporated hydrocarbons (HCs) and partial oxidation products such as

formaldehyde (HCHO). HCs and HCHO have two opposing effects. HCs enhance the autoignition process, while the HCHO has an opposite effect.

These opposing effects are being investigated by three different approaches. The first is experimentally in a multi-cylinder proto-type engine. The second is using high speed imaging in an optically accessible engine. The third is by using CFD and chemical kinetic simulation to gain a better understanding of the effect of the recirculated gases on the autoignition process during cold starting of a direct injection diesel engine. Cold start experiments are conducted on a 1.2L Ford DIATA 4-cylinder, 16-valve, 70 mm bore, 78 mm stroke and 19.5 compression ratio, water cooled, turbocharged and intercooled diesel engine. The engine is equipped with a common rail injection system, EGR system and a swirl control mechanism. The engine is installed in a cold room and the ambient temperature is electronically controlled. Before starting, the engine is soaked at the desired room temperature for at least eight hours. The analysis of the data demonstrated the effect of two CGR methods on reducing the cranking period and HCs emissions. The images showed the effect of aldehydes on hindering the autoignition and combustion processes. The simulation covered a wide range of the hydrocarbons and aldehydes concentrations and their effect on the ignition delay.

The simulation results agreed with the experimental findings. The results of this work will help in developing strategies to reduce the cranking period, fuel consumption and white smoke emitted during cold starting of diesel engines. In addition, a more understanding will be developed of the role of aldehydes in

combustion instability and misfiring after first firing experienced in cold starting of diesel engines.

PUBLICATIONS

- “Effect of HCR (Hydrocarbons Recirculation) on Cranking Period and Hydrocarbons Emissions during Cold Start of A Di Diesel Engine”, E11, Hurghada, Egypt, 2009.
- “Opposing Effects of Recirculated Gases during Cranking for Cold Start of Diesel Engines”, Institute of Mecanical Engineers, London, UK, JAUTO1785, 2011.
- “Simulation of the Effect of Recirculated Gases on Ignition Delay during Cold Starting of a Direct Injection Diesel Engine”, SAE 2011-01-0838, 2011.

AUTOBIOGRAPHICAL STATEMENT

Rafik N. Rofail was born on November 14th, 1979 in Cairo, Egypt. He joined Ain Shams University, college of engineering in Cairo, Egypt in September 1997. He received his Bachelor's degree in 2002. His major was concentrated on automotive engineering. Then he worked in GB as a design engineer from May 2003 to December 2003 then he worked as a demonstrator at Ain Shams University from December, 2003 to December, 2005.

He came to the United States and enrolled in the graduate program in Mechanical Engineering Department of Wayne State University in January 2006. He worked in the Center for Automotive Research, under the supervision of professor Naeim A. Henein, as a graduate research assistant from January 2006 to May 2011. During this period, he worked on the research projects related to DIATA diesel engine and its test rig setup, engine calibration and testing, diesel engine combustion and emissions testing and analysis, fuel injection system testing and simulation, diesel engine cold starting simulation.

He earned his Master's degree in December 2007 at the same university. Then he started working in his Ph.D. since January 2008 till May 2011 in Wayne State University. As an author, he has published 3 papers in the Society of Automotives Engineers (SAE), Institute of Mechanical Engineering Journal and EE11.